Regulation of Replication Fork Stability by ssDNA Binding Proteins

By

Kamakoti Prakash Bhat

Dissertation

Submitted to the Faculty of the

Graduate School of Vanderbilt University

in partial fulfillment of the requirements

for the degree of

DOCTOR OF PHILOSOPHY

in

BIOCHEMISTRY

March 31, 2018

Nashville, Tennessee

Approved:

Dr. Scott W. Heibert, Ph.D.

Dr. David K. Cortez, Ph.D.

Dr. Walter J. Chazin, Ph.D.

Dr. William P. Tansey, Ph.D.

Dr. Brandt F. Eichman, Ph.D.

To My Parents,

For inspiring me to reach for the stars.

To My Brother,

For always being there.

To My Husband,

For loving me unconditionally.

ACKNOWLEDGEMENTS

The last five years have been an amazing journey through graduate school and I am indebted to the Vanderbilt International Scholar's Program (VISP) for giving me the opportunity to come to Vanderbilt. I would like to thank the National Cancer Institute for awarding me an F99/K00 predoctoral to postdoctoral transition award (F99CA212345) to support my research. I am also grateful to the Vanderbilt Ingram Cancer Center and the Biochemistry department for distinguishing me with graduate student of the year awards in 2017 and 2018 respectively.

I would like to thank the members of my thesis committee Drs. Scott Heibert, William P. Tansey, Walter J. Chazin and Brandt Eichman. I always came out of committee meetings feeling better about myself as a scientist than I did going into them- and their support and encouragement have been invaluable. Walter, I have always appreciated your insights on DNA binding proteins; and thank you for all the travel stories and your constant support. I would like to thank Dr. Kathy Gould and Dr. Roger Colbran, who have been my mentors outside of my committee and who have championed me. I am grateful for your time, support and interest in my thesis. I also would like to thank Dr. Jennifer Pietenpol for her advice and encouragement.

None of this would have been possible without my mentor, David Cortez, and I owe my success as a graduate student to his encouragement and guidance. I feel privileged to have been part of the lab for five years and to have learnt from him what it means to be a scientist. His intelligence, critical thinking and passion for science have always inspired me and I shall be forever grateful for all the insights, thoughts and arguments we have had about experiments and science. I would like to thank him for always having a higher opinion of me than I have had of myself; for all the motivation, support, "nurturing" and lavish praise over the years. And most importantly, for always being willing to listen without taking offense. Dave, I will cherish the memories of you dancing at a conference in order to get purified protein for the RADX project, of

the times you randomly played music in the lab to boost morale and for all the non-science related talks we have had. I could not have asked for a better mentor- and I will miss you.

The members of the Cortez Lab have been instrumental in making this journey so memorable. Jami, thank you for helping me set up the fork remodeling assays in the lab and for all your insights. Jessica, thank you for all the long talks, for the movies, Bollywood dance nights and for your friendship. Lisa, it has been wonderful to go through grad school with you. Thank you for the Korean songs, food and for all the celebrations. Thomas, I could not have asked for a better bay-mate. Thank you for all the fun chats we have had and for being so awesome. Petria, I have enjoyed our Dosa Hut and Tacomamacita dinners. Sarah, thank you for the morning coffee breaks, cookies, decorations and fun. Kareem, it has been a lot of fun talking to you about random happenings in the world and about science. Gloria and Nancy, you have ensured that the lab ran smoothly, and thank you both for your help in my projects. Gina, Akosua and Clint – thank you for the jokes, motivation and laughter. Vaughn, Archana, Petria and Taha- you are all talented and I can't wait to hear about your achievements. Archana, thank you for helping me on the RADX project, for introducing me to "jimmikikammal" and for all the hundreds (or thousands) of fibers you measured.

Huzefa, we joined the lab in the same week. I am so glad you came up to me to say hi, and that you were not offended when I didn't realize you were Indian. We quickly became good friends- and working with you on CX has been a blast. I have learnt so much from you about being a persistent, methodical scientist, and I have always envied your ability to shrug things off and to be at peace. Thank you for all the waterfall-chasing, the long drives, for the sweet tea and coffee breaks, for movies, dinners, for driving me home and so much more. I know that I didn't make it easy, but thank you for trying to make me smile, every day. I am so glad you were at my wedding and you were the best "man of honor" I could have asked for at the sangeet. Mostly, thank you for being so constantly there- even at times when I was difficult to be around.

To all the friends I have made along the way- thank you for making this journey so much more fun. Rose, I will cherish our coffee walks and all your fun stories. To my friends from India- Kavya, Saranya, Nivedita, Lakshmi, Gokul, Shanmugam and Nijanthan- thank you for not letting the 12-hour time difference, the sheer distance or my busy hours come in the way of our friendship. You have always been there for me and I am so grateful for the love and support. Vatsi, you were there for me at one of the lowest points of my life, and I will never forget your support, patience and love.

My family has been my greatest strength. Mom and Dad, thank you for inspiring me to be the best I possibly can. You two have always been there for me, supported me, encouraged me to chase my dreams, given me the courage to face challenges and loved me more than I know. Thank you for not listening to society and for facing banal questions about why daughters need to study without letting it get to you. You both revolutionized the community, quietly, without a fuss- and I will always remain grateful to you both, for teaching me that I don't have to conform. You taught me about honesty, selfless love and cheerful duty, and I pray to, one day, be deserving of all your love and trust. To my brother, Adi - you are the smarter and the better one of us both and I love you more than you could ever know. You set the standard so high for all men, everywhere; and there is no one quite like you. I am so proud of the person you have grown up to be, and you are the best little brother in the world. I can't wait to live near you again.

I have been surrounded, all my life, by the very best of men. My father and brother set the standards so high I never thought I could find anyone who even came close. Kousik, you are all I could have ever asked for and more. You started me on this journey of getting a Ph.D. the day you taught me how to pipette in undergrad. You are the only one who can get me to smile amidst my tears, who can tolerate my rants about graduate school, lab and the state of the world and the only one I want to spend my life with. Thank you for seeing what I was capable of when I didn't know myself, for understanding me to the point that you know what I feel before I articulate it, for seeing the very worst of me and yet loving me. For the countless visits to Nashville during grad

school, for all the pep talks, jokes, happiness, joy and peace. I don't know anyone who is half as patient as you are - or half as giving. You are my better half, and I couldn't have survived graduate school if you weren't there. I love you.

TABLE OF CONTENTS

LIST OF TABLES

LIST OF FIGURES

LIST OF ABBREVIATIONS

γH2AX	Phosphoserine 139 H2AX
53BP1	p53 binding protein 1
ATM	Ataxia Telangiectasia Mutated
ATP	Adenosine Tri Phosphate
ATR	Ataxia Telangiectasia Mutated and Rad3-related
ATRi	Ataxia Telangiectasia Mutated and Rad3-related inhibitor
ATRIP	Ataxia Telangiectasia Mutated and Rad3-related Interacting Protein
BIR	Break Induced Replication
BLM	Bloom syndrome protein
BRCA1	Breast Cancer 1
BRCA2	Breast cancer 2
BrdU	Bromo deoxy uridine
CldU	5' chloro 2' deoxy uridine
CPT	Camptothecin
CRISPR	Clustered Regularly Interspaced Short Palindromic Repeats
CST complex	CST-Stn1-Ten1 complex
DDR	DNA Damage Response
DNA-PK	DNA-dependent Protein Kinase
dNTP	Deoxyribose Nucleotide Tri Phosphate
DSB	Double strand break
DSBR	Double Strand Break Repair
dsDNA	Double stranded DNA
EM	Electron Microscopy

EMSA	Electrophoretic Mobility Shift Assay
FA	Fanconi Anemia
FBS	Fetal Bovine Serum
GFP	Green Fluorescent Protein
GINS	Go-ichi-ni-san complex
gRNA	Guide RNA
HDR	Homology Directed Repair
HLTF	Helicase Like Transcription Factor
HU	Hydroxyurea
ICL	Intra-strand Cross Link
IdU	5’ Iodo 2’ deoxy uridine
IP	Immunoprecipitation
IR	irradiation
MCM	Mini Chromosome Maintenance
MGMT	O6-methylguanine DNA methyltransferase
MMS	Methyl-methane-sulfonate
MRN	Mre11-Rad50-Nbs1
MS	Mass-Spectrometry
NER	Nucleotide Excision Repair
NHEJ	Non-homologous End Joining
OB	Oligonucleotide/Oligosaccharide Binding protein
ORC	Origin Recognition Complex
PARPi	Poly ADP-ribosylase polymerase inhibitor
PBS	Phosphate-buffered saline
PCNA	Proliferating Cell Nuclear Antigen

PCR	Polymerase Chain Reaction
PEI	Poly-ethylene imine
PIKK	Phosphatidylinositol 3-kinase related kinase
PIP-box	PCNA-Interaction Protein-box
PML	Promyelocytic Leukemia
POT1	Protection of Telomeres Protein 1
PTIP	Pax Transactivation Domain-Interacting Protein
RECQ1	RECQ-like 1
RECQ5	RECQ-like 5
RPA	Replication Protein A
RSR	Replication Stress Response
SCE	Sister Chromatid Exchange
SILAC	Stable Isotope Labeling of Amino Acids in Cell Culture
siNT	Non-targeting siRNA
SIOD	Schimke immune osseous dysplasia
SMARCAL1	SWI-SNF related, Matrix associated, Actin-like, Regulator of Chromatin, subfamily A-like
SNF2	Sucrose Non Fermenting 2
SSB	Single Strand DNA Binding Protein
ssDNA	Single stranded DNA
UV	Ultra violet
WB	Western blot
WRN	Werner syndrome helicase
WT	Wild type
XPG/XPF	Xeroderma Pigmentosum, complementation group G

XPF	Xeroderma Pigmentosum, complementation group F
ZRANB3	Zinc finger RAN binding protein 2- type containing 3/ Annealing helicase 2

CHAPTER I

INTRODUCTION

Replication is fundamental for all life and requires the accurate and complete duplication of the organism's genome and epigenome. In humans, genomic replication involves the duplication of over six billion DNA bases in each cell; this process has to occur accurately trillions of times over the span of an average human lifetime. To further complicate this process, DNA replication is challenged by endogenous and exogenous sources of stress that can cause DNA damage at rates between 10,000-1 million DNA lesions in each cell, each day (Lindahl and Barnes, 2000). These sources of stress, such as UV rays, environmental carcinogens and cellular metabolites, can all interfere with the fidelity of replication and induce errors. Mistakes made during DNA replication are a large source of mutations and genome instability that can cause diseases like cancer.

Given that there are so many challenges to the accuracy of DNA replication, cells have evolved pathways to recognize and repair DNA damage and promote genome stability. These pathways are collectively termed the DNA Damage Response (DDR). The DDR promotes accurate replication and genome stability by regulating cellular checkpoints, transcriptional programs and repair pathways, and inducing senescence or apoptosis (Zeman and Cimprich, 2014). The DDR is a cellular signaling cascade regulated primarily by phosphorylation. The three major kinases that mediate the DDR are ataxia-telangiectasia mutated (ATM), ATM and RAD3-related (ATR), and DNA-dependent protein kinase (DNA-PK). All three kinases are related and belong to the phosphoinositide 3-kinase-related protein kinase (PIKK) family. While ATM and DNA-PK respond primarily to Double Strand Breaks (DSBs), ATR is activated following several types of DNA damage encountered during replication. ATR is thus essential

for the cellular viability of replicating cells whereas ATM and DNA-PK are not (Brown and Baltimore, 2000; De Klein et al., 2000; Saldivar et al., 2017). The pathways that maintain genome stability during replication that are regulated primarily by ATR are collectively termed the Replication Stress Response (RSR).

In this chapter, I will briefly discuss the pathways of the RSR, focusing primarily on replication fork remodeling, which is the topic of my thesis. I will also introduce the major ssDNA binding proteins in human cells, RPA (Replication Protein A) and RAD51 as the first responders to replication stress. I will then outline the functions of RPA and RAD51 in regulating fork remodeling and stability.

Replication stress responses at a stalled fork

Structure of a replication fork

DNA replication in mammalian cells occurs from defined regions known as "origins." Unlike in yeast, origins in human cells are not defined as much by sequence as by chromatin states and transcriptional activity. Additionally, not all origins are used during every round of replication (Bielinsky and Gerbi, 2001; Méchali, 2010). Regardless, replication occurs via bidirectional replication forks, with two forks moving in opposite directions from a single origin of replication (Figure 1.1A). Each sister fork is replicated by the "replisome", a copying machine consisting of several proteins, including the CMG (Cdc45-Mcm2-7-Gins) helicase that unwinds the dsDNA duplex, the polymerases and the polymerase processivity factor PCNA (Proliferating Cell Nuclear Antigen) that cooperate to "read" the parental template and synthesize the daughter "nascent" strands. Due to the polarity of DNA synthesis, one of the daughter strands is synthesized continuously, "leading strand", while the other strand is synthesized discontinuously, "lagging strand". Each daughter strand has a dedicated polymerase (Pol Δ for the

lagging strand and Polε for the leading strand (Burgers and Kunkel, 2017)) and an additional polymerase (Polα) synthesizes a RNA primer for each DNA strand. Since the lagging strand synthesis is discontinuous, Polα is required to synthesize a primer for each Okazaki fragment. At a replicating fork, the lagging strand synthesis lags behind the leading strand synthesis, generating ssDNA on the lagging strand template (Figure 1.1B).

Replication fork stalling leads to generation of ssDNA

When DNA replication is challenged by stress, including certain lesions on the template DNA or decreased availability of dNTP pools, replication forks "stall". In other words, the polymerases are unable to synthesize DNA; however, the helicases can continue to unwind the parental dsDNA, generating stretches of ssDNA on the leading and lagging strands (Byun et al., 2005) (Figure 1.1C). The ssDNA generated is almost immediately coated by the ssDNA binding protein, Replication Protein A (RPA). This RPA coated ssDNA serves as a platform for the recruitment and activation of the ATR kinase and the replication stress response (Zou and Elledge, 2003). The primary functions of the replication stress response are to repair the lesion, stabilize the replication fork and promote replication restart.

A

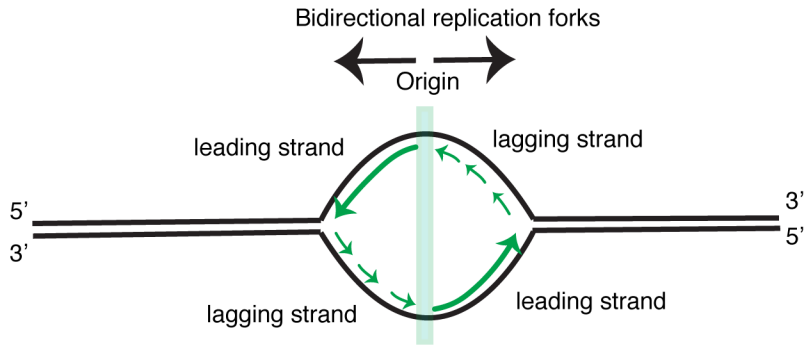

B *Elongating Fork*

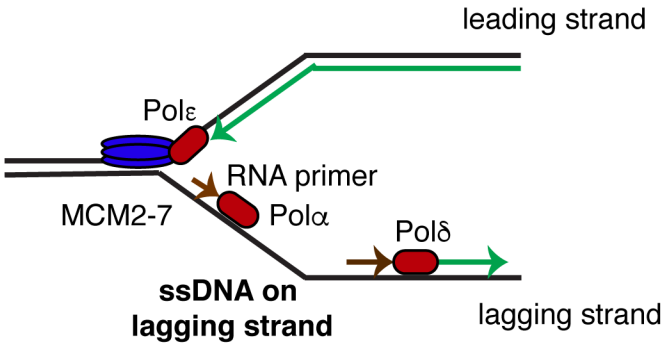

C *Stalled Fork*

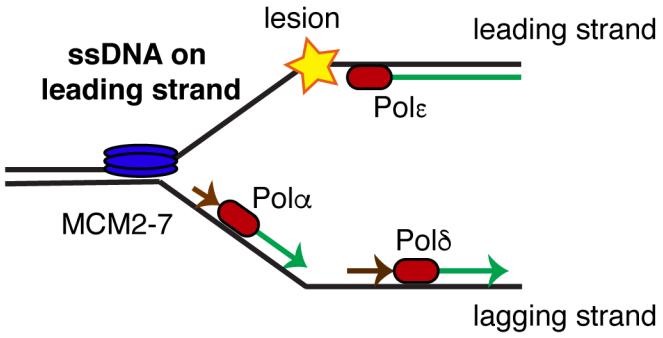

Figure 1.1. Structure of a replication fork. (A) DNA replication initiates from an origin of replication. Each origin gives rise to two sister forks, which move in opposite directions. The polarity of DNA synthesis causes the two strands to be replicated by different mechanisms. (B) A simplified schematic of an elongating fork (C) A simplified schematic of a stalled replication fork. See text for details.

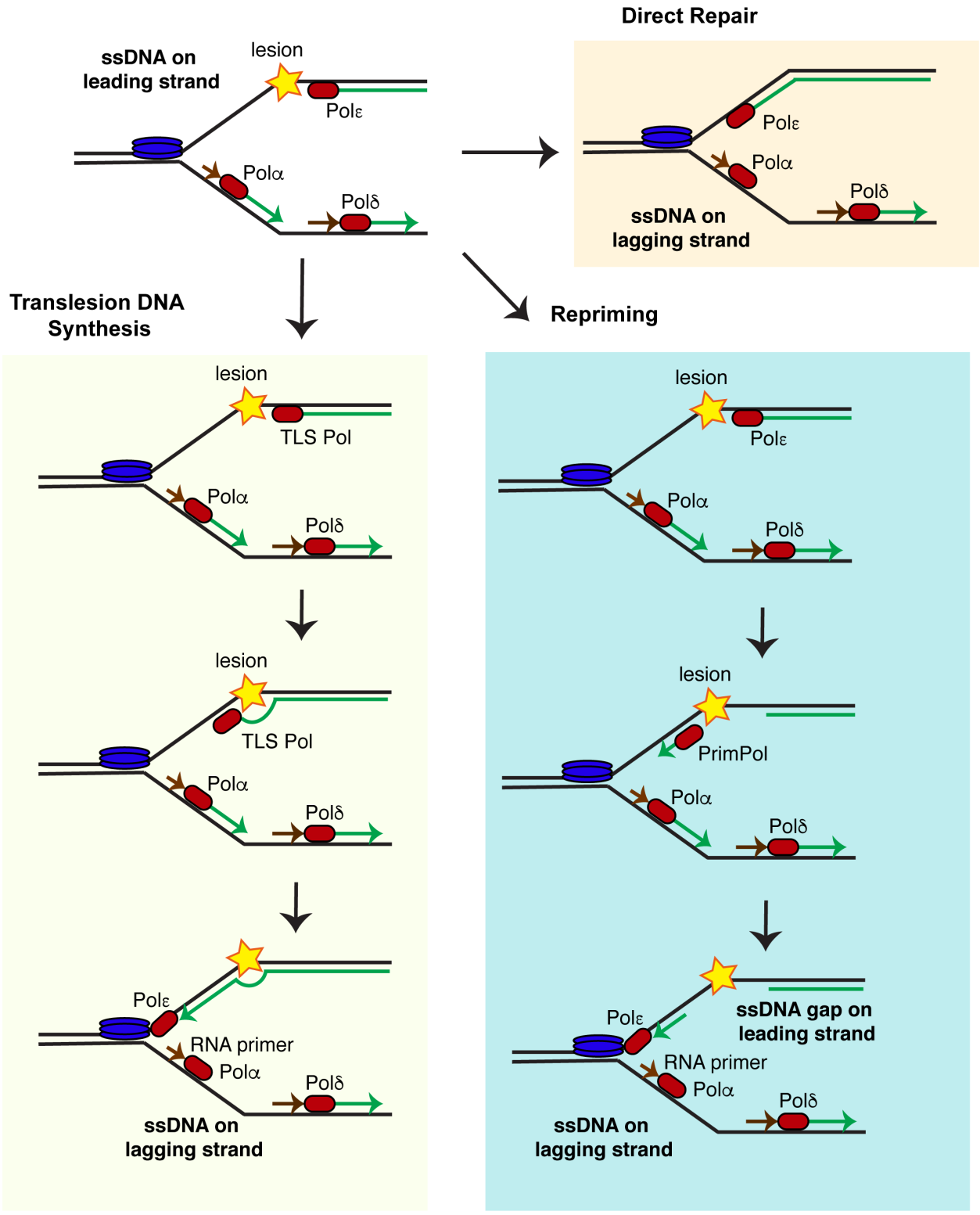

Figure 1.2. Pathways of replication fork restart. The stalled replication fork can be restarted by translesion DNA synthesis, repriming or direct repair of the lesion. See text for details.

Pathways of replication fork restart

There are several pathways that can operate at a stalled fork to promote replication restart- (i) repair and damage tolerance (ii) recombination-mediated restart and (iii) replication fork remodeling. By no means are these the only pathways; in most cases, the stalled fork can be replicated passively by an incoming fork. Another mechanism of damage tolerance and bypass at a stalled fork that was recently discovered is replication coupled proteolysis (Duxin et al., 2014; Stingele et al., 2014; Vaz et al., 2016). Additionally, most lesions on the lagging strand do not pose a challenge to replication since a new Okazaki fragment can be synthesized downstream of the lesion.

Direct repair and damage tolerance

In this section, I will discuss the following mechanisms – direct repair of DNA lesions, translesion mediated DNA synthesis and re-priming followed by post-replicative gap filling (Figure 1.2). Certain types of lesions, such as alkylated bases, can be directly repaired by enzymes such as MGMT (Fu et al., 2012), following which replication can resume. In the case of other lesions, the replisome simply bypasses the damage utilizing damage tolerance mechanisms, such as synthesis by translesion DNA polymerases. These are specialized polymerases that can allow replication to continue by inserting bases across from bulky adducts, such as UV-induced thymidine dimers. Several such polymerases have been implicated in stalled fork progression (Berti and Vindigni, 2016; Sale et al., 2012; Yang et al., 2015), and some, such as polκ are even known to switch with the replicative polymerases to promote replication at fragile sites (Barnes et al., 2017; Pillaire et al., 2014). Alternatively, the replisome can skip the lesion, and reinitiate synthesis downstream of the damaged DNA. The specialized translesion polymerase, PrimPol can reinitiate DNA replication in mammalian cells by repriming following dNTP depletion and UV-induced damage (Elvers et al., 2011; García-Gómez et al., 2013; Mourón et al., 2013). Repriming usually leaves

behind a ssDNA gap that can be filled through post-replicative mechanisms, including template switching, usually regulated by PCNA ubiquitination (Branzei, 2011).

Recombination-mediated fork restart

Lower organisms, including prokaryotes and *S. cerevisiae,* have a recombination-dependent pathway, Break Induced Replication (BIR), that allows replication restart from a collapsed replication fork (one-ended DSB) (Anand et al., 2013). In mammalian cells, most collapsed replication forks can be replicated passively from a neighboring origin or from a converging fork. However, in certain cases, HR-mediated restart of forks is required, including during Interstrand Crosslink repair (ICL). ICLs are repaired by a specialized Fanconi Anemia (FA) pathway that includes HR proteins such as BRCA1,2 and RAD51 (Ceccaldi et al., 2016). In addition, recent discoveries suggest that a BIR pathway exists in mammalian cells, although the mechanisms and factors that promote repair by such a pathway remain obscure(Bhowmick et al., 2016; Costantino et al., 2014; Dilley et al., 2016). BIR involves strand invasion of the collapsed fork, promoted by RAD51, into the sister chromatid (Figure 1.3). However, once initiated, BIR can synthesize DNA up to several kilobases by a conservative mechanism that is mutagenic(Donnianni and Symington, 2013; Hashimoto et al., 2012; Saini et al., 2013). This conservative DNA synthesis requires a different “replisome” than normal DNA synthesis and occurs during mitosis and at telomeres (Sakofsky and Malkova, 2017).

To prevent mutagenic BIR, structure specific nucleases, including MUS81, can cleave the recombination intermediate after strand invasion, regenerating a replication fork. Thus, in the presence of MUS81, BIR promotes replication restart and synthesizes DNA in short patches. MUS81 deletion promotes the mutagenic, long range BIR described above (Mayle et al., 2015)

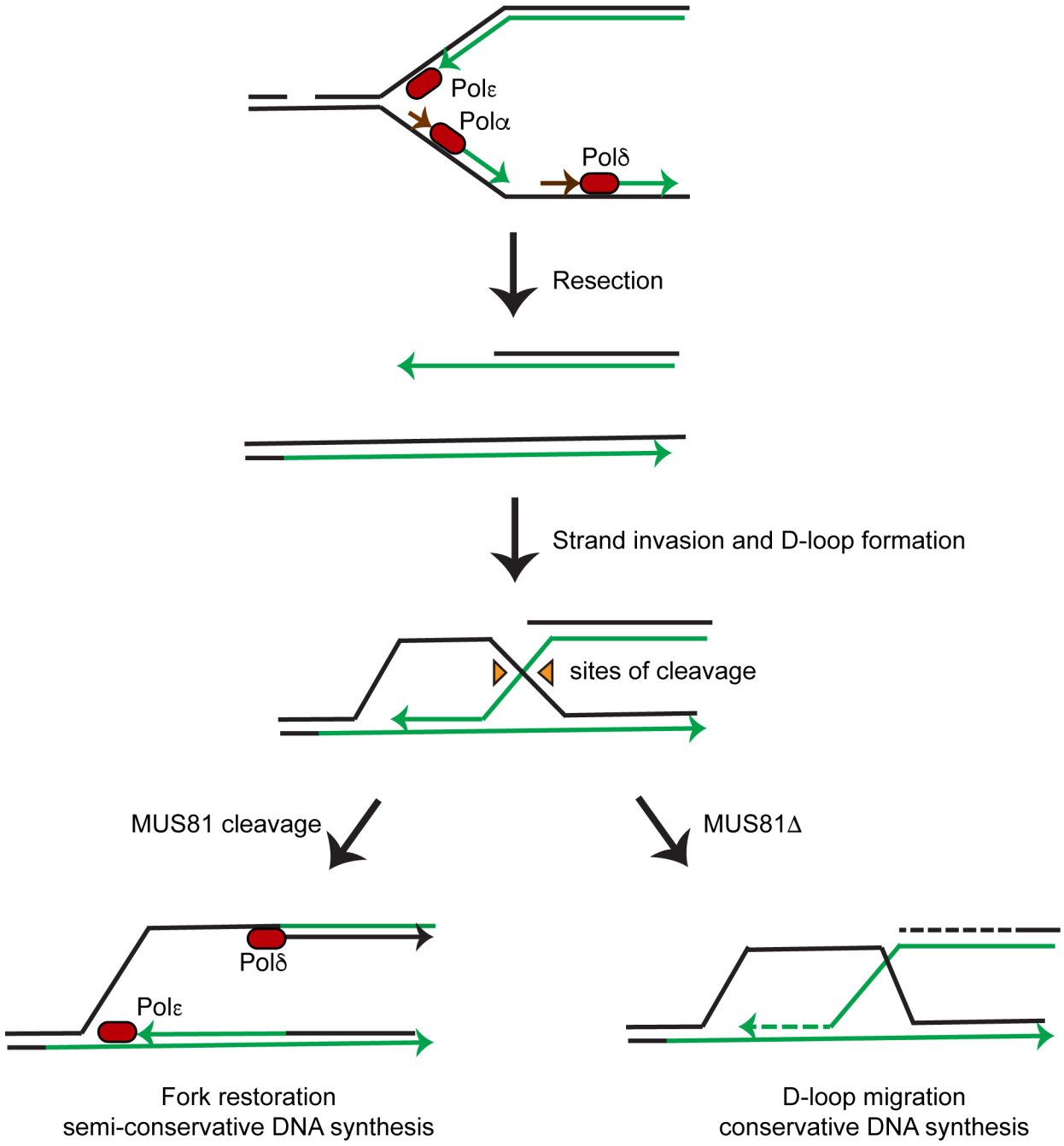

Figure 1.3. Mechanisms of break induced replication at a collapsed fork. A replication fork can collapse into a one-ended DSB when it encounters a lesion such as a single strand break. The fork can also be collapsed by nuclease mediated cleavage of the fork. The DNA end is resected to create a 3' overhang that invades the sister chromatid to form a D-loop. MUS81 cleavage of the D-loop intermediate results in semi conservative synthesis by restoration of a fork. In MUS81-deficient background, synthesis can occur through a migrating D-loop, resulting in conservative DNA synthesis over several kilobases of DNA.

Replication fork remodeling

Fork remodeling refers to both the processes of fork reversal and restoration. Fork reversal (or regression) is the process by which the replication fork essentially "backtracks", causing rewinding of the parental dsDNA duplex and causing the protrusion of the nascent DNA to form a four-way structure, the reversed replication fork or the "chicken-foot". The formation of a three-way junction (or an elongating fork) from the chicken foot structure is fork restoration (Figure 1.4).

Fork reversal: pathological consequence or physiological mechanism?

Fork reversal was initially proposed to be a genome maintenance mechanism as early as the 1970s (Hotchkiss, 1974). The evidence for the formation of the four-way junctions stemmed from the detection of heavy/heavy DNA duplexes by utilizing BrdU labelling of mammalian cells treated with UV or alkylating agents. Additionally, Four-armed DNA structures were observed using Electron Microscopy (EM) (Fujiwara and Tatsumi, 1976; Higgins et al., 1976; Nilsen and Baglioni, 1979). However, some studies suggested that the four way junctions were due to the spontaneous branch migration of replication forks and were an artifact of the processing steps, DNA labeling or extraction (Tatsumi and Strauss, 1978; Wanka et al., 1977). Additionally, the concept of fork regression suffered from the lack of evidence for a physiological role.

In the early 2000s, genetic evidence in bacteria, combined with 2D gel electrophoresis provided the first pieces of support for fork regression occurring *in vivo* as a genome maintenance pathway. Soon, the enzymes required for fork regression were identified, with RecG, RuvAB, RecQ helicases, and the recombinase RecA mediating reversal in different contexts. Thus, in prokaryotic systems, fork reversal was accepted as a mechanism that promoted genetic stability (Atkinson and McGlynn, 2009; Michel et al., 2004).

In eukaryotic cells, however, fork reversal was widely regarded as a very infrequent event that was pathological. Most of the evidence for this arose from the observation that in yeast, fork reversal occurred in checkpoint-defective mutants (Sogo et al., 2002). The size of mammalian genomes also excluded their analysis by 2D gel electrophoresis, resulting in EM being the only method to view reversed forks in human cells. Initial EM studies in mammalian systems identified reversed forks after Topoisomerase I poisoning or at difficult to repeat regions, reinforcing the idea that fork reversal was a consequence of replication failure (Follonier et al., 2013; Ray Chaudhuri et al., 2012).

However, several enzymes, including the SNF2 DNA translocase, SMARCAL1, were discovered as having the biochemical ability to reverse replication forks (Bétous et al., 2012). This, coupled with the observations that these proteins were required in cells to maintain genetic stability indicated that fork remodeling, in mammalian cells, is required for genome maintenance (Bansbach et al., 2009; Ciccia et al., 2012; Couch et al., 2013; Kile et al., 2015). EM analyses of replication fork intermediates in mammalian cells recently demonstrated that reversed forks accumulate after treatment of U2OS cells with sub-lethal doses of any of several exogenous stress-inducing agents, indicating that it was a global response to replication stress mediated by the essential RAD51 recombinase (Zellweger et al., 2015).

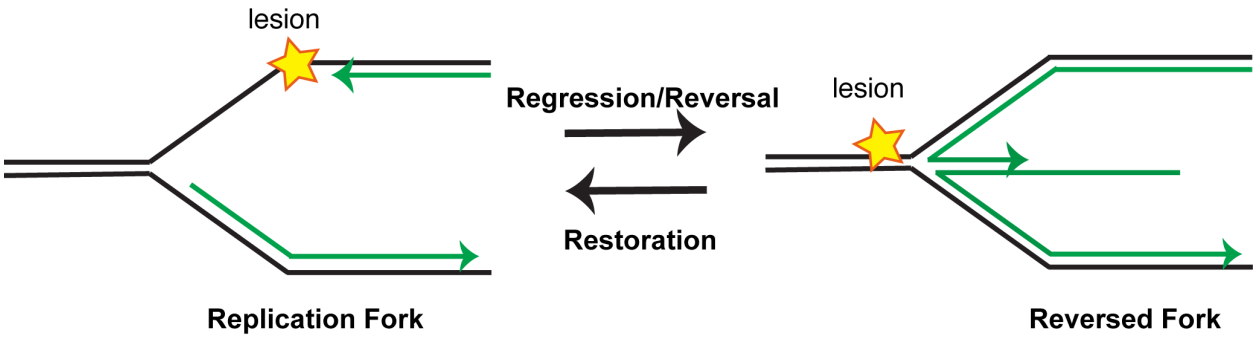

Figure 1.4. Fork remodeling reactions. A stalled replication fork with a lesion on the leading strand is reversed to form a four-way junction or a chicken foot structure. The process of fork reversal, or regression, places the lesion in the context of the parental dsDNA duplex, allowing repair processes to function. The process of fork restoration converts the reversed fork back into a three-way junction or a replication fork.

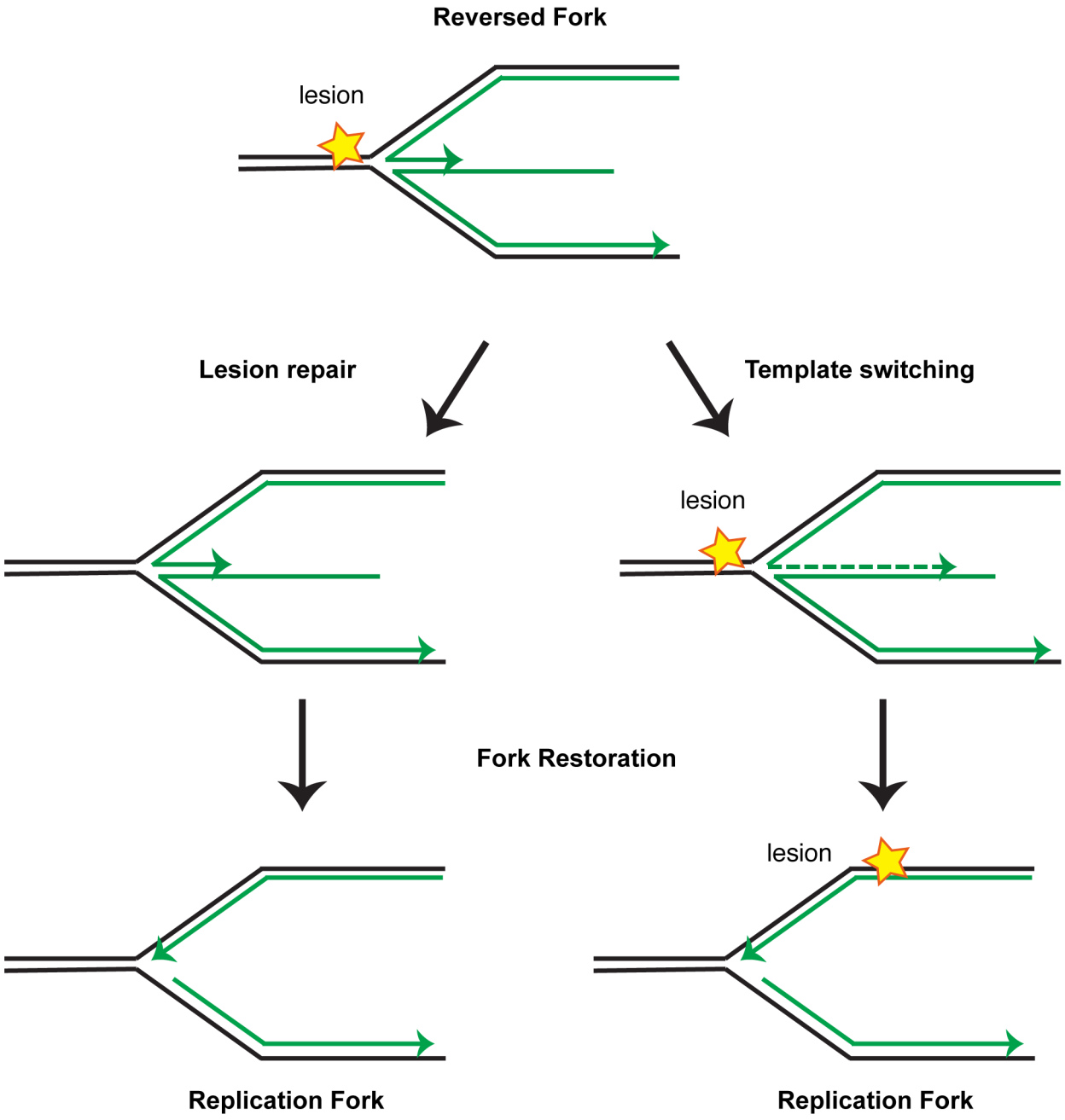

Figure 1.5. Possible pathways of replication fork restart following fork reversal. Replication fork regression can promote DNA repair by placing the lesion in the context of dsDNA. The presence of an undamaged template allows excision repair and mismatch repair mechanisms to fix the lesion, following which the fork can be restored and replication restarts. Alternatively, fork reversal allows the leading nascent strand to utilize the lagging nascent strand as a template. This allows the synthesis of DNA to extend past the lesion, after which the fork can be restored.

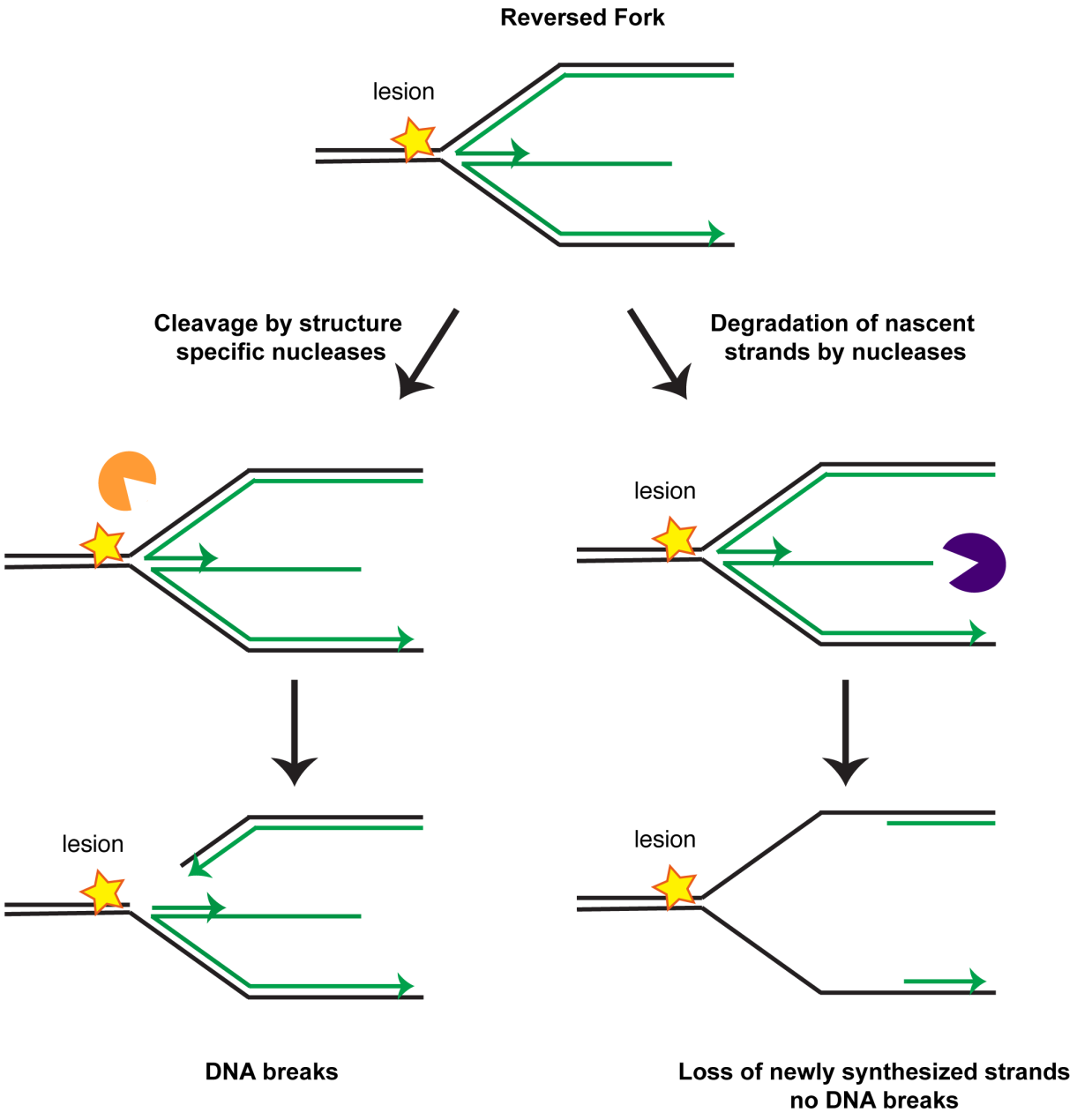

Figure 1.6. Fork reversal can cause genome instability and breaks. The reversed fork presents a substrate for structure-specific nucleases like MUS81 that can cleave the stalled fork, resulting in a one-ended DSB. The reversed fork is also an entry point for the action of nucleases such as MRE11 and DNA2 that degrade the newly synthesized DNA, resulting in genome instability.

Models for fork reversal promoting genetic stability

There are at least three models for how fork reversal could promote genetic stability (Atkinson and McGlynn, 2009; Neelsen and Lopes, 2015). Firstly, fork reversal could be a mechanism of stabilizing the stalled fork until an incoming fork from a nearby origin passively replicates the region. Second, the formation of the reversed fork and the resulting rewinding of the parental duplex places the DNA lesion on the template in the context of dsDNA. This would then allow repair of the damage by mechanisms such as mismatch repair (MMR), base excision repair (BER) or nucleotide excision repair (NER), all of which require an intact template strand. Third, the formation of the reversed fork could provide a template for the nascent leading strand to synthesize past the lesion, following which the fork can be restored. The last mechanism is a DNA damage tolerance pathway and invokes template switching. Additionally, the reversed fork can be cleaved by structure specific nucleases such as MUS81 or SLX4-dependent nucleases like SLX1 to promote recombination-mediated repair (Figure 1.5, also see below).

Excessive fork reversal can be detrimental to genome stability

While fork remodeling promotes genome stability, unregulated or excessive fork reversal can be detrimental to cells. The hyper recombination observed at the *E. coli* termination region has been proposed to arise from fork reversal (Louarn et al., 1994). Similarly, reversed forks have been implicated as the cause of DSBs associated with transcription-replication collisions (McGlynn and Lloyd, 2000), UV-induced DNA damage (Courcelle et al., 2003), and in bacterial strains deficient in the helicase DnaB (Atkinson and McGlynn, 2009). Additionally, reversed forks cause the genome instability associated with the rDNA region in *S. cerevisiae* (Defossez et al., 1999; Zou and Rothstein, 1997). In mammalian cells, deregulation of the fork remodeler, SMARCAL1, either by overexpression (Bansbach et al., 2009) or by ATR inhibition (Couch et al., 2013), causes increased genome instability and breaks. Additionally, deletion of RECQ1, a fork restoration enzyme, causes an accumulation of reversed forks. RECQ1 is also

required for replication fork progression after exogenous DNA damage, implying that excessive fork reversal causes replication problems (Berti et al., 2013).

This negative effect of fork reversal on genome stability could be because of three possibilities (Figure 1.6) - First, the reversed arm of the fork mimics a double strand break end and can thus catalyze inappropriate recombination by invading the parental duplex. Alternatively, the reversed fork can be recognized by structure-specific nucleases such as MUS81 that cleave the fork, generating DSBs and prompting recombination-based repair (Neelsen and Lopes, 2015). While regulated recombination may be beneficial to resume replication, it can also lead to chromosomal duplications, rearrangements and instability through inappropriate recombination and microhomology mediated recombination events (Carr and Lambert, 2013). Additionally, the reversed fork could also be an entry point for the actions of nucleases such as MRE11 or DNA2 that degrade the newly synthesized DNA strands, leading to chromosomal abnormalities (Higgs et al., 2015; Schlacher et al., 2011). This process is termed "**nascent strand degradation**" and occurs upon loss of "**fork protection**" proteins such as RAD51 and BRCA2 (explored in more detail in the next section).

ssDNA binding proteins: RPA as the first responder to replication stress

Replication forks that are stalled due to a block of the polymerases but not the helicase generate stretches of ssDNA. All organisms have ssDNA binding proteins (SSBs) that have high affinity for ssDNA and are required for all DNA metabolism including replication, repair and transcription. In mammalian systems, the exposed ssDNA at forks is immediately coated by the SSB, RPA. RPA binding to DNA at a fork serves at least three functions- (i) by binding to the DNA, RPA protects the DNA from the action of nucleases, such as DNA2 (Ruff et al., 2016) and SLX4-dependent structure specific nucleases(Couch et al., 2013; Toledo et al., 2013), that could cleave the fork generating DSBs. (ii) RPA-coated ssDNA acts as a platform for the recruitment of several DDR proteins, including the apical kinase ATR, the fork remodeling protein, SMARCAL1 and the essential recombinase, RAD51 (iii) Lastly, RPA can regulate the activities of several enzymes and proteins, directing their activity to the right context (Figure 1.7). These functions of RPA are critical to maintain genome integrity, since RPA exhaustion in cells drives replication fork breakage (Toledo et al., 2013). In this section, I will briefly introduce the biochemical properties of RPA and discuss concepts of how RPA regulates fork remodeling.

Domain organization of RPA

RPA is a heterotrimer of three subunits- RPA70, RPA32 and RPA14. Each subunit has several OB (Oligonucleotide/Oligosaccharide Binding) folds (Figure 1.8). These OB-folds consist of five β-strands arranged in a β-barrel, and are characteristic of several DNA binding proteins, including SSB, Telomeric POT1 as well as the recombination mediator BRCA2 (Flynn and Zou, 2010). The three subunits of RPA have a total of six OB-folds, labeled A-F (Fanning et al., 2006; Oakley and Patrick, 2010). RPA70, the

largest subunit, contains four OB folds- A,B, C and F. RPA 32 and RPA 14 have a single OB-fold each, D and E respectively. The OB folds A, B, C and D contribute to DNA binding. OB-E has extremely weak affinity for DNA and is required for the heterotrimerization of the complex. OB-F also has weak affinity for DNA and mediates protein-protein interactions (RPA70N). In addition to these OB-folds, RPA32 has a winged-helix C terminal domain (RPA32C) that is involved in mediating protein-protein interactions. RPA32 also has an unstructured N-terminal domain that is implicated in RPA regulation by phosphorylation.

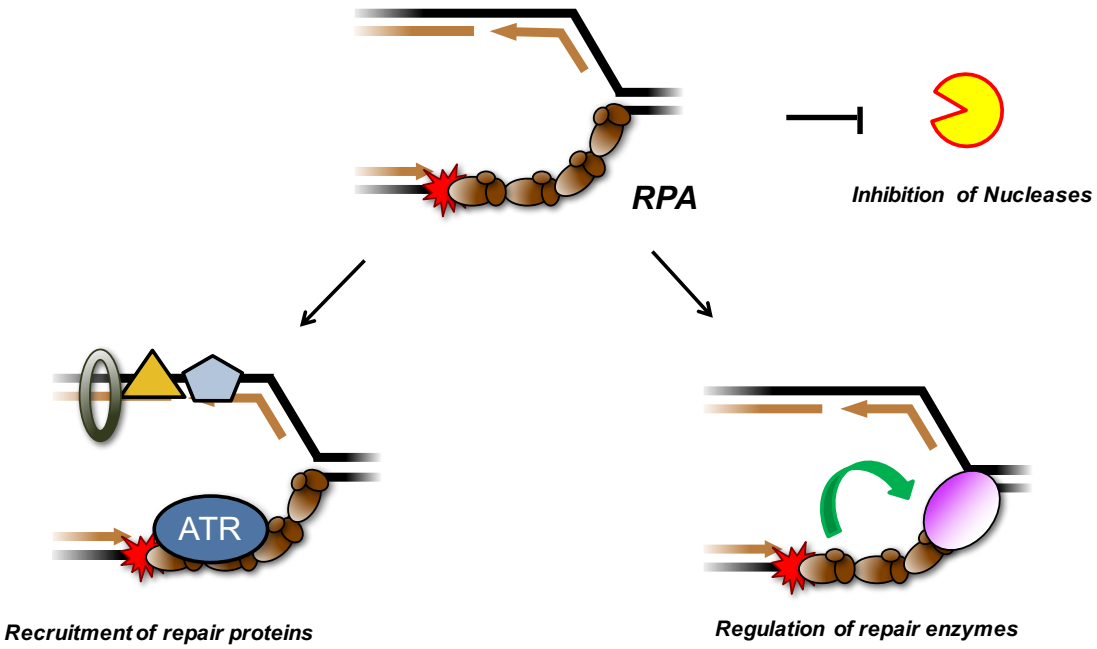

Figure 1.7. RPA is the first responder to replication stress. A stalled fork leads to the generation of ssDNA that is coated by RPA. RPA coated ssDNA at a fork promotes genome stability by recruiting repair proteins, regulating the activity of repair proteins and enzymes and by inhibiting nucleases from cleaving the exposed ssDNA. Thus, RPA prevents the accumulation of cytotoxic DSBs.

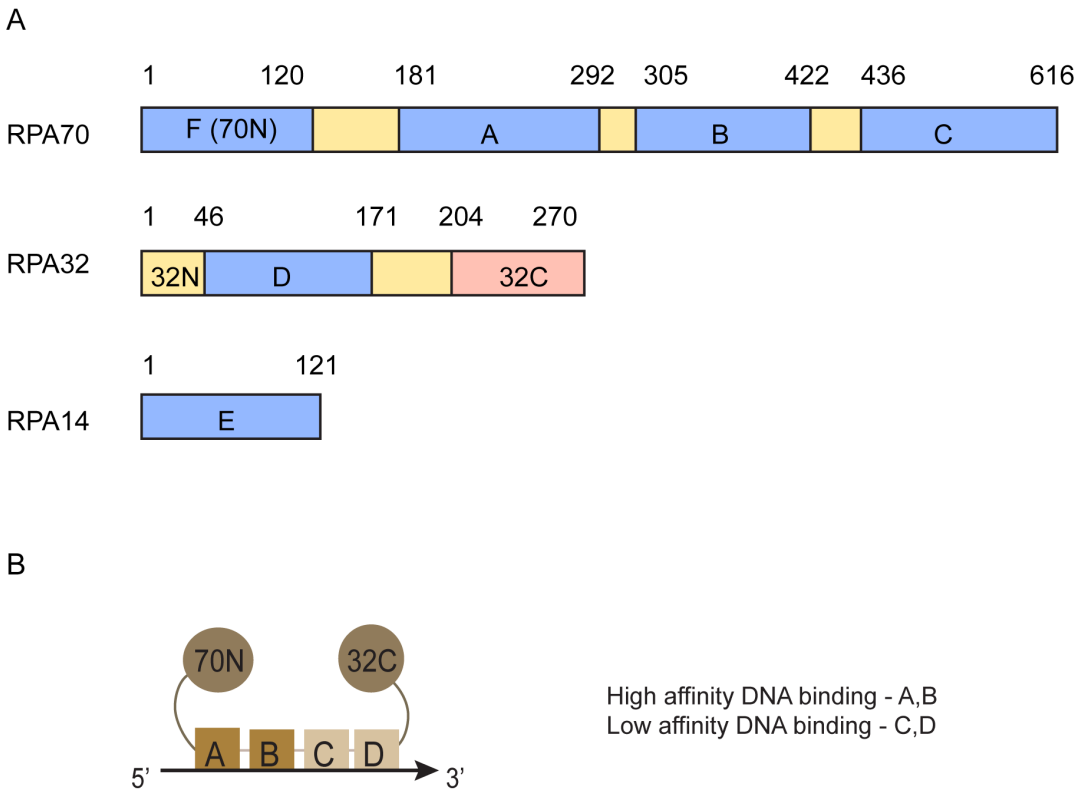

Figure 1.8. RPA has multiple DNA binding domains. (A) RPA has three subunits, RPA 70, RPA32 and RPA14. These subunits have six OB-folds (marked in blue). The 70N and 32C domains of RPA mediate protein-protein interactions. The 32N is heavily phosphorylated. The OB-C, OB-D and OB-E form the heterotrimerization core. (B) RPA binds DNA with a 5'-3' polarity. The high affinity DBDs A and B are at 5' end of ssDNA.

RPA DNA binding

RPA binds DNA with high affinity, with a K_d in the sub-nanomolar range. The binding is also polar, with DBDs A-D binding DNA 5'-3' (Figure 1.8) (Kolpashchikov et al., 2001; Wyka et al., 2003). RPA binds DNA in several 'modes'- in the first, lower affinity mode, 8-10nt of DNA are bound by DBD-A and DBD-B. In the second, high affinity mode, 28-30nt of DNA is bound by all four DBDs A-D. In addition, an intermediate 'mode' with 18-20nt of DNA has often been proposed with DBDs-A, B and C bound to DNA (Arunkumar et al., 2003; Bochkareva et al., 2001, 2002; Brosey et al., 2013; Iftode and Borowiec, 2000; de Laat et al., 1998). These results suggest that the DNA binding of RPA could have different modes. It is important to note that the binding of the different DBDs is not equivalent. Each DBD makes different contacts with ssDNA and therefore structures the underlying DNA differently (Fan and Pavletich, 2012). The four DBDs also do not have equal affinities for DNA; DBD-A has the highest affinity for ssDNA (~ 2μM), followed by BDBs-B, C and D. However, a very short linker separates DBDs A and B and the AB tandem domain usually binds as a single unit, with an affinity of ~0.1μM (Arunkumar et al., 2003).

The idea that RPA-DNA binding is very dynamic has recently been reinforced with the observation that the individual domains can microscopically dissociate from DNA (Chen and Wold, 2014; Gibb et al., 2014). In addition, RPA can rapidly diffuse along ssDNA, leading to melting of hairpins and other secondary structures or short regions of duplex DNA (Kemmerich et al., 2016; Nguyen et al., 2014). These observations have led to the model that the dynamic nature of RPA binding with individual domains dissociating and re-associating to ssDNA contributes to RPA function by allowing RPA to adopt different conformations, destabilize duplex regions and generate small ssDNA stretches that can act as nucleation sites for other DNA binding proteins - and thus help in the hand-off to different repair pathways (Chen et al., 2016).

RPA-Protein interactions

RPA interacts with several replication and repair proteins, primarily through the 70N and 32C domains. These interactions are required for the recruitment of several repair proteins, including ATRIP-ATR (Zou and Elledge, 2003) and SMARCAL1 (Bansbach et al., 2009; Ciccia et al., 2009; Postow et al., 2009; Yuan et al., 2009; Yusufzai et al., 2009) to sites of DNA damage. In addition, the interactions are essential for the regulation of the enzymatic activities of several DNA helicases, including the RECQ helicases BLM, WRN and FANCJ (Awate and Brosh, 2017). Several of these proteins all interact with the same site on RPA- indicating that at some level, there is a competition or hand-off between different proteins and pathways (Xu et al., 2008). How RPA coordinates these different pathways, recruits repair enzymes and directs their activity to the right place and right substrate is still unknown.

However, it is interesting that some protein interactions have been proposed to induce conformational changes that help load RPA on or evict RPA off DNA to allow repair processes to occur (Fanning et al., 2006). For example, the Sv40 T-antigen forms a stable complex with RPA70A and B domains and short stretches of ssDNA. However, on longer stretches of ssDNA, the T-antigen dissociates, allowing for stable RPA binding to ssDNA in its extended conformation (Jiang et al., 2006). Another interesting example of the coordination between DNA binding modes and protein interactions is in the case of nucleotide excision repair (NER). The polarity of RPA binding and specific interactions with the 70N and 32C domains are required for the proper assembly of the XPG and XPF nucleases at the 5' and 3' junctions respectively and to promote repair (de Laat et al., 1998).

RPA directs SMARCAL1 activity to the stalled fork

SMARCAL1 (SWI-SNF related, Matrix associated, Actin-dependent Regulator of Chromatin sub-family A-like 1) is a member of the SNF2 family of DNA translocases that have diverse functions as DNA-dependent ATPases. SMARCAL1 was identified as an "annealing helicase" (Yusufzai and Kadonaga, 2008); that is, it can couple the energy from ATP hydrolysis to anneal complimentary strands of DNA. This ability of SMARCAL1 to anneal strands allows it to remodel replication forks – and SMARCAL1 can catalyze both regression and restoration reactions *in vitro* (Bétous et al., 2012, 2013a).

Our lab and others discovered SMARCAL1 as a replication stress response protein that is recruited to stalled replication forks through an interaction with the 32C domain of RPA (Figure 1.9). The interaction with RPA is required for the genome maintenance functions of SMARCAL1 (Bansbach et al., 2009; Ciccia et al., 2009; Postow et al., 2009; Yuan et al., 2009; Yusufzai et al., 2009). Importantly, overexpression of SMARCAL1 as well as depletion leads to genome instability and DNA damage signaling, indicating that too much or too little SMARCAL1 activity is detrimental to cells (Bansbach et al., 2009). Additionally, we also discovered that SMARCAL1 is an ATR substrate and that ATR phosphorylation inhibits the enzymatic activity of SMARCAL1. Thus, ATR phosphorylation of SMARCAL1 is a regulatory mechanism to inhibit inappropriate fork reversal (Couch et al., 2013).

Interestingly, Rémy Bétous, a former post-doctoral fellow in the lab discovered that SMARCAL1 regression activity was specifically stimulated on stalled fork substrates, and the restoration activity was stimulated on normal forks by RPA. This led to a model where RPA regulated SMARCAL1 activity to promote genome stability (Figure 1.10) and inhibited inappropriate fork remodeling (Bétous et al., 2013a).

Other members of the SNF2 family that are biochemically similar to SMARCAL1, such as HLTF and ZRANB3 were also demonstrated to have fork remodeling activities *in vitro*. However, the regulation

by RPA seems to be specific to SMARCAL1 since RPA does not regulate or recruit ZRANB3 or HLTF. ZRANB3 is recruited by PCNA ubiquitination (Ciccia et al., 2012) and HLTF is likely regulated by other mechanisms (Kile et al., 2015). Recent EM data supports the model that all three proteins catalyze fork reversal in cells (Taglialatela et al., 2017); However, whether they cooperate with each other, catalyze reversal in different circumstances or in response to different kinds of damage is still unknown.

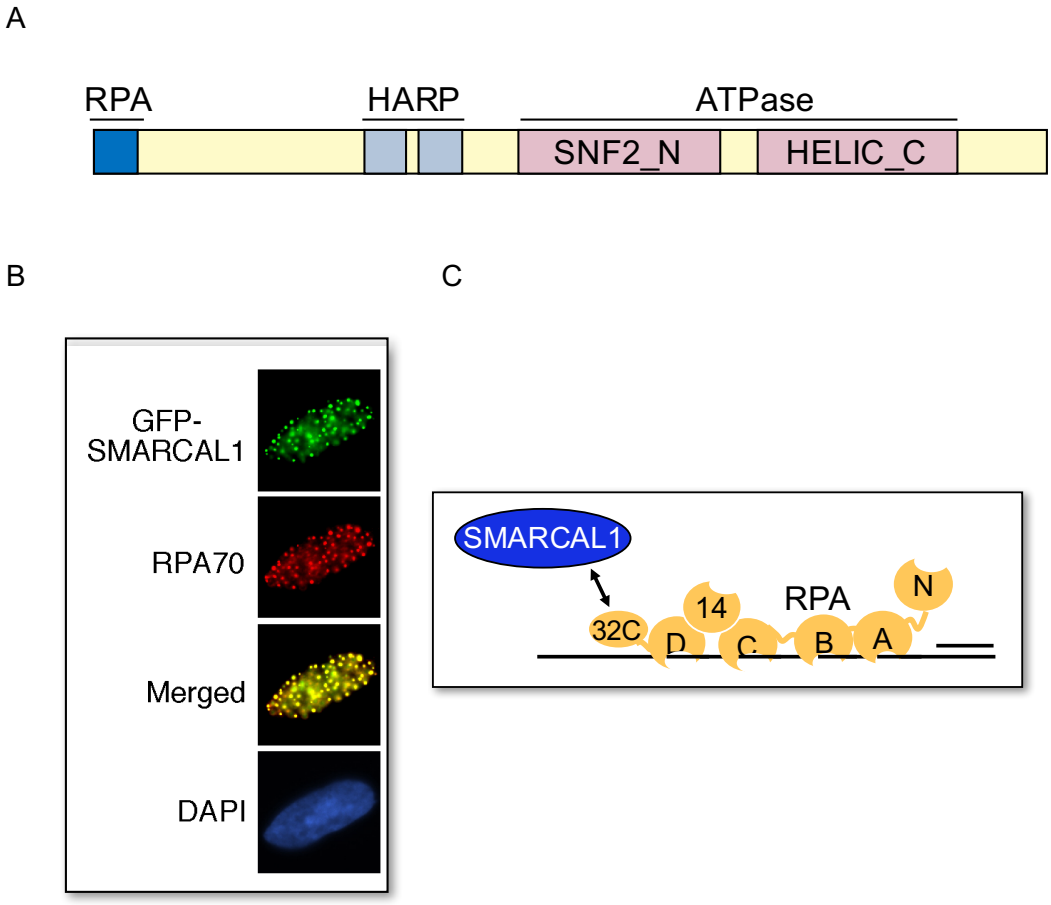

Figure 1.9. RPA recruits SMARCAL1 to sites of replication stress. A) Schematic of the domains of SMARCAL1 (B) immunofluorescence demonstrating colocalization of SMARCAL1 with RPA after DNA damage (C) schematic of the RPA-SMARCAL1 interaction. Figure adapted from Bansbach, et al, 2009.

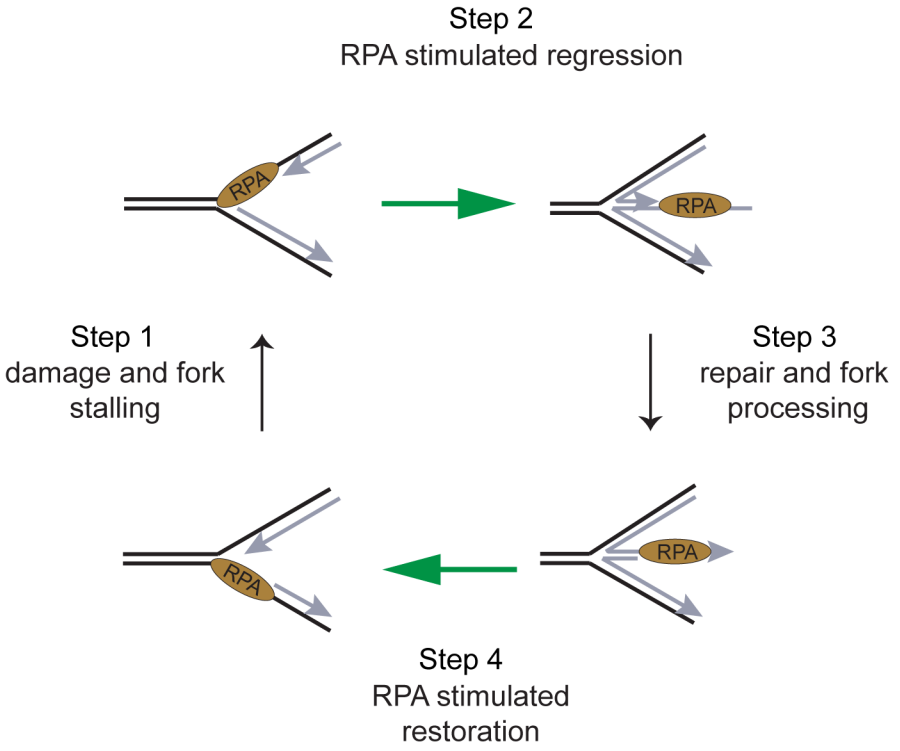

Figure 1.10. RPA directs SMARCAL1 activity to promote genome stability. Upon replication stress and fork stalling, RPA binds to the leading template strand. A replication fork with RPA bound to the leading strand stimulates SMARCAL1 mediated fork reversal. Following repair, the leading strand is processed to be longer than the lagging strand. RPA bound to the leading nascent strand stimulates SMARCAL1 mediated fork restoration, leading to the formation of an active replication fork.

Regulation of RPA by post-translational modifications

RPA undergoes several modifications, including phosphorylation, SUMOylation and ubiquitination. These post-translational modifications can affect the DNA-binding affinity of RPA, mediate or disrupt protein-protein interactions and thus influence DNA repair and replication pathways (Maréchal and Zou, 2015). RPA phosphorylation occurs primarily on the disordered N-terminal region of RPA32 during replication as well as after replication stress, and in certain cases, promotes protein-protein interactions, such as with RAD51(Wu et al., 2005). In other cases, phosphorylated RPA forms less stable interactions with DNA polα and the MRN complex (Oakley et al., 2003, 2009). Importantly, dephosphorylation of RPA is crucial for genome maintenance; phosphomimetic RPA causes defects in HR and an inability to resolve HU-induced fork damage (Feng et al., 2009; Lee et al., 2010). Phosphorylation state can also affect the DNA binding and helix destabilization ability of RPA (Binz et al., 2003; Oakley et al., 2003; Patrick et al., 2005). RPA SUMOylation is also proposed to regulate HR and cell sensitivity to drugs, although the mechanisms are less clear (Dou et al., 2010; Maréchal and Zou, 2015). RPA ubiquitination by the E3 ubiquitin ligase, RFWD3, is required to displace RPA off DNA, indicating that post-translational modifications, coupled with protein-protein interactions could help in evicting RPA off DNA (Elia et al., 2015). Thus, these diverse post-translational modifications are required to modulate RPA functions.

In summary, RPA binding to DNA serves several important functions in genome maintenance. The high affinity binding of RPA to DNA is dynamic process and the DNA binding modes, protein interactions and post-translational modifications all contribute to RPA function. How these different processes contribute to RPA coordination of multiple repair proteins and pathways to promote genetic stability is unknown.

ssDNA binding proteins: RAD51 as a second responder to replication stress

RAD51 is a DNA binding protein that is best known for its role in catalyzing double strand break repair (DSBR) by HR. However, RAD51 is recruited to stalled replication forks after treatments with DNA damaging agents that do not cause breaks (Petermann et al., 2010) and is at forks even in the absence of exogenous replication stress (Zellweger et al., 2015). In this section, I will briefly introduce the biochemical properties of RAD51, the need for mediators like BRCA2 and discuss the newly discovered functions of RAD51 in fork protection and reversal.

RAD51 domain organization

RAD51 is the central recombinase in eukaryotic cells and is similar in sequence and structure to the *E.coli* recombinase, RecA (Lusetti and Cox, 2002; Shinohara et al., 1992). Like RecA, RAD51 also forms nucleoprotein filaments on ssDNA and dsDNA to catalyze strand invasion in HDR. However, unlike in bacteria and yeast, RAD51 is essential in mammalian cells for viability (Lim and Hasty, 1996; Tsuzuki et al., 1996). RAD51 contains a central RecA/RAD51 conserved domain which consists of a walker A and walker B motif (Figure 1.11A). In addition, it contains a HnH domain and an N-terminal domain that has been shown to have DNA binding activity, although recent structures of RAD51 filaments bound to DNA appear to contradict this function of the N-terminus (Aihara et al., 1999; Baumann and West, 1998; Short et al., 2016). The structures of RAD51 filaments and RecA filaments are remarkably similar, indicating conservation of mechanism and functions (Yu et al., 2001).

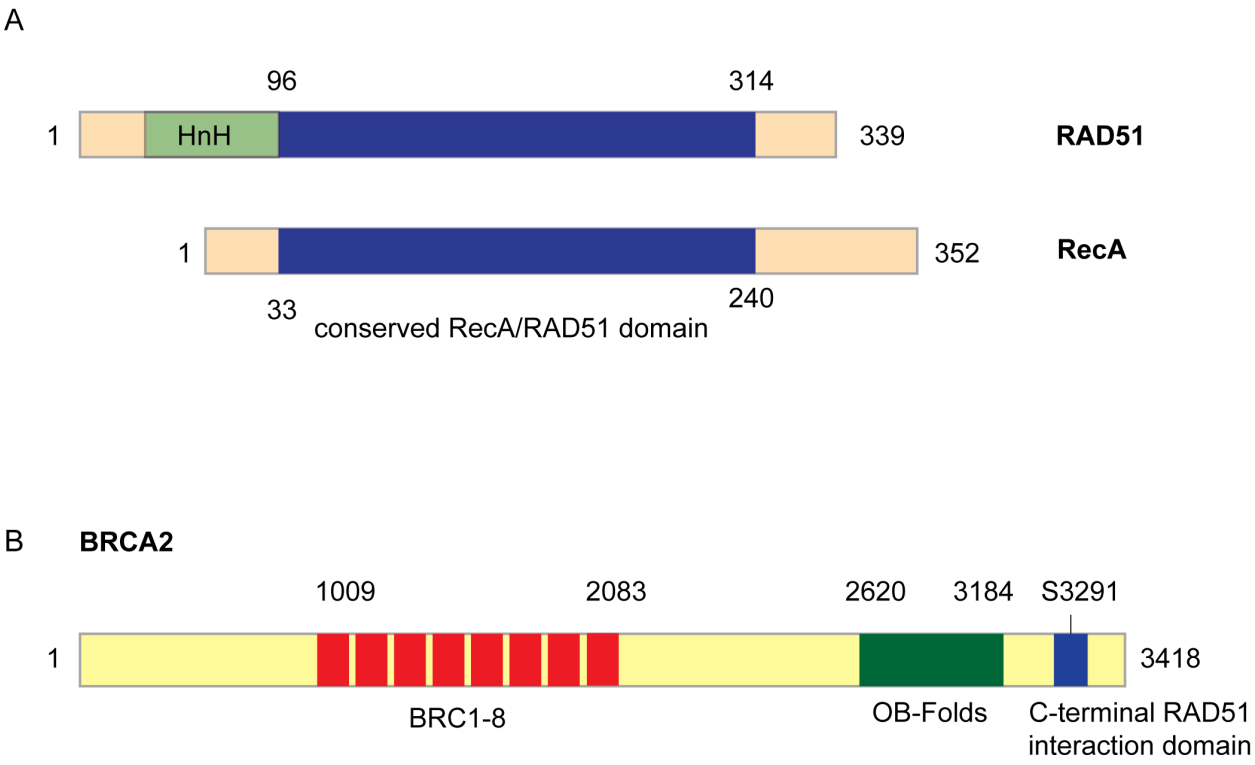

Figure 1.11. Schematic of the domains structures of (A) RAD51 and (B) BRCA2. See text for details.

RAD51 biochemical characteristics

Unlike RPA, which has extremely high affinity for ssDNA (K_d<10^{-9}) and very low affinity for dsDNA, RAD51 has modest affinity (K_d~10^{-6}) for both ssDNA and dsDNA (Baumann et al., 1996; Benson et al., 1994; Chen and Wold, 2014; Sung, 1994). RAD51 is a self-inactivating ATPase and requires ATP to bind DNA stably and form active filaments. The ATPase activity of RAD51 is stimulated by DNA binding, and upon ATP hydrolysis, RAD51 converts to an inactive form that cannot support strand exchange. This 'inactive' form also has decreased affinity for DNA in the ADP-bound form (Bugreev and Mazin, 2004; Chi et al., 2006). RAD51 binds DNA in several "modes" in vitro, depending on the nucleotide cofactors, divalent ions and pH. In the presence of ATP and Mg^{2+} or Ca^{2+} RAD51 binds ssDNA at a stoichiometry of 1 monomer to 3 or 4 nucleotides of DNA stably to 550mM NaCl. In the absence of ATP and divalent cations at low pH (probably not physiological), RAD51 binds DNA with a stoichiometry of 1 monomer to 7-9 nucleotides of DNA stable only up to 110mM NaCl. Interestingly, these two forms were inconvertible *in vitro* (Zaitseva et al., 1999).

RAD51 filaments on ssDNA are inherently unstable, even in the presence of ATP and divalent cations, and this inherent instability is proposed to be biologically relevant. The filaments are formed by several nucleation events which are rate-limiting, with the nucleation involving between 3-5 monomers(Hilario et al., 2009; Miné et al., 2007). Unlike RecA, which only dissociates from the end of the filament, dissociation of RAD51 monomers occurs from several points along the filament (Ristic et al., 2005). In summary, these studies indicate that RAD51 is very dynamic and has several DNA binding modes that may affect function (Forget and Kowalczykowski, 2010; Hilario et al., 2009; Miné et al., 2007; Ristic et al., 2005; Zaitseva et al., 1999). It is important to note, however, that several of these cryo-EM structures were obtained without mediators, which may contribute to filament stability in cells, and lead to more stable RAD51 structures.

Mediators for RAD51 function: BRCA2

RAD51, unlike RPA, requires mediators to regulate function and for loading onto ssDNA (Bochkarev and Bochkareva, 2004). In mammalian cells, this function is performed primarily by the tumor suppressor, BRCA2 (Breast Cancer 2). *BRCA2* is frequently mutated in several breast and ovarian cancers and BRCA2 is absolutely required for the error-free repair of DSBs by HR. Mutations in the related gene *BRCA1* (Breast Cancer 1) also causes cancer and BRCA1 functions in HR, although the mechanisms of these two proteins in genome maintenance are different (Liu and West, 2002; O'Donovan and Livingston, 2010; Roy et al., 2012; Venkitaraman, 2001). BRCA1 is an E3 ubiquitin ligase that has multiple functions in checkpoint activation, HR and other pathways of DSBR. The primary function of BRCA2 is to load and stabilize RAD51 filaments onto ssDNA (Kowalczykowski, 2015).

BRCA2 has several domains that interact with RAD51 (Figure 1.11B). The BRC1-8 repeats, in the central region of the protein interact with RAD51 monomers as well as with filaments *in vitro*. There is some ambiguity about the functions of the individual BRC repeats, although together, BRC1-8 promote RAD51 loading on ssDNA (Shivji et al., 2009). BRC1-4 at sub-stoichiometry promote RAD51-ssDNA nucleation by inhibiting the ATPase activity stimulated by ssDNA and reducing the association of RAD51 with dsDNA(Carreira et al., 2009). Additionally, the BRC1-4 peptides have a high affinity for free RAD51, and can bind ~ 5 monomers, consistent with a function in nucleation/loading (Jensen et al., 2010; Liu et al., 2010). However, at higher stoichiometry, (1:1 with RAD51), BRC1-4 bind with high affinity to RAD51 monomers and prevent their oligomerization. They can also disrupt pre-formed RAD51 filaments at sufficiently high concentrations (Galkin et al., 2005). The BRC5-8 repeats, on the other hand, have very low affinity for free RAD51, but bind to RAD51-ssDNA complexes with high affinity (Carreira and Kowalczykowski, 2011; Chatterjee et al., 2016). Thus, they are proposed to stabilize RAD51 filament formation on ssDNA.

BRCA2 also interacts with RAD51 using a C-terminal domain. This interaction is regulated by phosphorylation of S3291 by CDK1. Upon phosphorylation, the C-terminus does not interact with RAD51 (Esashi et al., 2005; Sharan et al., 1997). Interestingly, the C-terminus does not interact with RAD51 monomers at all and can only interact with RAD51 filaments on DNA (Davies and Pellegrini, 2007; Esashi et al., 2007). Thus, the C-terminus is required for RAD51 filament stabilization.

In addition to these RAD51 interaction domains, BRCA2 has several OB folds that mediate DNA binding (Bochkarev and Bochkareva, 2004). Interestingly, the methyl methane sulfonate (MMS) sensitivity of BRCA2-mutant CAPAN-1 cells could be completely restored by a fusion protein consisting of BRC3-4 and an RPA DBD (Saeki et al., 2006). This suggests that in response to DSBs, BRCA2's primary function is to load RAD51 onto DNA- rather than stabilization of filaments (see discussion for more details).

Other mediators have been proposed to stabilize RAD51 filaments and/or mediate recruitment in different contexts, including the RAD51 paralogs, MMS22L-TONSL and RAD52 (Chun et al., 2013; Piwko et al., 2016). Thus, it is plausible that different mediators regulate RAD51 loading/stabilization in different repair pathways.

RAD51 Functions

The most-well characterized function of RAD51, like RecA, is in DSBR. Upon induction of DSBs, repair protein, including RPA and RAD51 relocalize to sites of DNA damage or "foci". This function of RAD51 is completely dependent on BRCA2, and BRCA2-mutant cells cannot form RAD51 foci in response to DNA damage, including γ-irradiation (IR) (Sharan et al., 1997). Since the mechanisms of DSBR have been reviewed extensively, I will only briefly outline the process, and instead focus on the newer functions of RAD51 at stalled forks.

RAD51 and BRCA2: Obligate partners in DSBR

At a double-strand break, resection catalyzed by several nucleases including the MRN complex (Mre11-Nbs1-Rad50) leads to the generation of ssDNA. RPA-coated ssDNA at these ends is replaced by RAD51 by the mediator BRCA2, which helps in RAD51 loading and RPA eviction. RAD51-nucleoproteins mediate strand exchange, invading an intact DNA duplex for homology search. Once a template has been found, DNA synthesis occurs and RAD51-filaments are displaced allowing repair to finish (Figure 1.11). In the absence of BRCA2, RAD51 cannot replace RPA, resulting in a failure of HR (Kowalczykowski, 2015; Renkawitz et al., 2014; Symington, 2014). Thus, RAD51 functions are completely dependent on BRCA2 for DSBR.

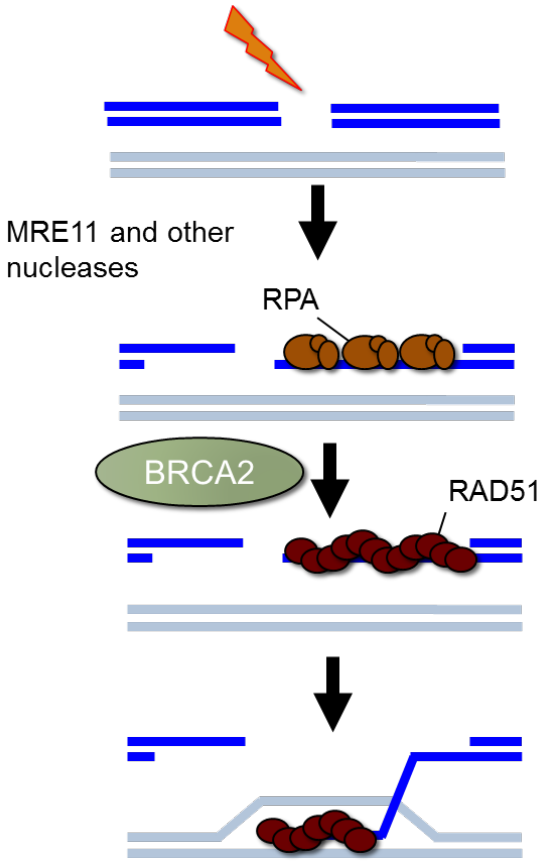

Figure 1.12. Simplified schematic of the process of homologous recombination. Upon induction of a DSB, several nucleases including MRE11 promote resection to generate 3' overhangs. The resected DNA is coated by RPA. BRCA2 replaces RPA with RAD51, which initiates strand exchange and D-loop formation.

A

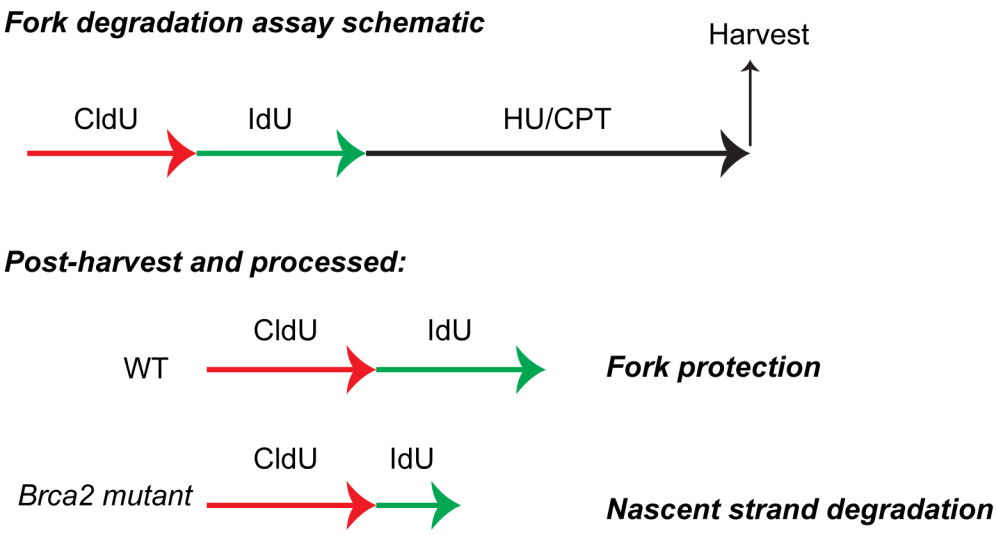

B

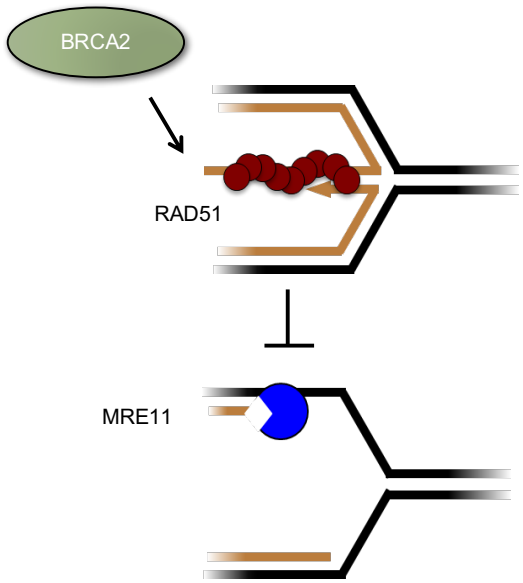

Figure 1.13. BRCA2 prevents fork degradation by inhibiting MRE11. (A) Schematic of the fork degradation assay. Cells are pulsed with two nucleoside analogs, CldU and Idu for 20 minutes each before release into HU. Following 5 hours of HU treatments, cells are harvested and stained for the two analogs. Wild type (WT) cells protect forks, and thus have the same length of IdU labeled DNA. BRCA2-mutant cells cannot protect forks and thus undergo nascent strand degradation, resulting in shorter IdU labelled DNA. (B) BRCA2 is required to form RAD51 filaments that prevent MRE11-dependent DNA degradation.

RAD51 and BRCA2: Obligate partners in Fork Protection

A DSBR independent function was recently identified for BRCA2 in fork protection (Hashimoto et al., 2010; Schlacher et al., 2011). *BRCA2*-deficient cells exhibit **fork instability or nascent strand degradation,** a phenomenon in which the newly synthesized DNA is degraded by the MRE11 nuclease following treatment with a fork stalling agent, such as hydroxyurea (HU) or camptothecin (CPT) (Figure 1.13)**.** Interestingly, the BRCA2 C-terminus, which is dispensable for the repair of a site-specific break, is required to restore **fork protection or fork stabilization**; **indicating that RAD51 filament stability** is critical for prevention of degradation by MRE11 (Schlacher et al., 2011). Additionally, this defect could be suppressed by overexpression of a mutant RAD51 that cannot hydrolyze ATP and thus forms hyper stable filaments (K133R). The protection conferred by RAD51 has been recapitulated in vitro; RAD51-ssDNA prevents MRE11-dependent degradation whereas an RPA-ssDNA complex does not (Kolinjivadi et al., 2017a).

From here on, when I use the terms **"fork protection" or "fork stability", I am referring to the function of RAD51 filaments in protecting replication forks from a specific process, "nascent strand degradation" or "fork degradation", catalyzed by the nucleases MRE11 or DNA2, at reversed forks.**

Several other HR proteins, including BRCA1, the RAD51 paralogs and the Fanconi Anemia (FA) proteins, have also been implicated in the prevention of nascent strand degradation (Higgs and Stewart, 2016). However, the mechanisms by which these proteins protect forks and promote RAD51 functions remain unclear. Another layer of complexity is the nuclease mediating degradation. While BRCA1/2 and the FA pathway prevent MRE11-dependent degradation by stabilizing RAD51 (Schlacher et al., 2011, 2012), other factors such as BOD1L prevent DNA2-mediated degradation, also by stabilizing RAD51 on ssDNA (Higgs et al., 2015). Thus, RAD51 loss can cause MRE11 or DNA2 dependent fork degradation, although the factors governing the choice of the nuclease are unclear.

In addition, there are RAD51-independent pathways that prevent fork degradation catalyzed by either MRE11 or DNA2, depending on the genetic contexts (Somyajit et al., 2015; Xu et al., 2017). Thus, it is still unclear how these different pathways affect fork stabilization, what governs the nuclease usage and if and how RAD51-independent mechanisms prevent nuclease mediated degradation of nascent DNA.

In spite of the ambiguity surrounding the mechanisms and pathways of fork protection, this function of RAD51 is also completely dependent on BRCA2. However, fork protection and HR require different domains of BRCA2, indicating that the functions of BRCA2 in these two processes are distinct.

RAD51-dependent and BRCA2-independent fork reversal is a pre-requisite for fork degradation

The model that the reversed fork is an entry point for nucleases to degrade the newly synthesized DNA has recently been demonstrated by EM analyses (Kolinjivadi et al., 2017a; Lemaçon et al., 2017; Mijic et al., 2017; Taglialatela et al., 2017). Thus, preventing fork reversal restores fork protection to BRCA2 deficient cells. Additionally, silencing or depleting RAD51 prevents the detection of reversed fork intermediates by EM, indicating RAD51 is required for fork reversal in cells (Mijic et al., 2017; Thangavel et al., 2015; Zellweger et al., 2015). However, this could be interpreted in two ways- RAD51 might catalyze reversal or could simply stabilize the reversed fork intermediate, allowing detection by EM. Importantly, BRCA2 is not required for this function of RAD51- reversed forks accumulate even in BRCA2-mutant cells (Dungrawala et al., 2017; Kolinjivadi et al., 2017a; Mijic et al., 2017). Thus, the function of RAD51 in reversal is independent of BRCA2.

In summary, RAD51 has several dynamic DNA binding modes and has three functions in cells 1) Double strand break repair by recombination 2) Fork protection and 3) Fork reversal. While break repair and fork protection functions depend entirely on BRCA2, the fork reversal function is BRCA2-

independent. However, the functions of RAD51 in fork reversal, the mechanisms of fork protection and the functions of other mediators of RAD51 is still not well understood.

Conservation of fork reversal and protection mechanisms

The functions of RAD51 and other recombination proteins in reversal and fork protection in mammalian cells is just being discovered. It is however, remarkable, that the prokaryotic homolog of RAD51, RecA is known to drive fork reversal and to protect nascent DNA from being degraded (Atkinson and McGlynn, 2009; Courcelle et al., 2003; Cox, 2007; Robu et al., 2001). Astonishingly similar to the case of BRCA2 and RAD51, RecA usually requires the RecFOR proteins to protect nascent DNA from degradation (Chow and Courcelle, 2004; Satta et al., 1979). It is also worth noting that bacterial cells have RecA dependent- and independent mechanisms of fork reversal; similar to the RAD51 dependent and independent mechanisms of fork protection(Atkinson and McGlynn, 2009). Interestingly, the bacteriophage recombinase UvsX is also capable of promoting fork regression (Kadyrov and Drake, 2004).

The fork remodeling enzyme SMARCAL1 is also conserved through prokaryotic systems; T4 bacteriophage UvsW and *E.Coli* RecG have fork remodeling activities and are regulated by their ssDNA binding proteins, gp32 and *E. coli* SSB, similar to the regulation of SMARCAL1 by RPA (Buss et al., 2008; Manosas et al., 2013; Mason et al., 2014a). Thus, while the individual proteins involved - RecA and RAD51, SMARCAL1 and RecG, RPA and SSB - differ significantly in biochemical properties and in certain aspects of function, fork protection and reversal mechanisms seem to be extraordinarily conserved through evolution.

Clinical Implications

Defects in fork processing enzymes cause a variety of genetic conditions and predispose to several diseases, including cancers. Biallelic loss of function mutations in SMARCAL1 cause a genetic condition, Schimke Immuno Osseous Dysplasia (SIOD), characterized by renal failure, growth defects, immune deficiencies and cancer predisposition (Boerkoel et al., 2002). Mutations in ZRANB3 predispose to endometrial cancers (Lawrence et al., 2014), while HLTF mutations predispose to colorectal and intestinal cancers (Moinova et al., 2002; Sandhu et al., 2012). While BRCA2 and RAD51 are essential for viability, BRCA2 is mutated in several cancers, including breast and ovarian cancers.

BRCA2 mutant cells are characterized by genome instability and defects in HR. PARP inhibitors, such as Olaparib, have been approved in the clinic for BRCA2- mutant cancers (Helleday et al., 2008; Lord and Ashworth, 2012; O'Connor, 2015). PARP inhibitors trap the enzyme poly ADP-ribose polymerase (PARP) on single strand DNA and negative affect single strand break repair. This in turn causes a greater dependence on DSBR factors, including BRCA2; and hence, PARP inhibitors are synthetic lethal with BRCA2 deficiency. However, several BRCA2 cancers develop chemoresistance. Most of the described mechanisms involve the restoration of a functional BRCA2 protein or restoration of HR (Lord et al., 2015). However, restoration of fork protection, in the absence of HR has also been shown to confer chemoresistance (Chaudhuri et al., 2016; Ding et al., 2016; Schubert et al., 2017; Yazinski et al., 2017), although other studies failed to find that fork protection contributed to resistance (Feng and Jasin, 2017). Finally, the best-documented mechanisms of resistance in patients involve restoration of the BRCA2 protein expression which restores both HR and fork protection functions. Thus, it is still unclear if fork protection is a resistance mechanism in BRCA2-mutant cancer patients.

Thesis Project

The Replication Stress Response (RSR) maintains genome stability and promotes the accurate duplication of the genome. ssDNA binding proteins are integral components of the RSR and have been extensively studied for years. However, the mechanisms by which they specifically direct enzymes to the right substrates and how they regulate replication fork remodeling is less well understood. My thesis projects have focused on the regulation of fork remodeling pathways by ssDNA binding proteins. In Chapter III, I discovered how RPA enforces SMARCAL1 substrate specificity to promote appropriate fork reversal. In chapter IV, I identified a new RPA-like ssDNA binding protein, RADX, at replication forks. I characterized the function of RADX as a negative regulator of RAD51 mediated fork reversal and described RADX loss as a chemo-resistance mechanism in BRCA2-deficient U2OS cells. In chapter V, I further explored the mechanisms by which RADX regulates RAD51. Utilizing RADX as a tool, I interrogated RAD51 functions in different pathways of fork protection and discovered the differential requirements of RAD51 in fork reversal and fork protection. Overall, my thesis has made significant contributions to our understanding of the processes of fork reversal and fork protection and has identified a potential chemo-resistance mechanism for BRCA2-mutant cancers.

CHAPTER II

MATERIALS AND METHODS

Protein purifications from baculovirus infected SF9 cells

Flag-RADX and Flag-SMARCAL1 were purified from baculovirus-infected insect cells using the same methodology as previously described for Flag-SMARCAL1 purification (Bétous et al. 2013). Briefly, cells were lysed in 20 ml buffer containing 20 mM Tris (pH 7.5), 150 mM NaCl, 0.1 mM EDTA, 1 mM DTT, 0.2 mM PMSF, 1 mg/mL leupeptin, 1 mg/mL aprotinin, and 0.1% Triton X-100. After high-speed centrifugation, the cleared lysates were incubated with 250 µl Flag-M2 beads (Sigma) for 4 h at 4°C. The beads were washed three times in LiCl buffer (lysis buffer containing 0.3 M LiCl) and twice in KCl buffer (20 mM HEPES at pH 7.6, 20% glycerol, 0.1 M KCl, 1.5 mM $MgCl_2$, 0.2 mM EDTA, 1 mM DTT, 0.2 mM PMSF, 0.01% IGEPAL CA-630). The bound proteins were eluted in 2 ml KCl buffer containing 0.25 mg/mL Flag peptide on ice, concentrated using Amicon Ultra-4 50K MWCO (Millipore) flash-frozen, and stored at −80°C. Generally, I would expect concentrations of SMARCAL1 around 1-5 µM and around 300-500 nM for RADX.

Protein Purifications from 293T cells

Flag-SMARCAL1 proteins and Flag-RADX were purified from 293T cells as previously described (Bétous et al., 2012) with the following modifications. Cells transfected with vectors expressing SMARCAL1 or RADX were lysed in 150mM NaCl, 20mM Tris pH 7.5, 1mM EDTA, 0.5% NP40, 0.2mM PMSF, 1mg/ml leupeptin and 1 mg/ml aprotinin. Following high-speed centrifugation, cleared lysates were incubated with Flag-M2 beads for 4 hours at 4 degrees. The beads were washed three times with the lysis buffer, twice with the LiCl buffer (10mM HEPES, 0.3M LiCl, 20% glycerol, 0.01% Triton X-100, 1 mM DTT, 1.5mM MgCl2, 0.2mM PMSF) and once with the 0.1M KCl buffer (10mM HEPES, 20% glycerol, 0.01% Triton X-100, 1 mM DTT, 1.5mM MgCl2, 0.2mM PMSF and 0.1M KCl). The protein was eluted in 80-100 µl of KCl buffer using Flag peptide at 300µg/ml concentration. For SMARCAL1 I would expect concentrations around 800nM-2 µM and around 100nM-300nM for RADX. The proteins were aliquoted, flash-frozen and stored at -80°C.

Radioactive labeling of substrates

2µl of 10µM oligonucleotide was labelled in a 40µl reaction with 6µl Hot ATP and 4µl 10X PNK for 2 hours at 37 degrees. Prior to adding Hot ATP, boil the oligonucleotide, water and PNK buffer at 95ºC for 2 minutes, and allow to cool by placing on ice for 1 minute. Following the reaction, the enzyme can be inactivated by heating the reaction to 65 degrees for twenty minutes. The labelled substrate was then separated from the $^{32}\gamma$P-ATP using a G25 column (GE). To use the G25 columns, mix the resin well before opening and removing the cap. Spin at 2,800 rpm in an Eppendorf tabletop centrifuge for 1 minute. Add up to 50µL of sample. Spin another 2 minutes at 2,800 rpm. The flow-through contains the labelled substrate at a final concentration of 0.5µM.

Preparation of Fork Restoration Substrates

Note: The oligonucleotides used for fork regression and restoration were described in (Bétous et al., 2013a). I have used the same nomenclature as Remy did for consistency, and have also depicted them in Table 2.1. The oligonucleotides were obtained from IDT and were PAGE purified.

Assays	Substrate structures	Label	5' to 3' oligonucleotide sequences
Fork regression	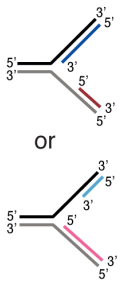	Lead122	CGTGACTTGATGTTAACCCTAACCCTAAGATATCGCGT**TA**TCAGAGTGTGAGGATACATGTAGG CAATTGCCACGTGTCTATCAGCTGAAGTTGTTCGCGACGTGCGATCGTCGCTGCGACG
		Lag122	CGTCGCAGCGACGATCGCACGTCGCGAACAACTTCAGCTGATAGACACGTGGCAATTGCCTA CATGTATCCTCACACTCTGA**AT**ACGCGATATCTTAGGGTTAGGGTTAACATCAAGTCACG
		Lead82	CGTCGCAGCGACGATCGCACGTCGCGAACAACTTCAGCTGATAGACACGTGGCAATTGCCTA CATGTATCCTCACACTCTGA
		Lag52	CCACGTGTCTATCAGCTGAAGTTGTTCGCGACGTGCGATCGTCGCTGCGACG
		Lead52	CGTCGCAGCGACGATCGCACGTCGCGAACAACTTCAGCTGATAGACACGTGG
		Lag82	TCAGAGTGTGAGGATACATGTAGGCAATTGCCACGTGTCTATCAGCTGAAGTTGTTCGCGACG TGCGATCGTCGCTGCGACG
Fork restoration	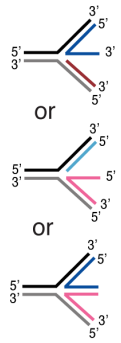	RD62P	TAGGCA**A**TTGCC**A**CGTGT**C**TATCA**G**CTGAA**GT**ACAAGCGCTGCACCCTAGGTCCGACGCTGC
		RG62P	CGTCGCAGCCTGGATCCCACGTCGCGAACA**AC**TTCAG**C**TGATA**G**ACACG**T**GGCAA**T**TGCCTA
		RD62N2.6	GCAGCGTCGGACCTAGGGTGCAGCGCTTGT**TG**TTCAG**G**TGATA**C**ACACG**C**GGCAA**A**TGCCTA
		RG30	TGTTCGCGACGTGGGATCCAGGCTGCGACG
		RD30	GCAGCGTCGGACCTAGGGTGCAGCGCTTGT
		RG62N2.6	TAGGCA**T**TTGCC**G**CGTGT**G**TATCA**C**CTGAA**CA**TGTTCGCGACGTGGGATCCAGGCTGCGACG

Table 2.1. List of oligonucleotides used for making fork regression and restoration substrates. This table was adapted from (Bétous et al., 2013a). The bolded underlined letters indicate mismatches to prevent spontaneous branch migration.

Oligonucleotide labeling: For lead gap fork restoration substrates, label 4μl of 50μM stock of RG-62P in a 40μl reaction with 10μl Hot ATP, 4μl 10X PNK and 4μl 10X PNK buffer for two hours at 37ºC. For lag gap fork restoration substrate, label 4μl of 50μM stock of RD-62P in a 40μl reaction with 10μl Hot ATP. Purify using G-25 columns as described above. The final concentration of the labelled oligo is 5 μM.

Annealing the oligonucleotides: For lead gap fork restoration substrates, anneal 35μl of the labelled RG-62P with 5μl of RD-62P (50μM stock) and 5μl of RD-30 (100μM stock) in 60μl containing a final concentration of 1X SSC buffer(10X SSC buffer contains 1.5M NaCl and 150 mM sodium citrate- final pH 7.0) . For lag gap fork restoration substrate, 35μl of the labelled RD-62P with 5μl of RG-62P (50μM stock) and 5μl of RG-30 (100μM stock). The reactions were then split into 20μl each, and annealed using the following PCR program-

RBanneal PCR Program

1. 95° for 30 seconds.

2. 95° (-3° per cycle) for 40 seconds.

3. 97° (-3° per cycle) for 40 seconds.

4. 96° (-3° per cycle) for 40 seconds.

5. GOTO 2, 24X. (25 total cycles).

6. 12° forever.

Creating the Substrate of the reaction: For lead gap fork restoration substrate, anneal 58 μl of the product from the RBAnneal program with 8 μl of RD62-N2.6 (50μM stock) in 80 μl of 1X annealing buffer (10X

annealing buffer contains 400 mM Tris pH 7.5, 50 mM MgCl2, 20 mM DTT, 200 mM KCl and 1 mg/ml BSA) using a water bath/heat block set at 37°C and then switched off for about 30 minutes. For lag gap fork restoration substrate, 58 µl of the product from the RBAnneal program with 8 µl of RG62-N2.6 (50µM stock). Following the annealing, the substrate was gel purified using a 5% (37.5:1) 0.25X TBE gel run at 100V for 60 minutes at room temperature and exposed to film, following which the band was transferred to a 3500 MWCO snake skin membrane and electro-eluted for 80 minutes at 80V in the EtBr-free box. The eluted buffer was concentrated using an Amicon Ultra-0.5 ml Centrifugal filter Ultracel-10K NMWL (Millipore) was utilized as per manufacturer's specifications. The concentration of the substrate was determined using the products (see below) as standards.

Creating the Products of the reaction: To create the reaction products for the lead gap fork restoration substrate, anneal 3.5µl of the labelled RG-62P with 5 µl of RD62N2.6 (50µM stock) in a 20µl reaction containing 2 µ1 of 10X SSC. For lag gap fork restoration substrate products, anneal 3.5µl of the labelled RD-62P with 5 µl of RG62N2.6 (50µM stock). This 20 µl reaction is also annealed using the RB Anneal PCR program. The concentration of the products is 0.875 µM.

Preparation of Fork Regression Substrates

The fork regression substrates were prepared in a similar manner as the restoration substrates. I will indicate in this section only the differences between the two methods.

Oligonucleotide Labeling: For lead gap fork regression substrate, Lag82 and Lag 122 are labeled in 40µl reactions with 6µl Hot ATP each. For lag gap fork regression, Lead 122 and Lead 82 are labeled. The final concentrations of labeled oligonucleotides are 2.5µM.

Annealing the oligonucleotides : For lead gap fork regression substrates, 14 µl each of 10µM stocks of Lead122 and Lead52 are mixed in a 40µl total reaction volume containing SSC, split into two tubes each of 20µl and annealed using the PCR program. In a separate reaction, 25µl of labelled Lag122 and 37.5µl of labelled Lag82 are also mixed in a total volume of 80µl before being split into 4 tubes of 20 µl each and annealed using RBanneal. For lag gap fork regression substrates, 14 µl each of 10µM stocks of Lag122 and Lag52 are mixed in a 40µl total reaction volume, split into two tubes each of 20µl and annealed using the PCR program. In a separate reaction, 25µl of labelled Lead122 and 37.5µl of labelled Lead82 are also mixed in a total volume of 80µl before being split into 4 tubes of 20 µl each and annealed using RBanneal.

Creating the substrate of the reaction : For lead and lag gap fork regression, 78µl of labelled product from the RBanneal step with 39µl of unlabeled annealed product were annealed in annealing buffer. Following the annealing, the substrates were gel purified, electro-eluted and concentrated as for the restoration substrates.

Creating the products of the reaction: For lead gap fork regression, 5 µl of labeled lag122 was annealed with 7.5 µl of unlabeled lead122 (2.5µM stock) in a 20µl reaction containing SSC. Also, 5 µl of labeled Lag82 was annealed in a separate reaction with 7.5µl of Lead52 (2.5µM stock) in a 20µl reaction using RB anneal. For lag gap fork regression, 5 µl of labeled lead122 was annealed with 7.5 µl of unlabeled lag122 (2.5µM stock) in a 20µl reaction containing SSC. Also, 5 µl of labeled Lead82 was annealed in a separate reaction with 7.5µl of Lag52 (2.5µM stock) in a 20µl reaction using RB anneal. The final concentrations of the products are 0.625µM.

Electrophoretic Mobility Shift Assays

Note: Each protein required different conditions in order to observe binding through an EMSA. In general, if it is an enzyme, utilize a protocol similar to what I have described here for RAD51 or SMARCAL1. Also, in my experience, the pre-run step is not required for RADX and RPA DNA binding assays, so I have omitted them.

Electrophoretic mobility shift assays for RPA binding- 3nM of ^{32}P-labeled substrate was incubated with different concentrations of RPA in binding buffer (40mM Tris, pH 7.5, 100mM KCl, 5mM $MgCl_2$, 100µg/ml BSA, 2mM DTT) for 20 minutes at room temperature. The reactions were separated by electrophoresis in an 8% (19:1 polyacrylamide, 1X TBE) gel at 80V for 80 minutes at room temperature. Gels were dried and quantified using a Molecular Imager FX (Bio-Rad).

SMARCAL1-DNA binding assays- 1nM of purified DNA substrate was incubated with increasing concentrations of SMARCAL1 (0.5,1 and 2 nM) in binding buffer (20mM HEPES, 0.1% NP40, 0.1M KCl, 5mM $MgCl_2$, 1% glycerol, 0.25mg/ml BSA, 0.05M EDTA and 1 mM DTT) for 30 minutes at room temperature. After adding 15% Ficoll dye to a final concentration of 2.5%, the reactions were separated at 40V for 200 minutes in a 5% (37.5:1 polyacrylamide, 0.5XTBE) gel that had been pre-run at 4 degrees for 30 minutes. The gels were dried and quantified using a Molecular Imager FX (Bio-Rad).

RADX-DNA binding assays- 0.5nM ^{32}P-labeled oligo-dT50 ssDNA was incubated with the indicated concentrations of RADX in binding buffer containing 40 mM Tris (pH 7.5), 100 mM KCl, 5 mM $MgCl_2$, 100 µg/ml BSA, and 2 mM DTT for 30 minutes at room temperature. After adding 15% Ficoll dye to a final

concentration of 2.5%, the reactions were separated by electrophoresis on an 8% gel (19:1 polyacrylamide, 1x TBE) at 80 V for 80 minutes at room temperature. Gels were dried and quantified using a Molecular Imager FX system (Bio-Rad). The dsDNA substrate was created by annealing the following oligonucleotide purchased from IDT with its complimentary oligo.

5'-3' sequence:

TCGATAGTCGGATCCTCTAGACAGCTCCATGTAGCAAGGCACTGGTAGAATTCGGCAGCGT.

RAD51-DNA binding assays- 0.5nM ^{32}P-labeled oligo-dT50 ssDNA was incubated with RAD51 in 20µl reactions of binding buffer containing 50 mM Tris pH7.5, 100 ug/ml BSA, 2 mM $CaCl_2$, 2 mM ATP, 100mM NaCl and 1 mM DTT. The reactions were incubated at 37 degrees for 30 minutes. 150 mg/ml of Ficoll was dissolved in water and utilized as 6X Loading buffer. The reactions were separated on 5% 0.5X TBE 37.5:1 gels run at 50V for 180 minutes at 4 degrees. The gels were pre-run at 50V for 30 minutes at 4 degrees. After separation, the gels were wrapped in saran wrap and exposed to a phosphorimager.

Biotin-DNA pull-down assays

Dynabeads T1 (Life Technologies) were washed twice in TE buffer and bound to biotinylated DNA substrates at room temperature for 30min. Beads were washed twice again in TE buffer followed with two washes in binding buffer (40mM Tris, pH 7.5, 100mM KCl, 5mM $MgCl_2$, 2mM DTT and 100µg/ml BSA in RNase/DNase free water). 1ul of beads with 4 picomoles of bound DNA was resuspended in binding buffer. Approximately 500 femtomoles of purified protein was added to the mix and rotated at room temperature for 30min. The supernatant was discarded and the beads were boiled in 2X sample

buffer for 5min. Captures were loaded on SDS-PAGE gels and analyzed by immunoblotting. The ssDNA oligo utilized for pulldown assays was a poly dT50. The dsDNA was created by annealing - 5'-/Biosg/GGATGATGACTCTTCTGGTCCGGATGGTAGTTAAGTGTTGAG-3' (IDT) with its complimentary oligo.

Fork Remodeling Assays

These assays were performed as described in (Bétous et al., 2013a) with minor modifications. 3nM of ^{32}P-labeled fork substrate was incubated with the indicated concentrations of RPA at Room temperature for 20 minutes in a reaction buffer containing 40mM Tris pH 7.5, 100 mM KCl, 5 mM MgCl2, 100μg/ml BSA, 2mM ATP and 2mM DTT. The indicated concentrations of SMARCAL1 were then added to the reaction and incubated at 37ºC for the fork regression and lead gap fork restoration assays. For lag gap fork restoration assays, the reaction was carried out at room temperature. The reactions were stopped and de-proteinized using 10μl of 3X STOP buffer (200 µl of 6X DNA dye + 655 µl of glycerol + 100 µl of 0.5 M EDTA and 45 µl of 20% SDS) and incubated on ice for 5 minutes. The reactions were separated on 8% 1X TBE gels for 80 minutes at 80V. The gels were dried and quantified using a phosphorimager.

Antibodies for western blotting

Antibody	***Species***	***Dilution***	***Company***	***Catalog No.***
RAD51	Rabbit	1:1000	Abcam	Ab63801

BRCA2	Mouse	1:250	Calbiochem	OP95
MUS81	Mouse	1:1000	Abcam	Ab14387
SMARCAL1-909	Rabbit	1:1000	Open	
ZRANB3	Rabbit	1:1000	Bethyl	A303-033A
RPA32	Mouse	1:1000	Abcam	Ab2175
RPA32 S4/S8	Rabbit	1:1000	Bethyl	A300-245A
Histone H3	Rabbit	1:10000	Abcam	Ab46765
RADX 846	Rabbit	1:500	Bethyl	Custom-directed against last 10 aa of RADX-HKIYSPENTS
γH2AX (JBW301)	Mouse	1:9000	Millipore	05-636
HA	Rat	1:1000	Roche	11 867 423 001
KU80	Rabbit	1:1000	Abcam	ab33242
KU70	Mouse	1:1000	Abcam	ab3114
BLM	Rabbit	1:1000	Santa Cruz	Sc 7790
BRCA1	Mouse	1:1000	Calbiochem	OP-92
HLTF	Rabbit	1:1000	Abcam	ab17984
MCM2-BM28	Mouse	1:1000	BD Transduction Labs	39289

GAPDH	Goat	1:10000	Santa Cruz	Sc 20357
RADX	Rabbit	1:1000	Novus Biologicals	NBP2-13887
DNA2	Rabbit	1:1000	Abcam	ab96488
FANCD2	Mouse	1:1000	Santa Cruz	sc-20022

Table 2.2: List of antibodies used for immunoblotting in these studies.

Antibodies for immunofluorescence

Antibody	***Species***	***Dilution***	***Company***	***Catalog No.***	***Notes***
HA	Rat	1:500	Roche	11 867 423 001	
RPA (9H8)	Mouse	1:200	Abcam	Ab 2175	3% BSA/PBS
γH2AX (JBW301)	Mouse	1:9000	Millipore	05-636	
BrdU	Mouse	1:50	BD	555627	3% BSA/PBS
CldU(anti-BrdU)	Rabbit	1:100	Abcam	Ab6326	

IdU (anti-BrdU)	Mouse	1:100	BD	347580	
53BP1	mouse	1:500	Millipore	7-c9	3% BSA/PBS
RAD51	Rabbit	1:200	Santa Cruz	Sc 8349	3% BSA/PBS
PCNA (PC10)	Mouse	1:50	Santa Cruz	Sc 056	Use acetone permeabilization

Table 2.3: List of antibodies used for immunofluorescence in these studies.

DNA Fiber Analysis

DNA fiber analysis of DNA replication was carried out essentially as described previously (Couch et al., 2013) with several modifications. Briefly, cells were labeled with 20 μM CldU for 30 minutes, washed twice with HBSS and labeled with 100 μM IdU for 30 minutes. Cells were washed twice again with HBSS and then treated with or without HU prior to collection. Cells were collected and resuspended at a concentration of $1x10^6$ cells/ml. The labelled cells were diluted 1:2 with unlabeled cells, and 2μl of the diluted mix was spread in a thin line onto a glass slide. The slide was allowed to dry for 5 minutes, following which 10μl of spreading buffer (0.5% SDS, 200 mM Tris-HCl pH 7.4, 50 mM EDTA) was added to the sample for 6 minutes. The fibers were then stretched and allowed to air-dry for 40 minutes before being fixed for two minutes with a 3:1 methanol: acetic acid mixture. The slides were dried for twenty minutes and stored at -20 degrees overnight.

The next day, DNA was denatured in 2.5M HCl for 70 minutes, washed three times with PBS and blocked in 10% goat serum/PBS with 0.1% triton X-100 for 1 hour. The DNA was stained with 100 µl of antibodies recognizing IdU and CldU for 2 hours (rat monoclonal anti-BrdU (anti-CldU) {ab6326} and mouse anti-BrdU (anti-IdU) {BD347580} 1/100 diluted in 10% goat serum/PBST) and probed subsequently with 100 µl of secondary antibodies (goat anti-rat IgG Alexa Fluor 594 and Goat anti-mouse Alexa Fluor 488 1:350 in 10% goat serum/PBST) for 1 hour in the dark. The slides were them mounted using 110 µl of prolong Gold with no DAPI and allowed to dry overnight in the dark. Between each incubation, rinse three times with 1X PBS. The slides can then be stored at 4 degrees. Images were obtained using a 40X oil objective (Nikon Eclipse Ti) and fiber lengths analyzed using NI-elements software. The percentage of asymmetric forks was calculated as those with greater than 33.3% length difference between sister forks.

ATPase assays with RAD51

This protocol was adapted from (Wang et al., 2015). Briefly, 1.0 µM of RAD51 was incubated with 3.0 µM nucleotides (ssDNA) in a buffer containing 20 mM TrisHCl (pH7.5), 0.5 mM ATP, 200 nCi [γ-^{32}P] ATP, 1 mM dithiothreitol (DTT) and 4 mM MgCl2. The reaction mixture was incubated at 37 °C for 1 hour and 1 µL of each reaction was spotted ontopolyethylene amine thin layer chromatography plates (EMD Chemicals), and the plates were allowed to air dry for five minutes. The separation of 32Pi from [γ-^{32}P] ATP was performed in buffer containing 0.8 M LiCl and 1 M formic acid for about 45 minutes.

Immunofluorescence

Cells were washed with 1X PBS three times before being pre-extracted with 0.5%Triton-X solution (20 mM HEPES pH 8, 50 mM NaCl, 3 mM MgCl2, 300 mM sucrose and 0.5% Triton-X) for 10 minutes

on ice. The coverslips were rinsed with PBS and then fixed with 3% paraformaldehyde/2%sucrose fix solution for 10 minutes at room temperature. The cells were then permeabilized with 0.5% triton X-100 for 15 minutes at 4 degrees, blocked with 5% BSA/PBS for 15 minutes at room temperature and then incubated with the primary and secondary antibodies in 1% BSA/PBS for an hour each before mounting with Prolong Gold with DAPI. The incubation with the secondary antibody should be done in the dark. Dry overnight before viewing on the microscope.

Paraformaldehyde fix solution:15g of paraformaldehyde was dissolved in 250mL water. The solution was incubated 20 minutes at 65 degrees in a water bath and then 3 drops of 10N NaOH were added. The solution was left in the water bath for an additional 5 minutes to allow the powder to completely dissolve. Then 50mL of 10X PBS and 10g of sucrose was added and the solution was brought to a final volume of 500mL with distilled water. The solution was sterile filtered, aliquoted into single use tubes, and stored at -20 degrees.

For immunofluorescence with EdU, follow the same protocol as above with a click reaction for thirty minutes in the dark before antibody incubations. The click reaction buffer is made by adding the following components in order - 875 μl PBS, 5 μl Azide – 488 or 594, 100 μl 20mg/ml Na ascorbate and 20μl 100 mM copper sulphate.

Neutral Comet Assays

Cells were seeded the day before treatment at $1x10^5$ cells per well in a 6-well tissue culture dish. On the day of treatment, cells were treated and harvested by trypsinization. Cells were washed once with cold PBS then resuspended at $2x10^5$ per mL in cold PBS. During this time, low melting temperature agarose (Trevigen) was melted at 95 deg and held in a 42 or 37-degree water bath. To prepare slides, 10μl of cell suspension was mixed with 100 μL of agarose and spread into one well of a

COMET slide (Trevigen). Slides were allowed to gel for 30 minutes at 4 degrees. Slides were then immersed in pre-chilled Lysis Buffer (Trevigen) for 1 hour at 4 degrees. Slides were rinsed once with pre-chilled TAE (40 mM Tris Base, 20 mM Acetic acid, 1 mM EDTA, pH 8.45), then washed for 30 minutes by immersing in TAE at 4 degrees. Slides were then electrophoresed for 1 hour at 1 V/cm immersed to a depth of at least 0.5 cm in TAE [this translates to 21V and 850 ml buffer on our apparatus]. After electrophoresis, slides were immersed in DNA Precipitation Solution (1M NH4Ac, 87% EtOH) for 30 minutes at room temperature. Next, slides were immersed in 70% ethanol for 30 minutes at room temperature then dried for 15 minutes at 45 degrees and stored overnight at room temperature. Slides were stained with 100 mL of 1X SYBR Green I (Trevigen) for 30 minutes at room temperature. SYBR Green solution was decanted and slides allowed to dry at least 30 minutes before visualizing. At least 100 cells were scored for each condition.

Alamar Blue assay to measure short-term cell viability

Cell Plating: 72 hours post siRNA transfection, U2OS cells were trypsinized and plated in 96-well plates at a density of 4,000 ($4x10^3$) cells per well in a volume of 100µL. For a full 96 wells 15mL of DMEM + 7.5% FBS with $6x10^5$ cells is required to give $4x10^3$ cells/100µL.

Preparing Drugs: Drug dilutions at 10X higher than the desired concentration were prepared and 200 µL was pipetted into one column of a 96 well plate. Using automatic pipettes, 10µL of drug per well was pipetted into the 96 well plates with cells.

Highest concentrations of some commonly used drugs:

ATRi 2µL of 100mM stock in 2mL of media for 100µM dilution

CHK1i 1µL of 20mM stock in 2mL of media for 10µM dilution

Cisplatin 1µL of 2.5mM stock in 2.5mL of media for 1µM dilution

80µL of 2.5mM stock in 2mL of media for 100µM dilution

Hydroxyurea 20µL of 1M stock in 2mL of media for 10mM dilution

Drug Ranges:

ATRi 10µM-0.1µM

CHK1i 1µM-0.01µM

Cisplatin 10µM-0.1µM

HU 10mM-0.1mM

CPT 0.01uM- 1µM

BMN673 10nM-1µM

Olaparib 1µM-100µM

Etoposide 1µM-100µM

MMC 1ng/µl- 100ng/µl

MMS 0.0005-0.05% (2 hours after attachment, change media)

NOTES: Media for high dose HU and CPT has to be changed the next day. BMN673-treated cells were analyzed on day 8 instead of day 7 (see below)

Day 7 after siRNA transfection: Cell viability was measured using Alamar Blue (Invitrogen) according to the manufacturer's instructions.

Clonogenic survival assays

For clonogenic survival assays, cells were plated and treated with Olaparib for approximately two weeks. Colonies were scored by methylene blue staining (48% methanol, 2% methylene blue, 50% water). All clonogenic survival assays were completed in triplicate.

Native BrdU assay to measure ssDNA

To measure parental ssDNA, cells were treated with 10μM BrdU for 22 hours, released into fresh media for 2 hours and then drug (usually 3mM HU) was added. To measure nascent ssDNA, cells were treated with 10μM BrdU for 10 minutes prior to harvest. Following pre-extraction, the cells were probed under non-denaturing conditions using a mouse anti-BrdU antibody (BD 555627 1:50 in 3% BSA/PBS).

Flow cytometry

For cell cycle analysis with BrdU, cells were labeled with 10 μM BrdU for 30 minutes before harvest. $5x10^5$ cells per sample were resupsended in 300 μL PBS on ice. 700 μL of ice cold 100%

ethanol was added and mixed gently by inverting tube. The tubes were fixed for at least 2 hours in -20 degrees. The tubes were centrifuged at 2000g (rcf) for 5 minutes. 1 mL of 0.5% BSA/PBS was added and cells were pelleted. Cells were then denatured in 1mL 2N HCl + 0.5% triton-x-100/PBS (5 mL 4N HCl, 5 mL PBS and 500 uL 10% triton) for 30 minutes at room temperature. Cells were pelleted and resuspended in 1mL 0.1M sodium borate for 2 mins before pelleting. Cells were washed with 1 mL 0.5%BSA/PBS before incubating with 100 uL of BrdU antibody (1:20 BrdU-488 in 0.5% BSA/PBS/0.5% Tween) for 30 minutes at room temperature. Cells were again washed with 0.5%BSA/PBS before incubating with 500 µL PBS with Propidium Iodide (25 µL of 5 mg/ml stock and 10 uL 4mg/ml RNAase A) at 37 degrees for 30 minutes. Cells were then filtered and analyzed.

For cell cycle analysis with just PI, 10^6 cells per sample was resuspended in 300 µL PBS on ice. 700 µL of ice cold 100% ethanol was added and mixed gently by inverting tube. The tubes were fixed for at least 2 hours in -20 degrees. The tubes were centrifuged at 2xg (rcf) for 5 minutes. Cells were washed with 1ml PBS and pelleted. 500 µL PBS with Propidium Iodide (25 µL of 5 mg/ml stock and 10 uL 4mg/ml RNAase A) was added and cells incubated at 37 degrees for 30 minutes. The cells were then filtered and analyzed.

DR-GFP assays

$0.25x10^6$ cells in each well of a 6 well dish were transfected with siRNA (200µl Optimem+ 5.9µl Dharmafect 1 in one tube and 200µl Optimem+ 40 pmol siRNA in a second tube). 24 hours later, Sce-1 expressing plasmids were transfected using FUGENE HD (For each well, 2ug of DNA and 6ul FUGENE in a total of 100ul of media was used). The mixture was incubated for 15min and added to cells with fresh media to a final volume of 3mls. Three days later, cells were filtered and analyzed for GFP-positive cells.

Generation of cell lines stably overexpressing cDNA

Virus production: 2-3x10^6 GP2-293 cells were plated in a 10cm dish. 24 hours later 1 μg of pVSV-G and 2μg of pLEGFP-CX (*neo*-RADX) was transfected using 1 mg/ml PEI. The next day, cells were washed with PBS and 5-6ml of complete media was added. 48 hours later, media was collected in a 15ml tube and placed at 4 degrees. Another 5-6 ml of complete media was added to transfected cells. 24 hours later, media was collected and pooled. 10-12 ml of collected media was spun at low speed to pellet any cell debris. The supernatant was transferred to a new 15ml tube, aliquoted and stored at -80 degrees for future use.

Viral knockdown: 0.2-0.3x10^6 of U2OS cells were plated in a 60mm dish. Extra plates were also prepared for mock infection controls. 24 hours later, the collected virus was filtered through 0.45μm pore filter paper. Polybrene (4mg/ml) was added to media at 2ul per 1ml of virus. 1.5-2ml of media containing virus was added to each dish after aspirating any remaining media. 24 hours later, fresh DMEM media was added and cells allow to recover. The next day, cells were transferred to a 10cm dish. A few hours later, selection media with Puromycin (2ug/ml) or G418 (1mg/ml) was added later in the day. Selection was allowed for 3-4 days until all the cells in the mock infection plates were dead.

Preparation of Nuclear Extracts

4μg of cDNA was transfected into each 10cm dish of 293T cells using 24μl 1mg/ml PEI. Typically, 20-30 dishes of 293T cells were transfected using PEI and then expanded into 15cm dishes the day after transfection. After 3 days, nuclear extracts were prepared as described in Current Protocols in Molecular Biology.

Cells were harvested, washed with PBS and transferred to 15ml tubes. The Packed Cell Volume (PCV) was noted and cells were rapidly resuspended in a volume of Hypotonic Buffer 5x the PCV. The cells were centrifuged at 2553g x 5min at 4 degrees. The cell pellet was again resuspended in hypotonic buffer to a final volume of 3 times the original PCV and allowed to swell on ice for 10 minutes. Cells were then transferred to a glass Dounce homogenizer (type B pestle). The cells were homogenized slowly with 10 up-and-down strokes (on ice) and then centrifuged at 3300g x 15min at 4C. The supernatant ("cytoplasm") was removed and saved. The packed nuclear volume (PNV) was noted. The nuclei were resuspended in a volume of Low Salt Buffer equal to ½ PNV. High Salt Buffer was then added to a volume equal to ½ PNV in a dropwise fashion to prevent clumping, and the tubes were allowed to rotate at 4 degrees for 30 minutes. The samples were pelleted at 13,200rpm for 30minutes at 4 degrees, and the supernatant is the nuclear extract. The extracts were then dialyzed at 4 degrees, cleared by high speed centrifugation, aliquoted and stored at -80 degrees.

Hypotonic Buffer: 10 mM HEPES pH 7.5, 1.5 mM MgCl2, 10 mM KCl, 0.2 mM PMSF and 0.5 mM DTT.

Low Salt Buffer: 20 mM HEPES pH 7.9, 25% Glycerol, 1.5 mM MgCl2, 20 mM KCl, 0.2 mM EDTA, 0.2 mM PMSF and 0.5 mM DTT.

High Salt Buffer: Low salt buffer with a final concentration of 1.2 M KCl.

Dialysis Buffer: 20 mM HEPES pH 7.9, 20% Glycerol, 100 mM KCl, 0.2 mM PMSF, 0.5 mM DTT and 0.2 mM EDTA

Flag-Immunoprecipitations from Nuclear extracts

The stored nuclear extracts can be thawed and pre-cleared by high speed centrifugation prior to IP. For a standard co-IP followed by western analysis, 1-2 mg of nuclear extract is sufficient. Flag-tagged protein was immunoprecipitated for one hour at 4 degrees using 3μg of Flag M2 antibody, following which 45μl of protein G dynabeads were added to the tube for a further 30 minutes. The beads were then pelleted using a magnetic rack, washed with Dialysis buffer and resuspended in 30μl elution buffer with 0.25 mg/ml flag peptide. The elution was carried out for 1.5 hours, with the tube being flicked every 15 minutes, following which the samples were centrifuged or pelleted, and the supernatant transferred to a new tube. If using for an immunoblot, 6X SDS loading buffer was added and the samples were boiled before being stored at -80 degrees. For IPs that were submitted for mass-spectrometry, the eluate was TCA precipitated and submitted to the Vanderbilt Mass Spectrometry core for trypsin digest and 1D or MudPit analyses.

Endogenous Immunoprecipitation from Nuclear Extracts

For endogenous immunoprecipitations, 2 mg of nuclear extracts were incubated with 3μg of antibody for 2 hours at 4 degrees. 50 μl of the appropriate dynabeads (Portein A for rabbit antibodies and protein G for mouse antibodies) were washed and added to the samples for an additional hour at 4 degrees. The beads were pelleted, washed, resuspended in 30μl of 2X SDS sample buffer and boiled for 10 minutes. Following pelleting, the samples were transferred to a new tube and analyzed by western blotting or stored at -80 degrees.

Transfection reagents

siRNA transfections were performed using Dharmafect-1 (Dharmacon) in a 60mm dish format for U2OS, A549 and BT549 cells, Dharmafect4 (Dharmacon) for CAPAN-1 cells and RNAiMax (Thermo Fisher) for RPE-hTERT and 293T cells according to manufacturer's instructions. Forward transfection protocol using RNAimax (Thermo Fisher) was performed in 35mm dishes for the fibroblast cell lines (BJ and T131P). Plasmid transfections were performed using Polyethyleneimine or FUGENE HD according to manufacturer's instructions.

Crispr/Cas9 Editing

HEK293T RADXΔ and U2OS RADXΔ cells were generated using CRISPR/Cas9. Briefly, cells were transfected with pSpCas9(BB)-2A-Puro 4 (Addgene plasmid no. 48139) containing guide RNAs that target the intron-exon junction of the second exon of RADX (3'-CACCGAATCAAAACTGCGATACTA-5' and 3'-CACCGTTACCATTACATGTTAAAC-5'), selected with 2 μg/ml puromycin for two days prior to plating for individual clones. Homozygous editing of the RADX locus was confirmed by genomic DNA PCR. The RADXΔcell lines were also validated for loss of RADX expression by immunoblotting and qRT-PCR of mRNA.

Isolation of Proteins from nascent DNA (iPOND)-SILAC

Changes in abundance of replication fork proteins in RADXΔ cells were determined using iPOND-SILAC MS as described previously(Dungrawala et al., 2015). For iPOND analysis in RADXΔ 293T cells, $4x10^8$ cells were utilized. For iPOND analysis in RADXΔ U2OS cells, $5x10^8$ cells were utilized. To examine

changes in response to HU, cells were incubated for 10 minutes with 10 μM EdU followed by 24 hours of 3 mM HU leaving EdU in the media.

Sister Chromatid Exchange Assay

24hrs post transfection with the indicated siRNAs, cells were labelled with 10 μM BrdU for approximately two cycles (48hrs). Colcemid was added to a final concentration of 150ng/ml to enrich for mitotic cells. Cells were trypsinized and spread for metaphases as described previously (German and Alhadeff, 2001). Cells were stained with 0.1mg/ml acridine orange and slides were mounted in Sorenson buffer (0.1 M Na2HPO4, 0.1 M NaH2PO4, pH 6.8).

Chromatin Fractionation

Chromatin fractionation experiments were performed as described previously(Lee et al., 2013). Briefly, cells were harvested and resuspended in Buffer A (100mM NaCl, 300mM Sucrose, 3mM $MgCl_2$, 10mM Pipes pH 6.8, 1mM EGTA, 0.2% TX-100, 1mM DTT, 1mM NaF, 1mM Na_2VO_3 and protease inhibitors) for 5 minutes on ice to collect the soluble fraction. The pellet was then washed once with Buffer A and then resuspended in Buffer B (50mM Tris-HCl pH 7.5, 150mM NaCl, 5mM EDTA, 1% TritonX-100, 0.1% SDS, 1mM DTT. 1mM NaF, 1mM Na_2VO_3 and protease inhibitors) for 10 minutes on ice. The insoluble fraction was collected following sonication and centrifugation.

Gateway cloning for CXORF57

The RADX cDNA was obtained from the ThermoScientific Open Biosystems Human ORFeome collection (Catalog number OHS-1770). Since this cDNA does not have a stop codon, I amplified the coding sequence and inserted a stop codon using PCR. I then utilized the gateway technology (Invitrogen) to create an expression vector containing the CXORF57 cDNA with a stop codon. For all of these steps, I followed the manufacturer's instructions (Invitrogen Gateway protocols).

Gene Blocks, Gibson Assembly and Site Directed Mutagenesis

For designing CXORF57 mutants, I utilized gene blocks synthesized from IDT. The gene blocks were designed to have atleast 30 bp of homology. The gene blocks were assembled using the Gibson Assembly Kit (NEB) according to manufacturer's instructions. I have successfully performed a six-piece assembly- for this reaction I utilized 50 bp of homology in each segment.

Site-directed mutagenesis was performed using Pfu Ultra according to manufacturer's instructions. I utilized the following PCR program:

Program name: KNM_SAM

95ºC - 1 min

<u>18 cycles of:</u>

95ºC - 50 s

60ºC - 50 s

68ºC - 1 min/kb

68ºC- 7 min

4 ºC- hold

Cell Culture

U2OS and HEK293T cells were cultured in DMEM with 7.5% fetal bovine serum (FBS). RPE-hTERT cells were cultured in DMEM F12, 7.5% FBS, and 7.5% sodium bicarbonate. A549 and BT549 cells were cultured in RPMI with 10% FBS. CAPAN-1 cells were cultured in RPMI with 20% FBS, and 1mM sodium pyruvate. The RA2630 FA-R fibroblast cell lines harboring a patient-derived RAD51 mutation and the matched controls were cultured in DMEM with 15% FBS and 1% MEM Non Essential Amino Acids (NEAA). All cells were incubated at 37 °C and 5% CO_2.

CHAPTER III

HIGH-AFFINITY DNA-BINDING DOMAINS OF REPLICATION PROTEIN A (RPA) DIRECT SMARCAL1-DEPENDENT REPLICATION FORK REMODELING[1]

Introduction

Replication is a fundamental process in all organisms and is challenged by DNA lesions, interference from transcription, and difficult to replicate sequences, all of which cause replication forks to stall (Zeman and Cimprich, 2014). Stalled forks activate the ATR checkpoint kinase, which phosphorylates hundreds of downstream targets to coordinate the replication stress response and promote replication restart and repair (Cimprich and Cortez, 2008).

SMARCAL1 is one ATR substrate that travels with the replication fork (Bétous et al., 2012). SMARCAL1 interacts with Replication Protein A (RPA), the major single-strand DNA (ssDNA) binding protein in human cells, and this interaction is required for SMARCAL1 localization (Bansbach et al., 2009; Ciccia et al., 2009; Postow et al., 2009; Yuan et al., 2009; Yusufzai et al., 2009). SMARCAL1-deficient cells are hypersensitive to replication stress (Bansbach et al., 2009; Ciccia et al., 2009; Postow et al., 2009; Yuan et al., 2009; Yusufzai et al., 2009), and accumulate DNA double strand breaks (DSBs) catalyzed by the MUS81 nuclease (Bétous et al., 2012). Too much SMARCAL1 activity either through overexpression or lack of restraining phosphorylation by

[1] The majority of this chapter has been published in (Bhat et al., 2015).

ATR, also causes an accumulation of DSBs due to fork cleavage by an SLX4-dependent endonuclease (Bansbach et al., 2009; Couch et al., 2013). In people, inherited loss of function mutations in *SMARCAL1* cause Schimke immunoosseous dysplasia (SIOD), a disease characterized by renal failure, immune deficiencies, cancer susceptibility, and growth defects (Boerkoel et al., 2002; Carroll et al., 2013; Elizondo et al., 2009).

Biochemically, SMARCAL1 is a DNA translocase that can evict RPA off DNA and anneal complementary strands (Yusufzai and Kadonaga, 2008). SMARCAL1 also performs branch migration and fork remodeling activities (Bétous et al., 2012). RPA confers substrate specificity to SMARCAL1, directing it to regress stalled forks caused by leading-strand lesions and restore normal forks with lagging-strand ssDNA (Bétous et al., 2013a), consistent with a function for SMARCAL1 in promoting genomic stability by catalyzing fork remodeling. However, the mechanism by which RPA selectively stimulates SMARCAL1 on certain substrates but inhibits it on others is unknown.

RPA is a heterotrimeric protein, with four DNA binding domains (DBDs) that bind to DNA with a specific orientation (Figure 3.1A). These four DBDs do not bind DNA equivalently, with DBD-A having the highest affinity followed by DBD-B, DBD-C and DBD-D (Arunkumar et al., 2003; Fanning et al., 2006; Wyka et al., 2003). RPA binds DNA with DBD-A and DBD-B making the initial contacts with 8 nucleotides (nts) of DNA (Arunkumar et al., 2003), and an additional 20 nts are protected when DBD-C and DBD-D bind (Brosey et al., 2013; Fan and Pavletich, 2012; Fanning et al., 2006). This 28-30 nt binding mode causes both the DNA and RPA to undergo major conformational changes and modifies the accessibility of protein interaction surfaces on RPA (Brosey et al., 2013; Fan and Pavletich, 2012; Fanning et al., 2006).

The regulation of DNA translocases by ssDNA binding proteins is an evolutionarily conserved feature of SMARCAL1-related enzymes. *E. coli* RecG and T4 UvsW are regulated by

interactions with their SSB proteins (Bétous et al., 2013a; Buss et al., 2008; Manosas et al., 2013). Furthermore, RPA regulates the specificity of many other reactions during replication and repair while being rapidly placed on and taken off DNA (Borgstahl et al., 2014; Fanning et al., 2006; Oakley and Patrick, 2010). The mechanisms underlying this fundamental aspect of DNA biology remain largely unknown. Although RPA can increase the local enzyme concentration to improve reaction rates, this mechanism does not explain how it generates substrate specificity for enzymes such as for SMARCAL1 (Bétous et al., 2013a).

In previous studies, we found that RPA regulation of SMARCAL1 is not due to a change in the ability of SMARCAL1 to bind DNA or hydrolyze ATP in the presence of RPA on the different substrates (Bétous et al., 2013a). In this study, we examined how RPA directs SMARCAL1 activity on specific substrates by testing two models. In the first model, we hypothesized that the location of the SMARCAL1 binding surface on RPA may be critical for generating substrate specificity. In the second model, we hypothesized that how RPA binds to the ssDNA in relation to the fork junction is important to create an optimal DNA-protein substrate for SMARCAL1. Our data support the second model and provide insights into how ssDNA binding proteins like RPA can generate substrate specificity for DNA translocases.

Results

The location of the SMARCAL1 interaction domain on RPA does not dictate substrate specificity

RPA activates SMARCAL1 on some fork substrates and inhibits it on others (Bétous et al., 2013a). Normal replication forks containing RPA bound to the lagging strand template are poor substrates for SMARCAL1-catalyzed fork regression; whereas stalled forks with RPA bound

to the leading strand template are good substrates (Figure 3.1B). Conversely, RPA bound to the chicken foot structures that are created by regression of stalled forks are poor substrates for SMARCAL1-catalyzed fork restoration, while chicken foot structures with RPA bound to the nascent leading strand are good substrates. Single molecule studies indicate that SMARCAL1 moves further on the good substrates than poor ones (Bétous et al., 2013a); however, how RPA dictates this specificity is unknown.

We hypothesized that the selective stimulation of SMARCAL1 is dictated by the orientation of RPA on DNA. Since the four RPA DNA binding domains bind with a 5' to 3' polarity (Bochkareva et al., 2002; Brosey et al., 2013; Fanning et al., 2006), the orientation of RPA with respect to the fork junction (and hence the DNA binding location of SMARCAL1) is different on the stalled fork and the normal fork (Figure 3.1B). This could translate into a difference in the location of the RPA32C domain that contacts SMARCAL1, and thereby alter whether RPA stimulates or inhibits SMARCAL1 (Figures 3.1B and 3.1C).

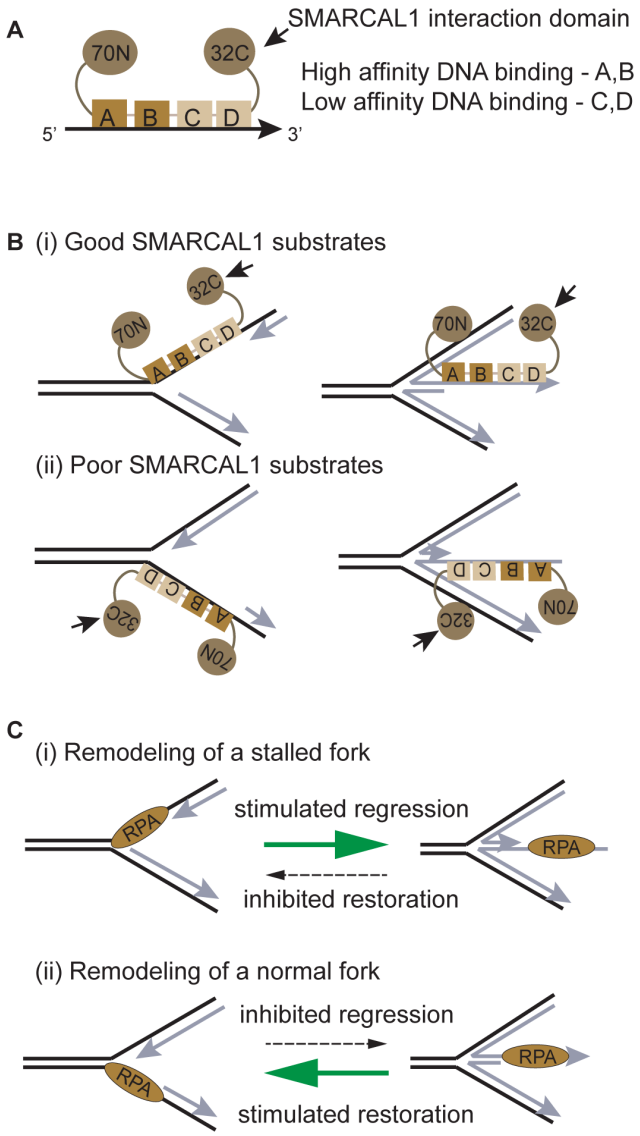

FIGURE 3.1. SMARCAL1 is regulated by RPA. (A) Schematic of RPA bound to ssDNA showing the polarity of the four DNA binding domains and location of the SMARCAL1-interaction domain. (B) Schematic of RPA orientation on the stimulatory and inhibitory substrates. The good SMARCAL1 substrates have the high-affinity DNA binding domains bound close to the fork junction. Also note that the position of RPA32C (the SMARCAL1 interaction domain) may be different on the good and bad SMARCAL1 substrates. The actual spatial locations of the DNA and proteins will be different in the three-dimensional structure of an actual replication fork. (C) Model for repair of stalled replication forks by SMARCAL1. (i) RPA bound to the leading template strand stimulates SMARCAL1-catalyzed fork regression. RPA should only be present on the leading strand when the polymerase is stalled. (ii) RPA bound to the lagging template strand inhibits SMARCAL1 catalyzed fork regression, thereby preventing aberrant remodeling of an actively elongating fork. However, RPA bound to the lagging nascent strand of a reversed fork stimulates SMARCAL1-mediated restoration to a normal fork structure.

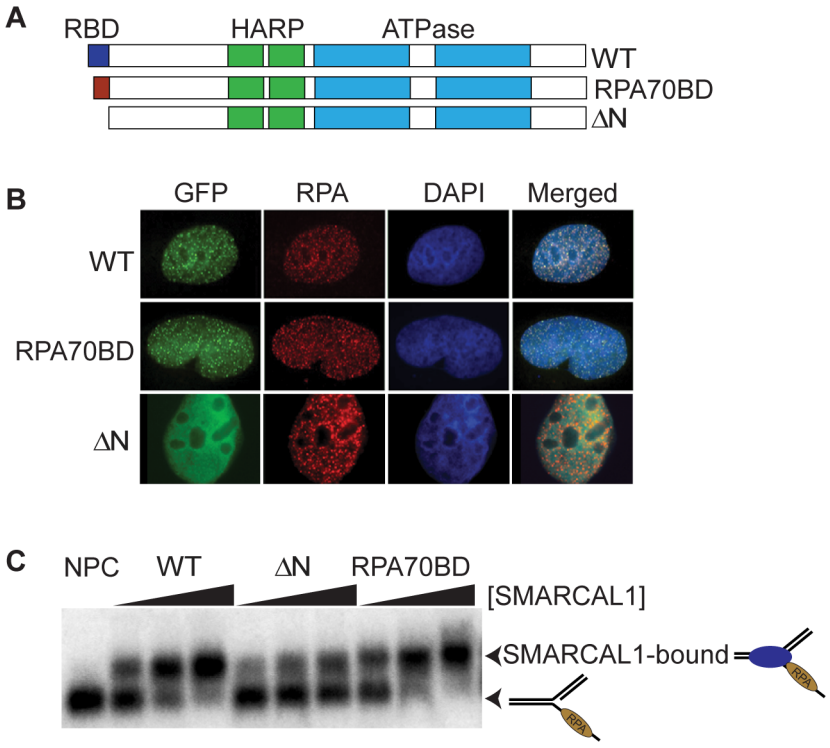

FIGURE 3.2. A SMARCAL1 mutant containing an RPA70N-interaction motif binds DNA and is recruited to RPA foci in cells after DNA damage. (A) Schematic of the wild type SMARCAL1 (WT) with an RPA32C interaction motif; SMARCAL1-ΔN, lacking an RPA interaction domain, and SMARCAL1-RPA70BD containing a RPA70N interaction motif. (B) U2OS cells were transfected with expression vectors for GFP-tagged SMARCAL1, SMARCAL1-RPA70BD, and SMARCAL1-ΔN. The cells were treated with hydroxyurea and imaged for RPA and SMARCAL1. (C) A model fork substrate was pre-bound with RPA (so that 100% of the substrate was bound) and incubated with increasing concentrations of the indicated SMARCAL1 protein for 30 minutes at room temperature. The products were then resolved on a 5% polyacrylamide gel. Remy Betous performed experiments for panels A and B.

To test if the location of the protein interaction domain on RPA is critical for directing SMARCAL1 to the right substrate, we utilized a SMARCAL1 mutant protein (SMARCAL1-RPA70BD) that interacts with the RPA70N domain instead of the 32C domain (Bétous et al., 2013b). This mutant substitutes an RPA70N binding motif for the RPA32C binding motif at the N-terminus of SMARCAL1 (Figure 3.2A). SMARCAL1-RPA70BD binds RPA with similar affinity as wild type SMARCAL1 (Bétous et al., 2013b), and colocalizes with RPA in DNA damage foci induced by hydroxyurea (Figure 3.2B) (Bansbach et al., 2009). In contrast, the SMARCAL1-ΔN protein missing any RPA interaction surface does not localize to stalled forks (Figure 3.2B and (Bansbach et al., 2009)). As expected, the DNA binding ability of SMARCAL1-RPA70BD in the presence of RPA is indistinguishable from the wild type protein (Figure 3.2C). Since the ΔN protein does not interact with RPA, the DNA binding ability of SMARCAL1-ΔN in the presence of RPA is slightly reduced as previously reported (Bétous et al., 2013a).

We then tested if the regulation of SMARCAL1 by RPA (Bétous et al., 2013a) is retained when SMARCAL1 binds RPA70N instead of RPA32C. RPA modestly stimulates both wild type SMARCAL1 and SMARCAL1-RPA70BD-catalyzed fork regression when the ssDNA is on the leading-strand template (Figures 3.3A and 3.3B). RPA inhibits SMARCAL1-ΔN-mediated regression, as previously described (Bétous et al., 2013a) suggesting that RPA acts as a block to SMARCAL1 when there is no interaction between RPA and SMARCAL1. Similarly, RPA stimulates wild type SMARCAL1 and SMARCAL1-RPA70BD to catalyze fork restoration to the same extent (Figures 3.3C and 3.3D). There is some stimulation of SMARCAL1-ΔN by RPA on the restoration substrate as previously described (Bétous et al., 2013a), suggesting an effect of RPA on the DNA substrate that is independent of a physical interaction with SMARCAL1. Also, RPA inhibits fork regression of SMARCAL1-RPA70BD when bound on the lagging template strand (Figure 3.4), similar to its inhibition of wild type SMARCAL1 and SMARCAL1-ΔN (Bétous et al., 2013a) suggesting that inhibition on some substrates is due to a physical block since RPA

must be removed during the reaction. This also further confirms that inhibition by RPA is independent of an RPA-SMARCAL1 interaction. Overall, these results support the conclusion that the regulation of SMARCAL1 by RPA is independent of how the two proteins interact, since there is no difference in the regulation of wild type SMARCAL1 and SMARCAL1-RPA70BD.

RPA high-affinity DNA binding is required to stimulate SMARCAL1

We next hypothesized that the DNA binding polarity of RPA might be important to regulate SMARCAL1 due to some change imparted on the DNA substrate. In contrast to the highly schematized cartoons in our models, the DNA bound to RPA adopts specific conformations(Brosey et al., 2013; Chen and Wold, 2014; Fan and Pavletich, 2012; Fanning et al., 2006) which would make the substrate presented to SMARCAL1 different depending on the orientation of the RPA DNA binding domains. To investigate if the affinity of RPA-DNA binding is important for stimulating SMARCAL1, we first utilized RPA mutants that have altered affinity for DNA due to mutations in either DBD-A or DBD-B (Haring et al., 2008; Hass et al., 2012; Walther et al., 1999). These mutations decrease but do not eliminate the affinity of these domains for ssDNA. Wild type and mutant RPA was added to the DNA substrates at concentrations sufficient to obtain full DNA binding (Figure 3.5A). Addition of excess wild type RPA to mimic the higher concentrations of the RPA mutants needed to obtain fully-bound substrates does not affect its regulation of SMARCAL1 (Figure 3.5B) as previously reported (Bétous et al., 2013a).

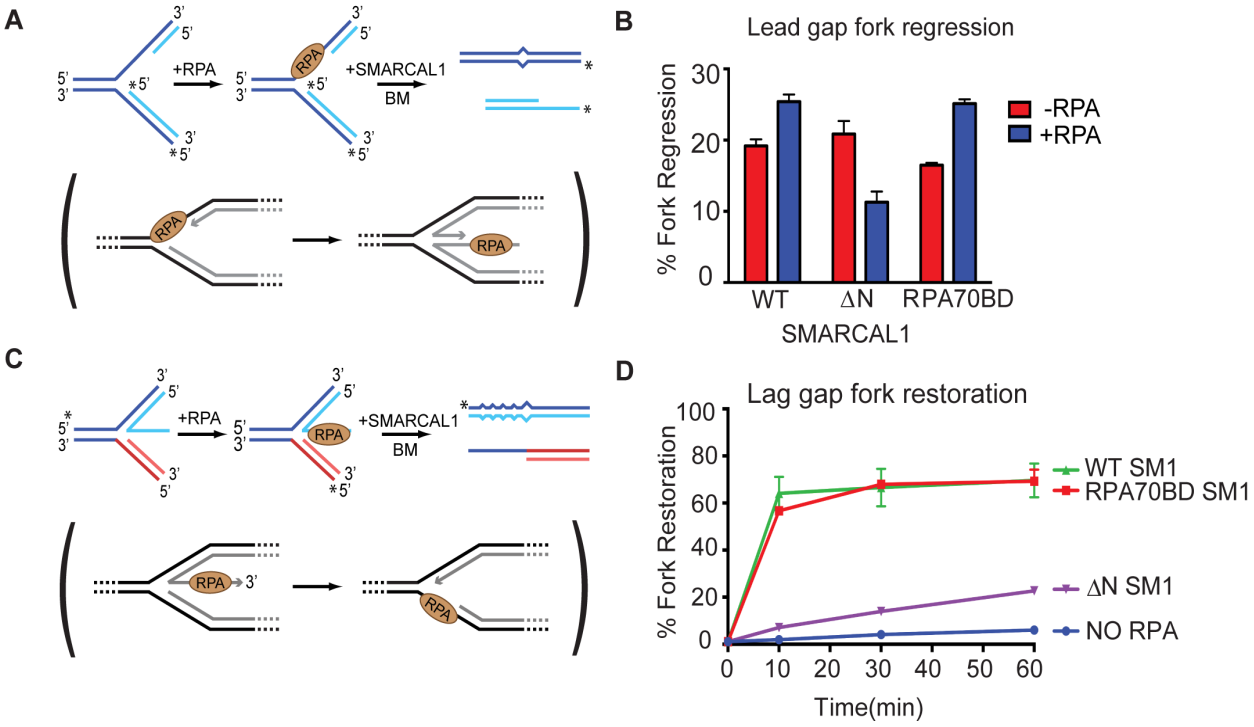

FIGURE 3.3. A SMARCAL1 mutant that binds to the 70N domain of RPA is regulated similarly to wild type SMARCAL1. (A and C) Schematic of the fork regression and restoration assays respectively; the ^{32}P-labeled strands are indicated by asterisks. The physiological reaction that is mimicked is indicated in the parentheses. The fork substrates were pre-bound with RPA and incubated with SMARCAL1 for (B) 60 minutes or (D) 10, 30 or 60 minutes. Products of the reactions were analyzed by native gel electrophoresis. The mean and standard deviations from three experiments are shown. Experiments for panel B were performed by Remy Betous.

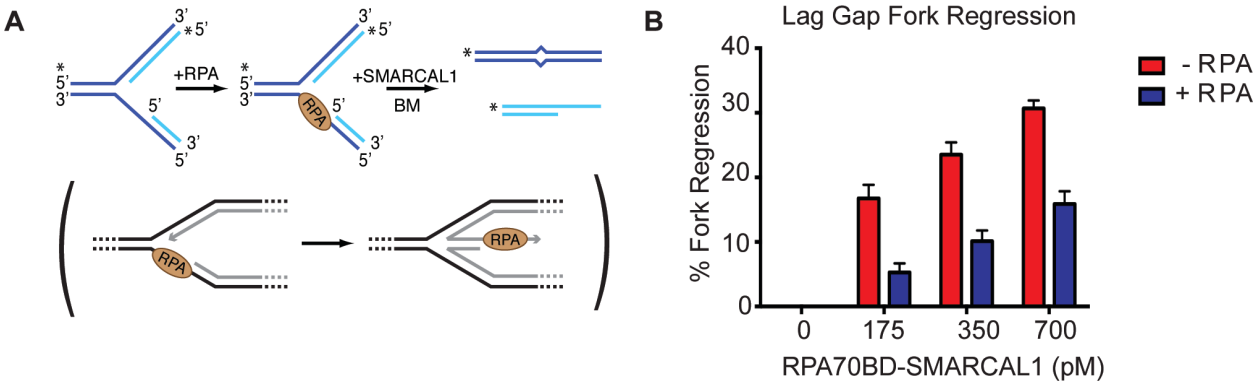

FIGURE 3.4. A SMARCAL1 mutant that binds to the 70N domain of RPA is inhibited by RPA on the normal fork substrate. (A) Schematic of the lag gap fork regression assay; the ^{32}P-labeled strands are indicated by asterisks. The physiological reaction that is mimicked is indicated in the parentheses. (B) The fork substrates were pre-bound with RPA and incubated with increasing concentrations of SMARCAL1-RPA70BD for 20 minutes at 30 degrees. Products of the reactions were analyzed by native gel electrophoresis. The mean and standard deviations from three experiments are shown. All experiments in this figure were performed by Remy Betous.

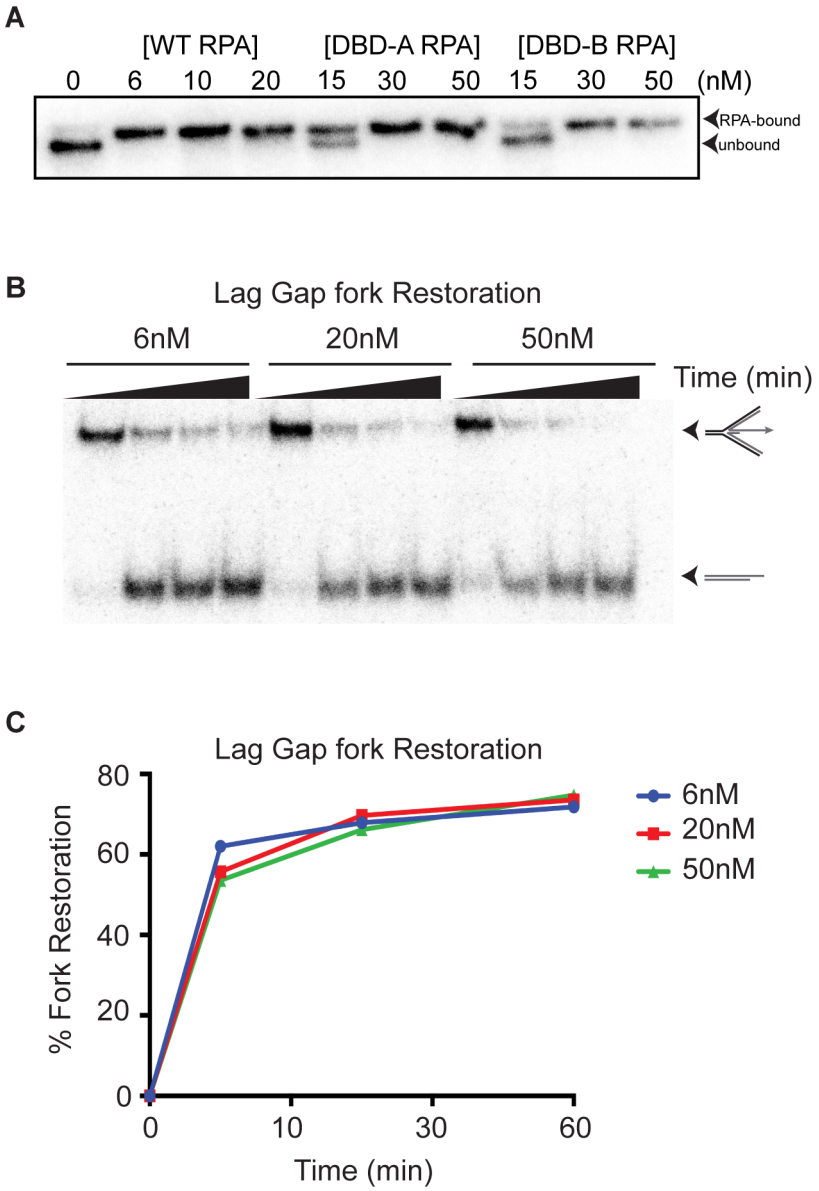

FIGURE 3.5. Excess RPA in the reaction does not affect the regulation of SMARCAL1. (A) Representative RPA binding assay. The fork regression substrate was incubated with the indicated concentrations of wild type, DBD-A or DBD-B RPA for 20 minutes and products were analyzed by native gel electrophoresis. The concentrations used in the remodeling assays were 6nM of wild type, and 30nM of DBD-A and DBD-B. (B and C) The fork restoration substrate was pre-bound with the indicated concentrations of full-length RPA for twenty minutes at room temperature, and then incubated with SMARCAL1 for 10, 30 or 60 minutes. The products were analyzed by native gel electrophoresis. (B) Autoradiograph. (C) Quantitation of B.

We then tested if the RPA proteins with mutated DBD-A or DBD-B stimulated SMARCAL1 in the fork remodeling assays. Since the DBD-A and DBD-B mutations should make it easier for RPA to be removed from the DNA during the reaction, we expected SMARCAL1 to remodel substrates with these mutants more rapidly. However, both the DBD-A and DBD-B mutants displayed a marked decrease in their ability to stimulate SMARCAL1, particularly in the fork restoration assay (Figures 3.6A, 3.6B and 3.6C). There is still some stimulation over the no RPA control since the mutations do not eliminate binding completely. An RPA protein with mutations in both DBD-A and DBD-B could not be tested because that mutant cannot bind the substrates in the conditions used in this assay. Nevertheless, these results indicate that mutations in the high-affinity DNA binding domains that should make it easier for SMARCAL1 to evict RPA actually interfere with the ability of RPA to stimulate SMARCAL1 translocation. However, the RPA DBD-A and DBD-B mutants do not inhibit SMARCAL1 as much as wild type RPA when bound to the poor substrates (Figure 3.6D) suggesting that the inhibitory action of RPA is due to a blocking effect on enzyme movement.

RPA DBD-A and DBD-B are sufficient to regulate SMARCAL1

RPA is removed from ssDNA in two or more steps with DBD-D and DBD-C coming off first, followed by DBD-B and DBD-A(Fanning et al., 2006; Haring et al., 2008; Jiang et al., 2006). Thus, during the fork remodeling reactions there should be an intermediate state where DBD-A and DBD-B are bound to DNA, but DBD-C and DBD-D are not. This could allow SMARCAL1 to access the ssDNA that was bound by DBD-C and DBD-D, and thus allow SMARCAL1 to translocate more efficiently depending on the orientation of the DNA binding domains.

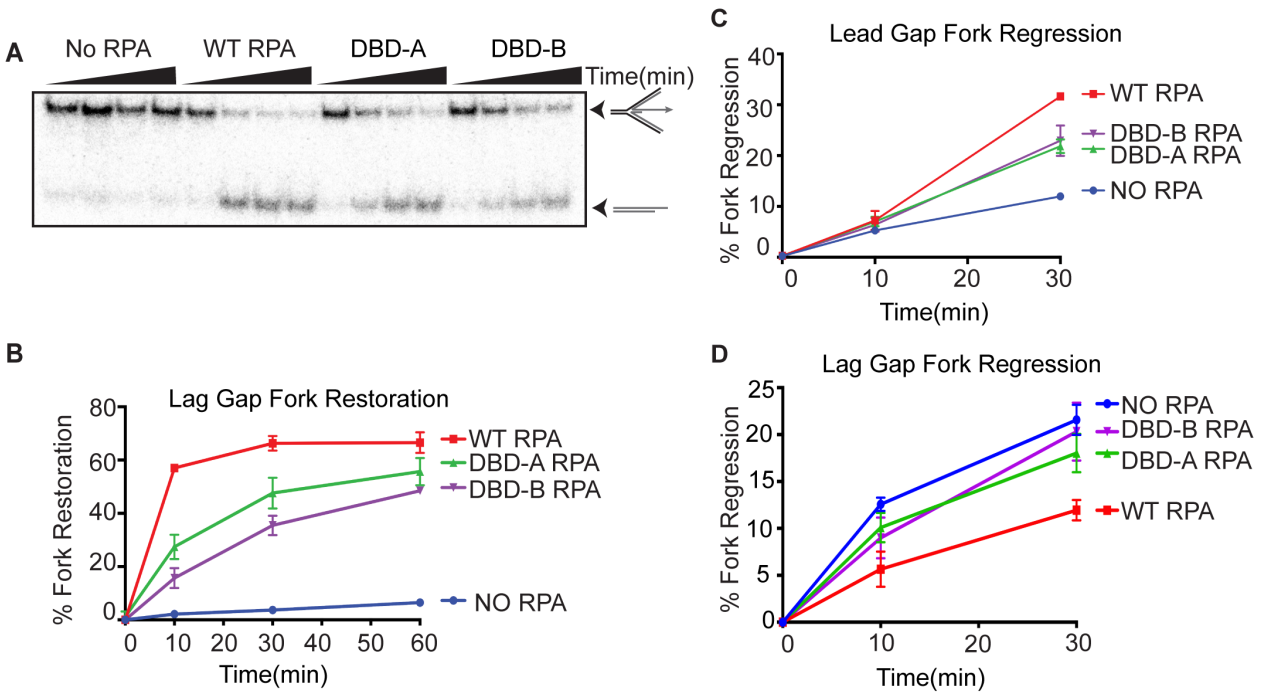

FIGURE 3.6. RPA mutants that are defective in binding DNA do not stimulate SMARCAL1 as well as wild type RPA. (A) Representative autoradiograph of the fork restoration assay with RPA mutants. The substrates and products are indicated. (B, C and D) The restoration and regression substrates were pre-bound with WT, DBD-A or DBD-B RPA as indicated for twenty minutes, and then incubated with SMARCAL1 for increasing times. The products were analyzed by native gel electrophoresis. The mean and standard deviations from three experiments are shown.

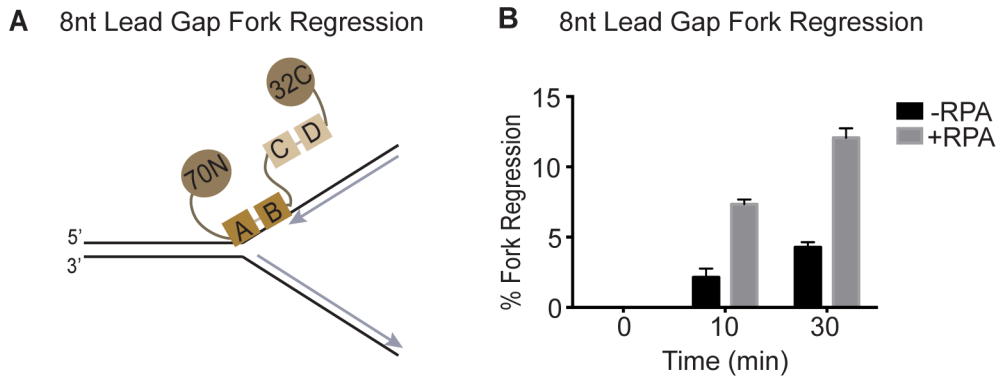

FIGURE 3.7. RPA bound to an 8nt gap is sufficient to stimulate SMARCAL1 regression of a stalled fork. (A) Schematic of the stalled fork substrate used in the assay. The ssDNA region is limited to 8nt, allowing the binding of only the RPA DBD-A and DBD-B domains. (B) The fork substrates were pre-bound with RPA and incubated with SMARCAL1 for increasing times. Products of the reactions were analyzed by native gel electrophoresis. The mean and standard deviations from three experiments are shown.

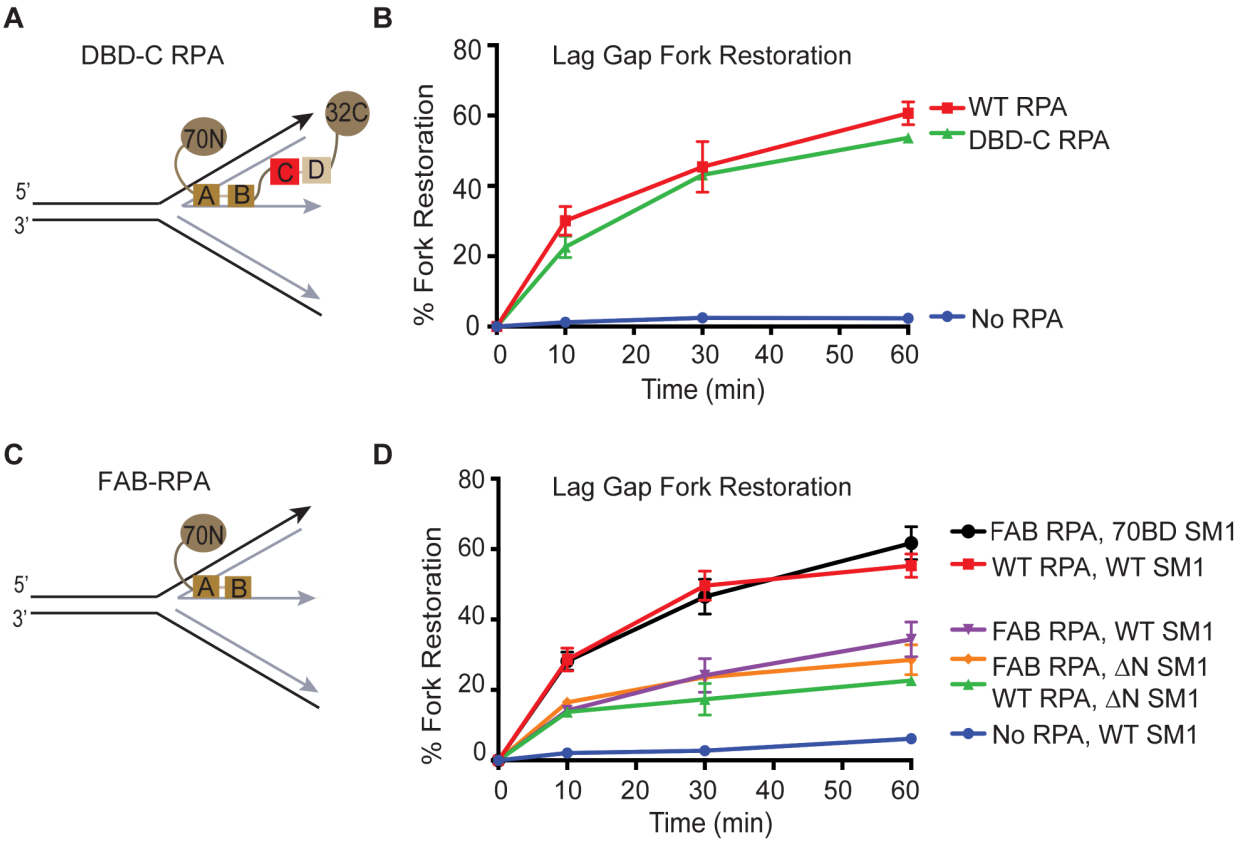

FIGURE 3.8. An RPA protein containing only DBD-A, DBD-B, and a SMARCAL1-interacting surface is sufficient to stimulate SMARCAL1. (A) Schematic of RPA DBD-C mutant (mutation in DBD-C that abrogates binding to DNA) bound to the substrate. (B) The fork substrates were pre-bound with the RPA DBD-C mutant and incubated with 1nM SMARCAL1 for increasing times. Products of the reactions were analyzed by native gel electrophoresis. The mean and standard deviations from three experiments are shown. (C) Schematic of the FAB-RPA protein (RPA that has only DBD-A and DBD-B along with the 70N domain) bound to the DNA substrate. D) The fork substrates were pre-bound with FAB-RPA and incubated with 1nM of the indicated SMARCAL1 proteins for increasing times. Products of the reactions were analyzed by native gel electrophoresis. The mean and standard deviations from three experiments are shown.

To test this idea and if the order of removal of the subunits of RPA off DNA is important, we designed fork substrates that have an 8-nucleotide ssDNA gap (Figure 3.7A), sufficient to allow only DBD-A and DBD-B binding to DNA (Jiang et al., 2006; Kolpashchikov et al., 2001; Lavrik et al., 1999; Wyka et al., 2003). Thus, any effect of DBD-C and DBD-D binding the DNA is eliminated. Binding of only the DBD-A and DBD-B RPA domains to ssDNA on the leading template strand is sufficient to stimulate SMARCAL1-catalyzed regression (Figure 3.7B). RPA does not stimulate SMARCAL1 when bound to an 8nt gap on the lagging template strand (data not shown). The activity of SMARCAL1 on the 8nt gap substrates is slightly less than on the 30nt gap substrates. Overall, these experiments suggest that the DNA binding and removal of the DBD-C and DBD-D RPA domains is not essential for regulation of SMARCAL1 and that only the DBD-A and DBD-B domains are critical.

To further test if the DNA binding of the C and D domains are dispensable for regulation of SMARCAL1, we utilized an RPA DBD-C mutant that abolishes binding of DBD-C and DBD-D to DNA (Bochkareva et al., 2000; Fanning et al., 2006; Hass et al., 2012; Walther et al., 1999) even on a 30nt ssDNA substrate (Figure 3.8A). Consistent with the results from the 8nt ssDNA regression substrates, the RPA DBD-C mutant stimulated SMARCAL1 activity to the same extent as wild type RPA (Figure 3.8B), suggesting that DBD-A and DBD-B binding to DNA is sufficient to selectively stimulate SMARCAL1 activity. Since the DBD-C mutant binds DNA with an overall affinity similar to the DBD-A and DBD-B mutants (Walther et al., 1999), this result also demonstrates that the decrease in the ability of those mutants to stimulate SMARCAL1 is not due to the overall decrease in DNA affinity of the mutant RPA proteins.

Finally, to confirm that the two, high-affinity RPA DNA binding domains are indeed sufficient to stimulate SMARCAL1 when attached to a SMARCAL1-interacting domain, we utilized FAB-RPA, an RPA truncation mutant that has only the DNA binding domains A and B, and the 70N protein interaction domain (Walther et al., 1999). SMARCAL1 does not interact with the FAB

mutant and hence would be expected to behave similarly to SMARCAL1-ΔN. However, SMARCAL1-RPA70BD, the SMARCAL1 mutant that interacts with 70N, should have a high level of stimulation with the FAB-RPA if the high-affinity DNA binding domains plus a SMARCAL1 interaction surface are sufficient for stimulation. Indeed, wild type SMARCAL1 behaves like SMARCAL1-ΔN in the presence of FAB-RPA, but SMARCAL1-RPA70BD is stimulated by FAB-RPA to the same extent as wild type SMARCAL1 by full-length RPA (Figures 3.8C and 3.8D). Thus, an RPA truncation mutant with only the high-affinity DNA binding domains stimulates a SMARCAL1 mutant that interacts with it.

Discussion

RPA is an essential regulator of DNA metabolism, serving as both a platform for protein recruitment and a director of enzymatic activities (Chen and Wold, 2014; Fanning et al., 2006). RPA interacts with many DNA translocases and can either stimulate or inhibit enzyme function. However, the mechanism by which it regulates enzymes in addition to increasing their local concentration is largely unknown. Our results reveal insights into the mechanism by which RPA regulates SMARCAL1, a fork remodeling enzyme, and provides a paradigm for understanding the dynamic nature of RPA-directed DNA metabolism.

Due to the high-affinity of RPA to ssDNA, RPA is almost always present when ssDNA forms during DNA replication or repair. Enzymes that translocate on DNA like helicases, translocases, and nucleases, must work in the presence of RPA (Bétous et al., 2013a; Brosh et al., 2000; Doherty et al., 2005; Machwe et al., 2011; Shen et al., 1998; Sommers et al., 2014). Regulation of DNA enzymes by ssDNA binding proteins is a conserved property in all organisms.

For example, both *E. coli* SSB and phage GP32 regulate the fork remodeling proteins RecG and UvsW (Bétous et al., 2013a; Buss et al., 2008; Manosas et al., 2013). However, differences in the structures of the prokaryotic, viral and eukaryotic SSBs suggest differences in mechanisms.

In some cases a change in enzyme recruitment or ATPase activity in the presence of the corresponding ssDNA binding protein is important (Abd Wahab et al., 2013; Ranalli et al., 2002; Shereda et al., 2007). However, the regulation of many helicases and translocases like SMARCAL1 cannot be explained by either mechanism. Also, in more complex examples, RPA stimulates enzymes like FANCJ and RECQ1 in a strand-specific manner (Suhasini et al., 2009). The basis of such regulation is largely not understood.

In the case of SMARCAL1, RPA selectively stimulates regression of a stalled fork and inhibits regression of a normal fork substrate (Figure 3.1C). It also stimulates SMARCAL1 to restore normal forks while inhibiting its restoration activity when the product would look like a stalled fork. We hypothesized that the polarity of RPA on DNA, which controls the location of the DNA binding domains and the location of the SMARCAL1 interaction surface with respect to the fork junction, conferred substrate specificity. Specifically, we developed two models. The first predicted that the location of the SMARCAL1-interaction surface on RPA is critical for regulation. This model was based on the idea that the RPA-protein interaction domain might be needed as an anchoring point for SMARCAL1 to remove RPA from DNA with the DBD-C and DBD-D low-affinity DNA binding domains being removed first (Chen and Wold, 2014; Fanning et al., 2006; Gibb et al., 2014). However, our results are inconsistent with this model, since a mutant SMARCAL1 that interacts with RPA70N is still regulated by RPA in the same way as wild type SMARCAL1 that interacts with RPA32C. Also, the crystal structure of RPA bound to DNA, as well as small angle X-ray scattering and NMR data suggest that RPA bends DNA and that its protein interaction domains are connected to the DNA binding domains with flexible tethers (Brosey et

al., 2013; Fan and Pavletich, 2012). Thus, the protein interaction domains could be close in space and incapable of providing firm anchoring points.

In our second model, we hypothesized that the way in which RPA binds replication forks, which is different between the normal fork and the stalled fork due to its asymmetry, is crucial for regulating SMARCAL1. This model predicts that alterations in the RPA DNA binding domains would impact regulation. Indeed, mutations in either of the two high-affinity RPA DNA binding domains caused a marked decrease in the ability of RPA to stimulate SMARCAL1 activity. Furthermore, an RPA protein with only a SMARCAL1-interaction domain and the two high-affinity DNA binding domains is sufficient to activate SMARCAL1. These results are consistent with observations that RPA with mutations in the high-affinity DNA binding domains are defective in DNA repair but can support DNA replication (Hass et al., 2012).

In summary, these results indicate that the placement of the RPA high-affinity DNA binding domains on DNA substrates dictates SMARCAL1 substrate specificity. Thus, although fork remodeling by SMARCAL1 must happen concurrently with displacement of RPA, some but not all mutations that decrease its DNA affinity actually make it more difficult for SMARCAL1 to translocate on the RPA-bound substrate. As might be expected, RPA mutants with lower affinity to DNA make the poor SMARCAL1 substrates better.

RPA binding to DNA is a highly dynamic process, and RPA can diffuse along ssDNA (Chen and Wold, 2014; Gibb et al., 2014; Nguyen et al., 2014). This diffusion of RPA along DNA may destabilize secondary structures, to allow access of other proteins to ssDNA (Chen and Wold, 2014; Nguyen et al., 2014). RPA diffusion can melt DNA hairpins efficiently when the hairpin is located at the 3' end. However, when the hairpin is located 5' to RPA, very little strand melting is observed (Nguyen et al., 2014). The high-affinity DBD-A and DBD-B domains are sufficient to induce hairpin destabilization (Nguyen et al., 2014). RPA can also promote unwinding of a duplex

DNA arm of a synthetic fork in an orientation-specific manner (Delagoutte et al., 2011). We speculate that RPA might stimulate SMARCAL1 in part by promoting the transient destabilization of the nascent-parental DNA duplex at the fork. This would explain why RPA selectively stimulates SMARCAL1 on some substrates but not others. Alternatively, the selective stimulation of SMARCAL1 could be because RPA induces specific DNA conformations that are more or less conducive to SMARCAL1 DNA translocation depending on its orientation with respect to the fork junction. Ultimately, high-resolution structures of enzyme-RPA-DNA complexes will be needed to distinguish between these ideas.

CHAPTER IV

RADX PROMOTES GENOME STABILITY AND MODULATES CHEMOSENSITIVITY BY REGULATING RAD51 AT REPLICATION FORKS[3]

Preamble

I joined the lab at the same time as Huzefa Dungrawala, a post-doctoral fellow who was interested in optimizing the iPOND protocol developed by Bianca Sirbu. I collaborated with Huzefa to perform several screens utilizing iPOND-SILAC-MS with the goal of identifying novel replication stress response genes (Dungrawala et al., 2015). One of our top hits from those screens was CXorf57 and we decided to collaborate to study the functions of this protein in genome maintenance. This chapter borrows heavily from our co-first author publication and almost every figure presented here was contributed to by both Huzefa and I. Since in many cases, the same experiments were repeated by both of us, I will not indicate in every figure our individual contributions.

Introduction

Single-strand DNA (ssDNA)-binding proteins (SSBs) are essential regulators of DNA metabolic processes including replication, recombination, and repair. SSBs in eukaryotic cells include Replication Protein A (RPA), hSSB1, POT1, and RAD51. These proteins protect ssDNA, recruit other proteins, and

[3] The majority of this chapter was published as a co-first author manuscript (Dungrawala et al., 2017).

regulate enzymatic activities in a variety of genomic contexts including at replication forks, sites of DNA damage, and at telomeres (Flynn and Zou, 2010; Oakley and Patrick, 2010; Richard et al., 2009).

RPA and RAD51 promote replication fork stability, especially in the context of replication stress. RPA dynamically associates with the replication fork to facilitate lagging strand DNA synthesis and binds stalled forks to regulate the replication checkpoint and prevent fork collapse. In this context, RPA recruits DNA damage response proteins including ATRIP and ETAA1 to activate ATR signaling, and also regulates fork processing enzymes like SMARCAL1 (Ball et al., 2005; Bass et al., 2016; Bétous et al., 2013a; Bhat et al., 2015; Duursma et al., 2013; Haahr et al., 2016; Myers and Cortez, 2006; Xu et al., 2008; Zou, 2017; Zou and Elledge, 2003). RPA exhaustion caused by defects in ATR signaling causes aberrant fork processing and fork collapse (Toledo et al., 2013).

RAD51 is best known for its ability to form filaments on ssDNA generated at resected double-strand breaks (DSBs) where it catalyzes a strand exchange reaction to initiate homology-directed repair (HDR) (Kowalczykowski, 2015; Symington, 2014). It also has at least two functions at stalled replication forks. First, it cooperates with motor proteins like SMARCAL1 and ZRANB3 to promote fork reversal as a mechanism to stabilize and repair stalled forks (Bétous et al., 2012, 2013a; Ciccia et al., 2012; Zellweger et al., 2015). Second, RAD51 protects forks from nuclease-catalyzed degradation of nascent DNA strands (Hashimoto et al., 2010; Schlacher et al., 2011). It may also promote strand invasion to restart a replication fork after cleavage by structure-specific nucleases like MUS81 (Sarbajna and West, 2014). The fork protection and HDR functions of RAD51 depend on BRCA2, which assists in replacing RPA with RAD51 at resected DSBs and stabilizes RAD51 at stalled forks (Kolinjivadi et al., 2017b). Thus, BRCA2-deficiency causes genomic instability and cancer predisposition due to a failure of HDR and fork degradation (Kass et al., 2016).

The break repair and fork protection defects in *BRCA2*-mutant cancer cells make them hypersensitive to DNA damaging agents used in cancer therapy and to drugs that target DNA repair like

PARP inhibitors (Lord and Ashworth, 2012; O'Connor, 2015). However, many patients develop drug resistance. One resistance mechanism is the acquisition of secondary *BRCA2* mutations that result in a functional protein (Edwards et al., 2008; Norquist et al., 2011; Sakai et al., 2008). In addition, re-acquisition of fork protection even in the absence of HDR restoration was recently demonstrated to yield PARP inhibitor resistance (Chaudhuri et al., 2016). The mechanisms by which this happen include inactivation of PTIP, PARP1, and other unidentified genetic alterations (Chaudhuri et al., 2016; Ding et al., 2016).

The HDR and replication fork protection functions of RAD51 are evolutionarily conserved in all kingdoms of life. For example, the bacterial RAD51 orthologue RecA also promotes replication fork reversal and protects newly synthesized DNA from being degraded by nucleases (Horii and Suzuki, 1968; Robu et al., 2001; Satta et al., 1979). RecA is both positively and negatively regulated to promote the proper balance between replication, recombination, and repair activities (Cox, 2007). This balance is partly achieved through the action of the RecX protein, a RecA antagonist (Drees et al., 2004; Stohl et al., 2003; Venkatesh et al., 2002; Vierling et al., 2000). No sequence homolog of RecX has been described in eukaryotic cells.

Here, we report the identification of a new replication stress response protein, RADX (RPA-related, RAD51-antagonist on X-chromosome) that has sequence similarity to RPA. RADX is recruited to replication forks and binds ssDNA via RPA-like OB-folds. RADX antagonizes the accumulation of RAD51 at forks. When RADX is inactivated, excessive RAD51 activity causes fork collapse in otherwise unstressed cells. In cells with reduced RAD51 function such as BRCA2-deficient cancer cells, RADX inactivation is sufficient to restore fork protection and confer chemoresistance. Thus, RADX is a novel regulator of RAD51 that functions at replication forks to maintain genome stability and may be an important determinant of chemosensitivity in cancer.

Results

RADX is recruited to stalled replication forks

We recently utilized iPOND (Isolation of Proteins on Nascent DNA) coupled with quantitative SILAC (stable isotope labeling of amino acids in cell culture) mass-spectrometry to identify proteins recruited to stalled replication forks (Dungrawala et al., 2015). Replication fork proteomes of cells treated with hydroxyurea (HU) for increasing amounts of time (0.5 hours to 24 hours) were compared to untreated cells (Figure 4.1A). In these analyses, the abundance of most chromatin proteins, like histones, are essentially unchanged through the replication stress time course (Dungrawala et al., 2015); replication proteins, like the MCM2-7 complex, decrease in abundance due to the slow completion of DNA synthesis and termination events in the absence of new origin firing; and replication stress response proteins like RPA and ATR are enriched at stalled forks (Dungrawala et al., 2015). We identified CXorf57 (Chromosome X open reading frame 57) as one the most highly enriched proteins at stalled forks (Figure 4.1B). We then performed iPOND-SILAC experiments comparing cells treated with EdU for 10 minutes (pulse) and cells treated and then incubated without EdU for an hour (chase) as described previously (Dungrawala et al., 2015) to identify proteins enriched at elongating replication forks (Figure 4.1C). We found that CXorf57 is modestly enriched even at unstressed replication forks (Figure 4.1D). Based on our functional analyses we have named this protein RADX.

RADX prevents replication fork collapse

To investigate its function, we utilized four siRNAs to deplete RADX (Figure 4.2B, inset). RADX knockdown causes elevated levels of the DNA damage marker γH2AX specifically in S-phase cells, both in the absence (Figure 4.2B) and presence of HU (Figures 4.2A, 4.2C).

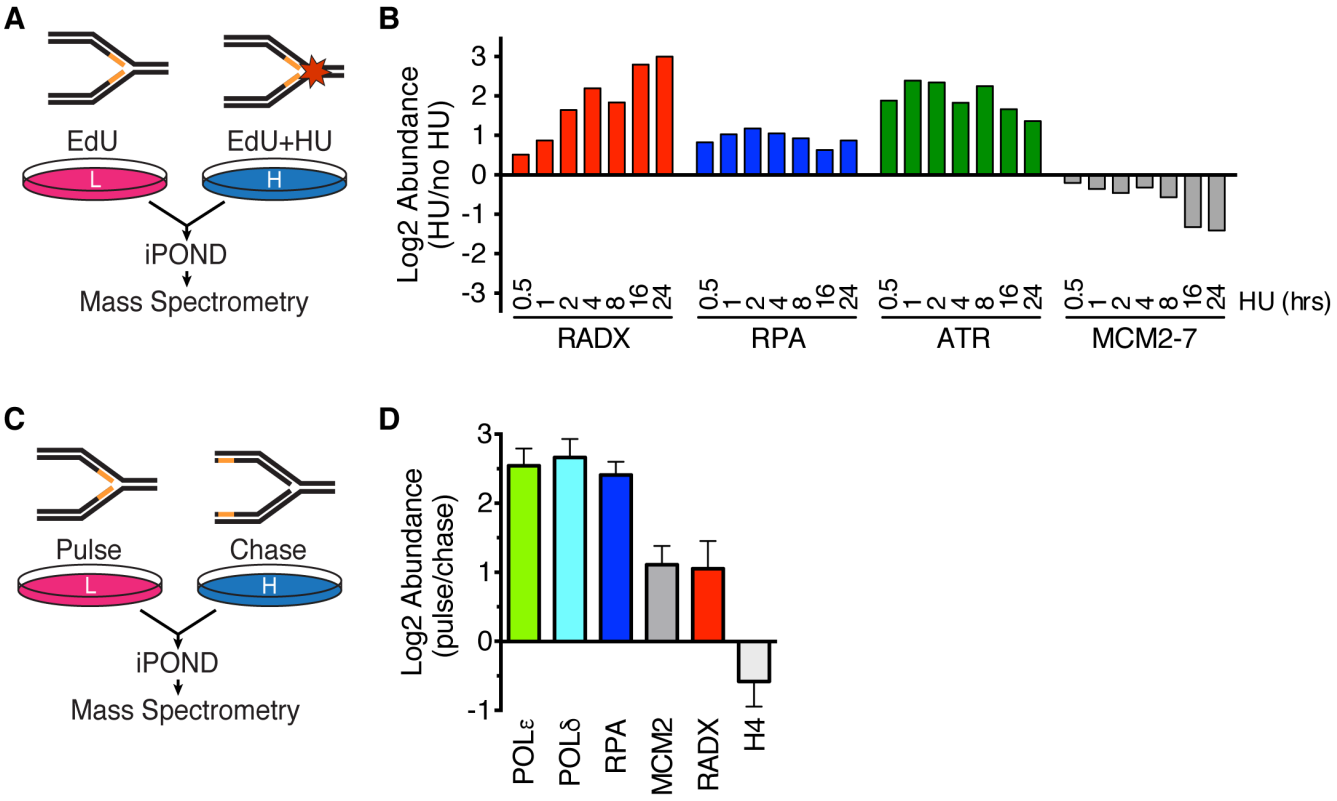

Figure 4.1. RADX is recruited to stalled replication forks. (A) iPOND-SILAC-MS was used to identify proteins enriched at forks in HU-treated cells. (B) Log_2 abundance ratios for selected proteins or complexes are depicted. P-values for RADX range from 0.04 to 10^{-14} at different time points (see (Dungrawala et al., 2015) for original data, n=12 total). (C) iPOND-SILAC-MS identified proteins enriched at elongating forks in the absence of exogenous stress. (D) Log_2 abundance ratios for selected proteins is depicted as mean +/- SEM, n=4 (n=2 each for HEK293T and HCT116). Panel A was published in (Dungrawala et al., 2015) and panel D was generated partly from Sarah Wessel's unpublished data.

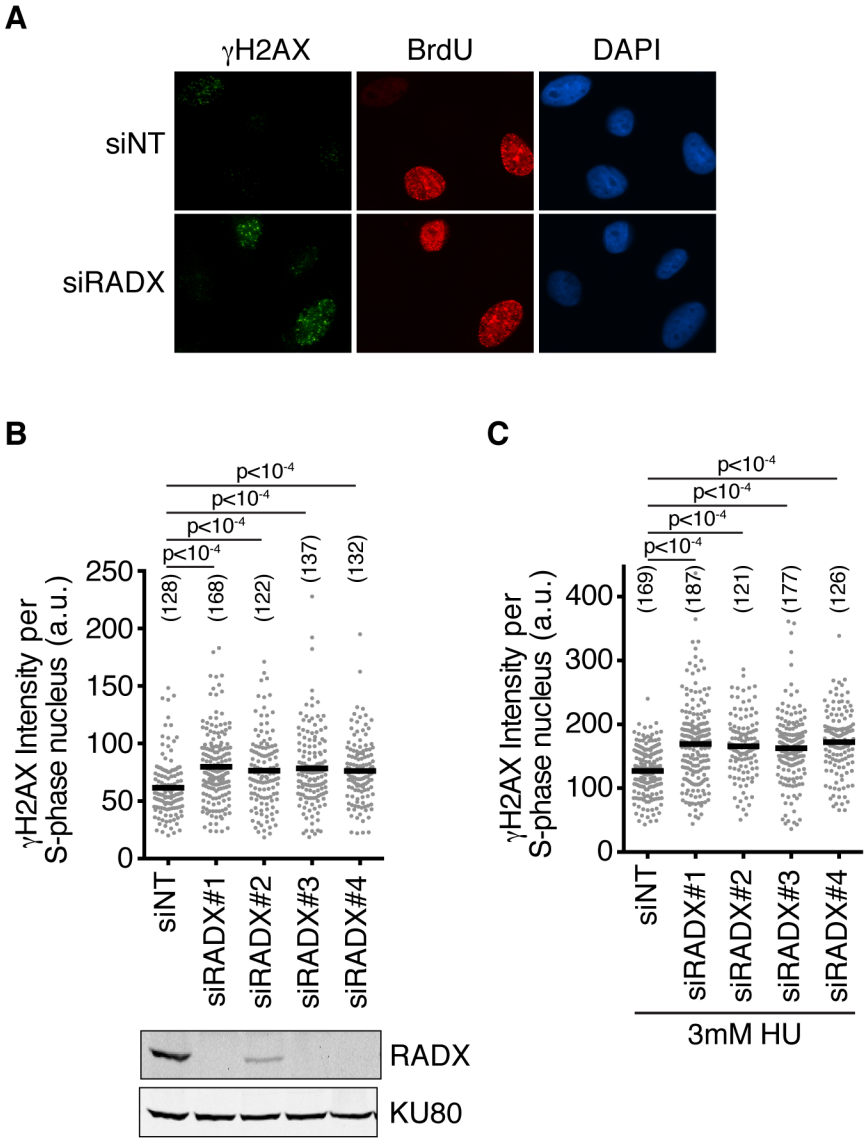

Figure 4.2. RADX silencing causes DNA damage signaling. (A) Representative images of U2OS cells transfected with non-targeting siRNA (siNT) or siRNA targeting the RADX gene (siRADX) treated with 3mM HU for 4 hours and stained for BrdU and γH2AX. (B-C) U2OS cells were transfected with siRNAs (siNT=non-targeting), labeled with EdU for 10 minutes, and γH2AX intensity in EdU-positive cells was measured by quantitative imaging. In C cells were treated with 3mM HU for four hours. Inset in B is an immunoblot to validate RADX siRNAs. The number of nuclei analyzed is indicated in parentheses. Black bars indicate the mean. P-values were calculated using a Kruskal-Wallis ANOVA with Dunn's posttest. All experiments are representative of at least two replicates.

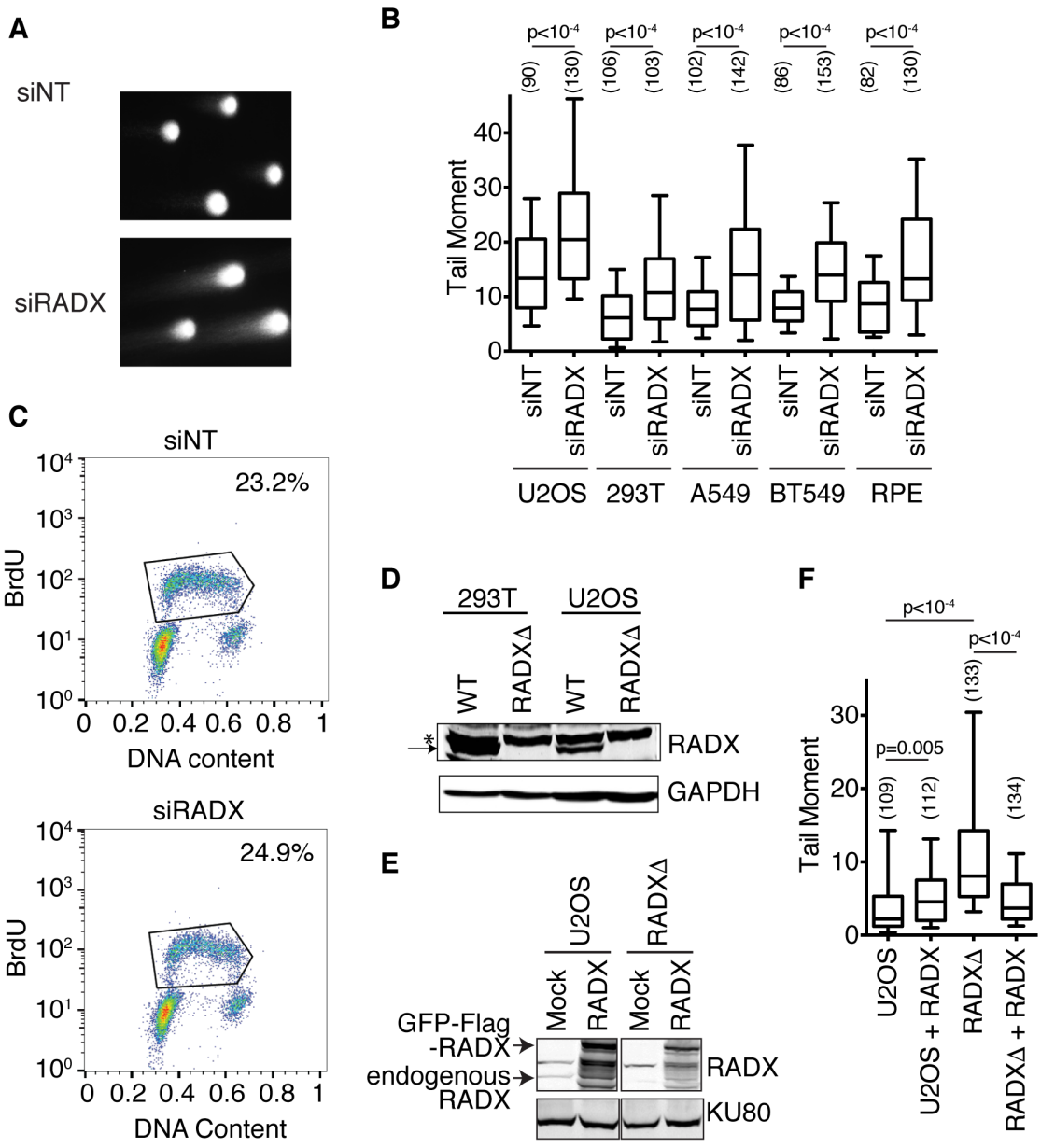

Figure 4.3. RADX is required to prevent double strand breaks. (A) Representative images of the neutral comet assay performed in the absence of exogenous damage. (B and F) DSBs were measured by neutral comet assay. For all box and whisker plots, the box depicts 25-75%, whiskers are 10-90%, and median is indicated. All experiments are representative of at least two replicates. P values were derived from a Mann-Whitney test in B and a Kruskal-Wallis ANOVA with Dunn's posttest in F. The number of nuclei analyzed is indicated in parentheses. (C) Cell cycle profiles of U2OS cells transfected with the indicated siRNAs were analyzed by flow cytometry using BrdU and propidium iodide staining. (D) Immunoblot to validate the RADX null cells obtained by CRISPR-CAS editing of the gene in U2OS and 293T cells (arrow points to RADX, *non-specific band). The non-specific band is not observed in other blots because of better separation on lower percentage gels. (E) Immunoblot of RADX expression levels in U2OS and RADXΔ cells before and after complementation. Aditya A Sathe performed the experiment in panel B.

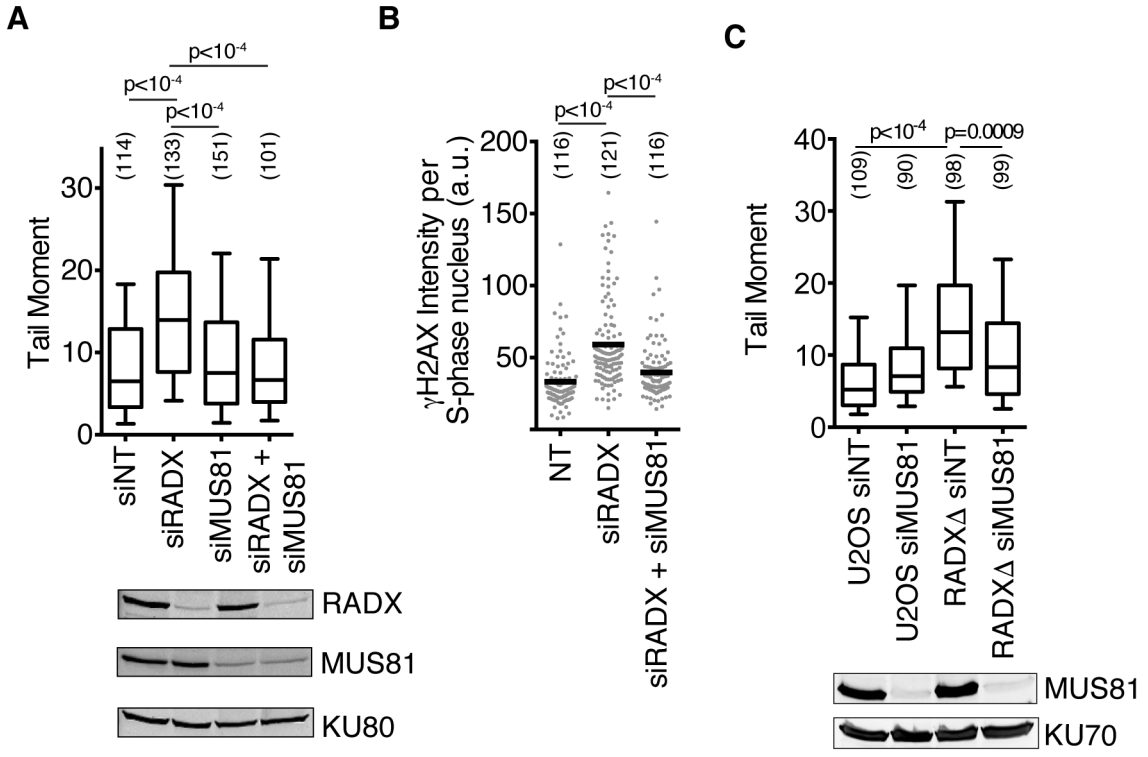

Figure 4.4. RADX is required to prevent MUS81-dependent DSBs. (A and C) DSBs were measured by neutral comet assay. For all box and whisker plots, the box depicts 25-75%, whiskers are 10-90%, and median is indicated. (B) γH2AX intensity in S-phase U2OS cells 72 hours post siRNA transfection. All experiments are representative of at least two replicates. P values were derived from a Kruskal-Wallis ANOVA with a Dunn's posttest. The number of nuclei analyzed is indicated in parentheses.

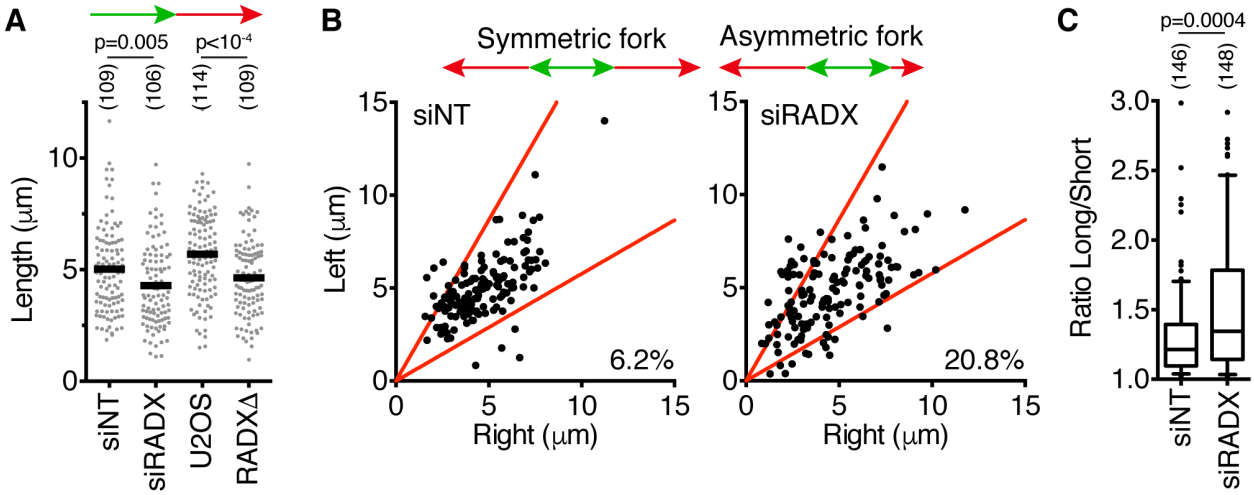

Figure 4.5. RADX prevents replication fork collapse. (A) U2OS cells transfected with siRNAs, or wild-type and RADXΔ cells, were labeled with IdU followed by CldU. CldU fiber length is plotted. (B and C) CldU lengths from left and right moving forks from the same origin were measured. In (I), the ratio of the sister fork lengths is plotted. The number of fibers (A and C) analyzed is indicated in parentheses. Black bars indicate the mean. P-values were calculated using a Kruskal-Wallis ANOVA with Dunn's posttest except in C where a Mann-Whitney test was used. All experiments are representative of at least two replicates.

RADX depletion, even in the absence of added replication stress, caused an increase in DSBs as measured by a neutral comet assay in both cancer and non-cancer human cell lines (Figures 4.3A, 4.3B). These effects are not due to large changes in the percentage of cells in S-phase (Figure 4.3C). RADXΔ cells derived using CRISPR-Cas9 targeting of the *RADX* gene in U2OS cells also displayed an increase in DSBs that could be rescued by complementation with an exogenously expressed RADX cDNA (Figures 4.3 D,E and F). We noticed in this complementation experiment that RADX cDNA expression did not fully complement the breaks caused by RADXΔ and modestly increased the level of DSBs in control U2OS cells, suggesting that overexpression of RADX also causes DNA damage. See below for a further exploration of overexpression phenotypes. Co-depletion of the structure-specific endonuclease MUS81 reduced both the DSBs and S-phase γH2AX phosphorylation caused by RADX silencing (Figure 4.4A and B) or *RADX* deletion (Figure 4.4C), suggesting that RADX prevents MUS81-catalyzed fork cleavage.

Finally, we utilized single molecule analysis of replicated DNA fibers to test if the increased DSBs in RADX-deficient cells affected replication fork progression. Indeed, both RADX siRNA and gene deletion decreased fork elongation rates (Figure 4.5A). In addition, RADX silencing also increased the frequency of asymmetric sister replication forks, confirming that RADX-deficient cells exhibit elevated rates of replication fork collapse (Figures 4.5B and C).

RADX binds DNA to maintain fork stability

An insight into the mechanism of RADX activity was obtained from analysis of the primary amino acid sequence and structural modeling, which predicts five structured domains, three of which are OB-folds (Figure 4.6A). The organization of the three OB-fold domains is reminiscent of the large subunit of RPA (RPA70). In addition, there is significant sequence similarity between RADX and RPA70 (Figure 4.7) leading us to hypothesize that RADX may bind ssDNA. To test this hypothesis, we purified a Flag-

RADX recombinant protein from baculovirus-infected insect cells (Figure S3A). Pull-down experiments of the purified protein with DNA conjugated to magnetic beads confirmed that RADX does bind ssDNA (Figure 4.6B). RADX also binds double-stranded DNA (dsDNA), although the interaction with dsDNA is significantly weaker (Figure 4.6C). We confirmed this observation using electrophoretic mobility shift assays which indicated that RADX has approximately 75-fold higher affinity for ssDNA than dsDNA (Figure 4.6D).

Sequence alignments indicate that the OB-1, OB-2, and OB-3 domains of RADX are most similar to the RPA70N protein recruitment domain, the RPA70A high-affinity ssDNA binding domain, and the telomeric ssDNA binding domain of POT1, respectively. Using the similarity of the RADX OB-2 domain to RPA70A and evolutionary conservation as guides, we designed mutations on surface amino acids of the OB-2 domain to determine if it is necessary to bind DNA (Figure 4.6A,4.6B, 4.8A and 4.8B). Indeed, the OB-2 domain mutant (OBm) RADX has reduced affinity for both ssDNA as well as dsDNA (Figure 4.8C). The OBm RADX protein has some residual ssDNA binding suggesting that like RPA, RADX likely contains multiple DNA binding domains.

We then tested whether DNA binding is required to protect replication forks from collapse. As observed previously, reconstituting RADXΔ cells with wild-type RADX reduces DSB formation (Figure 4.8D). In contrast, OBm RADX does not rescue the RADXΔ cells indicating that DNA binding is essential to maintain fork stability (Figure 4.8D). As noted previously, expression of wild-type RADX cannot fully complement the elevated DSB phenotype of RADXΔ cells, perhaps because it is overexpressed (Figure 4.8E). When tested directly in U2OS cells, high levels of overexpressed wild-type RADX, but not the OBm RADX protein, caused an increase in DSB formation (Figure 4.8D and 4.8E). We conclude that DNA binding is important for RADX function, and that either too much or too little RADX expression causes the accumulation of DSBs in otherwise unstressed cells.

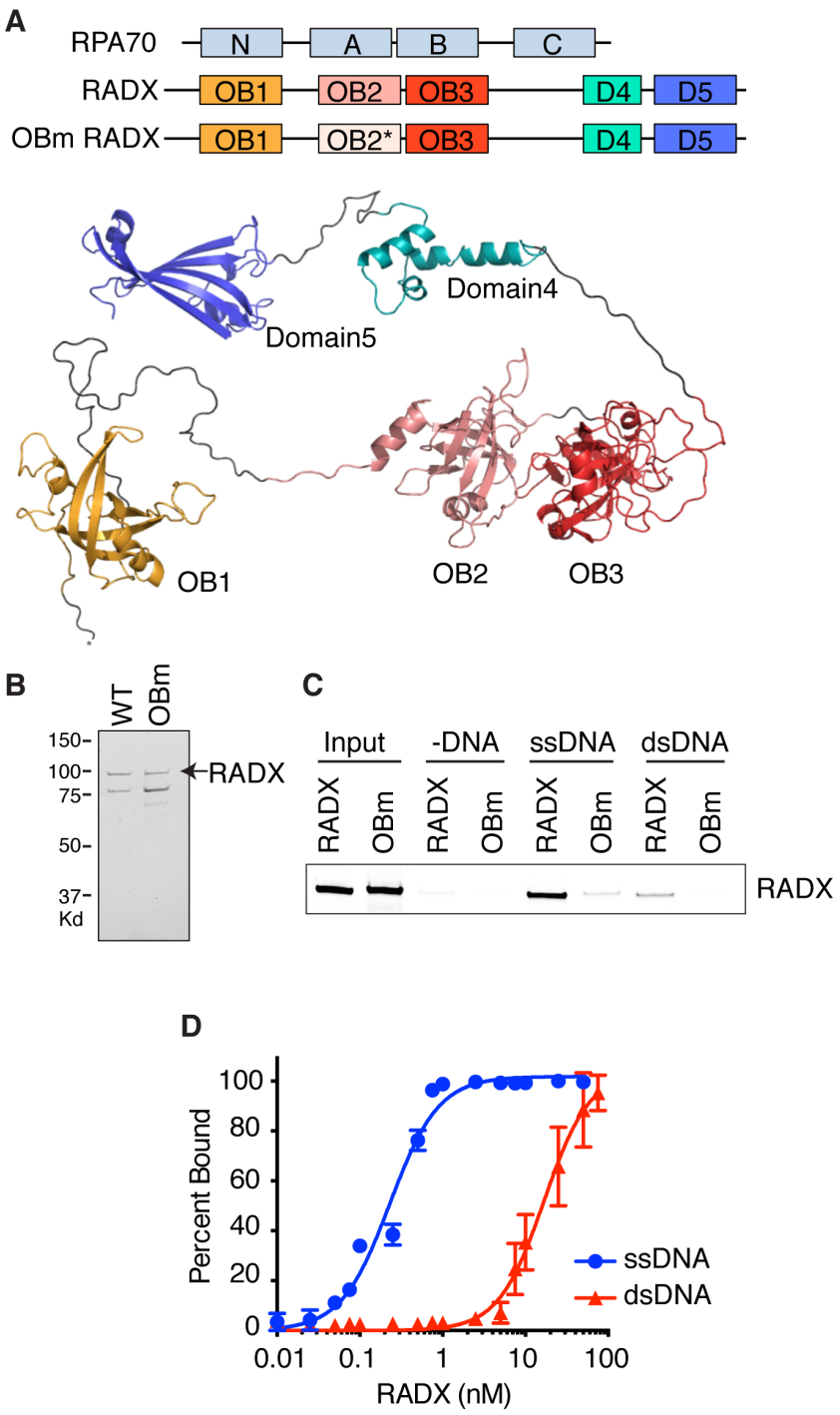

Figure 4.6. RADX binds DNA using its OB-fold domains. (A) Schematic of RADX and RPA70 depicting the OB-fold domains with a homology model of RADX generated using RaptorX. This was generated by Remy Le Meur. (B) Coomassie stained SDS-PAGE gels of purified RADX from insect cells. Mass spectrometry indicated that the smaller molecular weight band is a RADX degradation product. (C) DNA pull-down assays of purified RADX using ssDNA or dsDNA coupled to magnetic beads. (WT- wild type, OBm- OB mutant) (D) Electrophoretic mobility shift assays of RADX binding to ssDNA and dsDNA (mean+/-SD, n=3).

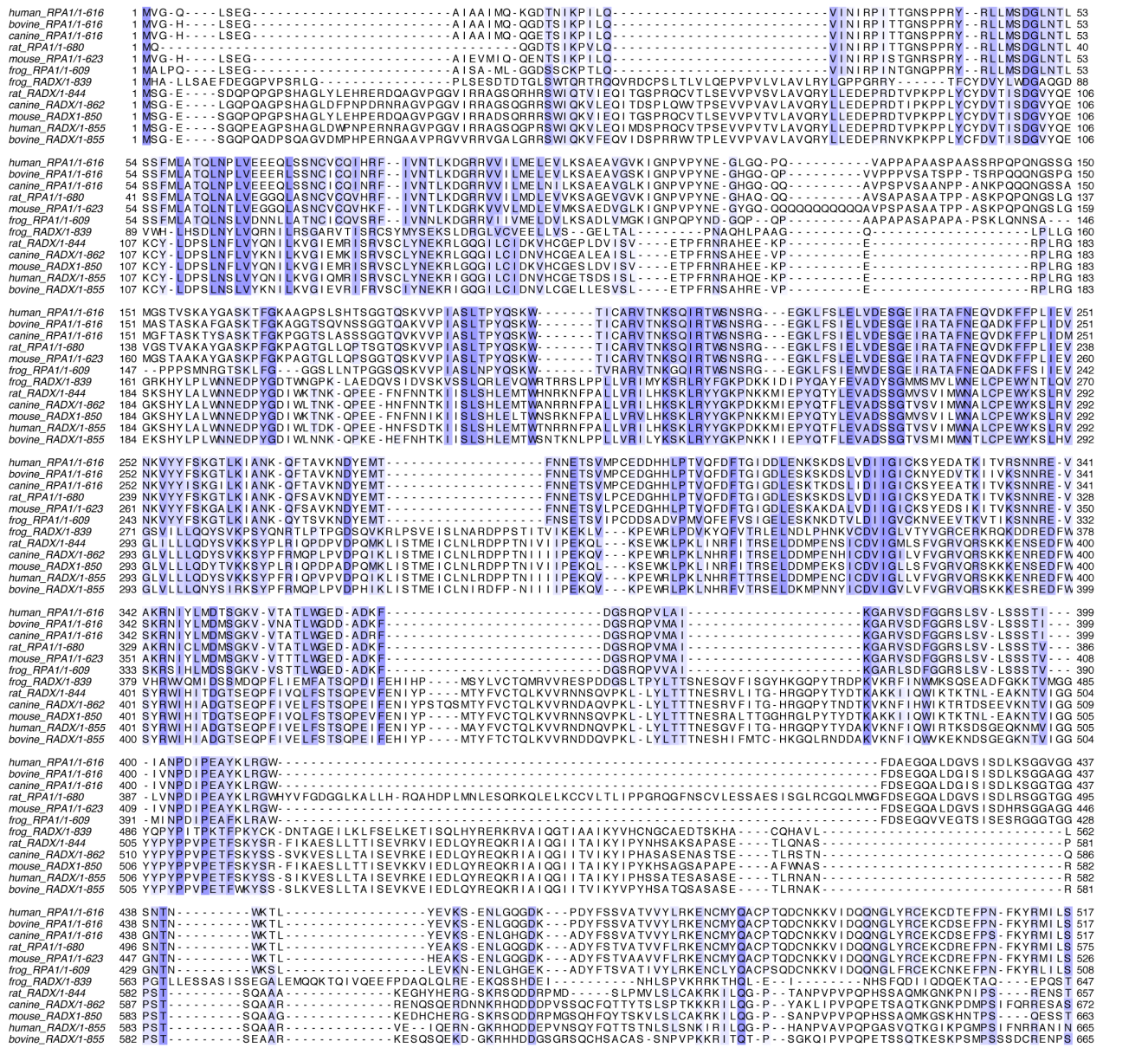

Figure 4.7. Multiple sequence alignment of RADX and RPA70g

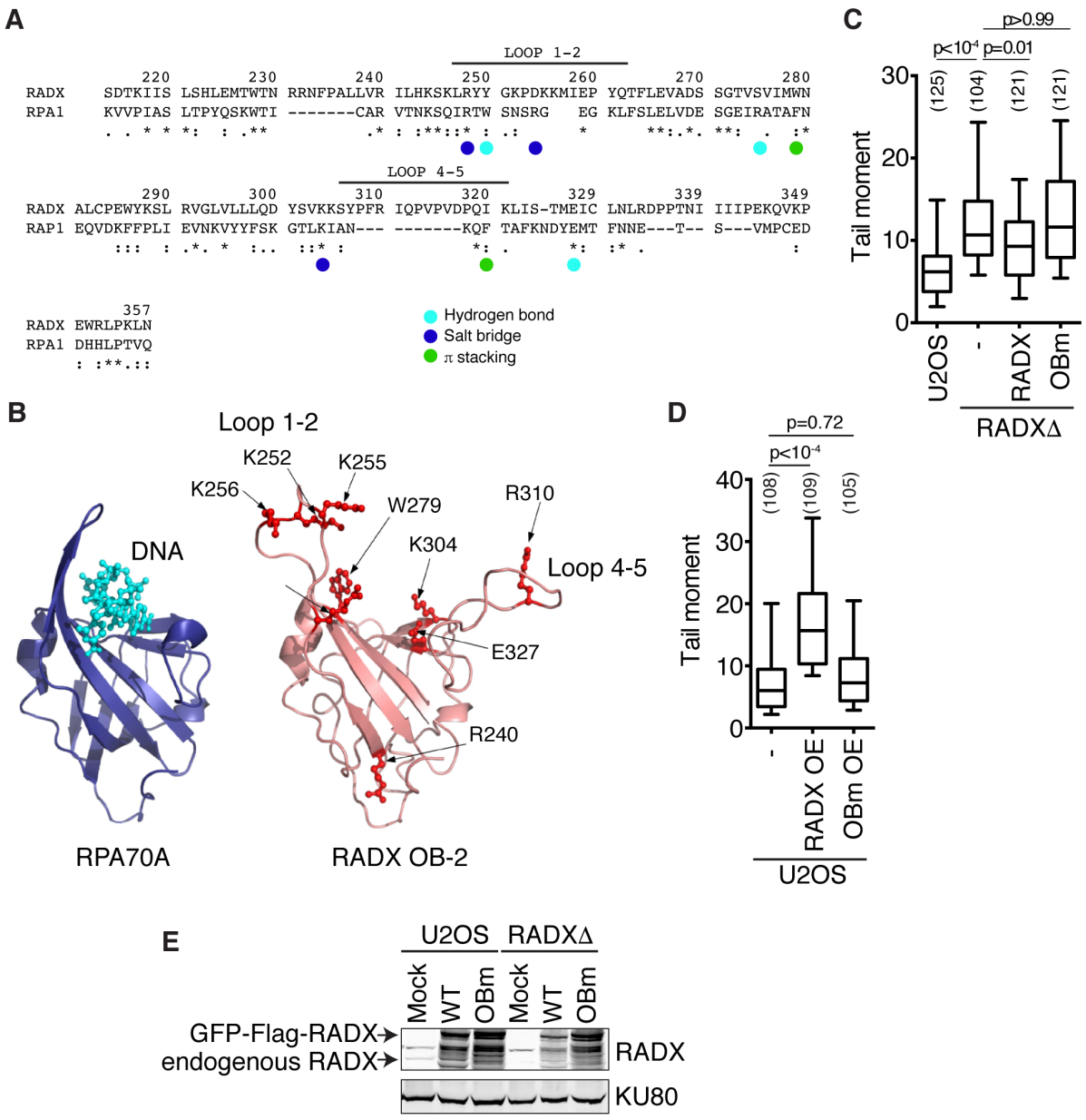

Figure 4.8 RADX binds DNA to prevent DSBs. (A) Sequence alignment of RPA70A and OB-2 of RADX. The cyan, blue and green dots indicate residues involved in hydrogen bonds, salt bridges and pi stacking interactions with DNA as observed in the crystal structure of RPA70AB in complex with DNA. (B) Ribbon representations of the RPA70-ssDNA complex (left, blue/cyan) extracted from the crystal structure of RPA70AB-dC8 (PDB code 1JMC) and a RADX OB-2 homology model (right, salmon). Residues selected for inclusion in the OBm mutant based on the model are highlighted. A and B were generated by Remy le Meur and David Cortez.(C) DSBs measured by neutral comet assay in RADXΔ cells expressing either wild-type or OBm RADX. The DSB level in parental U2OS cells is shown for comparison. (D) DSBs were measured after overexpression of wild-type or OBm RADX in U2OS cells. (-, mock). The number of nuclei analyzed is indicated. P-values were calculated by Kruskal-Wallis ANOVA with Dunn's posttest. Experiments are representative of at least two replicates. (E) Immunoblot depicting the complementation of RADX-proficient (WT) U2OS and RADXΔ cells with WT or OB-mutant RADX. Note that lanes 1,2,4, and 5 are also presented in Figure 4.3E.

RADX reduces RAD51 association with replication forks

To understand how RADX maintains replication fork stability, we performed iPOND-SILAC-mass spectrometry analyses to compare the stalled fork proteomes of RADXΔ cells to parental wild-type cells (Figure 4.9A). This experiment was completed in four different clones of HEK293T RADXΔ cells, and in one clone of U2OS RADXΔ cells. The median enrichment value of each protein observed in the datasets is depicted in Figure 4B and the full dataset is presented in Supplemental Table S1. Strikingly, of the 1060 proteins quantified in all five experiments, RAD51 was the highest enriched at stalled forks in the RADXΔ cells as compared to the parental cells (Figure 4.9B). In contrast, many other DNA damage response proteins like BRCA2, RPA, and the MRN complex were neither more nor less abundant at stalled forks in RADXΔ cells compared to control cells (Figure 4.9B).

Quantitative immunofluorescence imaging of chromatin-bound RAD51 confirmed an increase in RAD51 at replication forks corresponding to an increase in both the number of detectable foci and an increase in their size in RADX-silenced cells, even when cells were not stressed with HU (Figures 4.9C and 4.9D). These differences are not due to a difference in the total expression of RAD51 in RADX-silenced and RADXΔ cells (Figures 4.10A and 4.10B). In addition, this difference is unlikely to be due to increased end-resection of DSBs at forks since we did not observe an increase in RPA at forks (Figure 4.9B), an accumulation of more ssDNA in RADX-deficient cells as measured by native BrdU staining (Figure 4.10C), more RPA on chromatin (Figure 4.10D), or an increase in RPA S4/S8 phosphorylation which is often used as a marker for end resection (Figure 4.10D). Thus, even though the amount of ssDNA is not appreciably different than in wild-type cells, inactivating RADX allows more RAD51 to accumulate at forks.

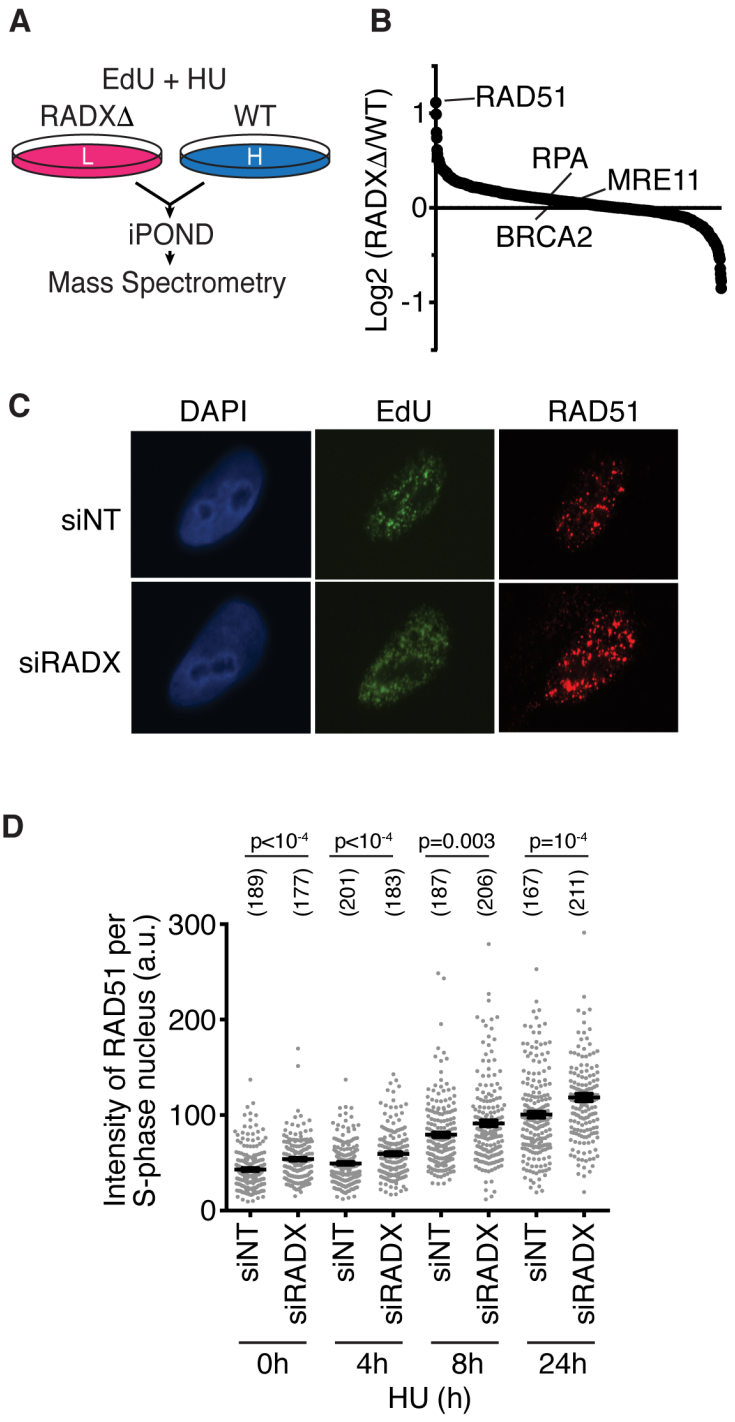

Figure 4.9. RADX loss causes increased RAD51 at replication forks. (A) Schematic of iPOND-SILAC-MS experiment. (B) The median of the $\log_2$ abundance ratios of the proteins identified in five cell clones is depicted. (C and D) U2OS cells transfected with siRNA were labeled with 10μM EdU for 30 minutes and were treated with 3mM HU. Cells were stained for RAD51 and EdU after detergent extraction. Representative images of RAD51 foci after 24h HU are shown in (C). In (D) the intensity of chromatin bound RAD51 in S phase cells is quantified. The number of nuclei analyzed is indicated and the mean+/-SEM is shown. P-value derived from a Mann-Whitney test. Experiment is representative of two replicates.

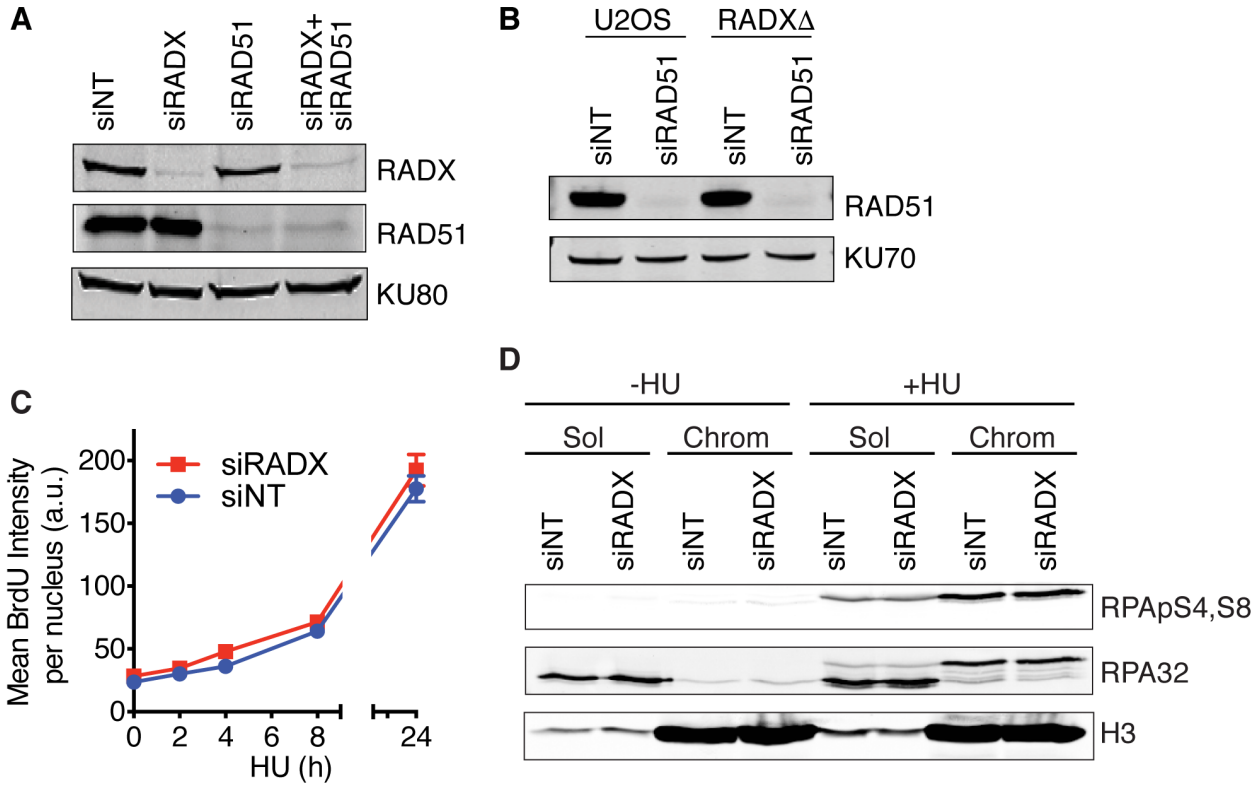

Figure 4.10. RADX loss does not affect end resection or RAD51 protein expression. (A and B) Immunoblots after transfection with the indicated siRNAs in wild-type or RADXΔ U2OS cells**.** (C) U2OS cells transfected with non-targeting (NT) or RADX siRNA were labeled with 10 μM BrdU for 22 hours prior to treatment with 3 mM HU for the indicated times. The cells were fixed and stained for BrdU using non-denaturing conditions to measure the amount of ssDNA. The mean+/-SEM from a representative experiment are depicted (n=107 per sample). (D) U2OS cells transfected with non-targeting (NT) or RADX siRNA were left untreated or treated with 3mM HU for 24 hours. The soluble and chromatin fractions were immunoblotted for the indicated proteins.

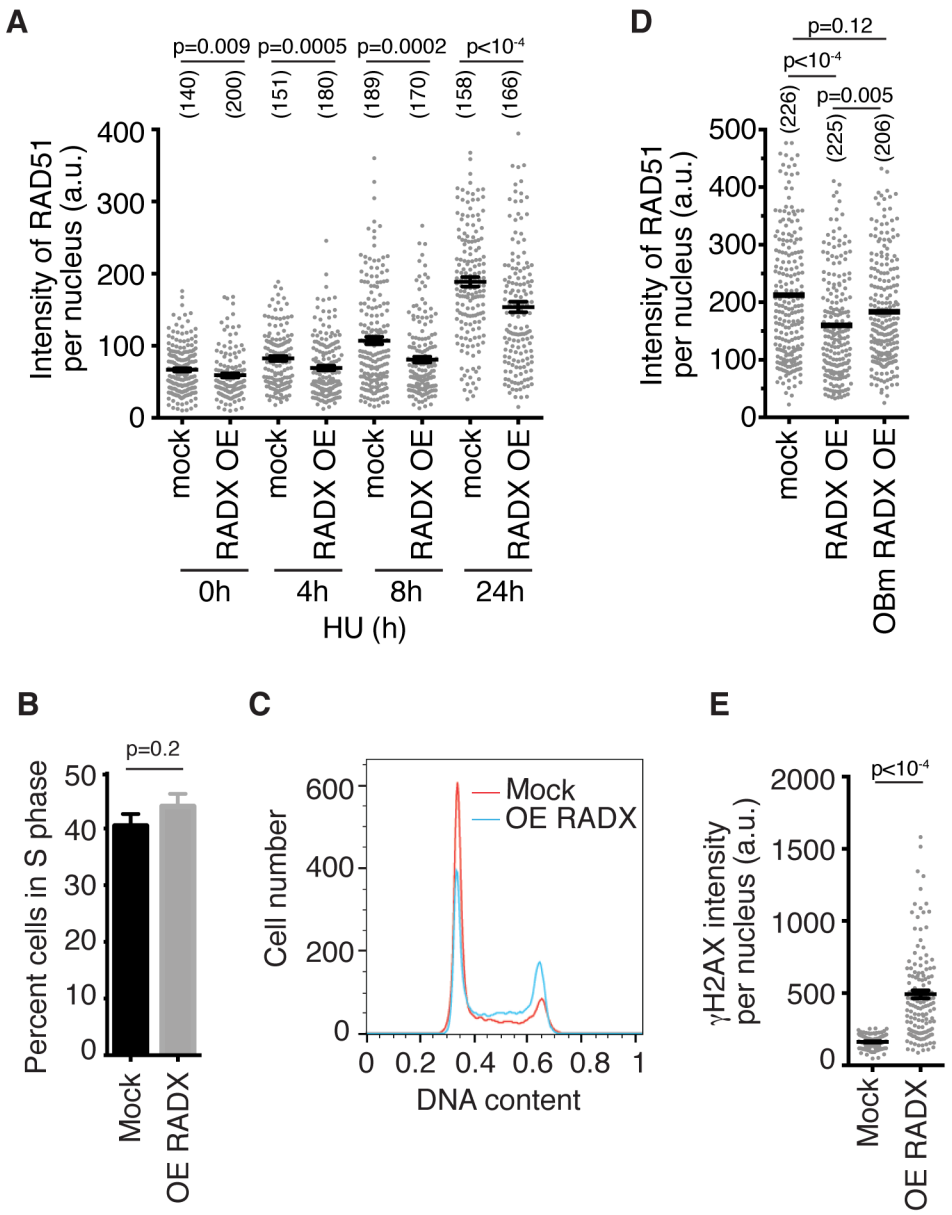

Figure 4.11. RADX overexpression suppresses RAD51 foci formation and causes DNA damage. (A) Cells overexpressing GFP-RADX (OE) or parental U2OS cells were treated with 3mM HU. Chromatin-bound RAD51 intensity after detergent extraction with mean+/-SEM is depicted. P-values were derived from a Mann-Whitney test. (B) Mock or Flag-RADX overexpressing U2OS cells were labeled with 10μM EdU for thirty minutes prior to staining for EdU and RADX. The percentage of EdU positive cells is presented (mean+/-SEM, n=3). P-value derived from a Mann Whitney test. (C) Cell cycle profiles of mock and GFP-RADX overexpressing U2OS cells were analyzed by propidium iodide staining and flow cytometry. (D) Cells overexpressing GFP-RADX or GFP-OBm were treated with 3mM HU for 24 hours Chromatin-bound RAD51 intensity with the mean is plotted. P-values were calculated by Kruskal-Wallis ANOVA with Dunn's posttest. (E) Mock and GFP-RADX overexpressing U2OS cells were stained for γH2AX. The mean+/-SEM from a representative experiment is presented (n=144). P-value was derived from a Mann Whitney test. All representative experiments were repeated at least twice.

These data collectively suggest that RADX might antagonize RAD51 recruitment. If so, then overexpression of RADX should reduce RAD51 accumulation at forks. As predicted, cells overexpressing GFP-RADX have decreased RAD51 accumulation in detergent-resistant foci, both in the absence of added exogenous stress, and in response to replication stress over a time course in HU (Figure 4.11A). The decreased RAD51 is not due to a decrease in the percentage of cells in S phase in the GFP-RADX cells (Figures 4.11B and 4.11C), but is dependent on the ability of RADX to bind DNA since it is less apparent in cells overexpressing OBm RADX (Figure 4.11D). As noted previously, RADX overexpression causes DNA damage as measured by both an increase in DSBs (Figure 4.8D) and increased γH2AX (Figure 4.11E), indicating that the differences in RAD51 accumulation at forks in RADXΔ and RADX overexpressing cells cannot simply be explained by changes in the amount of breaks and replication stress. Thus, we conclude that RADX inhibits RAD51 accumulation at forks, a function that is dependent on its ability to bind DNA.

Excessive RAD51 activity causes fork collapse in RADX-deficient cells

Since RADX causes decreased RAD51 at replication forks, we reasoned that the replication defects such as decreased replication elongation and increased fork collapse in RADX-deficient cells might be caused by too much RAD51 activity. This hypothesis predicts that RAD51 silencing should rescue the replication defects caused by RADX deficiency. Strikingly, reducing RAD51 expression with RNA interference rescues both the fork elongation defect and the increased DSBs observed in RADX-deficient cells (Figures 4.12A-C, and 4.10A and B). Thus, despite RAD51 being a DSB repair protein, RAD51 silencing decreases the DSBs caused by loss of RADX.

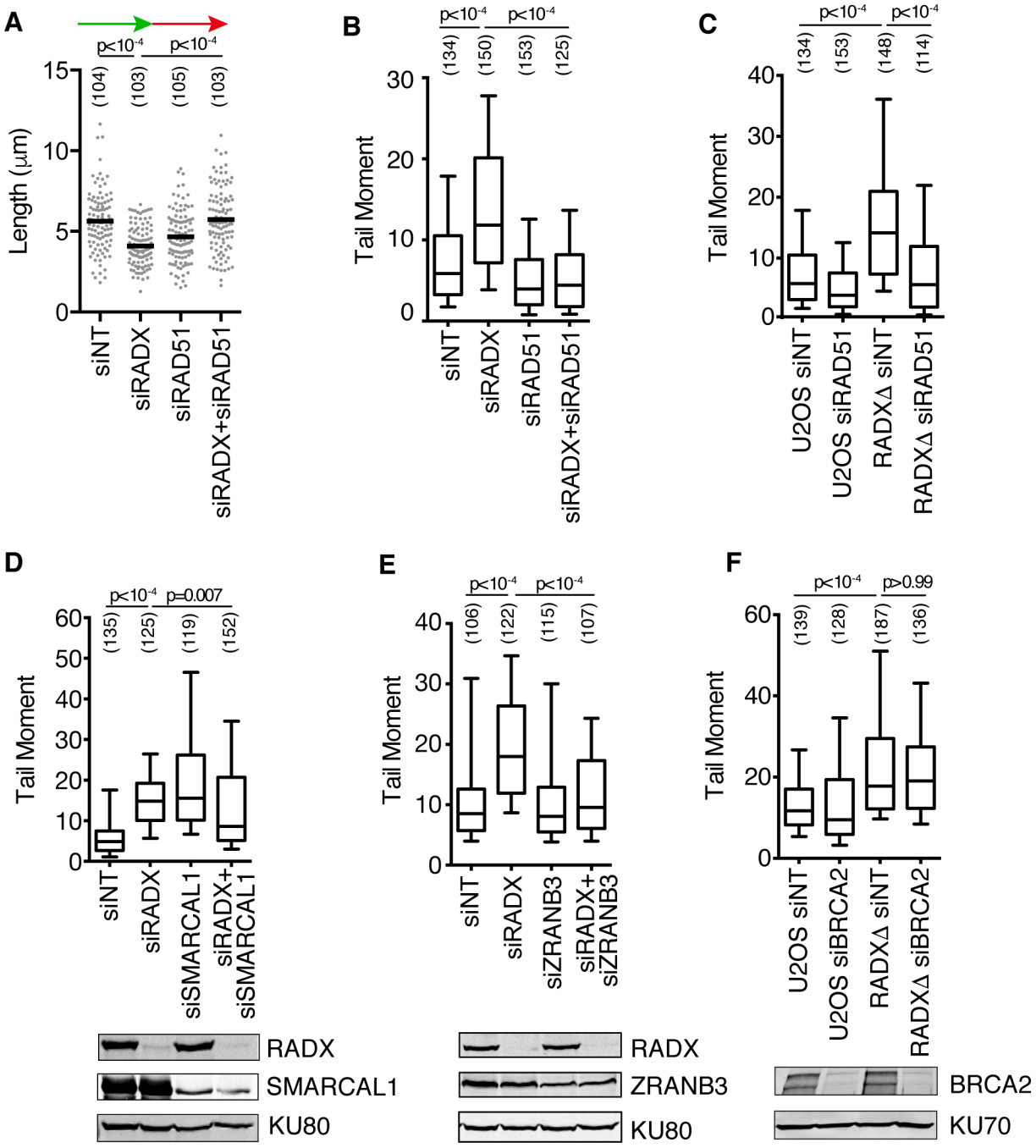

Figure 4.12. Excessive RAD51 activity causes fork collapse in RADX-deficient cells. (A) U2OS cells transfected with siRNAs were labeled with IdU (15 min) followed by CldU (15 min). CldU fiber lengths are plotted. (B-F) DSBs were measured by neutral comet assay in parental or RADXΔ U2OS cells transfected with siRNAs. The number of DNA fibers or comet tails examined is indicated in parentheses. P-values were calculated with a Mann Whitney test in A or a Kruskal-Wallis ANOVA and Dunn's post-test in all other panels. Experiments are representative of at least two replicates. Immunoblots depicting RADX, BRCA2, SMARCAL1 or ZRANB3 knockdown as indicated are provided as insets.

Since a DSB repair activity of RAD51 is unlikely to explain why we observe less fork breakage after silencing RAD51 in RADX-deficient cells, we considered the other known activities of RAD51 at replication forks. RAD51 is required for fork reversal (Zellweger et al., 2015) and replication fork stabilization (Schlacher et al., 2011). Unregulated fork reversal has previously been shown to lead to fork collapse (Bansbach et al., 2009; Couch et al., 2013; Sogo et al., 2002), so we considered the possibility that excessive fork reversal underlies the increase in DSBs observed in RADX-deficient cells. To test this idea, we asked whether depletion of the fork reversal enzymes SMARCAL1 and ZRANB3 could also rescue the fork collapse seen in RADX-deficient cells. As previously noted, SMARCAL1 depletion in wild-type cells increases DSB frequency (Bansbach et al., 2009; Ciccia et al., 2009; Yuan et al., 2009; Yusufzai et al., 2009). Nonetheless, depleting SMARCAL1 or ZRANB3 in RADX-deficient cells reduces the DSBs observed (Figures 4.12 D and 4.12E). Thus, these data suggest that RADX is needed to prevent inappropriate RAD51-, ZRANB3- and SMARCAL1-dependent fork remodeling that results in slow forks and cleavage by MUS81, and support the idea that the proper equilibrium between fork reversal and fork restoration is essential to prevent aberrant fork processing (Couch and Cortez, 2014). Interestingly, unlike RAD51, ZRANB3 and SMARCAL1, silencing BRCA2 did not decrease the DSBs seen in RADX-deficient cells (Figure 4.12F), consistent with previous observations that some RAD51 functions at forks are independent of BRCA2 (Chaudhuri et al., 2016; Tarsounas et al., 2003).

Deleting RADX restores fork protection to BRCA2-deficient cells without restoring HDR

BRCA2 is needed to stabilize RAD51 filaments and prevent fork degradation (Schlacher et al. 2011). Since our data indicates that RADX antagonizes RAD51 at replication forks, we tested whether removing this negative regulator might be sufficient to rebalance RAD51 functions and reverse the nascent strand degradation observed in BRCA2-deficient cells. Indeed, RADX silencing rescued the degradation phenotype that is observed upon BRCA2-silencing (Figures 4.13A, 4.13B and 4.13E). RADX

depletion also restored fork protection to the *BRCA2*-mutant CAPAN-1 pancreatic cell line (Figures 4.13C and 4.13E). Thus, RADX inactivation is capable of compensating for the decreased stability of RAD51 at forks in BRCA2-deficient cells. In addition, overexpression of RADX causes an increase in degradation, arguing that RADX antagonizes RAD51 at forks (Figures 4.13D and 4.13E).

We next asked whether RADX-silencing would affect the DSB repair activities of RAD51 and BRCA2. RADX silencing by itself has no effect on the rate of HDR (Figure 4.14A), as would be expected for a RAD51 antagonist since RAD51 overexpression does not change the rate of HDR (Stark et al., 2004). RADX silencing also does not restore the ability of RAD51- or BRCA2-deficient cells to perform HDR at a site-specific DSB (Figures 4.14A and B). This failure to restore HDR persists even when we titrated the amount of RAD51 siRNA to yield only a partial HDR-defect (Figure 4.14C). However, overexpression of RADX can interfere with RAD51 recruitment to DSBs and decrease the efficiency of HDR (Figures 4.14D,E), indicating that if RADX is too highly expressed it can interfere with DSB repair. If RADX is an antagonist of RAD51, then we would expect that silencing RADX might increase the frequency of single-strand annealing repair of DSBs since overexpression of RAD51 has this effect (Stark et al., 2004). As predicted, we did observe a modest increase in the frequency of single-strand annealing as measured by an SA-GFP assay in RADX-deficient cells (Figure 4.14F).

Finally, break repair at replication forks may be different than at site-specific DSBs (Willis et al., 2014). Therefore, we examined the rate of sister chromatid exchanges (SCEs) in RADX deficient cells to monitor HDR at forks. The BLM helicase, which functions as an anti-recombinase, prevents excessive SCEs (Sarbajna and West, 2014); however, we did not observe a large induction of SCEs in RADX deficient cells (Figure 4.14G). A small SCE increase (that was not statistically significant) was observed after RADX silencing in multiple experiments. This small increase may result from the increased fork breakage in these cells. However, these data suggest that RADX is not a general anti-recombinase.

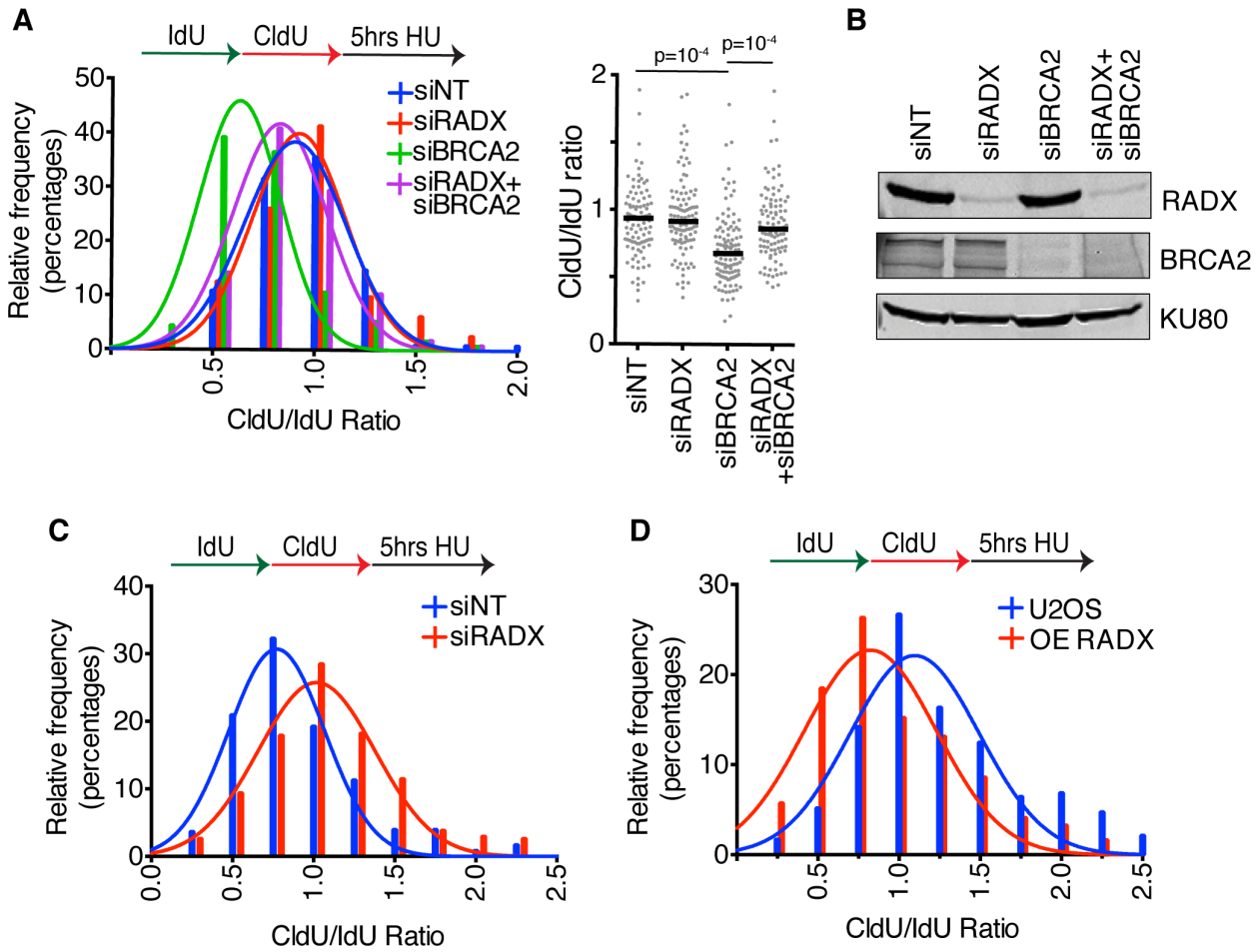

E

Figure	Sample	Median CldU/IdU ratio	Number of fibers analyzed
4.13A	U2OS siNT	0.93	101
	U2OS siRADX	0.91	111
	U2OS siBRCA2	0.67	112
	U2OS siRADX+siBRCA2	0.86	105
4.13B	CAPAN-1 siNT	0.78	203
	CAPAN-1 siRADX	0.99	204
4.13C	U2OS Mock	1.176	232
	U2OS RADX OE	0.87	243

Figure 4.13. RADX depletion in BRCA2-deficient cells prevents nascent strand degradation. (A, C and D) Cells were labeled with IdU and CldU prior to treatment with 3mM HU for five hours. The lengths of DNA fibers were scored and plotted as histograms and dot plots. P-values were derived using Mann Whitney test. Experiments are representative of at least two repeats. The cells used were U2OS cells with siRNA (A), CAPAN-1 cells transfected with siRNA (B), or (U2OS cells overexpressing RADX (OE) in (C). (E) Summary of the median CldU/IdU ratio and number of fibers analyzed for the single-molecule nascent strand degradation assay.

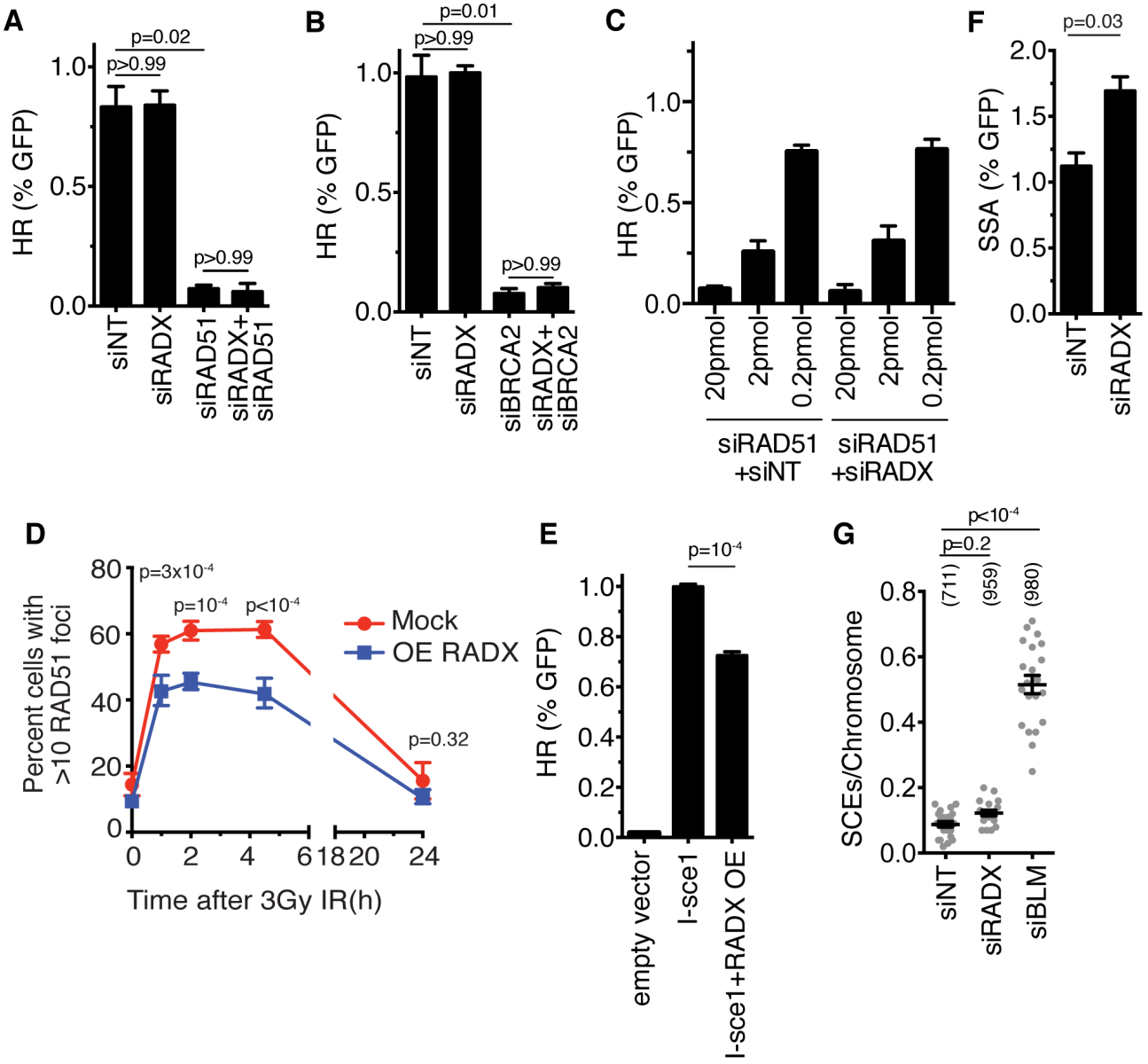

Figure 4.14. RADX deletion does not restore HR in BRCA2/RAD51-compromised cells (A-C) The percentage of DR-GFP-positive U2OS cells after transfection with siRNAs and I-SceI expression vector. In (C) the concentration indicates the amount of RAD51 siRNA used in each sample. (Mean+/-SD, n=3 in which 25,000 cells were scored per experiment). (D) Mock and GFP-RADX overexpressing U2OS cells were irradiated (3 Gy) and then allowed to recover for the indicated times before staining for RAD51. The number of cells with >10 RAD51 foci after detergent extraction is presented (Mean+/-SEM from n=3). P value derived from a two-way ANOVA with Sidak's post test for multiple comparisons. (E) The percentage of GFP-positive DR-GFP-U2OS cells after transfection with the indicated vectors was measured by flow cytometry. The mean and SEM from three experiments in which 25,000 cells were scored is depicted. (F) The percentage of SA-GFP-positive U2OS cells after transfection with siRNAs and I-SceI expression vector. (Mean+/-SD, n=3 in which 25,000 cells were scored per experiment). (G) The number of sister chromatid exchanges per chromosome were scored in U2OS cells transfected with siRNAs. The experiment is representative of three repeats. The number of chromosomes analyzed is indicated in parentheses.

RADX deletion causes chemo- and PARP-inhibitor resistance in BRCA2/RAD51-compromised cells

Although the ability of RADX to antagonize RAD51 function in the absence of replication stress may be important to prevent unwanted fork processing, RAD51 also has critical functions to protect and repair damaged replication forks (Hartlerode and Scully, 2009; Schlacher et al., 2011; Zellweger et al., 2015). Thus, reducing RAD51 expression with siRNA causes hypersensitivity to replication stress agents including HU, cisplatin, and camptothecin (Figures 14.15A-D). Since RADX antagonizes RAD51 activity at forks, and restores fork protection to BRCA2-depleted cells, we tested whether removing RADX might also be sufficient to suppress the hypersensitivity of cells with reduced BRCA2/RAD51 function. Indeed, siRNA depletion of RADX suppressed the HU, cisplatin, and camptothecin hypersensitivity of cells with reduced RAD51 expression (Figures 14.15A-D). I also observed similar results in the RADXΔ cells (Figure 14.16).

RADX deletion also increases the viability of BRCA2-silenced cells in the absence of damage (Figure 14.17A), and partially rescues the hypersensitivity of the BRCA2-silenced cells to low doses of PARP inhibitor (Figure 14.17B). However, RADX deficiency does not rescue the hyper-sensitivity of BRCA2-silenced cells to ionizing radiation, consistent with its function being largely confined to replication forks (Figure 14.17C). Thus, RADX silencing causes resistance to cancer therapies in BRCA2-compromised cells and this resistance correlates with restoration of replication fork stability without changes in HDR. Finally, overexpression of RADX increases cellular sensitivity to Olaparib consistent with overexpression causing fork degradation and inhibiting HDR (Figure 14.17D).

Brca2 is essential for the viability of mouse embryonic stem cells (mESC) (Kuznetsov et al., 2008). To test if RADX knockdown can rescue the lethality of *Brca2* null mESC, we knocked down RADX in PL2F7 mESC (Kuznetsov et al., 2008), which have one null and one conditional knockout allele of *Brca2* (Figure 14.17E). We then expressed Cre recombinase in these cells to delete the *Brca2* conditional allele and checked for the presence of viable *Brca2* null cells as described previously (Ding et al., 2016). Usually

deletion of *Brca2* in mESC results in no viable clones (Chaudhuri et al., 2016; Ding et al., 2016; Kuznetsov et al., 2008); however, 19% (18 out of 96) of the cell clones recovered from the RADX knockdown population were *Brca2* null (Figure 14.17F). Thus, RADX silencing can suppress the lethality caused by *Brca2* deletion, although these cells did grow more slowly than those that did not delete *Brca2*.

Intriguingly, breast and lung cancer patients with high levels of RAD51 tend to do poorly as compared to patients with lower levels (Figure 14.18). Conversely, patients with higher levels of RADX tend to survive better. These patients are often treated with chemotherapeutic agents that cause replication stress, suggesting that modulation of RAD51 function by RADX could impact cancer patient responses to treatments targeting DNA replication and DNA repair.

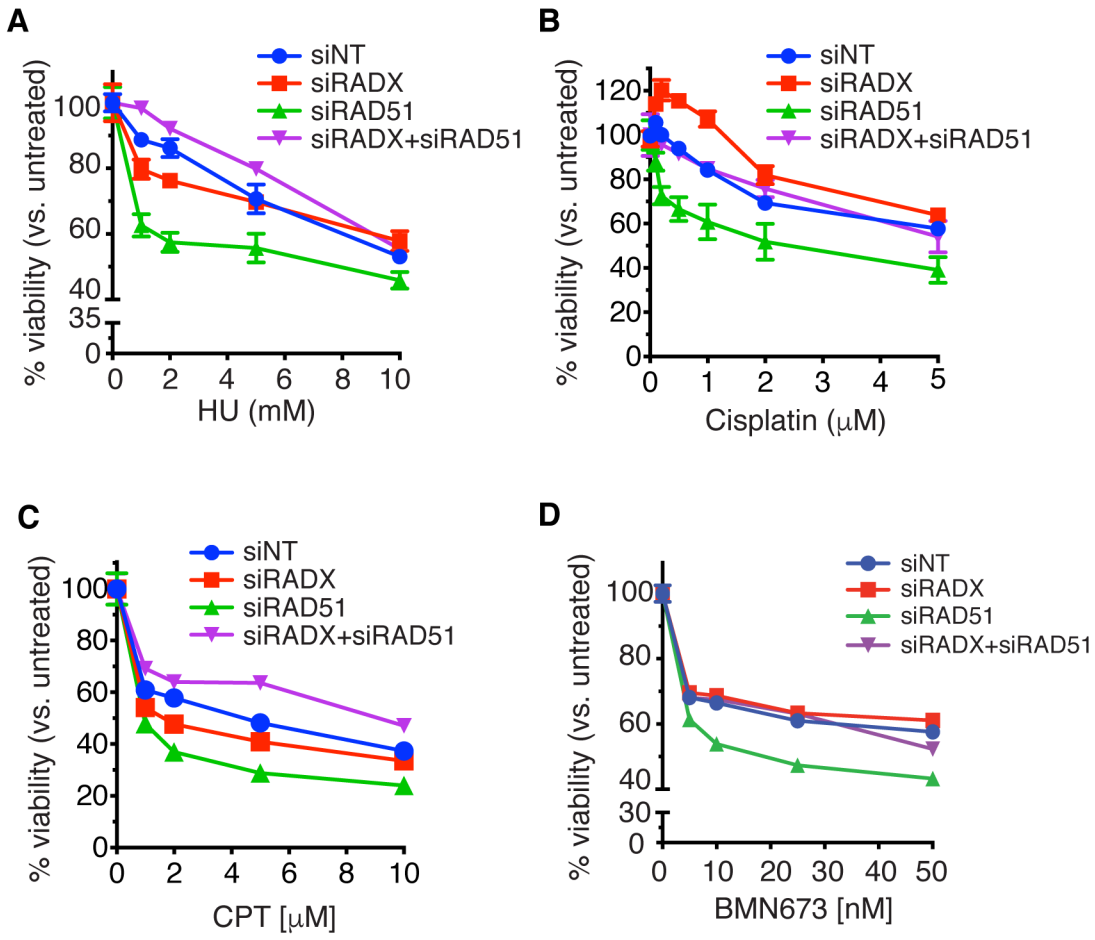

Figure 4.15. RADX depletion rescues the chemotherapy hypersensitivity of RAD51- depleted cells. (A-D) Cells transfected with siRNAs were treated with HU, camptothecin, cisplatin or BMN673 and viability was measured 72 hours later. (mean+/-SEM, n=3).

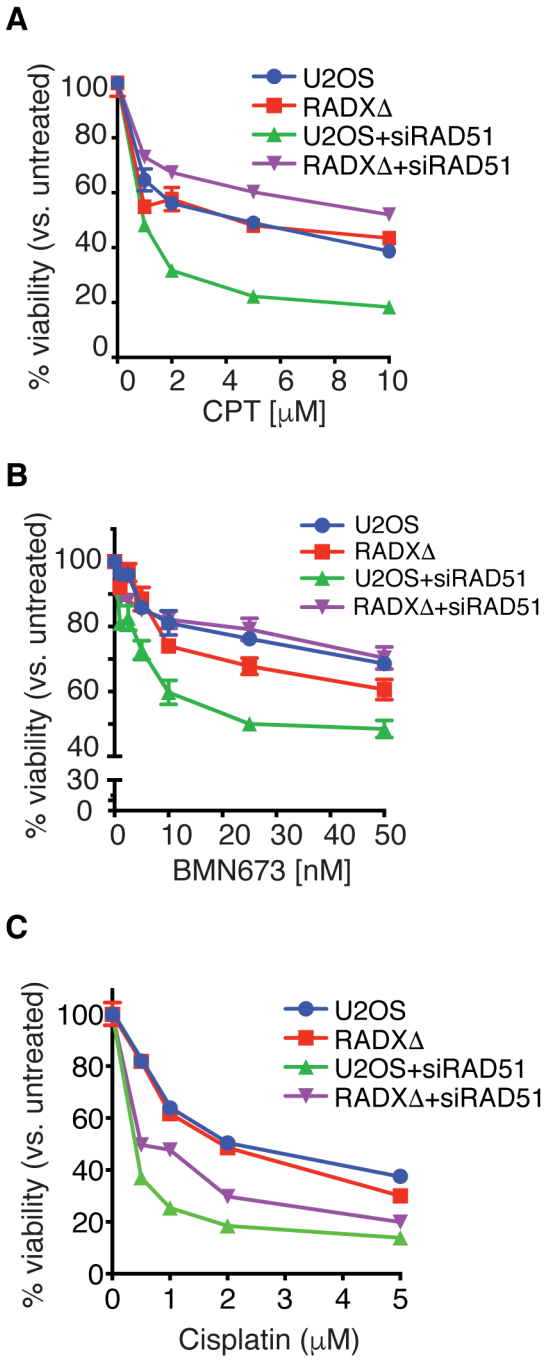

Figure 4.16. RADX deletion rescues the chemotherapy hypersensitivity of RAD51- depleted cells. (A-D) RADXΔ or WT U2OS cells transfected with siRNAs were treated with camptothecin, BMN673 or cisplatin and viability was measured 72 hours later. (mean+/-SEM, n=3).

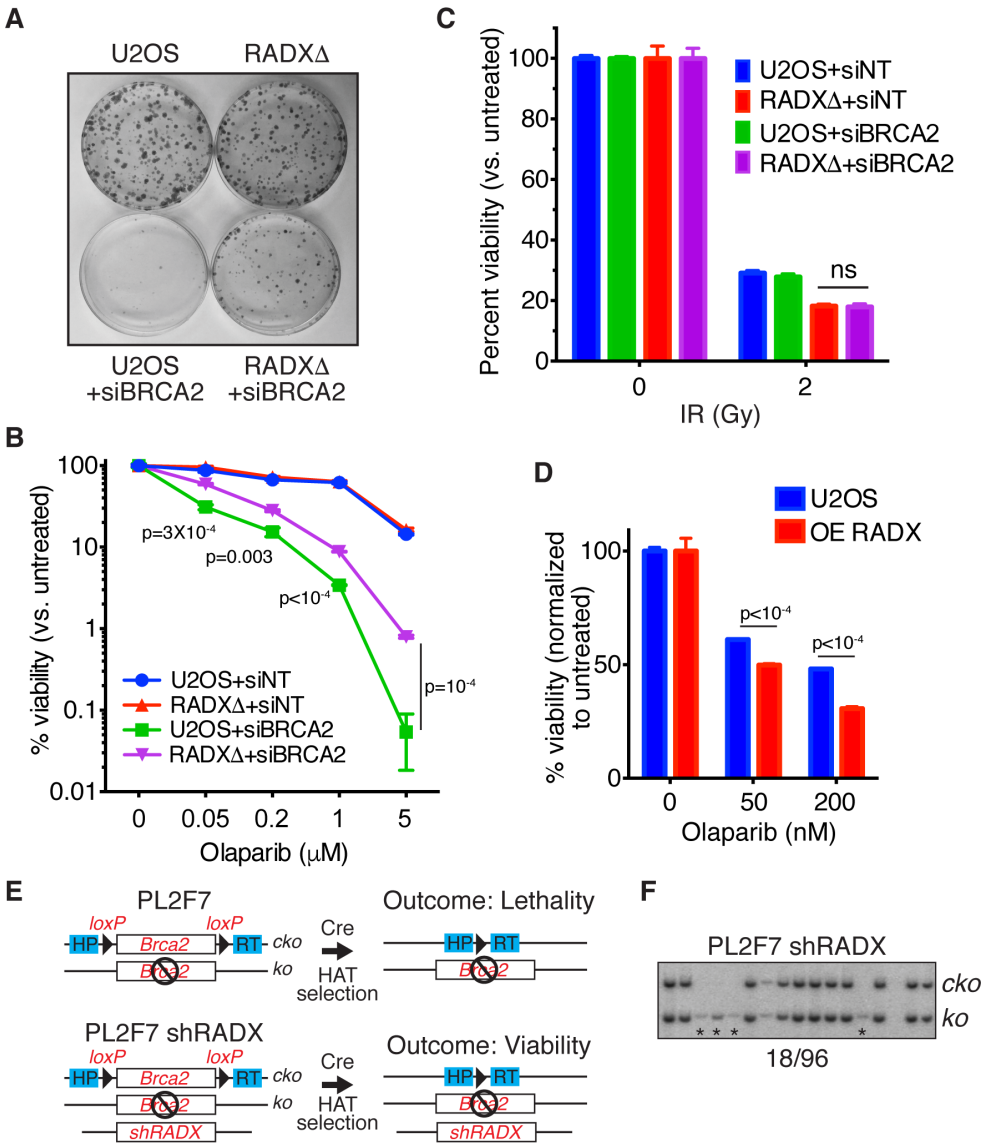

Figure 4.17. RADX depletion rescues the chemotherapy hypersensitivity of BRCA2-depleted cells. (A) Parental or RADXΔ U2OS cells transfected with non-targeting or BRCA2 siRNAs to achieve extensive knockdown were plated in the absence of drug and surviving colonies examined by methylene blue staining. (B) siRNA transfected cells were treated with the indicated concentrations of Olaparib, and surviving colonies were quantified. (mean+/-SD, n=3). P-values derived from unpaired t-tests corrected for a 1% FDR are shown for differences between siBRCA2 knockdown in U2OS and RADXΔ cells. The overall ANOVA-derived p value for these two curves is $<10^{-4}$. (C) Parental or RADXΔ U2OS cells transfected with the BRCA2 siRNAs were either untreated or treated with 2Gy. Surviving cell colonies were stained and scored. (mean+/-SD, n=3). The experiment was completed in triplicate. (D) Parental and RADX overexpressing U2OS cells were treated with Olaparib and viability of surviving colonies quantified (mean +/- SEM, n=3). P-values were derived from FDR-corrected, unpaired t-tests. (E) Schematic of the PL2F7 mESC cell model (*cko*, *Brca2* conditional knockout allele). (F) Representative southern blot from clones showing the rescue of *Brca2* null mESC cell lethality with RADX knocked-down by shRNA. Asterisks depict the rescued null cells, which grew slower yielding less genomic DNA. All viability experiments are representative of at least two replicates. This was performed by Xia Ding.

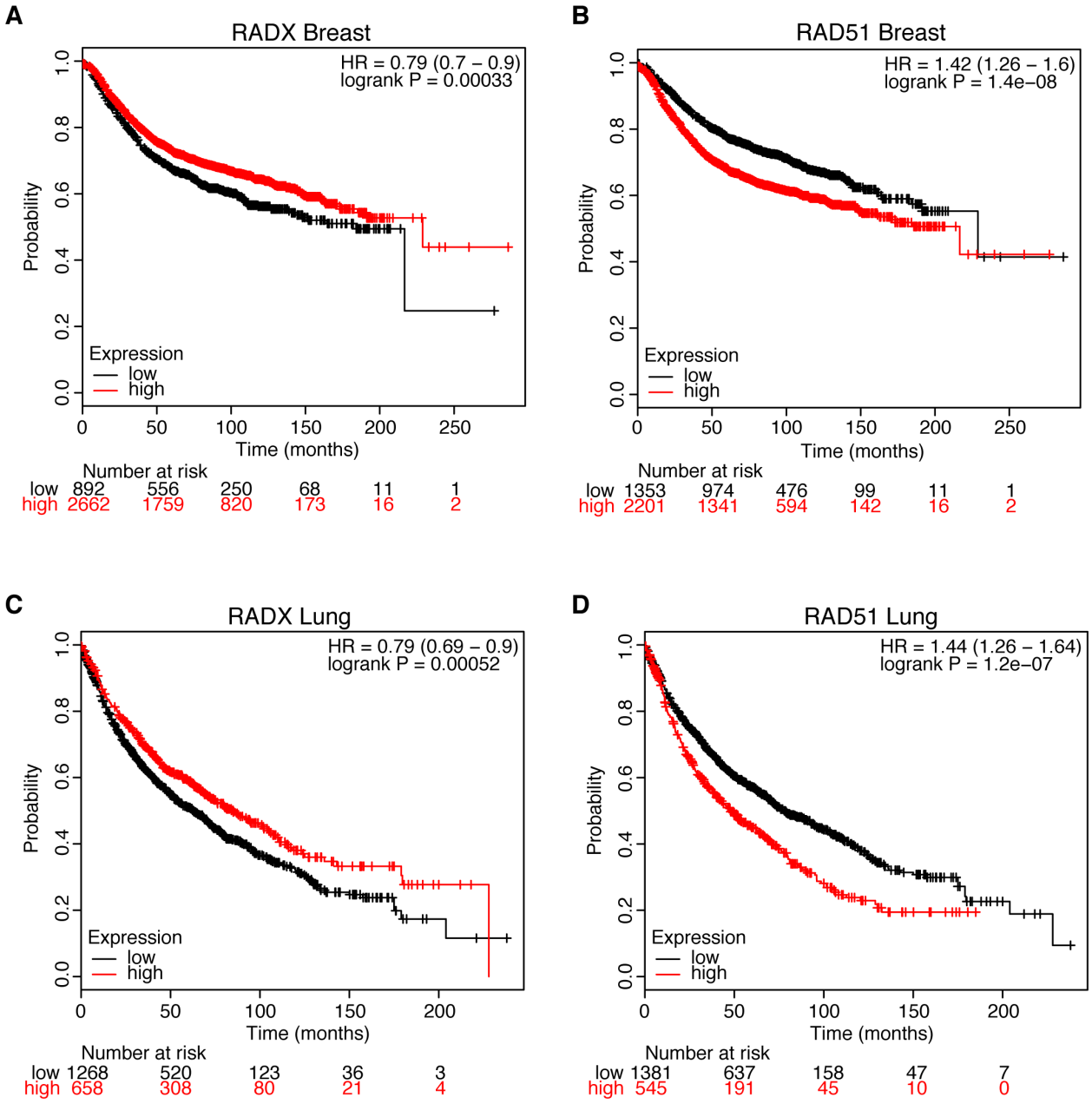

Figure 4.18. RADX and RAD51 expression correlations with patient outcome. (A-D) Kaplan Meier plots of RADX and RAD51 mRNA expression and correlation with patient outcome in breast and lung cancers were derived from KM plotter (Szász et al., 2016). Settings for all graphs were as follows: auto select best cutoff, only JetSet best probe, remove redundant samples, and exclude biased arrays. David Cortez generated this figure.

Discussion

Here, we report the identification of RADX as a new ssDNA binding protein with similarity to RPA, but with a specific activity in maintaining genome stability by regulating RAD51 function at replication forks. Strikingly, excessive RAD51 activity at forks slows elongation and leads to fork collapse when RADX is absent. In addition, loss of RADX confers chemotherapy resistance and restores fork protection in BRCA2-defcient cancer cells even though it cannot rescue HDR. We propose that RADX antagonizes RAD51 activities at replication forks to ensure the proper balance of fork remodeling and protection without interfering with the capacity of cells to complete HDR of DSBs. These results highlight that achieving the right balance of RAD51-dependent fork remodeling is critical for genome stability.

RADX prevents fork collapse

Our data support the following model: RAD51, SMARCAL1, and ZRANB3 promote fork reversal reactions to stabilize stalled replication forks (Bétous et al., 2012, 2013a; Ciccia et al., 2012; Zellweger et al., 2015). However, fork reversal can be dangerous since inappropriate fork reversal would slow fork elongation and can result in fork cleavage by structure specific nucleases (Bansbach et al., 2009; Couch and Cortez, 2014; Couch et al., 2013; Sogo et al., 2002). RADX is an essential regulator of these processes. It binds ssDNA and prevents inappropriate accumulation of RAD51 at replication forks. This regulation ensures the right balance of active fork elongation and RAD51/SMARCAL1/ZRANB3-mediated fork reversal (Figure 14.19A). Too much or too little fork reversal causes DNA damage and fork collapse. Thus, RADX works in parallel to other regulatory mechanisms of fork regression including phosphorylation of SMARCAL1 by ATR (Couch et al., 2013), and regulation of SMARCAL1 substrate preference by RPA (Bétous et al., 2013a; Bhat et al., 2015) to prevent fork collapse. Interestingly, while

RAD51-, SMARCAL1- and ZRANB3- silencing rescues the DSBs seen in RADX-deficient cells, BRCA2-loss does not. Mechanistically, this result indicates that RAD51 has BRCA2-independent functions and can be explained if BRCA2 is not required for RAD51-dependent fork reversal. This hypothesis will require direct testing with electron microscopy analyses of replication intermediates, but it is consistent with other reports which have found that BRCA2 is dispensable for some RAD51 functions at replication forks (Chaudhuri et al., 2016; Tarsounas et al., 2003).

BRCA2 stabilizes RAD51 at forks to protect them from MRE11-dependent degradation (Ciccia and Elledge, 2011; Schlacher et al., 2011) (Figure 14.19B). Lack of fork protection in *BRCA2*-mutant cells causes sensitivity to DNA damaging agents and PARP inhibitors (Schlacher et al. 2011; Chaudhuri et al. 2016). RADX deletion stabilizes the nascent DNA strands in BRCA2-deficient cells and causes chemoresistance. The simplest explanation is that it does so by rebalancing the functions of RAD51. In other words, removal of the negative RAD51 regulator (RADX) makes the positive regulator (BRCA2) dispensable at forks, but not at resected DSBs. This proposal is consistent with the ability of RAD51 overexpression to suppress the fork instability of BRCA2-deficient cells (Schlacher et al., 2012).

Importantly, HDR silencing RADX in BRCA2- or RAD51-deficient cells did not restore HDR. The amount of ssDNA at a stalled fork versus at resected DSBs may be key to explaining why RADX deletion suppresses RAD51 defects at forks, but not at DSBs. Moreover, this idea clarifies the need for a protein like RADX to regulate the fork protection activities of RAD51. Successful HDR involves extensive DSB resection and RAD51 filament formation; whereas electron microscopy analyses indicates that there are only short stretches of ssDNA at normal and stalled forks (Hashimoto et al., 2010; Ray Chaudhuri et al., 2012; Zellweger et al., 2015). Therefore, deletion of RADX may be sufficient to restore enough RAD51 function to maintain fork protection in BRCA2-deficient cells. However, it cannot suppress defects associated with DSBs because of a need for more RAD51 protein for HDR. Thus, modulation of RAD51 fork binding by RADX provides a finely tuned regulatory mechanism to yield the right amount of fork reversal and nascent strand stabilization while maintaining a high capacity for repair of DSBs by HDR.

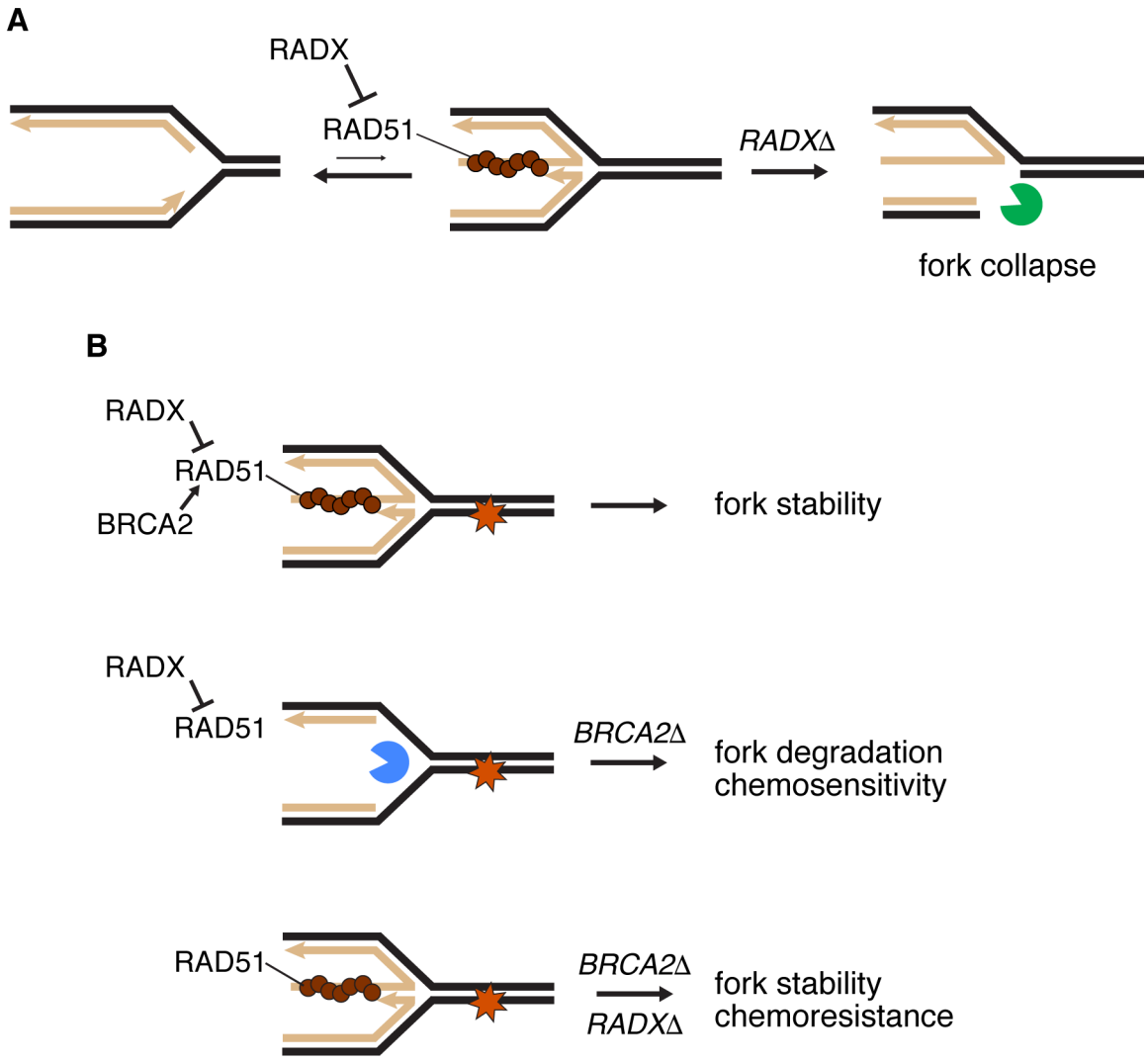

Figure 4.19. Model for RADX function. See text for details

Alternative models include the possibility that RADX directly recruits proteins such as MRE11 that degrade the nascent DNA in BRCA2- or RAD51-deficient cells, or that RADX binds to RAD51 directly to regulate its fork reversal and protection functions. Although these models cannot be excluded, we note that there was no RADX-dependent change in MRE11 levels at stalled forks and we have not been able to detect an interaction between RADX and MRE11 or RAD51 in preliminary screens for RADX-binding proteins.

In addition to RADX, cells have additional ways of fine-tuning RAD51 function through negative regulation. For example, the BLM helicase counteracts recombination during replication to prevent excessive sister chromatid exchanges (Larsen and Hickson, 2013). In addition, cyclin-dependent kinase phosphorylation of the C-terminus of BRCA2 disrupts its ability to stabilize RAD51 filaments and regulates fork protection (Davies and Pellegrini, 2007; Esashi et al., 2005; Schlacher et al., 2011). This multitude of both positive and negative regulatory mechanisms emphasizes the importance of appropriately balancing RAD51 activities.

Functional similarity to RecX

RAD51 is the eukaryotic homolog of bacterial RecA. Like RAD51, RecA also acts at stalled replication forks to promote fork reversal and block extensive nuclease degradation of DNA (Horii and Suzuki, 1968; Robu et al., 2001; Satta et al., 1979). RecA is aided in its fork protection function by the RecFOR proteins that mediate the loading and stabilization of RecA onto ssDNA similar to BRCA2 (Chow and Courcelle, 2004; Courcelle et al., 1997). The *recX* gene is often linked to *recA* in bacterial genomes. For example, *E. coli recX* is expressed from the *recA* promoter but at reduced transcript levels (Pagès et al., 2003). RecX suppresses the growth inhibitory consequences of RecA overexpression and acts to inhibit RecA by binding RecA-DNA filaments (Cox, 2007). Thus, RecX helps establish the proper balance

of RecA activities. We propose that RADX serves a similar function in vertebrate cells although the details of the mechanism differ.

Clinical implications

Many cancers are caused by inactivation of *BRCA2*, a property that makes the tumor cells hypersensitive to chemotherapies and PARP inhibitors. However, drug resistance is a problem. Most described resistance mechanisms involve the acquisition of secondary *BRCA2* mutations that result in a functional protein, or the re-establishment of HDR (such as by loss of 53BP1, a key antagonist of the HDR pathway) (Lord et al., 2015). However, resistance can be generated without restoring HDR (Guillemette et al., 2015), and recent studies described two mechanisms that contribute to resistance by restoring fork protection to *BRCA2*-deficient cells (Chaudhuri et al., 2016; Ding et al., 2016). These studies also indicated that there are as yet undiscovered mechanisms of fork protection that are relevant to tumor chemotherapy resistance. RADX inactivation should be considered as a candidate mechanism contributing to resistance.

The amount of functional RAD51 is important for both the etiology and treatment of cancer. Low activity can yield genome instability through defects in fork protection and HDR, but it also improves the cell killing by chemotherapeutics and PARP inhibitors (Budke et al., 2016; Quiros et al., 2011). On the other hand, RAD51 overexpression causes genome instability (Klein, 2008; Richardson et al., 2004), and RAD51 is frequently overexpressed in cancers (Klein, 2008). Thus, excessive RAD51 activity may drive tumorigenesis and generate drug resistance (Klein, 2008; Mason et al., 2014b; Tennstedt et al., 2013). Since RADX loss mimics RAD51 overexpression and reduces the PARP inhibitor sensitivity of BRCA2-deficient cells, it will be important to determine if RADX functionality is a determinant of how tumors respond to therapy.

CHAPTER V

RADX REGULATES FORK PROTECTION BY MODULATING RAD51 FUNCTION[3]

Introduction

RAD51 usually requires mediators like BRCA2 to be localized to sites of ssDNA. Thus, the functions of RAD51 in fork protection and DSBR are absolutely dependent on BRCA2. Interestingly, the fork reversal function of RAD51 is independent of BRCA2 (Dungrawala et al., 2017; Kolinjivadi et al., 2017a; Mijic et al., 2017; Taglialatela et al., 2017). Thus, *BRCA2*-deficient cells exhibit a loss of fork protection but do not have any defects in fork reversal (Mijic et al., 2017; Schlacher et al., 2011). How RAD51 gains access to the stalled fork without BRCA2 to mediate an exchange with RPA is unknown. Nonetheless, the need for RAD51 to promote reversal (which is a prerequisite for nascent strand degradation) explains why silencing RAD51 using RNA interference does not cause degradation (Mijic et al., 2017; Thangavel et al., 2015; Zellweger et al., 2015). However, some RAD51 mutations and inhibitors do yield fork degradation (Dungrawala et al., 2017; Kolinjivadi et al., 2017a; Leuzzi et al., 2016; Mijic et al., 2017; Su et al., 2014; Taglialatela et al., 2017; Zadorozhny et al., 2017) raising the possibility that either fork reversal is not always required for nucleases to degrade the nascent strands or these ways of inhibiting RAD51 only interfere with some of its activities.

[3] This chapter is derived from a manuscript currently in preparation and will be published as a first-author publication in 2018.

We recently identified a new SSB with similarity to RPA named RADX (RPA like, RAD51 antagonist on the X-chromosome). RADX negatively regulates RAD51 accumulation at replication forks (Dungrawala et al., 2017). Loss of RADX mimics RAD51 overexpression and RADX overexpression decreases RAD51 function. This regulation prevents inappropriate RAD51-dependent fork reversal in unstressed cells that can result in fork breakage by the structure-specific endonuclease MUS81 (Dungrawala et al., 2017). At persistently stalled forks, the negative regulation of RAD51 by RADX is overcome by the positive regulation conferred by BRCA2 to sustain fork protection. Consequently, knocking out RADX can restore fork protection to BRCA2-deficient cells (Dungrawala et al., 2017). This finding is consistent with the observation that RAD51 overexpression is also sufficient to confer fork protection to BRCA2-deficient cells (Schlacher et al., 2011). Thus, the data supports the hypothesis that the amount of RAD51 activity at forks determines whether they can be reversed and protected from nucleases, and upstream regulators of RAD51 including BRCA2 and RADX maintain the proper balance of these activities.

In addition to BRCA2-deficiency, loss of several other HR repair proteins, including BRCA1, also cause nascent-strand degradation (Higgs et al., 2015; Schlacher et al., 2012; Xu et al., 2017) (Figure 1). While the details of these pathways have not yet been fully worked out, they can be grouped into three categories (see Figure 1). First is the BRCA2 pathway in which MRE11-dependent nascent strand degradation arises from decreased RAD51 filament stability. BRCA1 and the Fanconi Anemia (FA) proteins are also proposed to be in this same genetic pathway since they also prevent MRE11-dependent degradation and their deficiency can be rescued by RAD51 overexpression (Schlacher et al., 2011, 2012). The second genetic pathway is exemplified by BOD1L, which is proposed to inhibit the anti-recombinases BLM and FBH1; thus, BOD1L promotes RAD51 stability indirectly by inhibiting negative regulators of RAD51. Interestingly, this pathway prevents DNA2-dependent degradation (Higgs and Stewart, 2016; Higgs et al., 2015); thus RAD51 destabilization causes MRE11-dependent degradation in some cases, and DNA2-

dependent degradation in others. The factors governing the choice of the nuclease in these pathways remain unclear.

The third pathway involves ABRO1 and also inhibits DNA2-dependent degradation of forks (Xu et al., 2017). Surprisingly, the ABRO1 pathway of fork protection is proposed to be distinct from the stabilization of RAD51 since RAD51 overexpression does not rescue nascent strand degradation in ABRO1-deficient cells (Xu et al., 2017).

How these pathways work together to maintain nascent strand stability and exactly what they do to control nuclease activity is still unclear (Higgs and Stewart, 2016; Kolinjivadi et al., 2017b). While RAD51 seems to be a nexus point in many of the mechanisms, there may be other control points. To add confusion, depleting RAD51 from cells has been reported to promote nascent strand stabilization in BRCA2 and ABRO1-defcient cells (Mijic et al., 2017; Taglialatela et al., 2017; Xu et al., 2017) and prevent fork breakage in RADX-deficient cells (Dungrawala et al., 2017).

In this study, we sought to further test the model that RADX acts as a RAD51 antagonist and use RADX as a tool to further investigate how fork protection pathways operate. If RADX is a RAD51 antagonist, then silencing RADX should restore fork protection in genetic conditions that interfere with the ability of RAD51 to stabilize the fork. Indeed, we find that RADX loss restores fork protection to BRCA1, BOD1L, FANCA and FANCD2-deficient cells as well as cells with mutant RAD51. Additionally, overexpression of RADX causes fork degradation that is genetically dependent on the same factors that are needed to degrade forks in BRCA2-deficient cells, including fork reversal enzymes and MRE11. Thus, RADX overexpression mimics loss of RAD51 function when forks are persistently stalled. We find that silencing RAD51 with RNA interference can yield either fork protection or fork reversal depending on how much RAD51 remains in the cell, reflecting a requirement for higher RAD51 levels to protect persistently stalled forks than to

promote fork reversal. Finally, RADX can compete with RAD51 to prevent it from forming filaments on ssDNA supporting the model that RADX is a RAD51 antagonist that ensures the right amount of RAD51 fork reversal and protection activities to maintain genome stability.

Results

RADX silencing suppresses MRE11-dependent fork degradation in cells with impaired RAD51 stability

Multiple proteins protect replication forks from nuclease digestion by promoting RAD51 filament stability (Figure 5.1). To test the hypothesis that reducing RADX levels would restore fork protection in genetic conditions that interfere with RAD51 filament stability, we utilized siRNA to silence BRCA1 in U2OS cells and induce nascent strand degradation as measured by the DNA fiber assay (Figure 5.2A and (Schlacher et al., 2012)). RADX silencing by itself had no significant effect. However, silencing RADX is sufficient to restore fork protection to BRCA1-depleted cells (Figure 5.2A).

In addition to their function in interstrand crosslink repair (Ceccaldi et al., 2016), the FA pathway proteins FANCA and FANCD2 are also required for replication fork protection and are thought to function in the same pathway as the BRCA1/2 proteins to prevent MRE11-dependent degradation (Schlacher et al., 2012). Indeed, silencing FANCA or FANCD2 in U2OS cells causes fork degradation (Figure 5.3A and 5.3B). Silencing RADX also restores fork protection to these cells (Figures 5.3A and B).

T131P is a FA-associated, dominant-negative RAD51 mutant allele (Wang et al., 2015). Patient derived fibroblasts harboring this mutation in one allele are defective in RAD51 fork protection, but are proficient in homologous recombination repair of double-strand breaks

(Kolinjivadi et al., 2017a; Mijic et al., 2017; Wang et al., 2015; Zadorozhny et al., 2017). As previously published, the T131P fibroblasts exhibit fork destabilization (Figure 5.3C and (Kolinjivadi et al., 2017a; Mijic et al., 2017; Zadorozhny et al., 2017)). We reasoned that since the cells harboring the T131P allele exhibit only a partial loss of RAD51 function (since they are completely proficient in HR and possess a WT allele), improving RAD51 function would restore fork protection in these cells. We tested this hypothesis by silencing RADX. As predicted, loss of RADX prevented the nascent strand degradation observed in the T131P cells (Figure 5.3C). This data further supports our model that RADX loss allows for increased RAD51 function.

Restoration of fork protection to BRCA1-deficient U2OS cells does not cause olaparib resistance

Fork protection has been proposed to be an important determinant of the chemosensitivity of BRCA-deficient cells to PARP inhibitors like olaparib (Chaudhuri et al., 2016; Ding et al., 2016). Consistent with this idea, RADX silencing not only confers fork protection to BRCA2-mutant cells, but also improves their viability and resistance to olaparib even though it does not alter homologous recombination (Dungrawala et al., 2017). Therefore, we tested if the restoration of fork protection in BRCA1-deficient *RADX*Δ cells is accompanied by an increase in cell viability and olaparib resistance. BRCA1 knockdown reduces the U2OS cell viability (Figure 3A). RADX deletion conferred a small, but significant, increase in viability to BRCA1-depleted cells in the absence of any drug (Figure 5.4A), consistent with what we observed after BRCA2-depletion (Dungrawala et al., 2017). However, unlike with BRCA2-silenced cells, RADX loss did not confer olaparib-resistance to BRCA1-depleted U2OS cells; suggesting that other functions of BRCA1 like HR are responsible for most of the sensitivity of BRCA1-deficient cells to olaparib (Figure 5.4B).

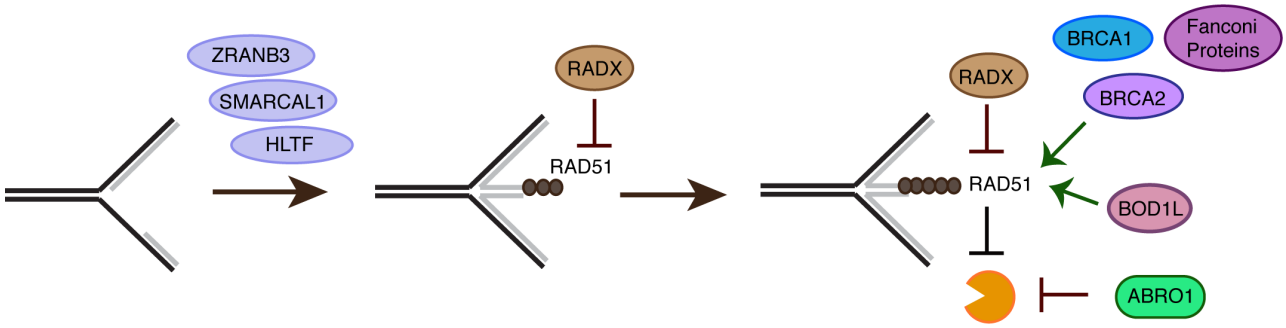

Figure 5.1. Model for RADX function at replication forks. Replication forks are reversed by SNF2 family DNA translocases, including SMARCAL1, ZRANB3 and HLTF, in cooperation with RAD51. BRCA2 stabilization of RAD51 filaments at the reversed fork is required for the inhibition of nuclease-mediated degradation of the nascent DNA. BRCA1 and the Fanconi Anemia (FA) proteins are also required for RAD51 stabilization and are thought to be in the same pathway as BRCA2. BOD1L promotes RAD51 stabilization by inhibiting the anti-recombinases BLM and FBH1, in a pathway that is distinct from BRCA2/BRCA1 and FA stabilization. ABRO1 protects replication forks from DNA2 dependent degradation in a RAD51-independent pathway. RADX negatively regulates RAD51 function in both fork reversal and protection.

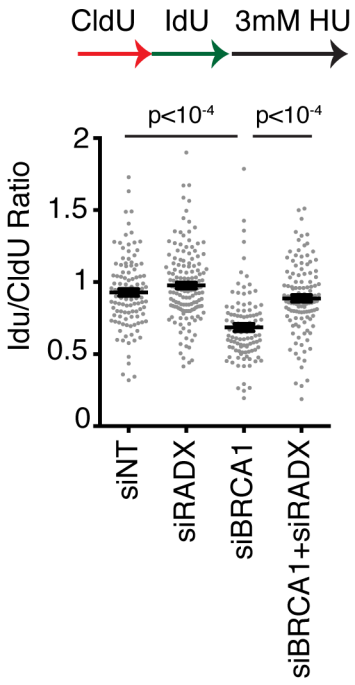

Figure 5.2. RADX loss restores fork protection to BRCA1-deficient cells. WT U2OS or transfected with the indicated siRNAs were labelled sequentially with CldU and IdU before treatment with 3mM HU for 5 hours. The lengths of 100 DNA fibers were measured and mean+/- SEM is depicted. P values derived from Kruskal-Wallis ANOVA with a Dunn's posttest.

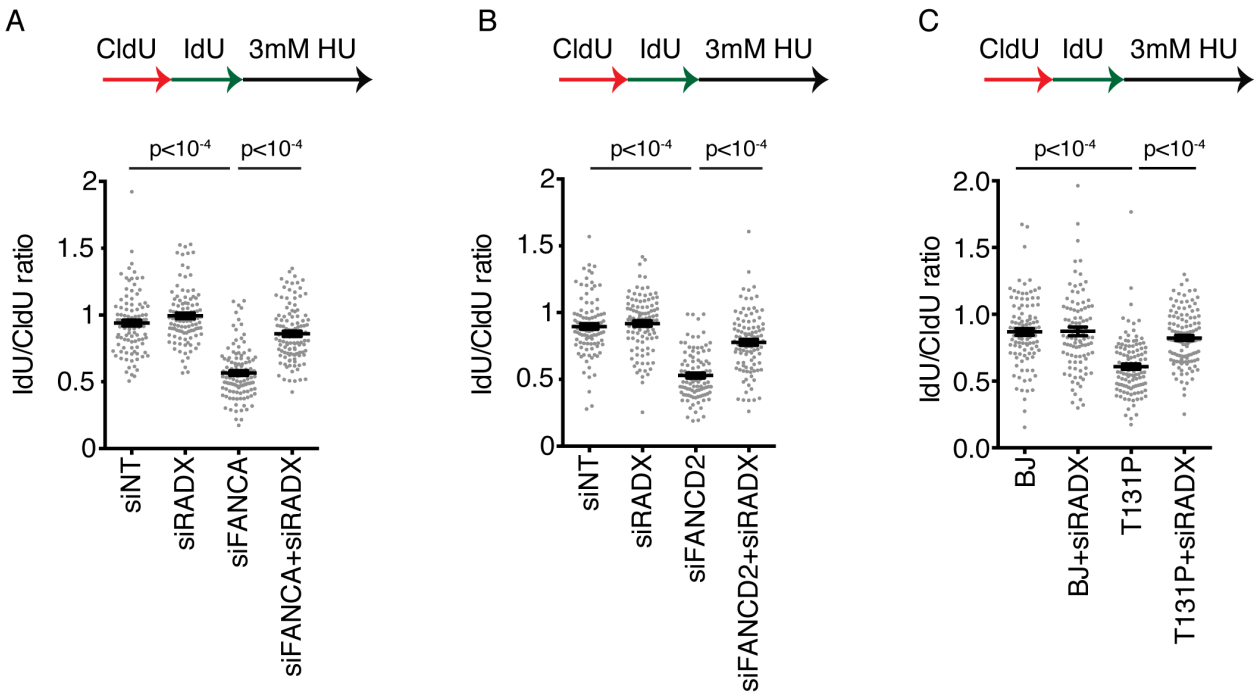

Figure 5.3. RADX silencing rescues the fork degradation caused by loss of the FA pathway or by partial loss of RAD51 function (A and B) U2OS cells transfected with the indicated siRNAs were labelled sequentially with CldU and IdU before treatment with 3mM HU for 5 hours. The lengths of 100 DNA fibers were measured and mean+/-SEM is depicted. P values derived from Kruskal-Wallis ANOVA with a Dunn's posttest. **(C)** Fibroblasts harboring a patient-derived mutation in RAD51 (T131P) and matched controls (BJ) were transfected with the indicated siRNAs and labelled sequentially with CldU and IdU, followed by treatment with 3mM HU for 5 hours. The lengths of 100 DNA fibers were measured and Mean+/-SEM is depicted. P values derived from Kruskal-Wallis ANOVA with a Dunn's posttest.

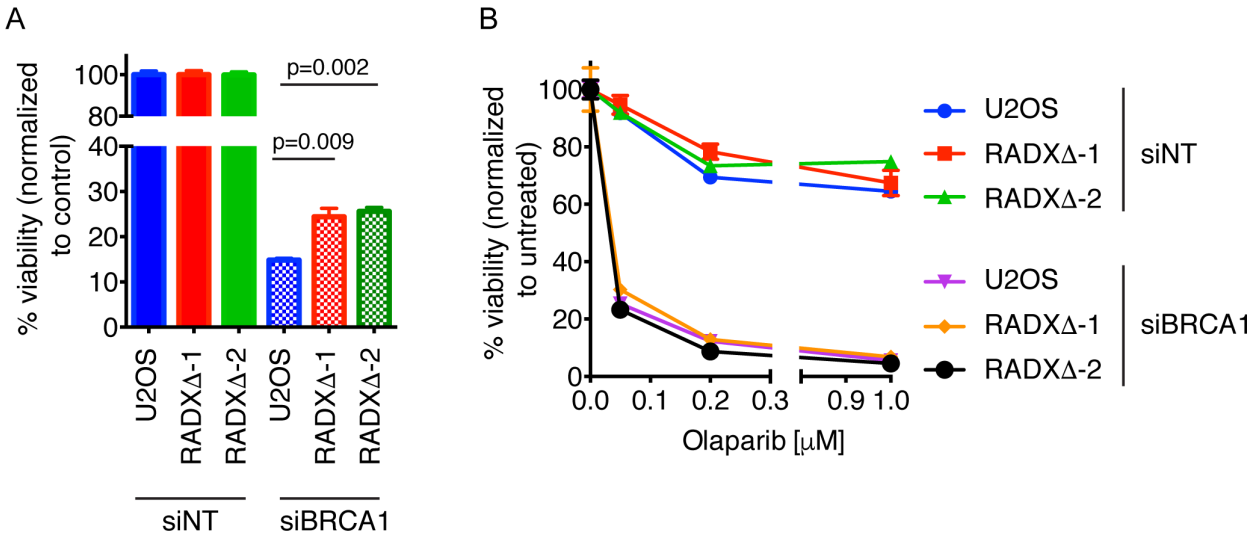

Figure 5.4. RADX loss does not confer chemoresistance to BRCA1-deficient U2OS cells.(A) Parental or RADXΔ U2OS cells were transfected with the indicated siRNAs and plated for clonogenic survival assays in the absence of drug. Mean+/-SEM is depicted. p values were calculated from a two-way ANOVA with Tukey's posttest. B) Parental or RADXΔ U2OS cells were transfected with the indicated siRNAs and plated for clonogenic survival assays. The cells were treated with the indicated concentrations of Olaparib, and surviving cell colonies were measured by methylene blue staining. Mean+/-SEM is depicted.

Loss of RADX protects against DNA2-dependent fork degradation

Thus far, our results indicate that silencing RADX can suppress fork degradation that is caused by RAD51 filament instability and MRE11 nuclease activity (Hashimoto et al., 2010; Mijic et al., 2017; Schlacher et al., 2011, 2012). Recently, the loss of BOD1L was reported to cause fork degradation that is MRE11-independent. Instead, DNA2 is required for degradation in BOD1L-deficient cells even though BOD1L is also thought to promote fork stability by promoting RAD51 stabilization at stalled forks (Higgs et al., 2015). To test if RADX also regulates fork protection in cases where the degradation is dependent on DNA2, we utilized siRNA against BOD1L and RADX. As reported previously, knocking down BOD1L causes DNA2-dependent nascent strand degradation (Figures 5.5A and 5.5B). RADX silencing restored fork protection to the BOD1L-deficient cells (Figure 5.5C). Thus, RADX deficiency restores fork protection irrespective of the nuclease mediating degradation.

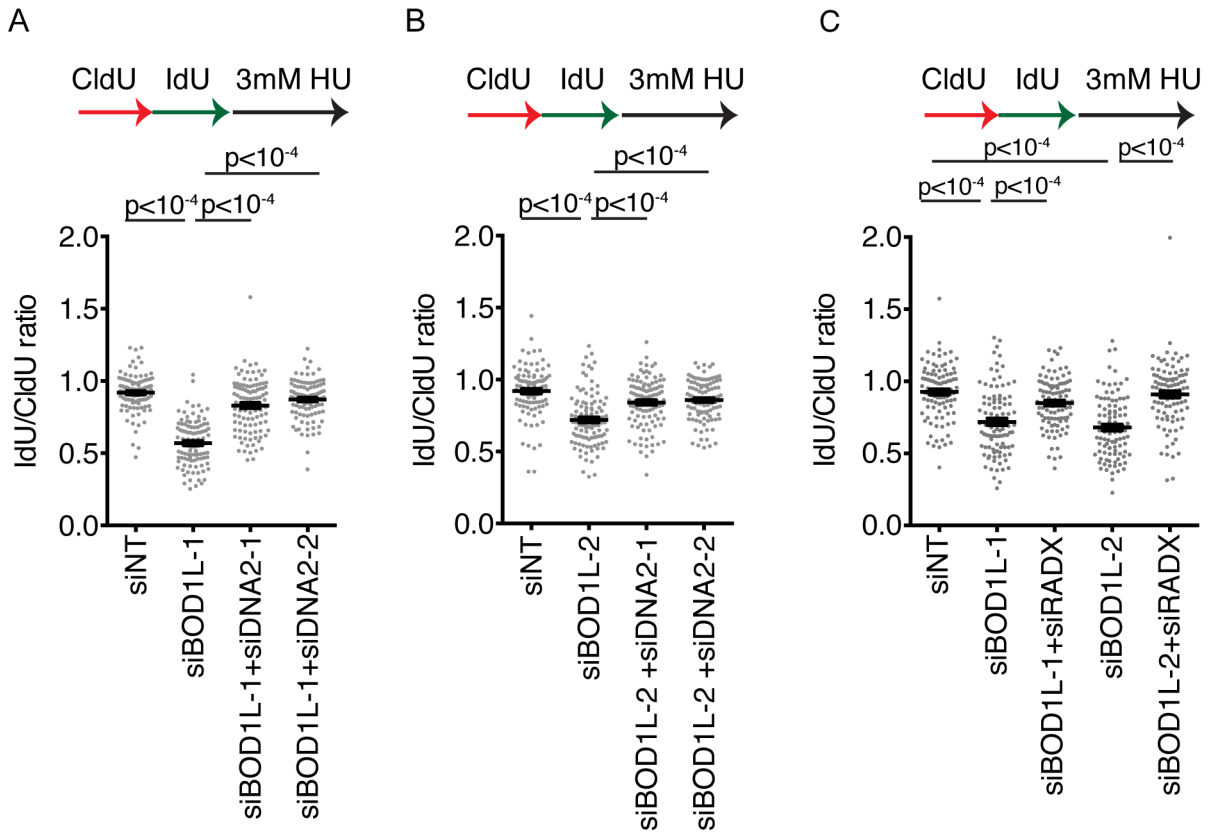

Figure 5.5. RADX silencing rescues DNA2 dependent fork degradation caused by loss of BOD1L. (A-C) U2OS cells transfected with the indicated siRNAs were labelled sequentially with CldU and IdU before treatment with 3mM HU for 5 hours. The lengths of 100 DNA fibers were measured and Mean+/-SEM is depicted. P values derived from Kruskal-Wallis ANOVA with a Dunn's posttest. All experiments in this figure were performed by Archana Krishnamoorthy.

Overexpression of RADX causes nascent strand degradation that is rescued by inhibition of MRE11 or ZRANB3

While silencing RADX can restore fork protection to RAD51-compromised cells, RADX overexpression causes nascent strand degradation (Dungrawala et al., 2017). If the fork degradation is due to reduced RAD51 function, then it should be dependent genetically on the same factors that cause nascent strand degradation in BRCA2-deficient cells including the MRE11 nuclease and ZRANB3 fork reversal enzyme (Figure 5.6A) (Kolinjivadi et al., 2017a; Mijic et al., 2017; Taglialatela et al., 2017). As predicted, inhibiting MRE11 (Figure 5.6B) or depleting ZRANB3 also rescue the fork degradation caused by RADX overexpression (Figure 5.6C). We also observed a partial rescue of the RADX overexpression-induced fork degradation by silencing DNA2 (Figure 5.7D). DNA2 silencing by itself led to a significant inhibition of fork degradation even in U2OS cells transfected with non-targeting siRNA (Figure 5.6D) – a result that is consistent with previous studies showing that these cells have a small amount of DNA2-dependent nascent strand degradation even without other genetic perturbations (Thangavel et al., 2015). Nonetheless, the ability of either DNA2 or MRE11 inhibition to rescue the fork degradation in RADX overexpression cells is consistent with the idea that RAD51 destabilization can lead to either MRE11-dependent degradation as in BRCA2-deficiient cells (Schlacher et al., 2011), or DNA2-dependent degradation, as in BOD1L-deficient cells (Higgs et al., 2015).

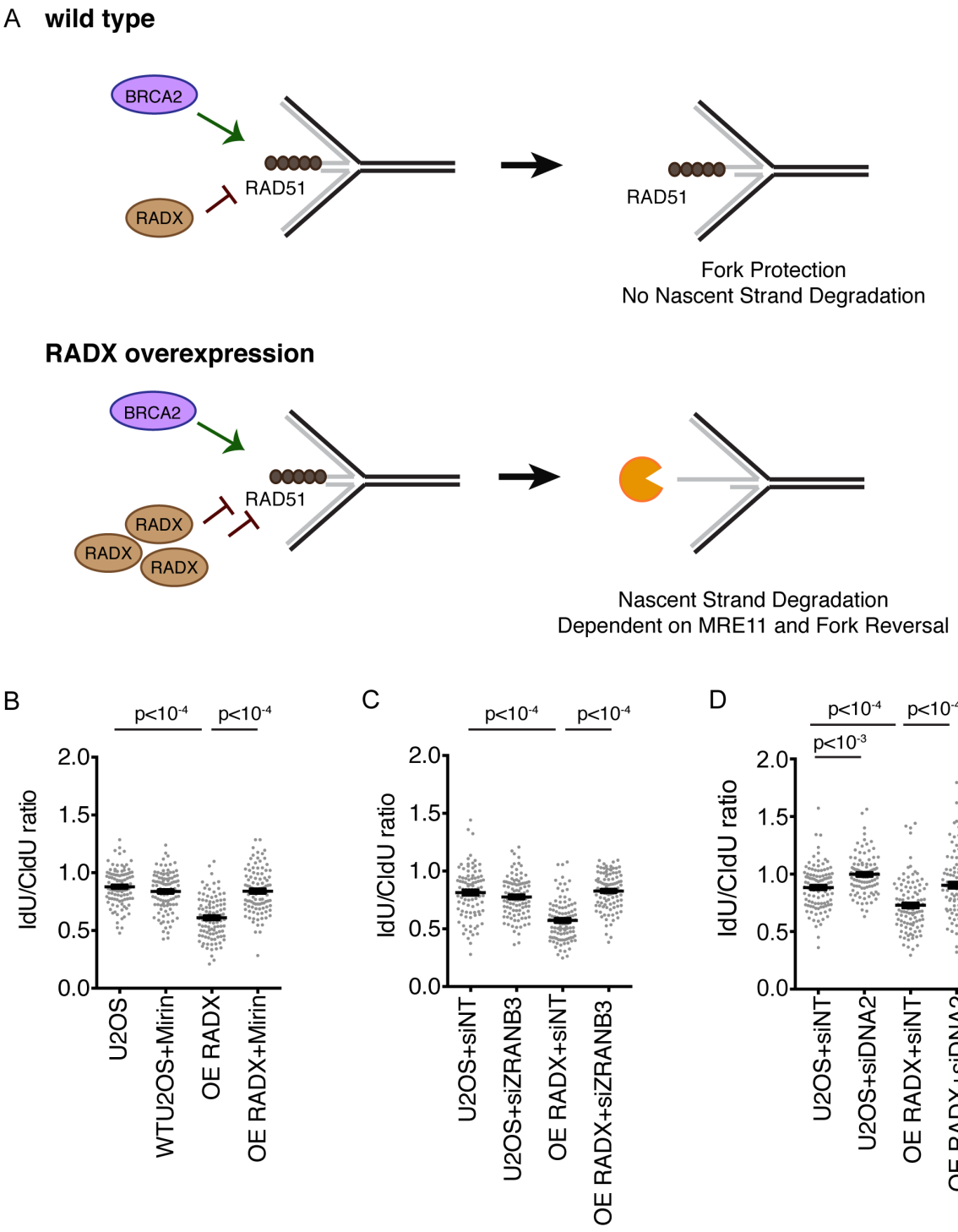

Figure 5.6. Overexpression of RADX causes fork degradation that is MRE11 and ZRANB3 dependent A) Model for RADX overexpression causing fork degradation (B-D) Parental or RADX overexpressing (OE RADX) U2OS cells were treated with mirin (B) or transfected with the indicated siRNAs (C and D). The cells were labelled sequentially with CldU and IdU before treatment with 3mM HU for 5 hours. The lengths of 100 DNA fibers were measured and are depicted as dot plots with mean+/-SEM. P values derived from Kruskal-Wallis ANOVA with a Dunn's posttest.

Differential requirements of RAD51 in fork reversal and protection

Paradoxically, RADX deficiency is proposed to cause excessive RAD51-dependent fork reversal in cells that are not exposed to added replication stress agents (Dungrawala et al., 2017). Thus, if RAD51 is required for fork reversal, which is in turn required for fork degradation, we might have expected that RADX overexpression would inhibit fork reversal and yield stable nascent strands. A possible explanation is that different RAD51 functions are needed for fork reversal and fork protection, and RADX only antagonizes the fork protection function. Alternatively, the same RAD51 function could be required for both reversal and protection, but more of it may be needed for fork protection than fork reversal. Consistent with the second hypothesis, we found that knocking down RAD51 with several different siRNAs yielded different phenotypic outcomes – fork stability or degradation, despite all of the siRNAs yielding almost no detectable RAD51 protein (Figures 5.7A). Importantly, titrating the amount of a potent RAD51 siRNA into cells initially yields fork degradation at low concentrations and fork protection at higher concentrations corresponding to increasing knockdown (Figure 5.7B). This result is consistent with the model that the amount of RAD51 determines whether forks reverse and are then protected from nucleases. HR factors including BRCA1/2 promote increased RAD51 functions while RADX appears to antagonize RAD51.

RADX outcompetes RAD51 for ssDNA but is expressed at lower levels than RAD51 in cells

To explore the mechanisms by which RADX could inhibit RAD51, we examined whether RADX could prevent RAD51 from binding to ssDNA. We performed competition experiments with RADX pre-bound to the DNA followed by addition of increasing amounts of RAD51 (Figure 5.8A); or experiments with RAD51 pre-bound to the DNA followed by incubation with increasing RADX

(Figure 5.8B). Extremely low concentrations of RADX (1nM) pre-bound to the DNA is sufficient to block binding by 10μM RAD51 (Figure 5.8A, lane 11). At 20μM RAD51, the 1nM prebound RADX is partially displaced to allow for RAD51-DNA complexes (Figure 5.8A lane 13), indicating that RAD51 can displace RADX from DNA at extremely high concentrations (20,000x excess compared to RADX). At the highest concentration of RADX that we tested (2nM), the RADX-DNA complex resists displacement even at 20μM RAD51 (Figure 5.8A lanes 17-19). Conversely, when RAD51 is prebound to the DNA, even 1nM RADX is sufficient to displace RAD51 to form RADX-DNA complexes (Figure 5.8B lane 1). This is the case even when 20μM RAD51 is prebound to the DNA (figure 5.8B lanes 6-9). Thus, RADX can outcompete RAD51 for DNA binding *in vitro* even when RAD51 is at 10,000-fold molar excess. This competition is dependent on the ability of RADX to bind DNA, since a RADX mutant that abrogates most of its DNA binding activity (OB-m RADX) cannot compete with RAD51 for ssDNA (Figure 5.8C).

We then calculated the levels of RAD51 and RADX in cells. We discovered that RAD51 is abundantly expressed in both 293T and U2OS cells (~$2X10^6$ molecules/cell in both cell types) (Figure 5.9). On the other hand, RADX is expressed at comparatively low levels (~$1X10^5$ molecules/cell in 293T and ~13,000 molecules/cell in U2OS) (Figure 5.9C). Thus, RADX is expressed approximately 24-fold and 170-fold lower than RAD51 in 293T and U2OS cells respectively. Regardless, these concentrations of RADX, coupled with its high affinity for DNA (see 5.9) would still allow for it to outcompete RAD51 for DNA binding in cells suggesting the need for additional regulatory mechanisms.

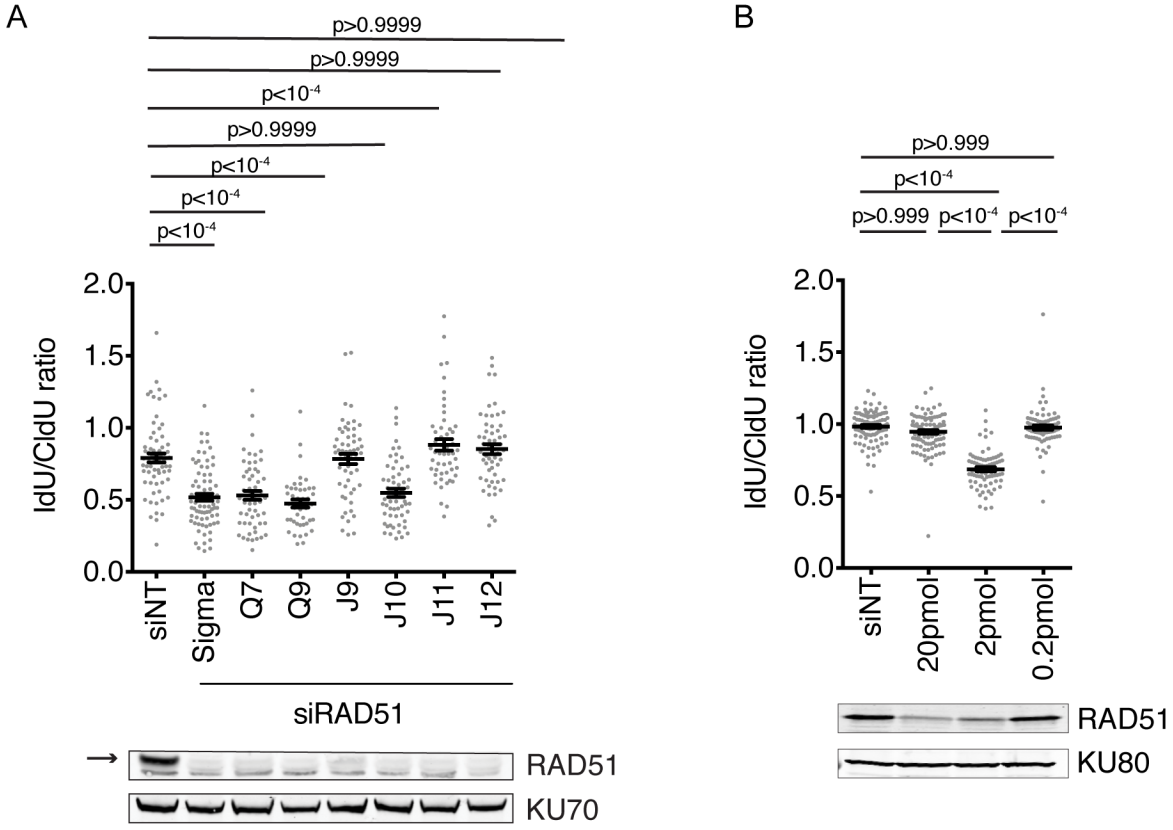

Figure 5.7. Differential requirements of RAD51 in causing reversal and protection of nascent strands. (A and B) U2OS cells transfected with the indicated siRNAs (A) or U2Os cells transfected with J10 at the indicated concentrations (B) were labelled sequentially with CldU and IdU before treatment with 3mM HU for 5 hours. The lengths of 100 DNA fibers were measured and Mean+/-SEM is depicted. P values derived from Kruskal-Wallis ANOVA with a Dunn's posttest. Immunoblot of knockdown efficiencies is also depicted. This experiment was performed by Huzefa Dungrawala and Archana Krishnamoorthy.

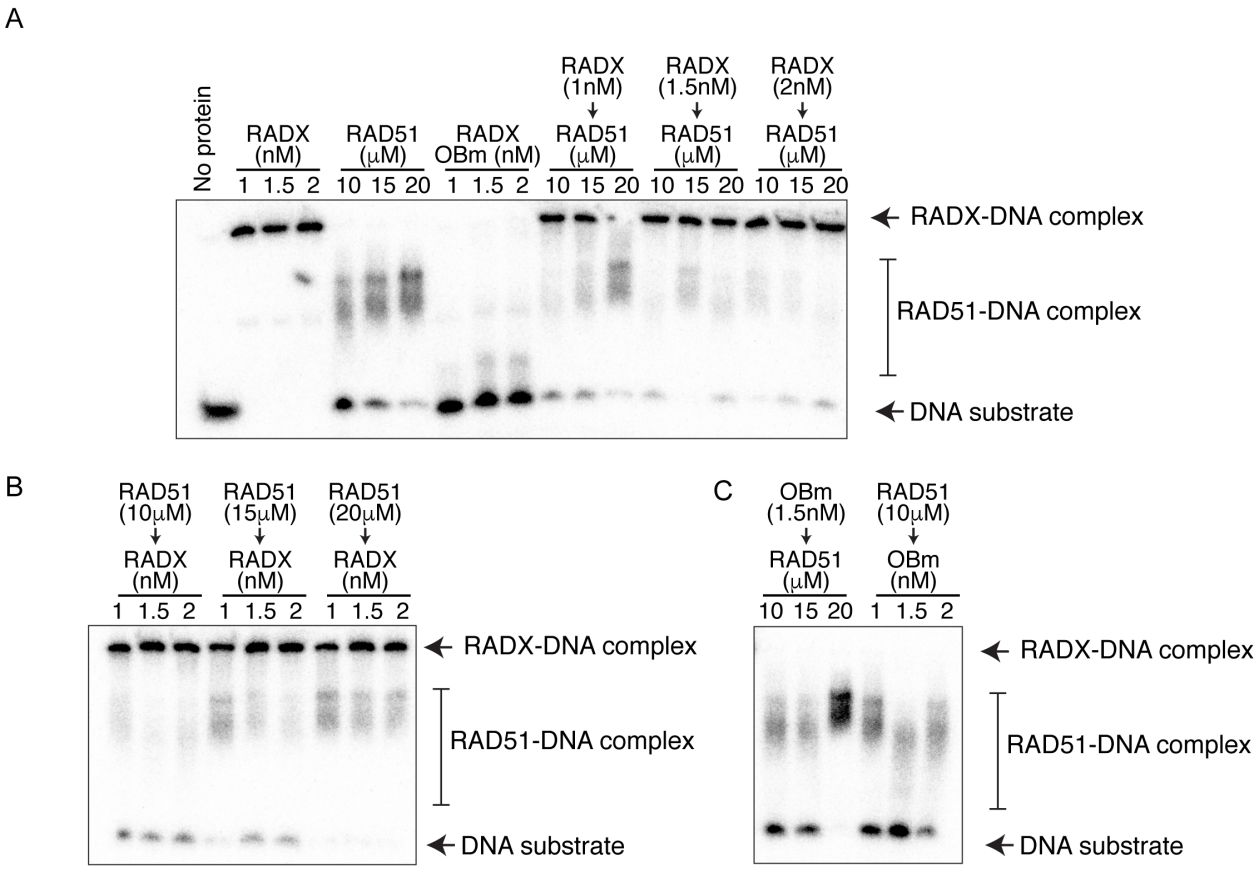

Figure 5.8. RADX can outcompete RAD51 for binding to ssDNA. (A-C) Electrophoretic Mobility Shift Assays for RADX and RAD51 binding to a dT-50 oligonucleotide. The experiment was performed by incubating DNA with RADX, RAD51, or both proteins in the indicated order and concentrations. The Ob-m is a DNA binding mutant of RADX that was utilized as a negative control. The experiments are representative of two repeats.

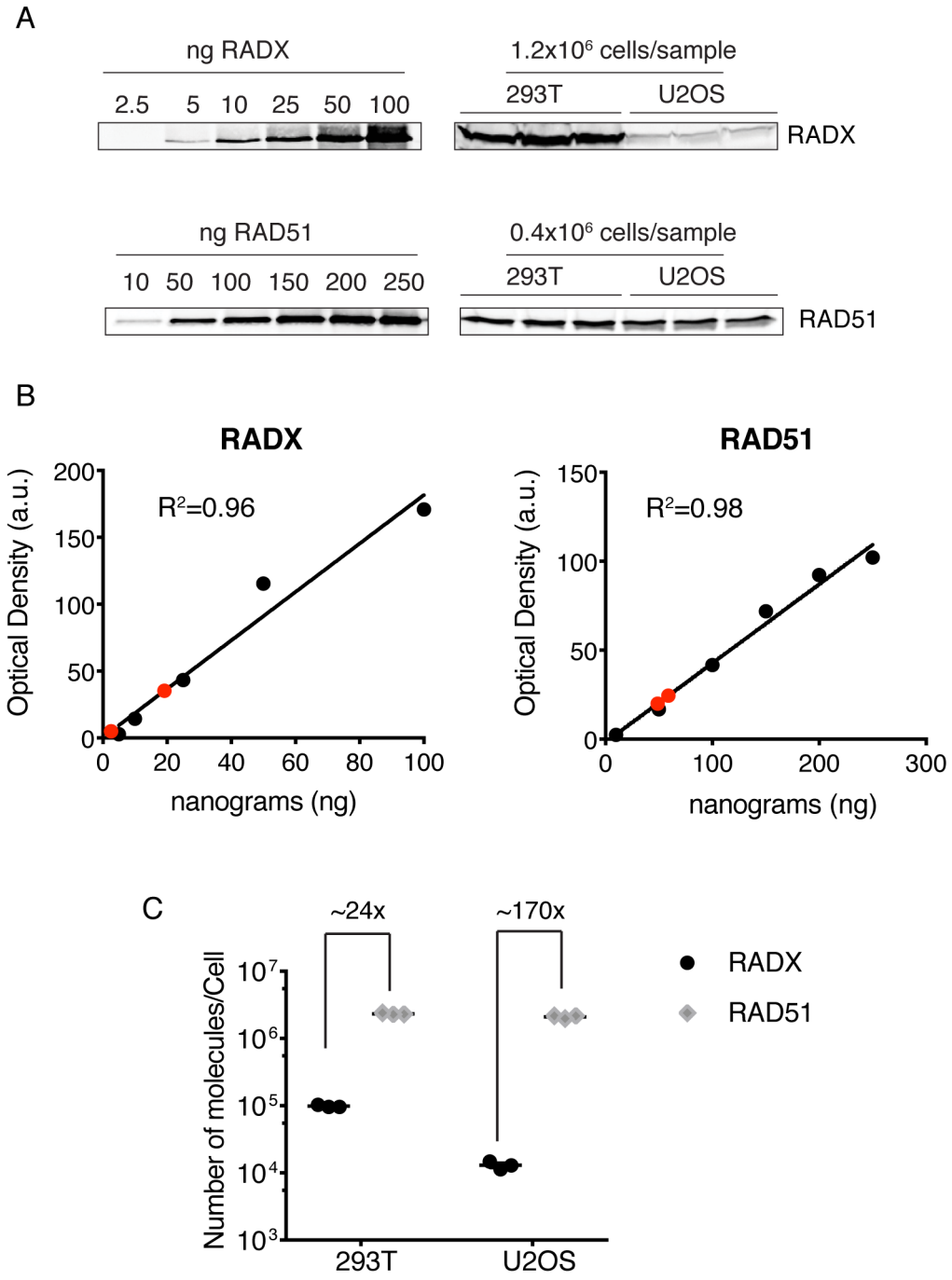

Figure 5.9. RADX is less abundant in cells as compared to RAD51. A) Immunoblot depicting RADX and RAD51 as indicated. Purified proteins were used to generate standard curves. B) Line plots depicting the R^2 goodness of fit for the standard curves of each protein. The red circles indicate the position of the sample means. C) Quantitation of the number of molecules per cell for RADX and RAD51 in two different cell lines. Mean+/-SEM is depicted for each replicate. This experiment was performed in triplicate by Huzefa Dungrawala.

Discussion

Fork Protection is an important function of several DNA repair proteins, including BRCA1/2, the FA pathway, BOD1L, the RAD51 paralogs and ABRO1 (Higgs et al., 2015; Schlacher et al., 2011, 2012; Somyajit et al., 2015; Xu et al., 2017). Loss of fork stability leads to extensive degradation of the nascent DNA at persistently stalled forks and genomic instability in BRCA1/2 defective cells due to destabilized RAD51 filaments (Schlacher et al., 2011, 2012).

RADX is an SSB that regulates the amount of RAD51 at replication forks (Dungrawala et al., 2017). Loss of RADX mimics RAD51 overexpression, and thus causes chemoresistance and fork protection in BRCA2 mutant cells (Dungrawala et al., 2017). In this study, we further tested the model that RADX antagonizes RAD51 at replication forks in different genetic backgrounds. We discovered that RADX loss confers fork protection to cells defective in BRCA1, FANCA, FANCD2 or BOD1L- all situations where RAD51 filament stability is compromised. In addition, ABRO1 was recently suggested to work independently of RAD51 since overexpression of RAD51 failed to rescue fork degradation in ABRO1-deficient mouse embryonic stem cells (Xu et al., 2017). We are thus currently testing if RADX deletion can also restore fork protection to

these cells. Our model would predict that if RAD51 overexpression cannot protect forks in ABRO1-deficient cells, RADX deletion should have no effect.

Importantly, RADX loss prevents both DNA2- and MRE11-dependent nascent strand degradation, consistent with the idea that RADX acts at the level of RAD51 and RAD51 stabilization prevents degradation by both nucleases (Higgs and Stewart, 2016; Higgs et al., 2015). Additionally, RADX overexpression causes fork destabilization dependent on the same genetic factors as those that cause fork degradation when RAD51 function is compromised; this result is also consistent with a RAD51 antagonist activity. RADX can outcompete RAD51 for ssDNA even when present at concentrations that are 10,000-fold less than RAD51. There are approximately 170x less RADX molecules per cell than RAD51 in U2OS cells. This result explains the need for positive RAD51 regulators like BRCA2 to stabilize it on reversed forks and to balance the antagonistic function of RADX.

Finally, as would be expected from this model, we found that the amount of RAD51 is critical to determining the fate of persistently stalled forks. Wild-type levels allow forks to be reversed which can serve as a way to accomplish template switching, repair DNA damage or otherwise promote fork restart. Moderately reduced levels of RAD51 can still facilitate fork reversal but are unable to stabilize the reversed fork leading to excessive nuclease action and genome instability. Finally, very low levels of RAD51 prevent any fork reversal yielding stable nascent strands but defects in fork restart and challenges in completion of DNA replication.

RADX does not regulate the recruitment of MRE11/DNA2 nucleases

An alternative model for how RADX depletion causes fork protection in different genetic backgrounds is if RADX mediates recruitment or regulation of the MRE11/DNA2 nucleases, as has been reported for other fork protection factors (Chaudhuri et al., 2016; Ding et al., 2016; Rondinelli et al., 2017; Xu et al., 2017). We do not favor this model due to several reasons. First, we observed no differences in the levels of MRE11 or DNA2 at replication forks upon RADXΔ (Dungrawala et al., 2017). Second, we also observed no differences in the amount of ssDNA or RPA S4/S8 phosphorylation upon RADX depletion in HU-treated cells, which we would expect if RADX worked by regulating these nucleases; Additionally RADX silencing does not cause any sensitivity to IR, which we might also expect if RADX modulated the activities of nucleases (Dungrawala et al., 2017). Third, RADX silencing prevents both MRE11 and DNA2 dependent degradation; this can only be explained if it regulated both nucleases, or if recruitment of one nuclease was dependent on the other. Since these nucleases can be separated genetically into different pathways (Higgs and Stewart, 2016; Higgs et al., 2015; Kolinjivadi et al., 2017b; Thangavel et al., 2015; Xu et al., 2017), it is unlikely that RADX controls both nucleases. Fourth, RADX overexpression causes decreased RAD51 accumulation at forks, which is the opposite of what we would expect if RADX positively regulated these nucleases. Thus, while we cannot exclude the possibility that RADX regulates the functions of both DNA2 and MRE11, we favor the model that RADX functions through RAD51.

Decreased RAD51 function in fork reversal and protection

Overexpression of RADX interferes with RAD51 function yielding fork degradation and modest defects in HR (Dungrawala et al., 2017). At replication forks, RADX overexpression causes degradation that is genetically dependent on the same factors as loss of RAD51 filament stability. This finding further supports our model that RADX overexpression causes decreased RAD51 function. Interestingly, since RADX overexpression results in fork degradation it must be insufficient to prevent the fork reversal function of RAD51. This is perhaps not surprising, since RADX overexpression results in only a partial decrease in RAD51 foci formation, both after HU and IR (Dungrawala et al., 2017). Thus, similar to the loss of BRCA2, the partial decrease in RAD51 function by RADX overexpression is sufficient to cause defects in fork protection, but not in fork reversal. It is important to note that there is, as yet, no identified genetic condition in humans where RAD51 function is sufficiently attenuated to prevent fork reversal. Neither loss of HR proteins nor mutations in RAD51 prevent fork degradation suggesting sufficient RAD51 activity remains to facilitate reversal (Kolinjivadi et al., 2017a; Mijic et al., 2017; Schlacher et al., 2011, 2012). There are multiple fork reversal enzymes in cells including ZRANB3, SMARCAL1, and HLTF (Bansbach et al., 2009; Bétous et al., 2012; Ciccia et al., 2012; Kile et al., 2015; Kolinjivadi et al., 2017a; Taglialatela et al., 2017; Vujanovic et al., 2017). SMARCAL1 is essential for normal development (Boerkoel et al., 2002) and deficiencies in the ZRANB3 and HLTF may cause cancer(Lawrence et al., 2014; Moinova et al., 2002; Sandhu et al., 2012). Thus, some ability to reverse a stalled fork may be essential at least in mammals.

Replication fork protection as a determinant of chemosensitivity

Replication fork protection has been reported to be an important determinant of chemosensitivity of both BRCA1 and BRCA2 mutant cells to PARP inhibitors, like olaparib (Chaudhuri et al., 2016; Ding et al., 2016; Dungrawala et al., 2017; Yazinski et al., 2017). However, other studies have found no contribution of fork protection in modulating chemosensitivity of BRCA-deficient tumors (Feng and Jasin, 2017). Additionally, loss of some factors like EZH2 and MUS81 have been found to restore fork protection and chemoresistance only to BRCA2-mutant cancer cells and not to BRCA1-mutant cells (Lemaçon et al., 2017; Rondinelli et al., 2017). Our results suggest RADX also differentiates between BRCA2 and BRCA1 since deleting RADX only confers chemoresistance to BRCA2-deficient cells and not BRCA1-deficient cells despite rescuing fork protection in both settings. One interpretation is that BRCA1 silencing might cause chemosensitivity largely due to a defect in HR at least in some cell types, as previously suggested (Feng and Jasin, 2017). Since RADX does not modulate HR (Dungrawala et al., 2017), it would not be expected to cause chemoresistance. It is also worth noting that our BRCA1-depeleted cells were more sensitive to olaparib than what we had previously reported for BRCA2 (Dungrawala et al., 2017). This may be due to differences in siRNA knockdown efficiencies. Thus, it is also possible the severity of the BRCA1/2 defect determines whether RADX deletion can generate drug resistance. Thus, the severity of the underlying cancer-causing HR gene mutation may determine whether restoring fork protection would be sufficient to generate drug resistance.

CHAPTER VI

DISCUSSION AND FUTURE DIRECTIONS

Summary of Dissertation Work

Stalled replication forks often lead to the generation of ssDNA and are thus a source of genome instability. Single Strand DNA Binding proteins (SSBs) like RPA and RAD51 are the first responders to replication forks stalling and protect the exposed ssDNA from the action of nucleases. Additionally, RPA bound ssDNA is a platform for the recruitment and regulation of several replication stress response enzymes and proteins, including the apical kinase ATR (Fanning et al., 2006). ATR regulates several mechanisms to promote replication restart and to protect stalled forks from collapse into cytotoxic Double Strand Breaks (DSBs). How these different pathways work in a coordinated manner to promote genomic stability is still not well understood (Saldivar et al., 2017). Also, we are just beginning to discover important functions of well-studied repair proteins in novel replication stress response pathways.

One such pathway of genome maintenance is replication fork remodeling. Fork remodeling was long considered to be a pathological consequence of replication stress (Follonier et al., 2013; Sogo et al., 2002). However recent electron microscopy data demonstrated that fork remodeling is a global response to stress and that at least 10% of forks were remodeled even in the absence of exogenous stress (Zellweger et al., 2015). Additionally, proteins that function as fork remodelers are required for genome maintenance (Bansbach et al., 2009; Ciccia et al., 2012;

Kile et al., 2015), providing evidence that fork remodeling is a physiological stress response pathway in mammalian cells.

My dissertation work has focused on the functions of single strand DNA binding proteins in regulating replication fork remodeling. Specifically, I have uncovered two mechanisms by which cells regulate fork reversal. In chapter III, I explored the mechanism by which RPA directed SMARCAL1 activity to promote genome stability. In chapter IV, I collaborated with Huzefa Dungrawala to identify and characterize a new RPA-like SSB at replication forks, RADX. In chapter V, I further investigated the mechanisms by which RADX regulates replication fork stability by modulating RAD51 functions.

How are fork reversal enzymes regulated?

Fork reversal promotes genome stability and replication fork stabilization. However, too much or unregulated fork reversal is also detrimental to cells, as has been demonstrated by SMARCAL1 overexpression (Bansbach et al., 2009), ATR inhibition (Couch et al., 2013) or by excessive RAD51 activity due to loss of RADX (Chapters IV, V and (Dungrawala et al., 2017)). The reversed fork is also an entry point for the MRE11 and DNA2 nucleases that promote nascent DNA degradation (Kolinjivadi et al., 2017a; Lemaçon et al., 2017; Mijic et al., 2017; Taglialatela et al., 2017; Vujanovic et al., 2017). Thus, maintaining the right amount or balance between fork reversal, restoration and protection is critical to promoting genomic stability. How cells achieve that balance is still unclear. This leads to the important question that I have tried to address in my thesis: What prevents inappropriate fork reversal?

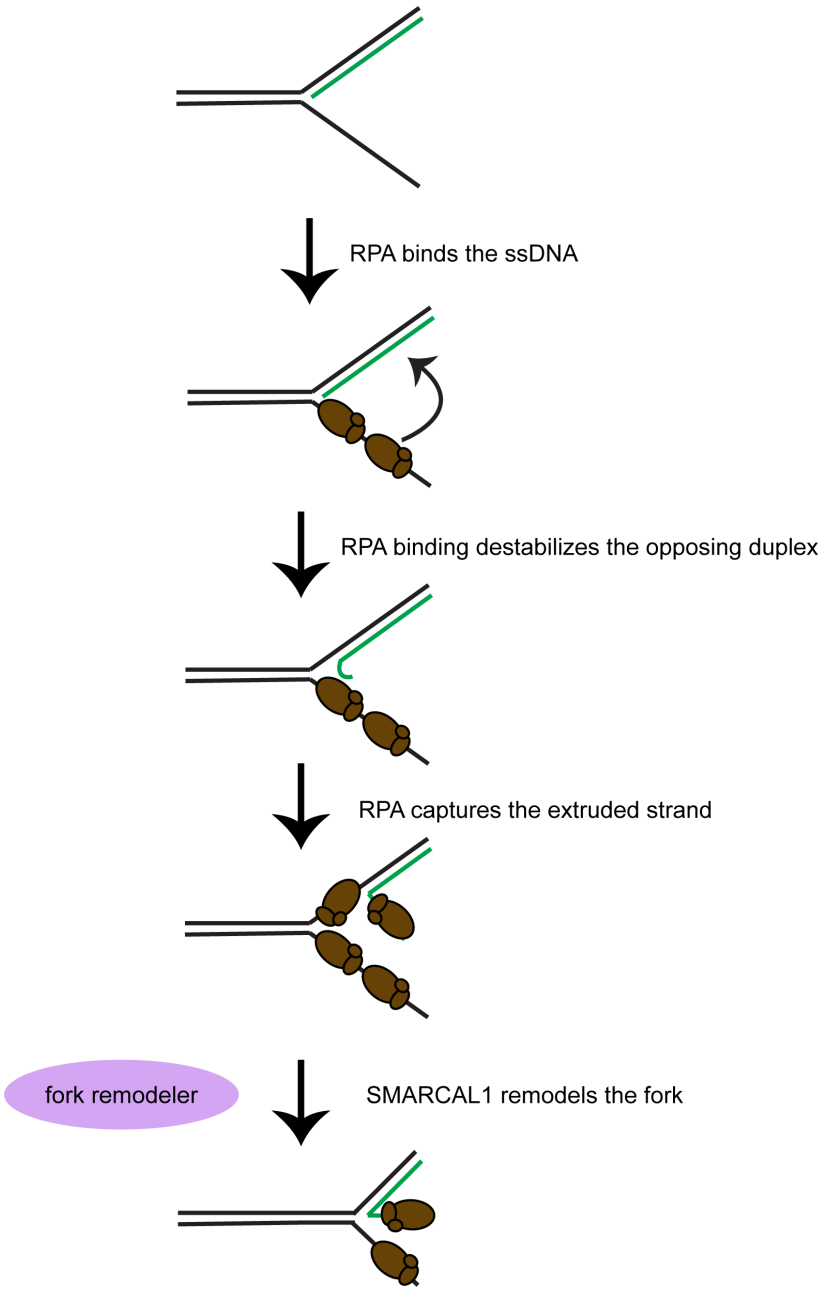

Figure 6.1. RPA promotes SMARCAL1-mediated fork regression by destabilization of the nascent-parental duplex. A possible model for RPA enforcement of SMARCAL1 specificity. When bound to the leading parental template, RPA can induce transient destabilization of the lagging strand duplex, thereby promoting SMARCAL1 mediated remodeling. Adapted from (Delagoutte et al., 2011)

RPA directs SMARCAL1 activity specifically at "stalled" forks

In the case of SMARCAL1, Remy Betous, a post-doctoral fellow in the lab had discovered that, *in vitro*, RPA stimulated SMARCAL1 specifically on model fork substrates that mimicked stalled replication forks and not on substrates that mimicked "normal" replication forks (Bétous et al., 2013a). Since RPA is almost always present at forks, it was an attractive candidate for preventing inappropriate SMARCAL1-mediated fork regression. I built upon Remy's findings to determine the mechanism by which RPA selectively stimulates SMARCAL1. I discovered that the intrinsic polarity with which RPA binds DNA determines SMARCAL1 stimulation or inhibition. Specifically, the orientation of the high-affinity DNA binding domains DBD-A and DBD-B of RPA with respect to the fork junction is critical for regulation of SMARCAL1. Additionally, the location of the interaction surface between RPA and SMARCAL1 does not affect regulation- as long as there is an interaction (Bhat et al., 2015). Thus, the regulation of SMARCAL1 by RPA is completely dependent on the intrinsic polarity of RPA binding to DNA. This model fits the idea that RPA has to direct the activity of several different enzymes and so regulatory mechanisms would not necessarily depend on the location of the protein-protein interaction surface.

As I pointed out in the discussion for chapter III, we don't really know why the orientation of the high affinity DNA binding domains is important. I speculate that it has to do with the transient destabilization or unwinding of the DNA duplexes in the fork substrate by RPA that promotes SMARCAL1-mediated fork remodeling (Figure 6.1). There is some evidence that this transient destabilization/unwinding by RPA is orientation-specific (Delagoutte et al., 2011; Nguyen et al., 2014). Additionally, the high affinity DNA binding domains of RPA are sufficient for this process (Nguyen et al., 2014), consistent with our findings that the high affinity DNA binding domains are sufficient for SMARCAL1 regulation. An alternate hypothesis is that RPA orientation on DNA determines the structuring of the underlying DNA substrate- and on some substrates, the orientation-dependent structuring make it more conducive to SMARCAL1 translocation and/or

annealing. This hypothesis is supported by the recent crystal structure of RPA bound to DNA, with each DBD making differential contacts with the DNA, resulting in a change in the overall conformation of DNA (Fan and Pavletich, 2012). FRET-based or single molecule fluorescence experiments and high-resolution structures of enzyme-RPA-DNA complexes will be critical to gain insights into these processes. Additionally, the T4 and *E.coli* SSBs have different polarity requirements to destabilization of short hairpins/duplexes compared to RPA and so can be used to test if it is truly helix destabilization that promotes SMARCAL1 activity. However, it must be noted that both these proteins have different DNA binding properties and therefore, structure the underlying DNA differently than RPA (Delagoutte et al., 2011).

RADX regulates RAD51 activity

RAD51 overexpression is associated with genomic instability (Klein, 2008; Richardson et al., 2004) and there are several anti-recombinases that regulate RAD51 activity negatively during DSBR, (Kowalczykowski, 2015). Like SMARCAL1, RAD51 is present at forks even in unperturbed S-phase cells (Zellweger et al., 2015) and thus has to be regulated to prevent inappropriate reversal. In collaboration with Huzefa Dungrawala, I identified RADX, a new RPA-like SSB at replication forks by iPOND. RADX functions to restrain RAD51 activity at replication forks and loss of RADX causes an increased accumulation of RAD51 at replication forks. Additionally, loss of RADX causes DNA breaks dependent on SMARCAL1-, ZRANB3- and RAD51- activities. Thus, I propose that RADX prevents inappropriate RAD51-mediated fork reversal.

There are several experiments that could further support the model. I think that one of the most critical experiments would be to perform EM analyses on RADX-depleted cells; specifically, if the model is right, we would expect to see an accumulation of reversed fork intermediates in RADXΔ cells. However, this experiment might need to be done with a co-depletion of MUS81,

which could process the reversed forks upon RADXΔ and thus prevent their detection by EM. Alternatively, silencing RADX in BRCA2-mutant cells should also result in an accumulation of reversed fork intermediates, similar to the effect of MRE11 inhibition in BRCA2-depleted cells (Mijic et al., 2017).The other key piece of information that we lack is the mechanism by which RADX regulates RAD51. In this section, I will discuss possible models for RADX function and present some preliminary data. Additionally, there are several questions left unanswered by my studies; and I will discuss these in the future directions section: (i) What does RADX interact with? (ii) How is RADX localized to replication forks? (iii) What are the functions of the different domains of RADX?

Mechanisms of RAD51 regulation by RADX

Competition between ssDNA binding proteins

The simplest model is that RADX outcompetes RAD51 for ssDNA at replication forks. Thus, depleting RADX from cells allows for more RAD51 to accumulate at replication forks, even without an increase in ssDNA (figure 6.2A). Similarly, this would also be consistent with our observations that overexpression of RADX causes decreased RAD51 foci after HU and IR, despite the fact that overexpression by itself causes an increase in breaks (Figures 4.8-4.11 and (Dungrawala et al., 2017)). The competition model is also supported by our in vitro biochemistry studies (Figure 5.8), since RADX can efficiently out-compete RAD51 for ssDNA even when RAD51 is present at 10,000-fold molar excess. Our measurements of the abundance of these proteins in 293T and U2OS cells also supports this model (Figure 5.9), although it should be noted that we don't yet know how many molecules of RAD51 and RADX are actually present at forks. To obtain these numbers, we would have to measure the amounts of RADX and RAD51 in the chromatin – bound fraction, rather than the nucleus or cellular amounts.

The problem with this model is that it does not account for any regulatory mechanisms- given the high affinity of RPA and its abundance in cells (Wold, 1997), a simple competition model would predict that RAD51 or even RADX never would bind ssDNA. However, both RADX and RAD51 are recruited to forks, indicating that this model is not likely to be simple competition.

A more complex model is that if RAD51 is being loaded onto DNA by a mediator, the mediator may be capable of only displacing RPA, but not RADX. Thus, in this model, RAD51 cannot form a continuous filament since it cannot replace RADX, and thus is inhibited for activity (Figure 6.2B). Surprisingly, EM and genetic data suggest that BRCA2, which usually loads RAD51 onto ssDNA ends, is not required for RAD51 loading for fork reversal (Dungrawala et al., 2017; Kolinjivadi et al., 2017a; Lemaçon et al., 2017; Mijic et al., 2017; Taglialatela et al., 2017; Vujanovic et al., 2017). However, other proteins including the MMS22L-TONSL heterodimer, XPG and the CST complex can mediate RAD51 loading in certain cases (Chastain et al., 2016; Piwko et al., 2016; Trego et al., 2016), and it is possible that some of them are required for fork reversal.

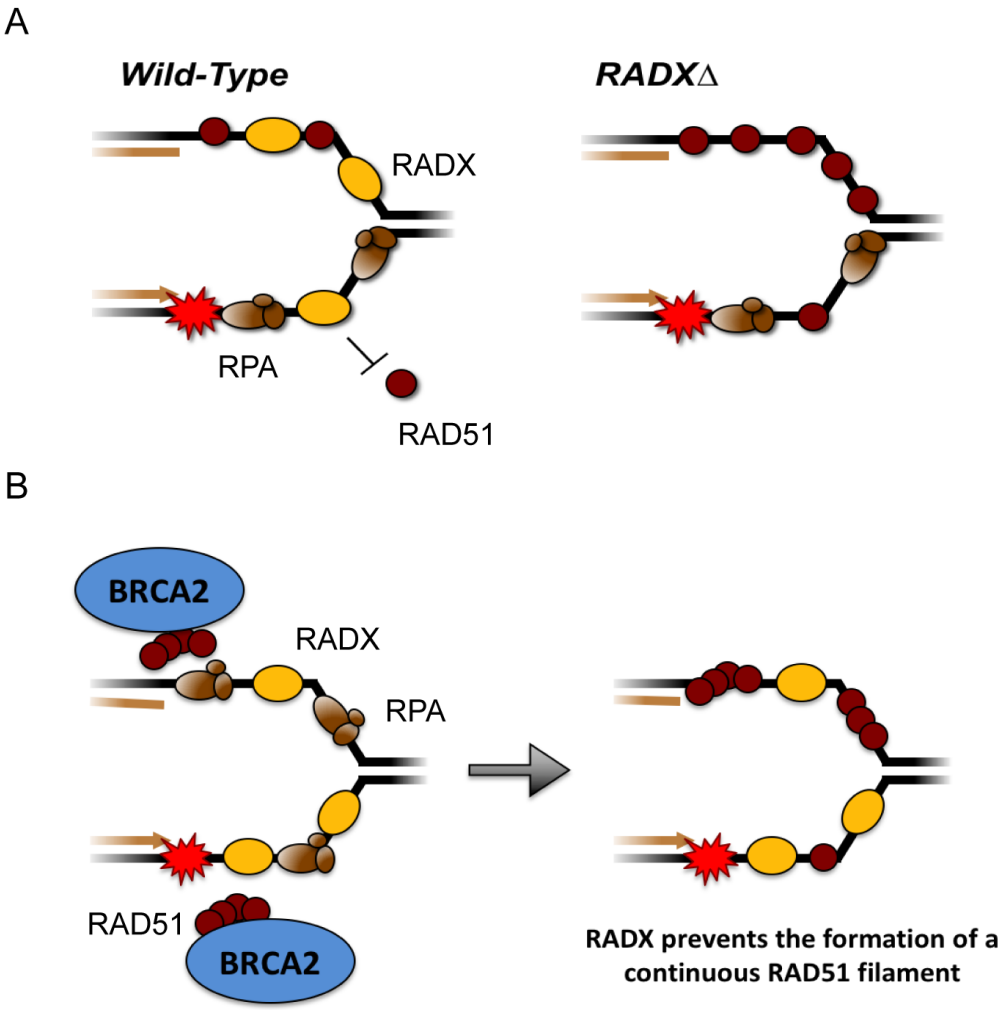

Figure 6.2. Competition between ssDNA binding proteins at stalled replication forks. (A) Schematic of replication forks in cells either WT or RADX∆. This model cannot explain how RADX and RAD51 bind DNA at forks in the presence of RPA. (B) In this model, BRCA2 can load RAD51 at forks by replacing RPA, but cannot replace RADX. Thus, RAD51 and RADX coexist at a fork, preventing the formation of a continuous RAD51 filament.

Modulation of RAD51 enzymatic activities

An alternate hypothesis is that RADX modulates the enzymatic or biochemical properties of RAD51. Since upon ATP hydrolysis, RAD51 dissociates from DNA (see Introduction for details), an increase in the ATPase activity of RAD51 by RADX would be one such mechanism of regulation. Similarly, changes in the ability of RAD51 to bind DNA or nucleotide cofactors or disruption of RAD51 filaments by RADX could all be other models to test. For example, the helicase RECQL5 disrupts RAD51 presynaptic filaments and HOP2-MND1 change RAD51-ATP binding in a manner that restores functionality to a K133A mutant of RAD51 that ordinarily has disrupted ATP binding ability (Bugreev et al., 2014; Hu et al., 2007).

Another interesting biochemical mechanism of inhibition of RecA (the RAD51 paralog in *E.Coli*) is by the protein, RecX. RecA filaments are nucleated slowly and extended 5'-3'. RecA monomers can also dissociate 5'-3' upon hydrolysis of ATP (Cox, 2007). Thus, extension has to be much faster than dissociation to promote filament assembly. RecX binds to RecA and prevents RecA filament extension (Figure 6.3), thereby disrupting the balance between filament growth and disruption (Drees et al., 2004).

The major caveat to all of these models is that it is hard to imagine how RADX would regulate RAD51 without a direct protein-protein interaction. Huzefa Dungrawala and I have both tried to determine if RADX and RAD51 interact through a variety of approaches, including Co-IPs from nuclear extracts, biotin-ssDNA pull downs as well as Co-IPs using purified proteins. However, we still do not have any convincing evidence that these proteins interact, although we have not exhausted all possibilities including testing if these interactions are DNA dependent.

RecA filament assembly - 5’ to 3’ - monomers added to the 3’ end of the filament

RecA filament disassembly - 5’ to 3’ - monomers dissociate from 5’ end

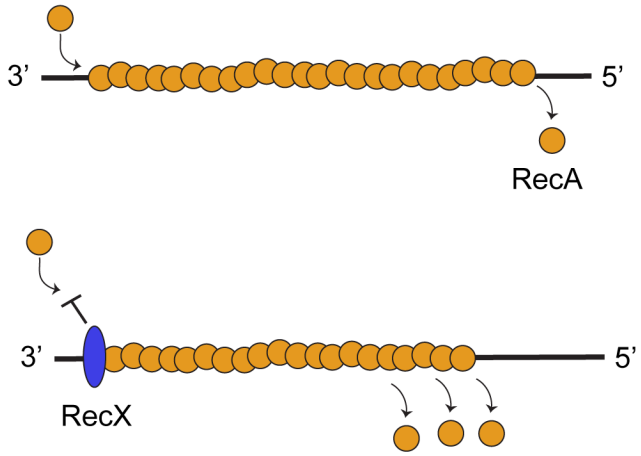

RecX caps the growing end of the filament; disassembly continues

Figure 6.3. Mechanism of RecX inhibiting RecA filament assembly. See text for details

RADX regulates the activity of RAD51 indirectly

It is also possible that the antagonistic effect of RADX on RAD51 is indirect. The hypothesis is that RADX mediates recruitment and/or function of a RAD51 regulator. This model predicts that we should have observed either loss or enrichment of the regulator upon RADXΔ or overexpression at forks. Our iPOND-MS analyses upon RADXΔ in different cell lines (Figure 4.9 and Figure 6.4) indicated that RAD51 was our strongest hit across all the different cell lines. There were, however, a few weaker hits. One of them is the anti-recombinase, RECQL5. RECQL5 is lost from forks upon RADXΔ, suggesting that its recruitment might be dependent on RADX. This model fits most of our data, since RECQL5 is known to disrupt RAD51 filaments (Hu et al., 2007). However, it does not fit our observations that RADXΔ cells are not sensitive to IR nor defective in DSBR, which we might predict given that RECQL5 is an anti-recombinase. Nevertheless, it is possible that RADX only regulates RECQL5 recruitment to forks and not to DSB ends. Also, we observed the strongest loss of RECQL5 upon RADXΔ in U2OS cells, where we observe our strongest phenotypes (Figure 6.4C). Thus, this model is a possibility that remains to be tested. Some initial experiments would be to validate if RECQL5 recruitment is indeed dependent on RADX, either by chromatin fractionation or IF imaging. Overexpression of RADX should cause an enrichment of RECQL5, whereas loss of RADX should result in a decrease of RECQL5. Additionally, experiments to test if RECQL5 depletion mimics loss of RADX and has the same genetic dependence on RAD51, SMARCAL1, ZRANB3 and MUS81 with respect to double strand breaks and fork protection assays would also be informative. The prediction would be that RECQL5 deletion can also restore fork protection and chemoresistance to BRCA2-depleted cells.

In summary, there are several possible models for how RADX regulates RAD51. Determining the mechanism of regulation will be crucial for further understanding RADX and RAD51 functions in regulating fork stability.

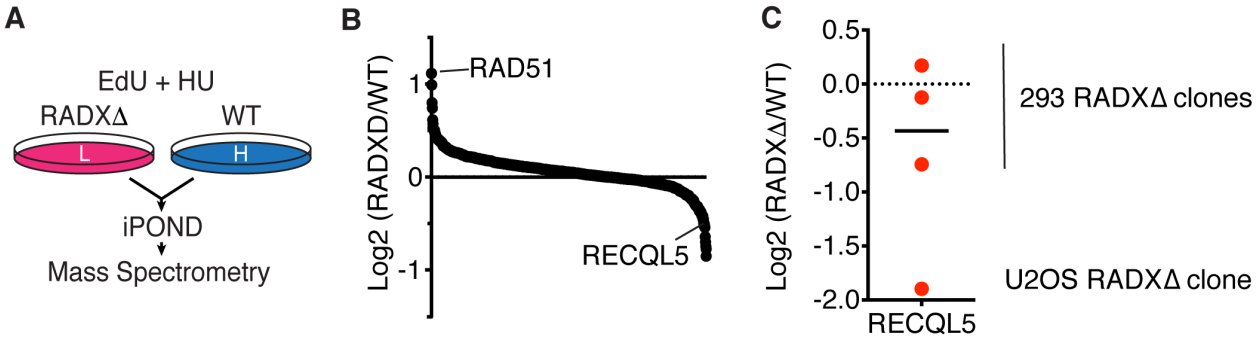

Figure 6.4. iPOND-MS analyses in RADXΔ cells. (A) Schematic of iPOND-SILAC experiment. (B) The median of the $\log_2$ abundance ratios of the proteins identified in five cell clones is depicted. (C) The abundance ratio for each individual clone is indicated for RECQL5.

Does RADX also regulate RPA?

RADX is a ssDNA binding protein and one of our models for its function is that it can compete for ssDNA with RAD51. This leads to the question- does RADX also affect RPA functions? A recent publication on RADX claimed that it could regulate RPA (Schubert et al., 2017). However, our preliminary data does not support this model. RADX silencing does not cause changes in the intensity of chromatin-bound RPA by IF (Figure 6.25A) or by iPOND (Figure 4.9).

We had previously observed that overexpression of RADX causes increased gamma-H2AX and double strand breaks (Figures 4.3F and 4.11E), likely due to interference with normal RAD51 function. This increase in breaks explains the increase in RPA intensity seen in GFP-RADX overexpression cells without any exogenous damage (Figure 6.5B). Despite this increased RPA intensity in GFP-RADX cells, upon induction of fork stalling by HU there is no further recruitment of RPA. This suggests that RADX, *when overexpressed, can suppress RPA recruitment to stalled forks*. However, I have observed no interactions between the two proteins by MS or by co-IPs. Additionally, given the relative affinities of RPA and RADX and that RPA is extremely abundant in cells, it is unlikely that endogenous RADX could compete with RPA for ssDNA.

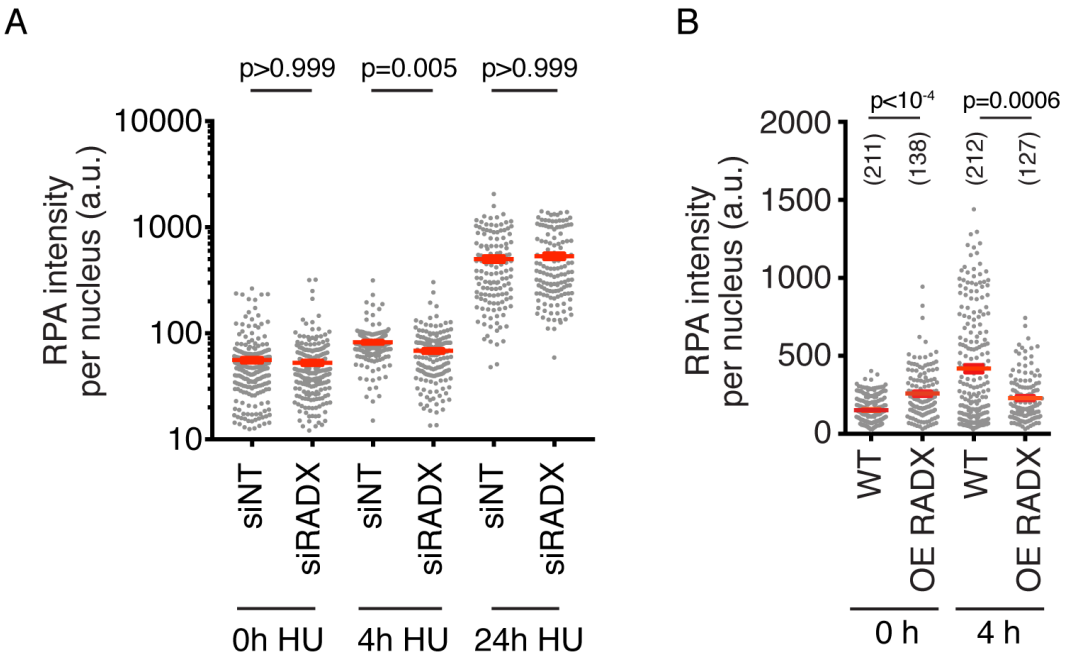

Figure 6.5. Chromatin bound RPA intensity after RADX silencing and overexpression. (A and B) WT or RADX OE U2OS cells were transfected with the indicated siRNA, treated with 3mM HU for the indicated times and stained for chromatin bound RPA after detergent extraction. P values derived from Mann-Whitney tests. Experiments are representative of two replicates.

RAD51 functions in Fork Reversal, Protection and HDR.

RAD51 has been extensively studied in DSBR, where it catalyzes strand invasion of the broken DNA end into an intact duplex (Kowalczykowski, 2015). More recently, RAD51 was described as a fork protection protein that functions by inhibiting MRE11 and DNA2-dependent degradation of the newly synthesized DNA strands (Hashimoto et al., 2010; Higgs et al., 2015; Schlacher et al., 2011). RAD51 has also been implicated in fork regression (Zellweger et al., 2015). In this section, I will discuss whether these are truly three distinct functions of RAD51 or if they are essentially the same and also address some important questions that remain unanswered in the field. Additionally, I would like to define the following terms:

RAD51 Loading: By RAD51 loading, I refer to the process by which RAD51 is brought to ssDNA. This is usually accomplished by BRCA2, which binds to ~4 or 5 RAD51 monomers using its BRC repeats. The BRC repeats are sufficient for HDR, but insufficient for fork protection.

RAD51 Stabilization: Here, I refer to the ability of BRCA2 to stabilize pre-loaded RAD51 monomers/oligomers on ssDNA and allow assembly into a fragment. This function is accomplished by the BRCA2-C terminus, which surprisingly is dispensable for HDR. However, the BRCA2 C terminus is absolutely required for the fork protection function of RAD51.

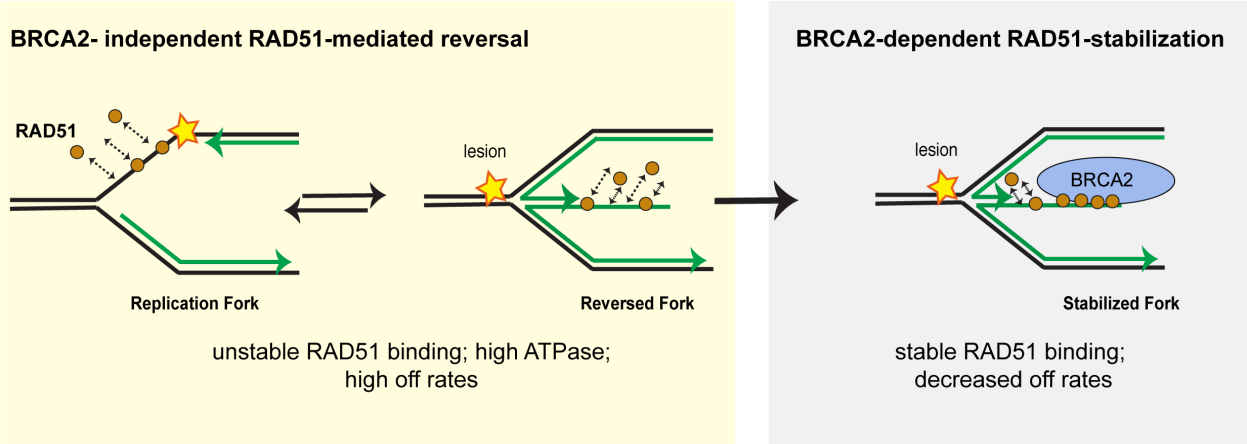

Figure 6.6. BRCA2 dependent and independent functions of Rad51 at replication forks. At replication forks, in the absence of BRCA2, RAD51 has high ATPase activity stimulated by ssDNA. This results in a dynamic on-off mode for RAD51. The model predicts that this unstable, dynamic RAD51 binding is sufficient for fork reversal. After fork regression, BRCA2 interacts with RAD51 monomers at the reversed fork through its C-terminal domain. This interaction results in an increased stability of RAD51 binding to DNA and prevents its dissociation.

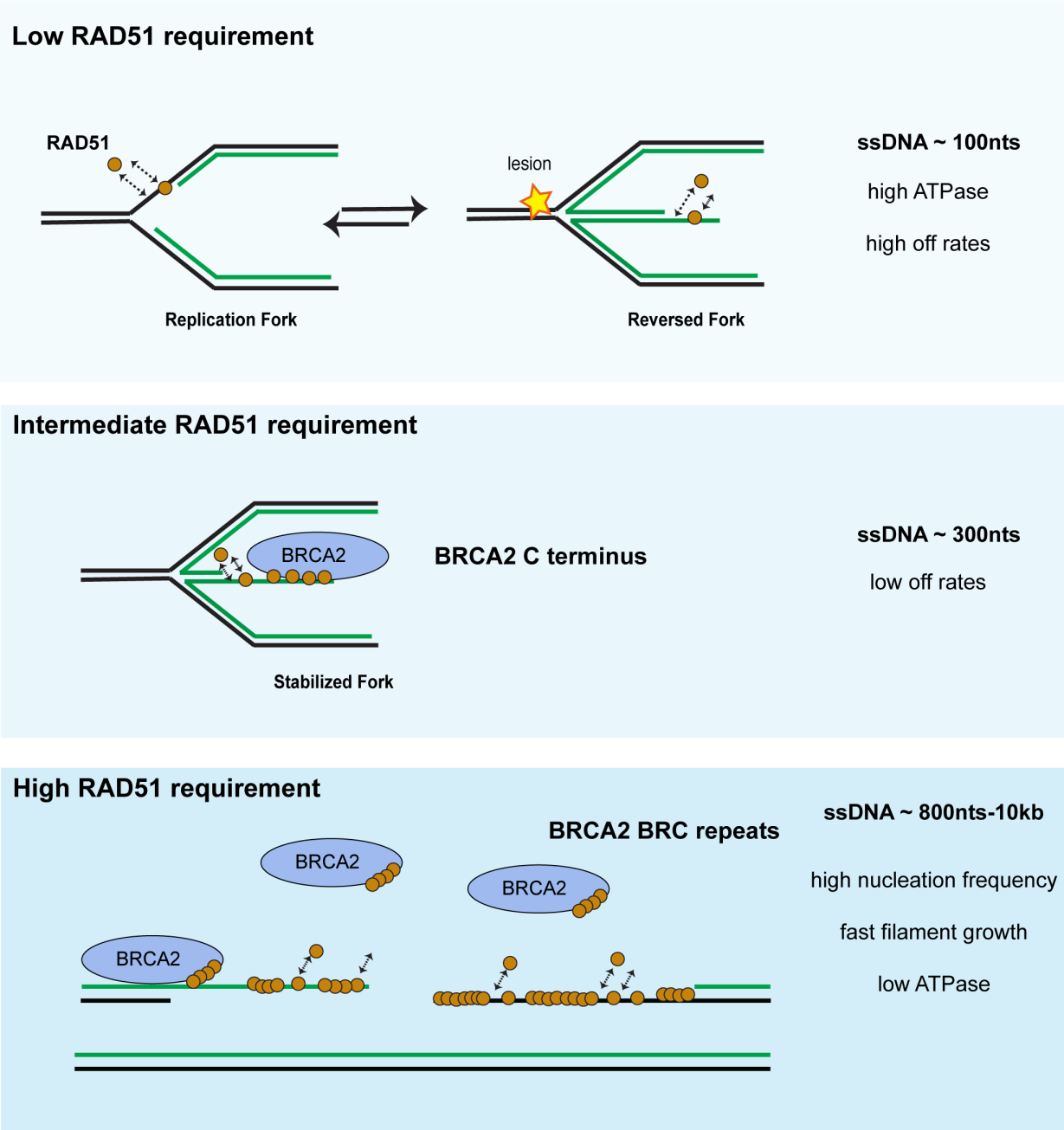

Figure 6.7. Differential requirements of RAD51 in fork reversal, protection and HR. During HR, the BRC peptides of BRCA2 promote RAD51 nucleation (the rate limiting step in filament assembly) on DNA. Following multiple nucleation events, filament assembly occurs fairly rapidly. RAD51 monomers also dissociate from different points along the filament, since the BRC-interaction does not change the ATPase activity of RAD51. See text for details.

Fork protection and HDR

Fork protection and HDR are two functions of RAD51 that are similar in one aspect: they both require BRCA2. However, a separation of function mutant of BRCA2 yields some insight into the differences between the two. While the BRC peptides of BRCA2 (which mediate RAD51 loading) are necessary and sufficient for HDR, they are not sufficient for fork protection. Additionally, a C-terminal mutant of BRCA2 that cannot stabilize RAD51 filaments is fully functional for HR, but deficient in fork protection (Schlacher et al., 2011). This indicates that in HR, RAD51 loading is dependent on BRCA2 and that BRCA2-mediated stabilization of RAD51 filaments is either not as important, or is mediated by other factors, such as the RAD51 paralogs (Chun et al., 2013; Taylor et al., 2016). Recent microscopy-based studies provide evidence for the first hypothesis; cells lacking the BRCA2 C-terminus, which have been demonstrated to have no defects in HR, do not form extended RAD51 filaments although they can initiate formation of RAD51 clusters at resected DNA ends (Haas et al., 2018). On the other hand, BRCA2 loading of RAD51 is not sufficient for fork protection. This suggests one of two possibilities- i) RAD51 can bind DNA at forks sufficiently without a mediator, complete fork reversal and then has a requirement for BRCA2 stabilization or ii) Mediators other than BRCA2 might load RAD51 at forks, such as the MM22L-TONSL complex (Piwko et al., 2016). Fork protection requires the C-terminus of BRCA2, implying that a stable RAD51 filament is critical for fork protection. This also indicates that fork protection might involve two steps- an initial, BRCA2 independent RAD51 loading and a second BRCA2-dependent stabilization (Figure 6.6).

Fork reversal and protection

The initial BRCA2 independent RAD51 loading in fork protection could occur during fork reversal. Recent data suggests that fork reversal is a prerequisite for nascent strand degradation

(Kolinjivadi et al., 2017a; Mijic et al., 2017; Taglialatela et al., 2017), and that RAD51-mediated fork reversal occurs independently of BRCA2 (Dungrawala et al., 2017; Lemaçon et al., 2017; Mijic et al., 2017; Vujanovic et al., 2017). While E. coli RecA can catalyze fork regression *in vitro* (Cox, 2007), RAD51 does not catalyze fork remodeling reactions *in vitro* (Bugreev et al., 2011). Thus, whether RAD51 actively drives regression by binding to the parental ssDNA at stalled forks, or if it simply captures and stabilizes the reversed arm of the fork remains to be explored. Determining the functions of RAD51 will be important to furthering our understanding of fork reversal. Some ways to test where RAD51 binds is to utilize PLA, as has been done recently for MRE11 (Taglialatela et al., 2017). If the experiment is done after treating cells with EdU for 24 hours to label all parental DNA and then releasing into fresh media, a positive signal would indicate that RAD51 binds the DNA at a stalled fork. On the other hand, if the experiment is performed by pulsing cells with EdU for a short duration such that only nascent DNA is labeled, a positive signal would indicate that RAD51 binds the DNA at the reversed arm of the fork. The disadvantage of this approach is that RAD51 is known to have dsDNA binding (Kowalczykowski, 2015), and thus the signal to noise might be a challenge. Additionally, utilizing proper controls will be critical to interpret the results confidently. For example, performing the PLA assay with and without fork remodelers such as SMARCAL1 or ZRANB3 would be required to ensure that the signal is dependent upon formation of a reversed fork. Another concern would be that the signal might appear positive because of the close proximity of the nascent and parental DNA. Alternatively, comparing RAD51 enrichment at forks (through chromatin fractionation or IF or iPOND) between wild type and cells depleted of the fork remodelers would be useful to determine if RAD51 is recruited to the reversed arm of forks rather than binding the ssDNA at stalled forks.

Interestingly, cells treated with B02, a RAD51 inhibitor that blocks DNA binding, exhibit fork degradation (Kolinjivadi et al., 2017a; Leuzzi et al., 2016). One interpretation of this result is that RAD51-DNA binding is dispensable for promotion of fork reversal because the inhibitor must

not block reversal if reversal is a prerequisite for degradation. Another interpretation is that fork protection is “more sensitive” to RAD51 inhibition. In other words, RAD51 might perform the same function in protection and reversal but there is less RAD51 required to perform reversal as compared to protection of forks. This is consistent with the differing requirements of BRCA2 for reversal and protection- BRCA2 is required for fork protection because there is a need for RAD51 filaments, whereas in reversal, RAD51 might not need to form filaments. This idea of having “less” RAD51 required for reversal is also consistent with our data with RADX overexpression (which presumably antagonizes RAD51) causing fork degradation rather than inhibiting reversal (Figure 4.13D). It is also consistent with our siRAD51 titration experiment, with fork degradation occurring at lower siRNA concentrations and fork protection at higher concentrations (Figure 5.7B).

An important determinant of the differential requirements of RAD51 in fork reversal, fork protection and HDR might be the amount of ssDNA. (Figure 6.7). HDR involves the generation of long stretches of ssDNA (between several hundred nucleotides and 10kb, depending on various cellular factors(Symington, 2014)) and therefore, there is a requirement for the most amount of RAD51. In *E. coli*, RecA filament formation involves several, slow nucleation steps followed by rapid extension steps (Cox, 2007); if we extend this to mammalian systems, HDR requires multiple RAD51 loading events, thus causing a need for the loading function of BRCA2. In the case of fork degradation, RAD51 is required to protect the reversed arm of replication forks from nucleases like MRE11(Kolinjivadi et al., 2017a; Mijic et al., 2017; Schlacher et al., 2011; Taglialatela et al., 2017; Vujanovic et al., 2017). This protective function requires RAD51 filaments at the regressed arm of the fork. EM analyses indicate that in most cases, the regressed arm is about 300 bp in length(Zellweger et al., 2015). Thus, there is a lesser need for RAD51 amount in fork protection as compared to HDR and thus a decreased requirement for RAD51 loading. However, there is a need to stabilize the filaments (i.e., prevent RAD51 dissociation- since loading either happens infrequently, RAD51 cannot reload as in HDR or even transient dissociation of RAD51 allows

nucleases to gain access to the DNA); and this requires the C-terminus of BRCA2 (Schlacher et al., 2011). Lastly, fork reversal can occur with about 40-100nts of ssDNA at the fork junction (Neelsen and Lopes, 2015; Zellweger et al., 2015); thus, very little RAD51 is required to bind DNA at the stalled and presumably, there are no stable filaments formed, since RAD51 needs to remodel the fork and stable binding would be counter-productive. Hence, this step could be completely independent of BRCA2. It is still important to remember that there might be other RAD51 mediators involved in fork reversal that we have not yet identified.

An alternate approach to genetics is to reconstitute the fork reversal reaction *in vitro*. While RAD51 can reverse forks *in vitro* in cooperation with RAD54 (Bugreev et al., 2011), it is unknown how SMARCAL1 and the other remodelers cooperate with RAD51 to facilitate this process. It is also interesting to note that silencing any one of the SNF2 family of remodelers is sufficient to restore fork protection to BRCA deficient cells by inhibiting fork reversal, indicating that these three proteins cooperate or function in a linear pathway (Taglialatela et al., 2017). However, a different study indicated that SMARCAL1 and RAD51 loss was additive, indicating they work in different pathways (Kolinjivadi et al., 2017a). Also, SMARCAL1, ZRANB3 and HLTF have different mechanisms of regulation and differing phenotypes upon loss, indicating that they are not redundant (Poole and Cortez, 2017). It is still unknown how they work in cells, why there are so many of them and if indeed, they are all performing the same reaction. One possibility is that SMARCAL1, ZRANB3 and HLTF are recruited at different points in the reversal reaction due to their differing mechanisms of regulation or substrate preference (See introduction and (Poole and Cortez, 2017) for details). For example, HLTF also has E3 ubiquitin ligase activity, and HLTF mediated ubiquitination of PCNA could serve as the signal for ZRANB3 recruitment. Alternatively, SMARCAL1 could initially reverse the fork until the leading nascent strand (with a 3'OH) is at the fork junction. This structure is a preferred substrate for HLTF, which could then continue the fork

regression reaction (Kile et al., 2015). However, it is still unclear how these enzymes would cooperate with RAD51.

A tool for studying RAD51 fork functions

The T131P Rad51 is a patient derived mutation that renders RAD51 incapable of fork protection, but proficient in fork reversal and HDR. It is interesting that T131P Rad51 is incapable of forming stable filaments (Wang et al., 2015; Zadorozhny et al., 2017), and yet is proficient in HDR. This is consistent with the idea that filament stabilization is less important in HDR as compared to fork protection. It is also consistent with the idea that there is a lesser requirement for RAD51 function is required for reversal as compared to fork protection (see Chapter V for details).

The model that RADXΔ causes increased breaks due to too much fork reversal predicts that RADXΔ should also cause an increase in breaks in a RAD51 mutant cell line that retains the ability to perform fork reversal. However, siRADX in the T131P mutant cells does not cause increased breaks (Figure 6.8). This suggests that the breaks do not arise from fork reversal alone but require some function of RAD51 that is missing from these cell lines. In other words, fork breakage has additional requirements than just fork reversal. If true, this cell line could prove to be a useful tool for studying RAD51 functions at forks.

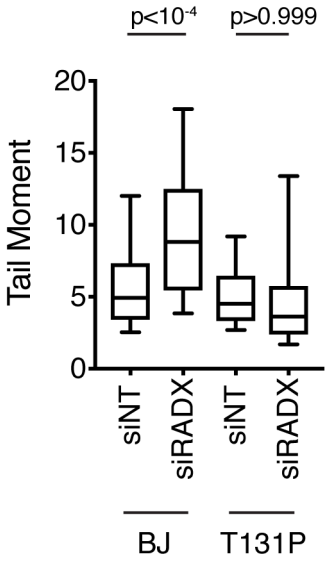

Figure 6.8. RADX silencing does not induce breaks in RAD51-mutant cells. Wild-type (BJ) or RAD51 mutant (T131P) fibroblasts were transfected with the indicated siRNA and the extent of breaks measured using a neutral comet assay. P values are derived from a Mann-Whitney test. Experiment is representative of three repeats.

Future Directions

Protein interactions for RADX

I performed several IP-MS screens to identify interaction partners for RADX. Unfortunately, my purifications were not very good and I observed no strong enrichment of protein interaction partners in my IP samples. These screens were performed with Flag-RADX overexpression and since RADX is expressed endogenously at very low levels, we reasoned that most of the overexpressed protein could be non-functional. Therefore, I tried to purify endogenous protein using commercially available and custom-generated antibodies. However, none of the antibodies were able to IP the protein. I also performed SILAC-IPs with overexpressed proteins in an effort to improve the signal to noise ratio, but did not see strong interactions. Some weak interactors that I observed in some of my datasets were the MCM2-6 complex, BRCA1, BLM and HLTF. I was able to confirm all of these by a Flag-IP followed by immunoblotting (Figure 6.4A). I was also able to validate the BLM interaction by endogenous-reverse IP of BLM (Figure 6.4B). The interactions with BRCA1, BLM and HLTF were insensitive to DNAse treatment, but the interaction with MCM2-6 seemed to be mediated by DNA (Data not shown). However, none of these proteins' abundance changed in iPOND-MS screens with RADXΔ or overexpression and so we did not follow up on the interactions. That said, the interaction with BLM would fit most of our data, since BLM negatively regulates RAD51 at forks.

An alternate approach would be to develop a system to purify endogenous RADX. While this has not worked in the past due to availability of good antibodies, we could use the CRISPR-CAS system to knock in a tag to RADX and purify the endogenous protein for MS analyses. Identification of interaction partners will help in understanding the mechanisms by which RADX regulates genome stability.

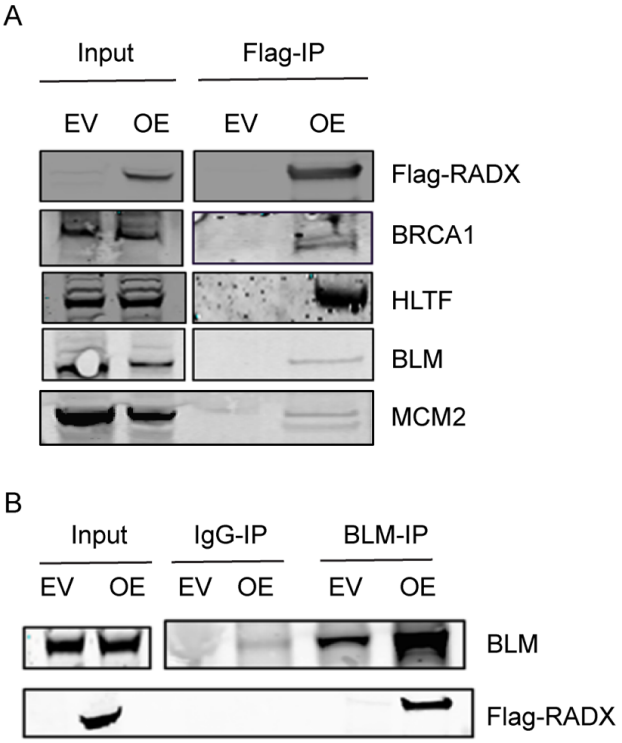

Figure 6.8. Co-immunoprecipitations for RADX-interacting proteins. (A and B) Cells were either transfected with an Empty Vector (EV) or Flag-RADX (OE). Nuclear extracts prepared from these cells were immunoprecipitated with a Flag antibody in A or an antibody recognizing Bloom (BLM) in B and probed with the indicated antibodies.

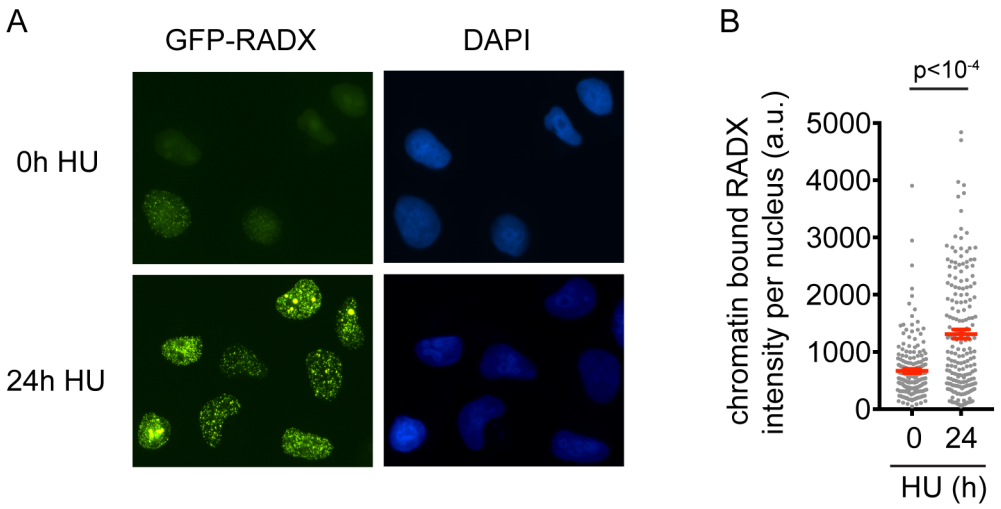

Figure 6.9. GFP-RADX is recruited to chromatin following DNA damage. (A) Representative image of U2OS cells overexpressing GFP-RADX treated with 3mM HU for the indicated times following detergent extraction. (B) The intensity of chromatin-bound GFP-RADX per nucleus was quantified. The experiment is representative of three repeats. P value derived from a Mann-Whitney test.

Localization of RADX to replication forks

RADX localizes to unperturbed replication forks and is highly enriched at stalled forks by iPOND (Figure 4.1 and (Dungrawala et al., 2017)). To investigate its colocalization with other replication fork proteins, I performed immunofluorescence imaging with overexpression of a GFP-tagged RADX cDNA that we have utilized for complementing RADXΔ cells (Chapter IV). GFP-RADX forms detergent-resistant foci even in unperturbed cells and the intensity of foci increases upon treatment with DNA damage (Figure 6.5). However, despite several attempts, I could not obtain convincing colocalization data for GFP-RADX foci with PCNA or RPA. There were some foci that co-localized with EdU, but it was hard to distinguish if those were real since the majority of the foci did not colocalize. The GFP-RADX foci also did not colocalize with telomeres or PML bodies.

These results, combined with our IP-MS lead us to speculate that the majority of overexpressed RADX forms aggregates and is non-functional. Another group studying RADX also observed similar immunofluorescence results as we did with overexpressed protein and arrived at the same conclusion (Schubert et al., 2017). However, it is worth noting that the foci are dependent on the ability to bind DNA, since a DNA binding mutant of RADX does not form foci (Data not shown). Additionally, it is also worth noting that protein truncations of the C-terminus (which leaves the predicted OB-folds intact) also do not form foci, despite being expressed at the same levels as wild-type (see next section for more details).

The approach of tagging endogenous protein should also be a great system to investigate RADX localization and to test if its recruitment is dependent on other factors. Alternatively, we have just started utilizing Proximity Ligation Assays (PLA) in our lab and this might be another approach to look at RADX localization/recruitment. The limitation for PLA thus far has been the

lack of a good antibody to RADX, but the endogenously-tagged RADX should be amenable to the protocol.

Structure-Function analyses of RADX

RADX is predicted to have five domains, three of which are N-terminal RPA like OB-Folds (Figure 4.6A). The fourth and fifth domains, at the C-terminus of the protein, are predicted to resemble the oligomerization domains of bacterial transcription factors DasR and NrtR (Remy Le Meur, unpublished observations). To test if RADX could oligomerize, I co-transfected Flag-tagged and HA-tagged RADX cDNA into cells, immuno-precipitated the Flag-RADX and blotted for the HA-RADX. My preliminary experiments suggest that RADX can oligomerize (Figure 6.6), although the experiment has to be repeated with additional controls to test if the oligomerization was DNA mediated and to perform the reverse-IP.

Apart from the knowledge that OB-2 of RADX is required for DNA binding, there is little we know about the rest of the domains and what their functions are. One possibility is that the C-terminus mediates protein interactions while the N-terminus is required for DNA binding. This would help explain why C-terminal truncations of the protein do not form foci despite having their OB-folds intact. Alternatively, the C-terminus could also be required for DNA binding. Thus, identifying the minimum unit of RADX that is required to bind DNA, and required for localization would provide insights into the mechanisms of its function. It would also be worthwhile to perform IPs for interacting proteins with the C-terminus of RADX.

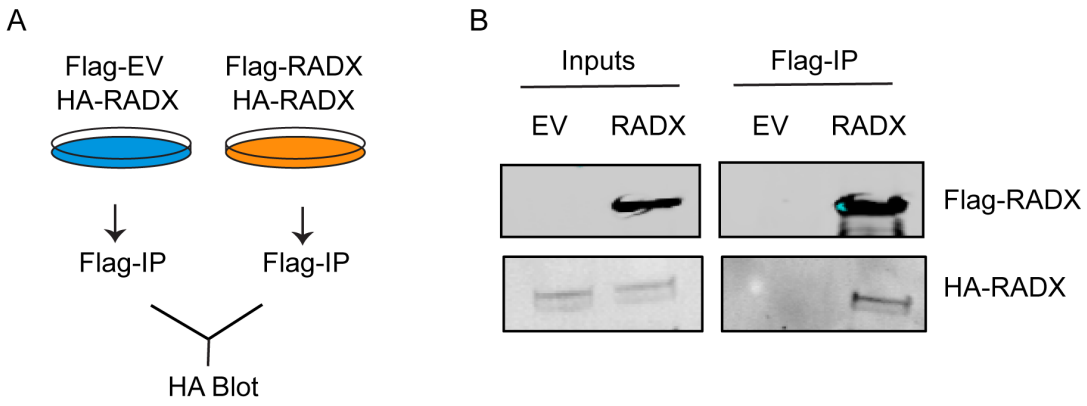

Figure 6.10. Co-immunoprecipitation to test if RADX can form oligomers. A) Schematic of the experiment. Cells were transfected with HA-RADX and Flag-Empty Vector (EV) or Flag-RADX. A flag-IP was done, following which the samples were probed with an anti-HA antibody. B) Immunoblot for Flag and HA as indicated.

APPENDIX A

This appendix contains information about an in vivo assay to measure fork regression that I attempted to develop.

Design of an assay to detect nascent DNA duplexes in cells

DNA replication is semiconservative, and DNA molecules in cells are always composed of parental-nascent DNA duplexes. Fork reversal causes an unwinding of this nascent-parental duplex and forces the formation of a “chicken foot” or a DNA duplex composed entirely of nascent DNA. I proposed to purify reversed forks by taking advantage of the fact that fork regression results in a transient DNA duplex composed of two nascent DNA molecules.

In order to stabilize the transient nascent DNA duplex through the process of purification, I used 6-thioguanine (6-TG), a nitrogenous base that can be incorporated into DNA. The advantage of utilizing 6-TG as compared to other well-known DNA analogues, including BrdU, IdU or CldU is that when exposed to long wavelength UV light, 6-TG is capable of forming an inter-molecular disulfide bond with an opposing molecule of 6-TG present on the other strand of the duplex (Brem et al., 2011). Based on this property, I designed a protocol (Figure AA.1) that involves pulsing cells with 6-TG for a short period of time such that 6-TG is only incorporated into the nascent DNA. In this situation, disulfide bonds upon UV treatment can be formed only if there are instances of nascent-nascent DNA duplex formation. Thus, performing this assay in instances

where fork reversal is induced would cause, in theory, the stabilization of all reversed forks through disulfide bond crosslinking.

Following the UV-mediated crosslinking of these replication intermediates, the challenge is to purify these crosslinked DNA duplexes away from the rest of the genomic DNA. To do this, I decided to employ a rapid DNA denaturation process that renders all non-crosslinked DNA single-stranded. The crosslinked DNA would remain double stranded as it is resistant to the denaturation. I then incubated the DNA with a single-stranded DNA nuclease (S1 nuclease) that degrades all denatured DNA. At the end of this process, the crosslinked replication intermediates should be the only double stranded, intact DNA left, which can be visualized by agarose gel electrophoresis or detected by other methods.

Optimization and Preliminary Results

To maximize the signal for optimization of the protocol, I performed preliminary experiments where I treated cells with 6-TG for 48 hours to label all genomic DNA. Using this strategy, I was able to optimize the individual steps in the protocol including the crosslinking time, heat denaturation process, and the S1 digestion. I observed that the formation of intact, double-stranded DNA at the end of the protocol increased as more DNA was labeled with 6-TG and required UV-induced crosslinking of 6-TG labeled DNA (Figure AA.2). Additionally, the reduction of disulfide bonds with DTT resulted in the disappearance of intact DNA after S1 nuclease digestion (Figure AA.3). These DNA duplexes were also not affected by RNase H, suggesting that they were not composed of RNA-DNA hybrids (Figure AA.4). These data led me to conclude that the purified DNA at the end of the protocol was crosslinked with disulfide bonds dependent on 6-TG incorporation. Thus, this methodology was capable of purifying crosslinked 6-TG containing DNA duplexes.

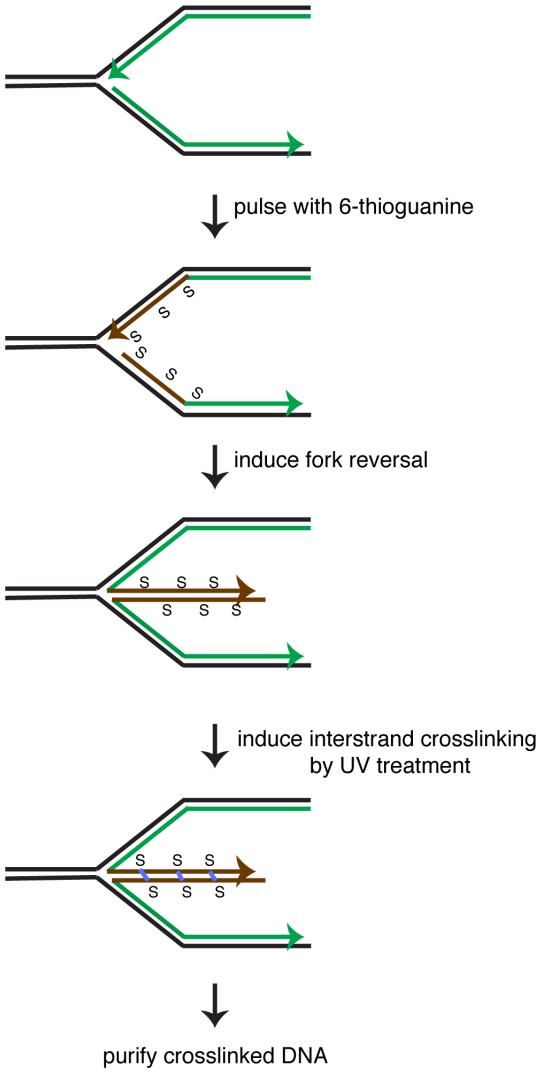

Figure AA.1. Schematic of the assay to detect fork reversal in cells. See text for details.

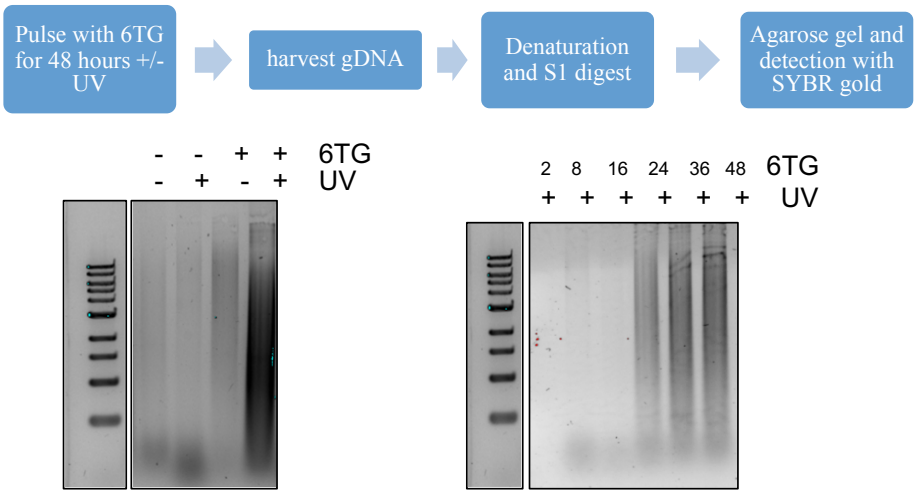

Figure AA.2. The protocol purifies crosslinked DNA. The formation of S1 resistant DNA is dependent on UV treatment (left) and on treatment with 6-thioguanine (right). The schematic of the process is also depicted.

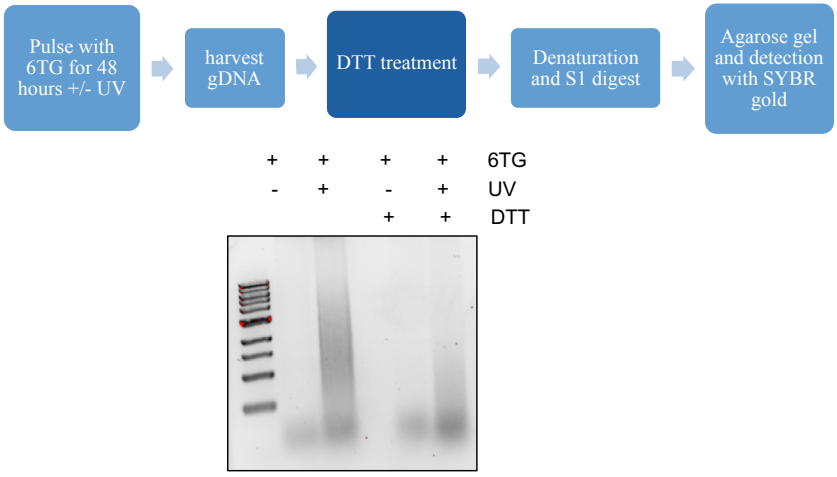

Figure AA.3. The crosslinks are mediated by disulfide bonds. The resistance of crosslinked DNA to S1 digestion is reversed by DTT treatment.

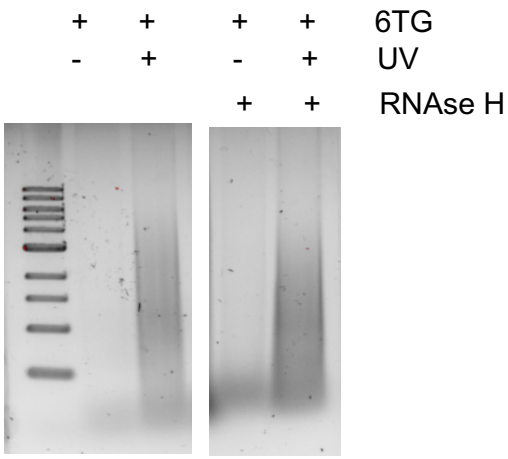

Figure AA.4. The crosslinks are not composed of RNA-DNA hybrids. The resistance of crosslinked DNA to S1 digestion is not altered by RNAse H treatment.

Utilization of the assay to detect fork reversal events

I next applied this method to purifying fork reversal events in my experimental conditions by decreasing the pulse time to 2-4 hours, such that only newly synthesizing DNA incorporates 6-TG. I induced fork reversal using different genotoxic treatments (Zellweger et al., 2015) and scaled up the amount of starting material for detection purposes. My results from these experiments with asynchronous cells were highly variable with no clear pattern for the formation of S1 nuclease-resistant DNA (Figure AA.5). In an attempt to maximize the signal, I synchronized the cells with thymidine blocks to enrich for replicating cells as fork reversal is a replication associated phenomenon. Unfortunately, this experiment indicated that the formation of the S1-resistant DNA was not dependent on S phase and hence could not be a measure of fork reversal events (Figure AA.6). The DNA detected under these circumstances is probably due to the background contributed by incomplete denaturation and/or incomplete S1 digestion. I changed the denaturation method from a single cycle to multiple cycles and also tried multiple rounds of S1 digestion to optimize the S1 nuclease digestion; however, these changes resulted in the loss of intact DNA in my positive control (Figure AA.7). Despite performing several other experiments, including changing the detection method to a radioactive end-labeling protocol, I was unable to develop a consistent method for monitoring fork reversal.

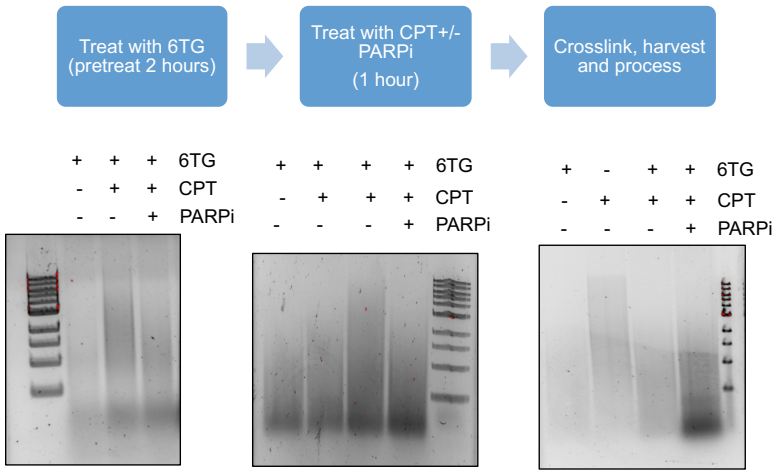

Figure AA.5. There is no consistency in the formation of S1 resistant DNA after short treatments with 6TG and camptothecin. Three representative experiments are depicted.

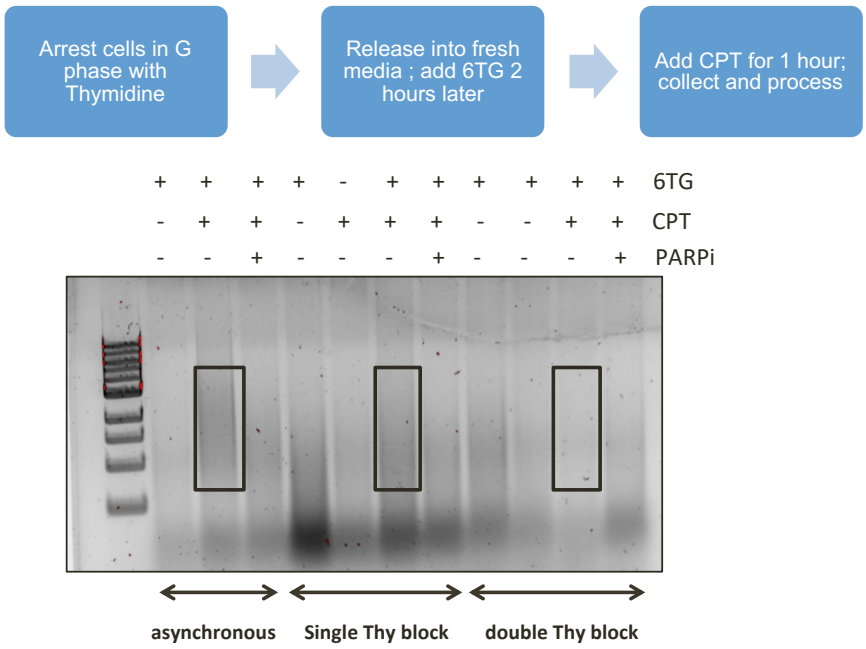

Figure AA.6. The formation of S1 resistant DNA does not depend on DNA replication. There is no correlation between the formation of S1 resistant DNA and cells in S-phase. The black outlines indicate the lanes in which we would expect to see an accumulation of reversed forks, and thus increased S1-resistant DNA.

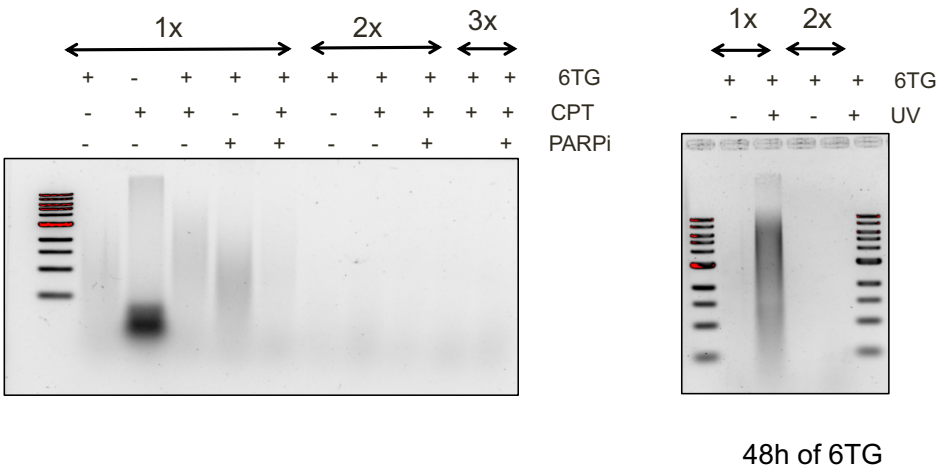

Figure AA.7. Multiple cycles of S1 digestion results in loss of all crosslinked DNA. The samples were processed in a similar way as described previously (1x) or were heat denatured followed by rapid cooling and nuclease digestion two or three times (2x or 3x). The gel on the right are samples after 2 hours of 6TG treatment, while the gel on the right contains cells treated with 6TG for 48 hours.

REFERENCES

1. Abd Wahab, S., Choi, M., and Bianco, P.R. (2013). Characterization of the ATPase Activity of RecG and RuvAB Proteins on Model Fork Structures Reveals Insight into Stalled DNA Replication Fork Repair. J. Biol. Chem. *288*, 26397–26409.

2. Aihara, H., Ito, Y., Kurumizaka, H., Yokoyama, S., and Shibata, T. (1999). The N-terminal domain of the human Rad51 protein binds DNA: structure and a DNA binding surface as revealed by NMR. J. Mol. Biol. *290*, 495–504.

3. Anand, R.P., Lovett, S.T., and Haber, J.E. (2013). Break-induced DNA replication. Cold Spring Harb. Perspect. Biol. *5* (12).

4. Arunkumar, A.I., Stauffer, M.E., Bochkareva, E., Bochkarev, A., and Chazin, W.J. (2003). Independent and coordinated functions of replication protein A tandem high affinity single-stranded DNA binding domains. J. Biol. Chem. *278*, 41077–41082.

5. Atkinson, J., and McGlynn, P. (2009). Replication fork reversal and the maintenance of genome stability. Nucleic Acids Res. *37*, 3475–3492.

6. Awate, S., and Brosh, R.M. (2017). Interactive roles of DNA helicases and translocases with the single-stranded DNA binding protein RPA in nucleic acid metabolism. Int. J. Mol. Sci. *18*, 1233.

7. Ball, H.L., Myers, J.S., and Cortez, D. (2005). ATRIP binding to replication protein A-single-stranded DNA promotes ATR-ATRIP localization but is dispensable for Chk1 phosphorylation. Mol. Biol. Cell *16*, 2372–2381.

8. Bansbach, C.E., Bétous, R., Lovejoy, C.A., Glick, G.G., and Cortez, D. (2009). The annealing helicase SMARCAL1 maintains genome integrity at stalled replication forks. Genes Dev. *23*, 2405–2414.

9. Barnes, R.P., Hile, S.E., Lee, M.Y., and Eckert, K.A. (2017). DNA polymerases eta and kappa exchange with the polymerase delta holoenzyme to complete common fragile site synthesis. DNA Repair (Amst). *57*, 1–11.

10. Bass, T.E., Luzwick, J.W., Kavanaugh, G., Carroll, C., Dungrawala, H., Glick, G.G., Feldkamp, M.D., Putney, R., Chazin, W.J., and Cortez, D. (2016). ETAA1 acts at stalled replication forks to maintain genome integrity. Nat. Cell Biol. *18*, 1185–1195.

11. Baumann, P., and West, S.C. (1998). Role of the human RAD51 protein in homologous recombination and double-stranded-break repair. Trends Biochem. Sci. *23*, 247–251.

12. Baumann, P., Benson, F.E., and West, S.C. (1996). Human Rad51 protein promotes ATP-dependent homologous pairing and strand transfer reactions in vitro. Cell *87*, 757–766.

13. Benson, F.E., Stasiak, A., and West, S.C. (1994). Purification and characterization of the

human Rad51 protein, an analogue of E. coli RecA. EMBO J. *13*, 5764–5771.

14. Berti, M., and Vindigni, A. (2016). Replication stress: getting back on track. Nat. Struct. Mol. Biol. *23*, 103–109.

15. Berti, M., Chaudhuri, A.R., Thangavel, S., Gomathinayagam, S., Kenig, S., Vujanovic, M., Odreman, F., Glatter, T., Graziano, S., Mendoza-Maldonado, R., et al. (2013). Human RECQ1 promotes restart of replication forks reversed by DNA topoisomerase I inhibition. Nat. Struct. Mol. Biol. *20*, 347–354.

16. Bétous, R., Mason, A.C., Rambo, R.P., Bansbach, C.E., Badu-Nkansah, A., Sirbu, B.M., Eichman, B.F., and Cortez, D. (2012). SMARCAL1 catalyzes fork regression and holliday junction migration to maintain genome stability during DNA replication. Genes Dev. *26*, 151–162.

17. Bétous, R., Couch, F.B., Mason, A.C., Eichman, B.F., Manosas, M., and Cortez, D. (2013a). Substrate-selective repair and restart of replication forks by DNA translocases. Cell Rep. *3*, 1958–1969.

18. Bétous, R., Glick, G.G., Zhao, R., and Cortez, D. (2013b). Identification and Characterization of SMARCAL1 Protein Complexes. PLoS One *8*, e63149.

19. Bhat, K.P., Bétous, R., and Cortez, D. (2015). High-affinity DNA-binding domains of replication protein A (RPA) direct SMARCAL1-dependent replication fork remodeling. J. Biol. Chem. *290*, 4110–4117.

20. Bhowmick, R., Minocherhomji, S., and Hickson, I.D. (2016). RAD52 Facilitates Mitotic DNA Synthesis Following Replication Stress. Mol. Cell *64*, 1117–1126.

21. Bielinsky, a K., and Gerbi, S. a (2001). Where it all starts: eukaryotic origins of DNA replication. J. Cell Sci. *114*, 643–651.

22. Binz, S.K., Lao, Y., Lowry, D.F., and Wold, M.S. (2003). The phosphorylation domain of the 32-kDa subunit of replication protein A (RPA) modulates RPA-DNA interactions: Evidence for an intersubunit interaction. J. Biol. Chem. *278*, 35584–35591.

23. Bochkarev, A., and Bochkareva, E. (2004). From RPA to BRCA2: Lessons from single-stranded DNA binding by the OB-fold. Curr. Opin. Struct. Biol. *14*, 36–42.

24. Bochkareva, E., Korolev, S., and Bochkarev, a (2000). The role for zinc in replication protein A. J. Biol. Chem. *275*, 27332–27338.

25. Bochkareva, E., Belegu, V., Korolev, S., and Bochkarev, A. (2001). Structure of the major single-stranded DNA-binding domain of replication protein A suggests a dynamic mechanism for DNA binding. EMBO J. *20*, 612–618.

26. Bochkareva, E., Korolev, S., Lees-Miller, S.P., and Bochkarev, A. (2002). Structure of the RPA trimerization core and its role in the multistep DNA-binding mechanism of RPA. EMBO J. *21*, 1855–1863.

27. Boerkoel, C.F., Takashima, H., John, J., Yan, J., Stankiewicz, P., Rosenbarker, L., André,

J.-L.L., Bogdanovic, R., Burguet, A., Cockfield, S., et al. (2002). Mutant chromatin remodeling protein SMARCAL1 causes Schimke immuno-osseous dysplasia. Nat. Genet. *30*, 215–220.

28. Borgstahl, G.E.O., Brader, K., Mosel, A., Liu, S., Kremmer, E., Goettsch, K. a., Kolar, C., Nasheuer, H.-P., and Oakley, G.G. (2014). Interplay of DNA damage and cell cycle signaling at the level of human replication protein A. DNA Repair (Amst). *21*, 12–23.

29. Branzei, D. (2011). Ubiquitin family modifications and template switching. FEBS Lett. *585*, 2810–2817.

30. Brem, R., Daehn, I., and Karran, P. (2011). Efficient DNA interstrand crosslinking by 6-thioguanine and UVA radiation. DNA Repair (Amst). *10*, 869–876.

31. Brosey, C. a, Yan, C., Tsutakawa, S.E., Heller, W.T., Rambo, R.P., Tainer, J. a, Ivanov, I., and Chazin, W.J. (2013). A new structural framework for integrating replication protein A into DNA processing machinery. Nucleic Acids Res. *41*, 2313–2327.

32. Brosh, R.M., Li, J.L., Kenny, M.K., Karow, J.K., Cooper, M.P., Kureekattil, R.P., Hickson, I.D., and Bohr, V. a (2000). Replication protein A physically interacts with the Bloom's syndrome protein and stimulates its helicase activity. J. Biol. Chem. *275*, 23500–23508.

33. Brown, E.J., and Baltimore, D. (2000). ATR disruption leads to chromosomal fragmentation and early embryonic lethality. Genes Dev. *14*, 397–402.

34. Budke, B., Lv, W., Kozikowski, A.P., and Connell, P.P. (2016). Recent Developments Using Small Molecules to Target RAD51: How to Best Modulate RAD51 for Anticancer Therapy? ChemMedChem *11*, 2468–2473.

35. Bugreev, D. V, and Mazin, A. V (2004). Ca2+ activates human homologous recombination protein Rad51 by modulating its ATPase activity. Proc. Natl. Acad. Sci. U. S. A. *101*, 9988–9993.

36. Bugreev, D. V., Rossi, M.J., and Mazin, A. V. (2011). Cooperation of RAD51 and RAD54 in regression of a model replication fork. Nucleic Acids Res. *39*, 2153–2164.

37. Bugreev, D. V., Huang, F., Mazina, O.M., Pezza, R.J., Voloshin, O.N., Daniel Camerini-Otero, R., and Mazin, A. V. (2014). HOP2-MND1 modulates RAD51 binding to nucleotides and DNA. Nat. Commun. *5*: 4198.

38. Burgers, P.M.J., and Kunkel, T.A. (2017). Eukaryotic DNA Replication Fork. Annu. Rev. Biochem. *86*, 417–438.

39. Buss, J. a, Kimura, Y., and Bianco, P.R. (2008). RecG interacts directly with SSB: implications for stalled replication fork regression. Nucleic Acids Res. *36*, 7029–7042.

40. Byun, T.S., Pacek, M., Yee, M., Walter, J.C., and Cimprich, K.A. (2005). Functional uncoupling of MCM helicase and DNA polymerase activities activates the ATR-dependent checkpoint. Genes Dev. *19*, 1040–1052.

41. Carr, A.M., and Lambert, S. (2013). Replication stress-induced genome instability: the

dark side of replication maintenance by homologous recombination. J. Mol. Biol. *425*, 4733–4744.

42. Carreira, A., and Kowalczykowski, S.C. (2011). Two classes of BRC repeats in BRCA2 promote RAD51 nucleoprotein filament function by distinct mechanisms. Proc. Natl. Acad. Sci. *108*, 10448–10453.

43. Carreira, A., Hilario, J., Amitani, I., Baskin, R.J., Shivji, M.K.K., Venkitaraman, A.R., and Kowalczykowski, S.C. (2009). The BRC Repeats of BRCA2 Modulate the DNA-Binding Selectivity of RAD51. Cell *136*, 1032–1043.

44. Carroll, C., Badu-Nkansah, A., Hunley, T., Baradaran-Heravi, A., Cortez, D., and Frangoul, H. (2013). Schimke immunoosseous dysplasia associated with undifferentiated carcinoma and a novel SMARCAL1 mutation in a child. Pediatr. Blood Cancer *60,* 88-90.

45. Ceccaldi, R., Sarangi, P., and D'Andrea, A.D. (2016). The Fanconi anaemia pathway: New players and new functions. Nat. Rev. Mol. Cell Biol. *17*, 337–349.

46. Chastain, M., Zhou, Q., Shiva, O., Fadri-Moskwik, M., Whitmore, L., Jia, P., Dai, X., Huang, C., Ye, P., and Chai, W. (2016). Human CST Facilitates Genome-wide RAD51 Recruitment to GC-Rich Repetitive Sequences in Response to Replication Stress (Cell Rep. *16*, 1300–1314.

47. Chatterjee, G., Jimenez-Sainz, J., Presti, T., Nguyen, T., and Jensen, R.B. (2016). Distinct binding of BRCA2 BRC repeats to RAD51 generates differential DNA damage sensitivity. Nucleic Acids Res. *44*, 5256–5270.

48. Chaudhuri, A.R., Callen, E., Ding, X., Gogola, E., Duarte, A.A., Lee, J.-E., Wong, N., Lafarga, V., Calvo, J.A., Panzarino, N.J., et al. (2016). Replication fork stability confers chemoresistance in BRCA-deficient cells. Nature *535*, 382–387.

49. Chen, R., and Wold, M.S. (2014). Replication protein A: Single-stranded DNA's first responder: Dynamic DNA-interactions allow replication protein A to direct single-strand DNA intermediates into different pathways for synthesis or repair. Bioessays *36*, 1156–1161.

50. Chen, R., Subramanyam, S., Elcock, A.H., Spies, M., and Wold, M.S. (2016). Dynamic binding of replication protein a is required for DNA repair. Nucleic Acids Res. *44*, 5758–5772.

51. Chi, P., Van Komen, S., Sehorn, M.G., Sigurdsson, S., and Sung, P. (2006). Roles of ATP binding and ATP hydrolysis in human Rad51 recombinase function. DNA Repair (Amst). *5*, 381–391.

52. Chow, K.H., and Courcelle, J. (2004). RecO Acts with RecF and RecR to Protect and Maintain Replication Forks Blocked by UV-induced DNA Damage in Escherichia coli. J. Biol. Chem. *279*, 3492–3496.

53. Chun, J., Buechelmaier, E.S., and Powell, S.N. (2013). Rad51 Paralog Complexes BCDX2 and CX3 Act at Different Stages in the BRCA1-BRCA2-Dependent Homologous Recombination Pathway. Mol. Cell. Biol. *33*, 387–395.

54. Ciccia, A., and Elledge, S.J. (2011). The DNA Damage Response: Making It Safe to Play with Knives.

55. Ciccia, A., Bredemeyer, A.L., Sowa, M.E., Terret, M.-E., Jallepalli, P. V, Harper, J.W., and Elledge, S.J. (2009). The SIOD disorder protein SMARCAL1 is an RPA-interacting protein involved in replication fork restart. Genes Dev. *23*, 2415–2425.

56. Ciccia, A., Nimonkar, A. V, Hu, Y., Hajdu, I., Achar, J., Izhar, L., Petit, S.A., Adamson, B., Yoon, J.C., Kowalczykowski, S.C., et al. (2012). The ZRANB3 translocase associates with poly-ubiquitinated PCNA to promote fork restart and limit recombination after replication stress. Mol. Cell *47*, 396–409.

57. Cimprich, K.A., and Cortez, D. (2008). ATR: an essential regulator of genome integrity. Nat. Rev. Mol. Cell Biol. *9*, 616–627.

58. Costantino, L., Sotiriou, S.K., Rantala, J.K., Magin, S., Mladenov, E., Helleday, T., Haber, J.E., Iliakis, G., Kallioniemi, O.P., and Halazonetis, T.D. (2014). Break-induced replication repair of damaged forks induces genomic duplications in human cells. Science *343*, 88–91.

59. Couch, F.B., and Cortez, D. (2014). Fork reversal, too much of a good thing. Cell Cycle *13*, 1049–1050.

60. Couch, F.B., Bansbach, C.E., Driscoll, R., Luzwick, J.W., Glick, G.G., Bétous, R., Carroll, C.M., Jung, S.Y., Qin, J., Cimprich, K. a, et al. (2013). ATR phosphorylates SMARCAL1 to prevent replication fork collapse. Genes Dev. *27*, 1610–1623.

61. Courcelle, J., Carswell-Crumpton, C., and Hanawalt, P.C. (1997). recF and recR are required for the resumption of replication at DNA replication forks in Escherichia coli. Proc. Natl. Acad. Sci. U. S. A. *94*, 3714–3719.

62. Courcelle, J., Donaldson, J.R., Chow, K.H., and Courcelle, C.T. (2003). DNA damage-induced replication fork regression and processing in Escherichia coli. Science *299* , 1064 –1067.

63. Cox, M.M. (2007). Regulation of Bacterial RecA Protein Function. Crit. Rev. Biochem. Mol. Biol. *42*, 41–63.

64. Davies, O.R., and Pellegrini, L. (2007). Interaction with the BRCA2 C terminus protects RAD51-DNA filaments from disassembly by BRC repeats. Nat. Struct. Mol. Biol. *14*, 475–483.

65. Defossez, P.A., Prusty, R., Kaeberlein, M., Lin, S.J., Ferrigno, P., Silver, P.A., Keil, R.L., and Guarente, L. (1999). Elimination of replication block protein Fob1 extends the life span of yeast mother cells. Mol. Cell *3*, 447–455.

66. Delagoutte, E., Heneman-Masurel, A., and Baldacci, G. (2011). Single-stranded DNA binding proteins unwind the newly synthesized double-stranded DNA of model miniforks. Biochemistry *50*, 932–944.

67. Dilley, R.L., Verma, P., Cho, N.W., Winters, H.D., Wondisford, A.R., and Greenberg, R.A.

(2016). Break-induced telomere synthesis underlies alternative telomere maintenance. Nature *539*, 54–58.

68. Ding, X., Chaudhuri, A.R., Callen, E., Pang, Y., Biswas, K., Klarmann, K.D., Martin, B.K., Burkett, S., Cleveland, L., Stauffer, S., et al. (2016). Synthetic viability by BRCA2 and PARP1/ARTD1 deficiencies. Nat. Commun. *7*, 12425.

69. Doherty, K.M., Sommers, J. a, Gray, M.D., Lee, J.W., von Kobbe, C., Thoma, N.H., Kureekattil, R.P., Kenny, M.K., and Brosh, R.M. (2005). Physical and functional mapping of the replication protein a interaction domain of the werner and bloom syndrome helicases. J. Biol. Chem. *280*, 29494–29505.

70. Donnianni, R. a, and Symington, L.S. (2013). Break-induced replication occurs by conservative DNA synthesis. Proc. Natl. Acad. Sci. U. S. A. *110*, 13475–13480.

71. Dou, H., Huang, C., Singh, M., Carpenter, P.B., and Yeh, E.T.H. (2010). Regulation of DNA Repair through DeSUMOylation and SUMOylation of replication protein A complex. Mol. Cell *39*, 333–345.

72. Drees, J.C., Lusetti, S.L., Chitteni-Pattu, S., Inman, R.B., and Cox, M.M. (2004). A RecA filament capping mechanism for RecX protein. Mol. Cell *15*, 789–798.

73. Dungrawala, H., Rose, K.L., Bhat, K.P., Mohni, K.N., Glick, G.G., Couch, F.B., and Cortez, D. (2015). The replication checkpoint prevents two types of fork collapse without regulating replisome stability. Mol. Cell *59*, 998–1010.

74. Dungrawala, H., Bhat, K.P., Le Meur, R., Chazin, W.J., Ding, X., Sharan, S.K., Wessel, S.R., Sathe, A.A., Zhao, R., and Cortez, D. (2017). RADX Promotes Genome Stability and Modulates Chemosensitivity by Regulating RAD51 at Replication Forks. Mol. Cell *67*, 374–386.

75. Duursma, A.M., Driscoll, R., Elias, J.E., and Cimprich, K.A. (2013). A Role for the MRN Complex in ATR Activation via TOPBP1 Recruitment. Mol. Cell *50*, 116–122.

76. Duxin, J.P., Dewar, J.M., Yardimci, H., and Walter, J.C. (2014). Repair of a DNA-protein crosslink by replication-coupled proteolysis. Cell *159*, 349–357.

77. Edwards, S.L., Brough, R., Lord, C.J., Natrajan, R., Vatcheva, R., Levine, D. a, Boyd, J., Reis-Filho, J.S., and Ashworth, A. (2008). Resistance to therapy caused by intragenic deletion in BRCA2. Nature *451*, 1111–1115.

78. Elia, A.E.H., Wang, D.C., Willis, N.A., Boardman, A.P., Hajdu, I., Adeyemi, R.O., Lowry, E., Gygi, S.P., Scully, R., and Elledge, S.J. (2015). RFWD3-Dependent Ubiquitination of RPA Regulates Repair at Stalled Replication Forks. Mol. Cell *60*, 280–293.

79. Elizondo, L.I., Cho, K.S., Zhang, W., Yan, J., Huang, C., Huang, Y., Choi, K., Sloan, E.A., Deguchi, K., Lou, S., et al. (2009). Schimke immuno-osseous dysplasia: SMARCAL1 loss-of-function and phenotypic correlation. J. Med. Genet. *46*, 49–59.

80. Elvers, I., Johansson, F., Groth, P., Erixon, K., and Helleday, T. (2011). UV stalled replication forks restart by re-priming in human fibroblasts. Nucleic Acids Res. *39*, 7049–

7057.

81. Esashi, F., Christ, N., Gannon, J., Liu, Y., Hunt, T., Jasin, M., and West, S.C. (2005). CDK-dependent phosphorylation of BRCA2 as a regulatory mechanism for recombinational repair. Nature *434*, 598–604.

82. Esashi, F., Galkin, V.E., Yu, X., Egelman, E.H., and West, S.C. (2007). Stabilization of RAD51 nucleoprotein filaments by the C-terminal region of BRCA2. Nat. Struct. Mol. Biol. *14*, 468–474.

83. Fan, J., and Pavletich, N.P. (2012). Structure and conformational change of a replication protein A heterotrimer bound to ssDNA. Genes Dev. *26*, 2337–2347.

84. Fanning, E., Klimovich, V., and Nager, A.R. (2006). A dynamic model for replication protein A (RPA) function in DNA processing pathways. Nucleic Acids Res. *34*, 4126–4137.

85. Feng, W., and Jasin, M. (2017). BRCA2 suppresses replication stress-induced mitotic and G1 abnormalities through homologous recombination. Nat. Commun. *8*:525.

86. Feng, J., Wakeman, T., Yong, S., Wu, X., Kornbluth, S., and Wang, X.-F. (2009). Protein phosphatase 2A-dependent dephosphorylation of replication protein A is required for the repair of DNA breaks induced by replication stress. Mol. Cell. Biol. *29*, 5696–5709.

87. Flynn, R.L., and Zou, L. (2010). Oligonucleotide/oligosaccharide-binding fold proteins: a growing family of genome guardians. Crit. Rev. Biochem. Mol. Biol. *45*, 266–275.

88. Follonier, C., Oehler, J., Herrador, R., and Lopes, M. (2013). Friedreich's ataxia-associated GAA repeats induce replication-fork reversal and unusual molecular junctions. Nat. Struct. Mol. Biol. *20*, 486–494.

89. Forget, A.L., and Kowalczykowski, S.C. (2010). Single-molecule imaging brings Rad51 nucleoprotein filaments into focus. Trends Cell Biol. *20*, 269–276.

90. Fu, D., Calvo, J.A., and Samson, L.D. (2012). Balancing repair and tolerance of DNA damage caused by alkylating agents. Nat. Rev. Cancer *12*, 104–120.

91. Fujiwara, Y., and Tatsumi, M. (1976). Replicative bypass repair of ultraviolet damage to DNA of mammalian cells: Caffeine sensitive and caffeine resistant mechanisms. Mutat. Res. - Fundam. Mol. Mech. Mutagen. *37*, 91–109.

92. Galkin, V.E., Esashi, F., Yu, X., Yang, S., West, S.C., and Egelman, E.H. (2005). BRCA2 BRC motifs bind RAD51-DNA filaments. Proc. Natl. Acad. Sci. *102*, 8537–8542.

93. García-Gómez, S., Reyes, A., Martínez-Jiménez, M.I., Chocrón, E.S., Mourón, S., Terrados, G., Powell, C., Salido, E., Méndez, J., Holt, I.J., et al. (2013). PrimPol, an Archaic Primase/Polymerase Operating in Human Cells. Mol. Cell *52*, 541–553.

94. German, J., and Alhadeff, B. (2001). Analysis of sister-chromatid exchanges. Curr. Protoc. Hum. Genet. *Chapter 8*, Unit 8.6.

95. Gibb, B., Ye, L.F., Gergoudis, S.C., Kwon, Y., Niu, H., Sung, P., and Greene, E.C. (2014).

Concentration-dependent exchange of replication protein A on single-stranded DNA revealed by single-molecule imaging. PLoS One *9*, e87922.

96. Guillemette, S., Serra, R.W., Peng, M., Hayes, J.A., Konstantinopoulos, P.A., Green, M.R., Green, M.R., and Cantor, S.B. (2015). Resistance to therapy in BRCA2 mutant cells due to loss of the nucleosome remodeling factor CHD4. Genes Dev. *29*, 489–494.

97. Haahr, P., Hoffmann, S., Tollenaere, M.A.X., Ho, T., Toledo, L.I., Mann, M., Bekker-Jensen, S., Räschle, M., and Mailand, N. (2016). Activation of the ATR kinase by the RPA-binding protein ETAA1. Nat. Cell Biol. *18*, 1196–1207.

98. Haas, K.T., Lee, M., Esposito, A., and Venkitaraman, A.R. (2018). Single-molecule localization microscopy reveals molecular transactions during RAD51 filament assembly at cellular DNA damage sites. Nucleic Acids Res. gkx*1303.*

99. Haring, S.J., Mason, A.C., Binz, S.K., and Wold, M.S. (2008). Cellular functions of human RPA1: Multiple roles of domains in replication, repair, and checkpoints. J. Biol. Chem. *283*, 19095–19111.

100. Hartlerode, A.J., and Scully, R. (2009). Mechanisms of double-strand break repair in somatic mammalian cells. Biochem. J. *423*, 157–168.

101. Hashimoto, Y., Chaudhuri, A.R., Lopes, M., and Costanzo, V. (2010). Rad51 protects nascent DNA from Mre11-dependent degradation and promotes continuous DNA synthesis. Nat. Struct. Mol. Biol. *17*, 1305–1311.

102. Hashimoto, Y., Puddu, F., and Costanzo, V. (2012). RAD51- and MRE11-dependent reassembly of uncoupled CMG helicase complex at collapsed replication forks. Nat. Struct. Mol. Biol. *19*, 17–24.

103. Hass, C.S., Lam, K., and Wold, M.S. (2012). Repair-specific functions of replication protein A. J. Biol. Chem. *287*, 3908–3918.

104. Helleday, T., Petermann, E., Lundin, C., Hodgson, B., and Sharma, R. a (2008). DNA repair pathways as targets for cancer therapy. Nat. Rev. Cancer *8*, 193–204.

105. Higgins, N.P., Kato, K., and Strauss, B. (1976). A model for replication repair in mammalian cells. J. Mol. Biol. *101*, 417–425.

106. Higgs, M.R., and Stewart, G.S. (2016). Protection or resection: BOD1L as a novel replication fork protection factor. Nucleus *7*, 34–40.

107. Higgs, M.R., Reynolds, J.J., Winczura, A., Blackford, A.N., Borel, V., Miller, E.S., Zlatanou, A., Nieminuszczy, J., Ryan, E.L., Davies, N.J., et al. (2015). BOD1L Is Required to Suppress Deleterious Resection of Stressed Replication Forks. Mol. Cell *59*, 462–477.

108. Hilario, J., Amitani, I., Baskin, R.J., and Kowalczykowski, S.C. (2009). Direct imaging of human Rad51 nucleoprotein dynamics on individual DNA molecules. Proc. Natl. Acad. Sci. *106*, 361–368.

109. Horii, Z.I., and Suzuki, K. (1968). DEGRADATION OF THE DNA OF ESCHERICHIA COLI

K12 REC- (JC1569b) AFTER IRRADIATION WITH ULTRAVIOLET LIGHT*. Photochem. Photobiol. *8*, 93–105.

110. Hotchkiss, R.D. (1974). Models of Genetic Recombination. Annu. Rev. Microbiol. *28*, 445–468.

111. Hu, Y., Raynard, S., Sehorn, M.G., Lu, X., Bussen, W., Zheng, L., Stark, J.M., Barnes, E.L., Chi, P., Janscak, P., et al. (2007). RECQL5/Recql5 helicase regulates homologous recombination and suppresses tumor formation via disruption of Rad51 presynaptic filaments. Genes Dev. *21*, 3073–3084.

112. Iftode, C., and Borowiec, J.A. (2000). 5' - 3' molecular polarity of human replication protein A (hRPA) binding to pseudo-origin DNA substrates. Biochemistry *39*, 11970–11981.

113. Jensen, R.B., Carreira, A., and Kowalczykowski, S.C. (2010). Purified human BRCA2 stimulates RAD51-mediated recombination. Nature *467*, 678–683.

114. Jiang, X., Klimovich, V., Arunkumar, A.I., Hysinger, E.B., Wang, Y., Ott, R.D., Guler, G.D., Weiner, B., Chazin, W.J., and Fanning, E. (2006). Structural mechanism of RPA loading on DNA during activation of a simple pre-replication complex. EMBO J. *25*, 5516–5526.

115. Kadyrov, F.A., and Drake, J.W. (2004). UvsX recombinase and Dda helicase rescue stalled bacteriophage T4 DNA replication forks in vitro. J. Biol. Chem. *279*, 35735–35740.

116. Kass, E.M., Moynahan, M.E., and Jasin, M. (2016). When Genome Maintenance Goes Badly Awry. Mol. Cell *62*, 777–787.

117. Kemmerich, F.E., Daldrop, P., Pinto, C., Levikova, M., Cejka, P., and Seidel, R. (2016). Force regulated dynamics of RPA on a DNA fork. Nucleic Acids Res. *44*, 5837–5848.

118. Kile, A.C., Chavez, D.A., Bacal, J., Eldirany, S., Korzhnev, D.M., Bezsonova, I., Eichman, B.F., and Cimprich, K.A. (2015). HLTF's Ancient HIRAN Domain Binds 3' DNA Ends to Drive Replication Fork Reversal. Mol. Cell *58*, 1090–1100.

119. Klein, H.L. (2008). The consequences of Rad51 overexpression for normal and tumor cells. DNA Repair (Amst). *7*, 686–693.

120. De Klein, A., Muijtjens, M., Van Os, R., Verhoeven, Y., Smit, B., Carr, A.M., Lehmann, A.R., and Hoeijmakers, J.H.J. (2000). Targeted disruption of the cell-cycle checkpoint gene ATR leads to early embryonic lethality in mice. Curr. Biol. *10*, 479–482.

121. Kolinjivadi, A.M., Sannino, V., De Antoni, A., Zadorozhny, K., Kilkenny, M., Técher, H., Baldi, G., Shen, R., Ciccia, A., Pellegrini, L., et al. (2017a). Smarcal1-Mediated Fork Reversal Triggers Mre11-Dependent Degradation of Nascent DNA in the Absence of Brca2 and Stable Rad51 Nucleofilaments. Mol. Cell *67*, 867–881.

122. Kolinjivadi, A.M., Sannino, V., de Antoni, A., Técher, H., Baldi, G., and Costanzo, V. (2017b). Moonlighting at replication forks: a new life for homologous recombination proteins BRCA1, BRCA2 and RAD51. FEBS Lett. *591*, 1083–1100.

123. Kolpashchikov, D.M., Khodyreva, S.N., Khlimankov, D.Y., Wold, M.S., Favre, a, and

Lavrik, O.I. (2001). Polarity of human replication protein A binding to DNA. Nucleic Acids Res. *29*, 373–379.

124. Kowalczykowski, S.C. (2015). An Overview of the Molecular Mechanisms of Recombinational DNA Repair. Cold Spring Harb. Perspect. Biol. *7 (11)*.

125. Kuznetsov, S.G., Liu, P., and Sharan, S.K. (2008). Mouse embryonic stem cell-based functional assay to evaluate mutations in BRCA2. Nat. Med. *14*, 875–881.

126. de Laat, W.L., Appeldoorn, E., Sugasawa, K., Weterings, E., Jaspers, N.G., and Hoeijmakers, J.H. (1998). DNA-binding polarity of human replication protein A positions nucleases in nucleotide excision repair. Genes Dev. *12*, 2598–2609.

127. Larsen, N.B., and Hickson, I.D. (2013). RecQ helicases: Conserved guardians of genomic integrity. Adv. Exp. Med. Biol. *767*, 161–184.

128. Lavrik, O.I., Kolpashchikov, D.M., Weisshart, K., Nasheuer, H.P., Khodyreva, S.N., and Favre, a (1999). RPA subunit arrangement near the 3'-end of the primer is modulated by the length of the template strand and cooperative protein interactions. Nucleic Acids Res. *27*, 4235–4240.

129. Lawrence, M.S., Stojanov, P., Mermel, C.H., Robinson, J.T., Garraway, L.A., Golub, T.R., Meyerson, M., Gabriel, S.B., Lander, E.S., and Getz, G. (2014). Discovery and saturation analysis of cancer genes across 21 tumour types. Nature *505*, 495–501.

130. Lee, D.H., Pan, Y., Kanner, S., Sung, P., Borowiec, J.A., and Chowdhury, D. (2010). A PP4 phosphatase complex dephosphorylates RPA2 to facilitate DNA repair via homologous recombination. Nat. Struct. Mol. Biol. *17*, 365–372.

131. Lee, K.Y., Fu, H., Aladjem, M.I., and Myung, K. (2013). ATAD5 regulates the lifespan of DNA replication factories by modulating PCNA level on the chromatin. J. Cell Biol. *200*, 31–44.

132. Lemaçon, D., Jackson, J., Quinet, A., Brickner, J.R., Li, S., Yazinski, S., You, Z., Ira, G., Zou, L., Mosammaparast, N., et al. (2017). MRE11 and EXO1 nucleases degrade reversed forks and elicit MUS81-dependent fork rescue in BRCA2-deficient cells. Nat. Commun. *8*, 860.

133. Leuzzi, G., Marabitti, V., Pichierri, P., Franchitto, A., Ammazzalorso, F., Pirzio, L., Bignami, M., Franchitto, A., Pichierri, P., Basile, G., et al. (2016). WRNIP1 protects stalled forks from degradation and promotes fork restart after replication stress. EMBO J. *35*, 1437–1451.

134. Lim, D.S., and Hasty, P. (1996). A mutation in mouse rad51 results in an early embryonic lethal that is suppressed by a mutation in p53. Mol. Cell. Biol. *16*, 7133–7143.

135. Lindahl, T., and Barnes, D.E. (2000). Repair of endogenous DNA damage. In Cold Spring Harbor Symposia on Quantitative Biology *65*, 127–133.

136. Liu, Y., and West, S.C. (2002). Distinct functions of BRCA1 and BRCA2 in double-strand break repair. Breast Cancer Res. *4*, 9–13.

137. Liu, J., Doty, T., Gibson, B., and Heyer, W.D. (2010). Human BRCA2 protein promotes RAD51 filament formation on RPA-covered single-stranded DNA. Nat. Struct. Mol. Biol. *17*, 1260–1262.

138. Lord, C.J., and Ashworth, A. (2012). The DNA damage response and cancer therapy. Nature *481*, 287–294.

139. Lord, C.J., Tutt, A.N.J., and Ashworth, A. (2015). Synthetic Lethality and Cancer Therapy: Lessons Learned from the Development of PARP Inhibitors. Annu. Rev. Med. *66*, 455–470.

140. Louarn, J., Cornet, F., Francois, V., Patte, J., and Louarn, J.M. (1994). Hyperrecombination in the terminus region of the Escherichia coli chromosome: Possible relation to nucleoid organization. J. Bacteriol. *176*, 7524–7531.

141. Lusetti, S.L., and Cox, M.M. (2002). The Bacterial RecA Protein and the Recombinational DNA Repair of Stalled Replication Forks. Annu. Rev. Biochem. *71*, 71–100.

142. Machwe, A., Lozada, E., Wold, M.S., Li, G.-M., and Orren, D.K. (2011). Molecular cooperation between the Werner syndrome protein and replication protein A in relation to replication fork blockage. J. Biol. Chem. *286*, 3497–3508.

143. Manosas, M., Perumal, S.K., Bianco, P., Ritort, F., Benkovic, S.J., and Croquette, V. (2013). RecG and UvsW catalyse robust DNA rewinding critical for stalled DNA replication fork rescue. Nat. Commun. *4*, 2368.

144. Maréchal, A., and Zou, L. (2015). RPA-coated single-stranded DNA as a platform for post-translational modifications in the DNA damage response. Cell Res. *25*, 9–23.

145. Mason, A.C., Rambo, R.P., Greer, B., Pritchett, M., Tainer, J. a, Cortez, D., and Eichman, B.F. (2014a). A structure-specific nucleic acid-binding domain conserved among DNA repair proteins. Proc. Natl. Acad. Sci. U. S. A. *111*, 7618-7623

146. Mason, J.M., Logan, H.L., Budke, B., Wu, M., Pawlowski, M., Weichselbaum, R.R., Kozikowski, A.P., Bishop, D.K., and Connell, P.P. (2014b). The rad51-stimulatory compound rs-1 can exploit the rad51 overexpression that exists in cancer cells and tumors. Cancer Res. *74*, 3546–3555.

147. Mayle, R., Campbell, I.M., Beck, C.R., Yu, Y., Wilson, M., Shaw, C.A., Bjergbaek, L., Lupski, J.R., and Ira, G. (2015). Mus81 and converging forks limit the mutagenicity of replication fork breakage. Science *349*, 742–747.

148. McGlynn, P., and Lloyd, R.G. (2000). Modulation of RNA polymerase by (p)ppGpp reveals a RecG-dependent mechanism for replication fork progression. Cell *101*, 35–45.

149. Méchali, M. (2010). Eukaryotic DNA replication origins: Many choices for appropriate answers. Nat. Rev. Mol. Cell Biol. *11*, 728–738.

150. Michel, B., Grompone, G., Florès, M.-J., and Bidnenko, V. (2004). Multiple pathways process stalled replication forks. Proc. Natl. Acad. Sci. U. S. A. *101*, 12783–12788.

151. Mijic, S., Zellweger, R., Chappidi, N., Berti, M., Jacobs, K., Mutreja, K., Ursich, S., Ray Chaudhuri, A., Nussenzweig, A., Janscak, P., et al. (2017). Replication fork reversal triggers fork degradation in BRCA2-defective cells. Nat. Commun. *8*, 859.

152. Miné, J., Disseau, L., Takahashi, M., Cappello, G., Dutreix, M., and Viovy, J.L. (2007). Real-time measurements of the nucleation, growth and dissociation of single Rad51-DNA nucleoprotein filaments. Nucleic Acids Res. *35*, 7171–7187.

153. Moinova, H.R., Chen, W.-D., Shen, L., Smiraglia, D., Olechnowicz, J., Ravi, L., Kasturi, L., Myeroff, L., Plass, C., Parsons, R., et al. (2002). HLTF gene silencing in human colon cancer. Proc. Natl. Acad. Sci. *99*, 4562–4567.

154. Mourón, S., Rodriguez-Acebes, S., Martínez-Jiménez, M.I., García-Gómez, S., Chocrón, S., Blanco, L., and Méndez, J. (2013). Repriming of DNA synthesis at stalled replication forks by human PrimPol. Nat. Struct. Mol. Biol. *20*, 1383–1389.

155. Myers, J.S., and Cortez, D. (2006). Rapid activation of ATR by ionizing radiation requires ATM and Mre11. J. Biol. Chem. *281*, 9346–9350.

156. Neelsen, K.J., and Lopes, M. (2015). Replication fork reversal in eukaryotes: from dead end to dynamic response. Nat. Rev. Mol. Cell Biol. *16*, 207–220.

157. Nguyen, B., Sokoloski, J., Galletto, R., Elson, E.L., Wold, M.S., and Lohman, T.M. (2014). Diffusion of Human Replication Protein A along Single-Stranded DNA. J. Mol. Biol. *426*, 3246–3261.

158. Nilsen, T., and Baglioni, C. (1979). Unusual base-pairing of newly synthesized DNA in HeLa cells. J. Mol. Biol. *133*, 319–338.

159. Norquist, B., Wurz, K.A., Pennil, C.C., Garcia, R., Gross, J., Sakai, W., Karlan, B.Y., Taniguchi, T., and Swisher, E.M. (2011). Secondary Somatic Mutations Restoring BRCA1/2 Predict Chemotherapy Resistance in Hereditary Ovarian Carcinomas. J. Clin. Oncol. *29*, 3008–3015.

160. O'Connor, M.J. (2015). Targeting the DNA Damage Response in Cancer. Mol. Cell *60*, 547–560.

161. O'Donovan, P.J., and Livingston, D.M. (2010). BRCA1 and BRCA2: Breast/ovarian cancer susceptibility gene products and participants in DNA double-strand break repair. Carcinogenesis *31*, 961–967.

162. Oakley, G.G., and Patrick, S.M. (2010). Replication protein A: directing traffic at the intersection of replication and repair. Front. Biosci. (Landmark Ed). *15*, 883–900.

163. Oakley, G.G., Patrick, S.M., Yao, J., Carty, M.P., Turchi, J.J., and Dixon, K. (2003). RPA phosphorylation in mitosis alters DNA binding and protein-protein interactions. Biochemistry *42*, 3255–3264.

164. Oakley, G.G., Tillison, K., Opiyo, S.A., Glanzer, J.G., Horn, J.M., and Patrick, S.M. (2009). Physical interaction between replication protein A (RPA) and MRN: Involvement of RPA2 phosphorylation and the N-terminus of RPA1. Biochemistry *48*, 7473–7481.

165. Pagès, V., Koffel-Schwartz, N., and Fuchs, R.P.P. (2003). recX, a new SOS gene that is co-transcribed with the recA gene in Escherichia coli. DNA Repair (Amst). *2*, 273–284.

166. Patrick, S.M., Oakley, G.G., Dixon, K., and Turchi, J.J. (2005). DNA damage induced hyperphosphorylation of replication protein A. 2. Characterization of DNA binding activity, protein interactions, and activity in DNA replication and repair. Biochemistry *44*, 8438–8448.

167. Petermann, E., Orta, M.L., Issaeva, N., Schultz, N., and Helleday, T. (2010). Hydroxyurea-Stalled Replication Forks Become Progressively Inactivated and Require Two Different RAD51-Mediated Pathways for Restart and Repair. Mol. Cell *37*, 492–502.

168. Pillaire, M.-J., Bétous, R., and Hoffmann, J.-S. (2014). Role of DNA polymerase κ in the maintenance of genomic stability. Mol. Cell. Oncol. *1*, e29902.

169. Piwko, W., Mlejnkova, L.J., Mutreja, K., Ranjha, L., Stafa, D., Smirnov, A., Brodersen, M.M., Zellweger, R., Sturzenegger, A., Janscak, P., et al. (2016). The MMS22L–TONSL heterodimer directly promotes RAD51-dependent recombination upon replication stress. EMBO J. *35*, 2584–2601.

170. Poole, L.A., and Cortez, D. (2017). Functions of SMARCAL1, ZRANB3, and HLTF in maintaining genome stability. Crit. Rev. Biochem. Mol. Biol. *52*, 696–714.

171. Postow, L., Woo, E.M., Chait, B.T., and Funabiki, H. (2009). Identification of SMARCAL1 as a component of the DNA damage response. J. Biol. Chem. *284*, 35951–35961.

172. Quiros, S., Roos, W.P., and Kaina, B. (2011). Rad51 and BRCA2--New molecular targets for sensitizing glioma cells to alkylating anticancer drugs. PLoS One *6*, e27183.

173. Ranalli, T. a, DeMott, M.S., and Bambara, R. a (2002). Mechanism underlying replication protein a stimulation of DNA ligase I. J. Biol. Chem. *277*, 1719–1727.

174. Ray Chaudhuri, A., Hashimoto, Y., Herrador, R., Neelsen, K.J., Fachinetti, D., Bermejo, R., Cocito, A., Costanzo, V., and Lopes, M. (2012). Topoisomerase I poisoning results in PARP-mediated replication fork reversal. Nat. Struct. Mol. Biol. *19*, 417–423.

175. Renkawitz, J., Lademann, C. a, and Jentsch, S. (2014). Mechanisms and principles of homology search during recombination. Nat. Rev. Mol. Cell Biol. *15*, 369-383.

176. Richard, D.J., Bolderson, E., and Khanna, K.K. (2009). Multiple human single-stranded DNA binding proteins function in genome maintenance: structural, biochemical and functional analysis. Crit. Rev. Biochem. Mol. Biol. *44*, 98–116.

177. Richardson, C., Stark, J.M., Ommundsen, M., and Jasin, M. (2004). Rad51 overexpression promotes alternative double-strand break repair pathways and genome instability. Oncogene *23*, 546–553.

178. Ristic, D., Modesti, M., van der Heijden, T., van Noort, J., Dekker, C., Kanaar, R., and Wyman, C. (2005). Human Rad51 filaments on double- and single-stranded DNA: Correlating regular and irregular forms with recombination function. Nucleic Acids Res. *33*, 3292–3302.

179. Robu, M.E., Inman, R.B., and Cox, M.M. (2001). RecA protein promotes the regression of stalled replication forks in vitro. Proc. Natl. Acad. Sci. U. S. A. *98*, 8211–8218.

180. Rondinelli, B., Gogola, E., Yücel, H., Duarte, A.A., Van De Ven, M., Van Der Sluijs, R., Konstantinopoulos, P.A., Jonkers, J., Ceccaldi, R., Rottenberg, S., et al. (2017). EZH2 promotes degradation of stalled replication forks by recruiting MUS81 through histone H3 trimethylation. Nat. Cell Biol. *19*, 1371–1378.

181. Roy, R., Chun, J., and Powell, S.N. (2012). BRCA1 and BRCA2: Different roles in a common pathway of genome protection. Nat. Rev. Cancer *12*, 68–78.

182. Ruff, P., Donnianni, R.A., Glancy, E., Oh, J., and Symington, L.S. (2016). RPA Stabilization of Single-Stranded DNA Is Critical for Break-Induced Replication. Cell Rep. *17*, 3359–3368.

183. Saeki, H., Siaud, N., Christ, N., Wiegant, W.W., van Buul, P.P.W., Han, M., Zdzienicka, M.Z., Stark, J.M., and Jasin, M. (2006). Suppression of the DNA repair defects of BRCA2-deficient cells with heterologous protein fusions. Proc. Natl. Acad. Sci. U. S. A. *103*, 8768–8773.

184. Saini, N., Ramakrishnan, S., Elango, R., Ayyar, S., Zhang, Y., Deem, A., Ira, G., Haber, J.E., Lobachev, K.S., and Malkova, A. (2013). Migrating bubble during break-induced replication drives conservative DNA synthesis. Nature *502*, 389–392.

185. Sakai, W., Swisher, E.M., Karlan, B.Y., Agarwal, M.K., Higgins, J., Friedman, C., Villegas, E., Jacquemont, C., Farrugia, D.J., Couch, F.J., et al. (2008). Secondary mutations as a mechanism of cisplatin resistance in BRCA2-mutated cancers. Nature *451*, 1116–1120.

186. Sakofsky, C.J., and Malkova, A. (2017). Break induced replication in eukaryotes: mechanisms, functions, and consequences. Crit. Rev. Biochem. Mol. Biol. *52*, 395–413.

187. Saldivar, J.C., Cortez, D., and Cimprich, K.A. (2017). The essential kinase ATR: Ensuring faithful duplication of a challenging genome. Nat. Rev. Mol. Cell Biol. *18*, 622–636.

188. Sale, J.E., Lehmann, A.R., and Woodgate, R. (2012). Y-family DNA polymerases and their role in tolerance of cellular DNA damage. Nat. Rev. Mol. Cell Biol. *13*, 141–152.

189. Sandhu, S., Wu, X., Nabi, Z., Rastegar, M., Kung, S., Mai, S., and Ding, H. (2012). Loss of HLTF function promotes intestinal carcinogenesis. Mol. Cancer *11*: 18

190. Sarbajna, S., and West, S.C. (2014). Holliday junction processing enzymes as guardians of genome stability. Trends Biochem. Sci. *39*, 409–419.

191. Satta, G., Gudas, L.J., and Pardee, A.B. (1979). Degradation of Escherichia coli DNA: Evidence for limitation in vivo by protein X, the recA gene product. Mol. Gen. Genet. *168*, 69–80.

192. Schlacher, K., Christ, N., Siaud, N., Egashira, A., Wu, H., and Jasin, M. (2011). Double-strand break repair-independent role for BRCA2 in blocking stalled replication fork degradation by MRE11. Cell *145*, 529–542.

193. Schlacher, K., Wu, H., and Jasin, M. (2012). A Distinct Replication Fork Protection Pathway Connects Fanconi Anemia Tumor Suppressors to RAD51-BRCA1/2. Cancer Cell *22*, 106–116.

194. Schubert, L., Ho, T., Hoffmann, S., Haahr, P., Guérillon, C., and Mailand, N. (2017). RADX interacts with single-stranded DNA to promote replication fork stability. EMBO Rep. *18*, 1991-2003

195. Sharan, S.K., Morimatsu, M., Albrecht, U., Lim, D.S., Regel, E., Dinh, C., Sands, a, Eichele, G., Hasty, P., and Bradley, a (1997). Embryonic lethality and radiation hypersensitivity mediated by Rad51 in mice lacking Brca2. Nature *386*, 804–810.

196. Shen, J., Gray, M., Oshima, J., and Loeb, L. (1998). Characterization of Werner syndrome protein DNA helicase activity: directionality, substrate dependence and stimulation by replication protein A. Nucleic Acids Res. *26*, 2879–2885.

197. Shereda, R.D., Bernstein, D. a, and Keck, J.L. (2007). A central role for SSB in Escherichia coli RecQ DNA helicase function. J. Biol. Chem. *282*, 19247–19258.

198. Shinohara, A., Ogawa, H., and Ogawa, T. (1992). Rad51 protein involved in repair and recombination in S. cerevisiae is a RecA-like protein. Cell *69*, 457–470.

199. Shivji, M.K.K., Mukund, S.R., Rajendra, E., Chen, S., Short, J.M., Savill, J., Klenerman, D., and Venkitaraman, A.R. (2009). The BRC repeats of human BRCA2 differentially regulate RAD51 binding on single- versus double-stranded DNA to stimulate strand exchange. Proc. Natl. Acad. Sci. U. S. A. *106*, 13254–13259.

200. Short, J.M., Liu, Y., Chen, S., Soni, N., Madhusudhan, M.S., Shivji, M.K.K., and Venkitaraman, A.R. (2016). High-resolution structure of the presynaptic RAD51 filament on single-stranded DNA by electron cryo-microscopy. Nucleic Acids Res. *44*, 9017–9030.

201. Sogo, J.M., Lopes, M., and Foiani, M. (2002). Fork Reversal and ssDNA Accumulation at Stalled Replication Forks Owing to Checkpoint Defects. Science *297*, 599–602.

202. Sommers, J. a, Banerjee, T., Hinds, T., Wold, M.S., Lei, M., and Brosh, R.M. (2014). Novel Function of the Fanconi Anemia Group J or RECQ1 Helicase to Disrupt Protein-DNA Complexes in a Replication Protein A-Stimulated Manner. J. Biol. Chem. *289*, 19928–19941.

203. Somyajit, K., Saxena, S., Babu, S., Mishra, A., and Nagaraju, G. (2015). Mammalian RAD51 paralogs protect nascent DNA at stalled forks and mediate replication restart. Nucleic Acids Res. *43*, 9835–9855.

204. Stark, J.M., Pierce, A.J., Oh, J., Pastink, A., and Jasin, M. (2004). Genetic Steps of Mammalian Homologous Repair with Distinct Mutagenic Consequences. Mol. Cell. Biol. *24*, 9305–9316.

205. Stingele, J., Schwarz, M.S., Bloemeke, N., Wolf, P.G., and Jentsch, S. (2014). A DNA-dependent protease involved in DNA-protein crosslink repair. Cell *158*, 327–338.

206. Stohl, E.A., Brockman, J.P., Burkle, K.L., Morimatsu, K., Kowalczykowski, S.C., and

Seifert, H.S. (2003). Escherichia coli RecX inhibits RecA recombinase and coprotease activities in vitro and in vivo. J. Biol. Chem. *278*, 2278–2285.

207. Su, F., Mukherjee, S., Yang, Y., Mori, E., Bhattacharya, S., Kobayashi, J., Yannone, S.M., Chen, D.J., and Asaithamby, A. (2014). Nonenzymatic Role for WRN in Preserving Nascent DNA Strands after Replication Stress. Cell Rep. *9*, 1387–1401.

208. Suhasini, A.N., Sommers, J.A., Mason, A.C., Voloshin, O.N., Camerini-Otero, R.D., Wold, M.S., and Brosh, R.M. (2009). FANCJ helicase uniquely senses oxidative base damage in either strand of duplex DNA and is stimulated by replication protein A to unwind the damaged DNA substrate in a strand-specific manner. J. Biol. Chem. *284*, 18458–18470.

209. Sung, P. (1994). Catalysis of ATP-dependent homologous DNA pairing and strand exchange by yeast RAD51 protein. Science *265*, 1241–1243.

210. Symington, L.S. (2014). End resection at double-strand breaks: Mechanism and regulation. Cold Spring Harb. Perspect. Biol. *6*(8).

211. Szász, A.M., Lánczky, A., Nagy, Á., Förster, S., Hark, K., Green, J.E., Boussioutas, A., Busuttil, R., Szabó, A., Győrffy, B., et al. (2016). Cross-validation of survival associated biomarkers in gastric cancer using transcriptomic data of 1,065 patients. Oncotarget *7*, 49322–49333.

212. Taglialatela, A., Alvarez, S., Leuzzi, G., Sannino, V., Ranjha, L., Huang, J.-W., Madubata, C., Anand, R., Levy, B., Rabadan, R., et al. (2017). Restoration of Replication Fork Stability in BRCA1- and BRCA2-Deficient Cells by Inactivation of SNF2-Family Fork Remodelers. Mol. Cell *68*, 414–430.

213. Tarsounas, M., Davies, D., and West, S.C. (2003). BRCA2-dependent and independent formation of RAD51 nuclear foci. Oncogene *22*, 1115–1123.

214. Tatsumi, K., and Strauss, B. (1978). Production of DNA bifilarly substituted with bromodeoxyuridine in the first round of synthesis: Branch migration during isolation of cellular DNA. Nucleic Acids Res. *5*, 331–347.

215. Taylor, M.R.G., Špírek, M., Jian Ma, C., Carzaniga, R., Takaki, T., Collinson, L.M., Greene, E.C., Krejci, L., and Boulton, S.J. (2016). A Polar and Nucleotide-Dependent Mechanism of Action for RAD51 Paralogs in RAD51 Filament Remodeling. Mol. Cell *64*, 926–939.

216. Tennstedt, P., Fresow, R., Simon, R., Marx, A., Terracciano, L., Petersen, C., Sauter, G., Dikomey, E., and Borgmann, K. (2013). RAD51 overexpression is a negative prognostic marker for colorectal adenocarcinoma. Int. J. Cancer *132*, 2118–2126.

217. Thangavel, S., Berti, M., Levikova, M., Pinto, C., Gomathinayagam, S., Vujanovic, M., Zellweger, R., Moore, H., Lee, E.H., Hendrickson, E.A., et al. (2015). DNA2 drives processing and restart of reversed replication forks in human cells. J. Cell Biol. *208*, 545–562.

218. Toledo, L.I., Altmeyer, M., Rask, M.-B., Lukas, C., Larsen, D.H., Povlsen, L.K., Bekker-Jensen, S., Mailand, N., Bartek, J., and Lukas, J. (2013). ATR prohibits replication

catastrophe by preventing global exhaustion of RPA. Cell *155*, 1088–1103.

219. Trego, K.S., Groesser, T., Davalos, A.R., Parplys, A.C., Zhao, W., Nelson, M.R., Hlaing, A., Shih, B., Rydberg, B., Pluth, J.M., et al. (2016). Non-catalytic Roles for XPG with BRCA1 and BRCA2 in Homologous Recombination and Genome Stability. Mol. Cell *61*, 535–546.

220. Tsuzuki, T., Fujii, Y., Sakumi, K., Tominaga, Y., Nakao, K., Sekiguchi, M., Matsushiro, a, Yoshimura, Y., and MoritaT (1996). Targeted disruption of the Rad51 gene leads to lethality in embryonic mice. Proc. Natl. Acad. Sci. U. S. A. *93*, 6236–6240.

221. Vaz, B., Popovic, M., Newman, J.A., Fielden, J., Aitkenhead, H., Halder, S., Singh, A.N., Vendrell, I., Fischer, R., Torrecilla, I., et al. (2016). Metalloprotease SPRTN/DVC1 Orchestrates Replication-Coupled DNA-Protein Crosslink Repair. Mol. Cell *64*, 704–719.

222. Venkatesh, R., Ganesh, N., Guhan, N., Reddy, M.S., Chandrasekhar, T., and Muniyappa, K. (2002). RecX protein abrogates ATP hydrolysis and strand exchange promoted by RecA: Insights into negative regulation of homologous recombination. Proc. Natl. Acad. Sci. U. S. A. *99*, 12091–12096.

223. Venkitaraman, a R. (2001). Functions of BRCA1 and BRCA2 in the biological response to DNA damage. J. Cell Sci. *114*, 3591–3598.

224. Vierling, S., Weber, T., Wohlleben, W., and Muth, G. (2000). Transcriptional and mutational analyses of the Streptomyces lividans recX gene and its interference with recA activity. J. Bacteriol. *182*, 4005–4011.

225. Vujanovic, M., Krietsch, J., Raso, M.C., Terraneo, N., Zellweger, R., Schmid, J.A., Taglialatela, A., Huang, J.W., Holland, C.L., Zwicky, K., et al. (2017). Replication Fork Slowing and Reversal upon DNA Damage Require PCNA Polyubiquitination and ZRANB3 DNA Translocase Activity. Mol. Cell *67*, 882–890.

226. Walther, a P., Gomes, X. V, Lao, Y., Lee, C.G., and Wold, M.S. (1999). Replication protein A interactions with DNA. 1. Functions of the DNA-binding and zinc-finger domains of the 70-kDa subunit. Biochemistry *38*, 3963–3973.

227. Wang, A.T., Kim, T., Wagner, J.E., Conti, B.A., Lach, F.P., Huang, A.L., Molina, H., Sanborn, E.M., Zierhut, H., Cornes, B.K., et al. (2015). A Dominant Mutation in Human RAD51 Reveals Its Function in DNA Interstrand Crosslink Repair Independent of Homologous Recombination. Mol. Cell *59*, 478–490.

228. Wanka, F., Brouns, R.M.G. m. e., Aelen, J.M.A., and Eygensteyn, J. (1977). The origin of nascent single-stranded DNA extracted from mammalian cells. Nucleic Acids Res. *4*, 2083–2098.

229. Willis, N. a, Chandramouly, G., Huang, B., Kwok, A., Follonier, C., Deng, C., and Scully, R. (2014). BRCA1 controls homologous recombination at Tus/Ter-stalled mammalian replication forks. Nature *510*, 556–559.

230. Wold, M.S. (1997). Replication protein A: a heterotrimeric, single-stranded DNA-binding protein required for eukaryotic DNA metabolism. Annu. Rev. Biochem. *66*, 61–92.

231. Wu, X., Yang, Z., Liu, Y., and Zou, Y. (2005). Preferential localization of hyperphosphorylated replication protein A to double-strand break repair and checkpoint complexes upon DNA damage. Biochem. J. *391*, 473–480.

232. Wyka, I.M., Dhar, K., Binz, S.K., and Wold, M.S. (2003). Replication protein A interactions with DNA: differential binding of the core domains and analysis of the DNA interaction surface. Biochemistry *42*, 12909–12918.

233. Xu, S., Wu, X., Wu, L., Castillo, A., Liu, J., Atkinson, E., Paul, A., Su, D., Schlacher, K., Komatsu, Y., et al. (2017). Abro1 maintains genome stability and limits replication stress by protecting replication fork stability. Genes Dev. *31*, 1469–1482.

234. Xu, X., Vaithiyalingam, S., Glick, G.G., Mordes, D. a, Chazin, W.J., and Cortez, D. (2008). The basic cleft of RPA70N binds multiple checkpoint proteins, including RAD9, to regulate ATR signaling. Mol. Cell. Biol. *28*, 7345–7353.

235. Yang, Y., Liu, Z., Wang, F., Temviriyanukul, P., Ma, X., Tu, Y., Lv, L., Lin, Y.F., Huang, M., Zhang, T., et al. (2015). FANCD2 and REV1 cooperate in the protection of nascent DNA strands in response to replication stress. Nucleic Acids Res. *43*, 8325–8339.

236. Yazinski, S.A., Comaills, V., Buisson, R., Genois, M.M., Nguyen, H.D., Ho, C.K., Kwan, T.T., Morris, R., Lauffer, S., Nussenzweig, A., et al. (2017). ATR inhibition disrupts rewired homologous recombination and fork protection pathways in PARP inhibitor-resistant BRCA-deficient cancer cells. Genes Dev. *31*, 318–332.

237. Yu, X., Jacobs, S.A., West, S.C., Ogawa, T., and Egelman, E.H. (2001). Domain structure and dynamics in the helical filaments formed by RecA and Rad51 on DNA. Proc. Natl. Acad. Sci. U. S. A. *98*, 8419–8424.

238. Yuan, J., Ghosal, G., and Chen, J. (2009). The annealing helicase HARP protects stalled replication forks. Genes Dev. *23*, 2394–2399.

239. Yusufzai, T., and Kadonaga, J.T. (2008). HARP Is an ATP-driven Annealing Helicase. *322*, 748–750.

240. Yusufzai, T., Xiangduo, K., Kyoko, Y., and Kadonaga, J.T. (2009). The annealing helicase HARP is recruited to DNA repair sites via an interaction with RPA. Genes Dev. *23*, 2400–2404.

241. Zadorozhny, K., Sannino, V., Beláň, O., Mlčoušková, J., Špírek, M., Costanzo, V., and Krejčí, L. (2017). Fanconi Anemia Associated Mutations Destabilize RAD51 Filaments and Impair Replication Fork Protection. Cell Rep. *21*, 333–340.

242. Zaitseva, E.M., Zaitsev, E.N., and Kowalczykowski, S.C. (1999). The DNA binding properties of Saccharomyces cerevisiae Rad51 protein. J. Biol. Chem. *274*, 2907–2915.

243. Zellweger, R., Dalcher, D., Mutreja, K., Berti, M., Schmid, J.A., Herrador, R., Vindigni, A., and Lopes, M.,(2015). Rad51-mediated replication fork reversal is a global response to genotoxic treatments in human cells. J. Cell Biol. *208*, 563–579.

244. Zeman, M.K., and Cimprich, K. a (2014). Causes and consequences of replication stress.

Nat. Cell Biol. *16*, 2–9.

245. Zou, L. (2017). DNA Replication Checkpoint: New ATR Activator Identified. Curr. Biol. *27*, R33–R35.

246. Zou, H., and Rothstein, R. (1997). Holliday junctions accumulate in replication mutants via a RecA homolog- independent mechanism. Cell *90*, 87–96.

247. Zou, L., and Elledge, S.J. (2003). Sensing DNA damage through ATRIP recognition of RPA-ssDNA complexes. Science *300*, 1542–1548.